Engineering the Next-generation Type I Reaction Centers

Specializing in Hydrogen Production in Vivo

by

Andrey Kanygin

A Dissertation Presented in Partial Fulfillment
of the Requirements for the Degree
Doctor of Philosophy

Approved July 2022 by the
Graduate Supervisory Committee:

Kevin E. Redding, Chair
Anne Katherine Jones
Yuval Mazor

ARIZONA STATE UNIVERSITY

August 2022

ABSTRACT

The growing global energy demand coupled with the need for a low-carbon economy requires innovative solutions. Microalgal oxygenic photosynthesis provides a sustainable platform for efficient capture of sunlight and storage of some of the energy in the form of reduced carbon derivatives. Under certain conditions, the photosynthetic reductant can be shunted to molecular hydrogen production, yet the efficiency and longevity of such processes are insufficient. In this work, re-engineering of the heterodimeric type I reaction center, also known as photosystem I (PSI), in the green microalga *Chlamydomonas reinhardtii* was shown to dramatically change algal metabolism and improve photobiological hydrogen production in vivo. First, an internal fusion of the small PsaC subunit of PSI harboring the terminal photosynthetic electron transport chain cofactors with the endogenous algal hydrogenase 2 (HydA2) was demonstrated to assemble on the PSI core in vivo, albeit at ~15% the level of normal PSI accumulation, and make molecular hydrogen from water oxidation. Second, the more physiologically active algal endogenous hydrogenase 1 (HydA1) was fused to PsaC in a similar fashion, resulting in improved levels of accumulation (~75%). Both algal hydrogenases chimeras remained extremely oxygen sensitive and benefited from oxygen removal methods. On the example of PSI-HydA1 chimera, it was demonstrated that the active site of hydrogenase can be reactivated in vivo after complete inactivation by oxygen without the need for new polypeptide synthesis. Third, the hydrogenase domain of *Megasphaera elsdenii* bacterial hydrogenase (*Me*HydA) was also fused with psaC, resulting in expression of a PSI-hydrogenase chimera at ~25% the normal level. The heterologous hydrogenase chimera could be activated with the algal maturation system, despite only 32 % sequence identity (43 % similarity). All constructs demonstrated diminished ability to reduce PSI electron acceptors (ferredoxin and flavodoxin) in vitro and indirect evidence indicated that this was true in vivo as well. Finally, chimeric design considerations are discussed in light of the models generated by Alphafold2 and how could they be used to further optimize stability of the PSI-hydrogenase chimeric complexes.

ACKNOWLEDGMENTS

First, I would like to thank my advisor Kevin Redding for his continuous support through the years and shared moments of excitement for scientific discovery. His passion for science drew me to the lab as an undergraduate with pre-med aspirations and then, sparked my interest in photosynthesis in the graduate school.

I owe thanks to the former and current members of the Redding lab who created a positive and encouraging environment. Especially I would like to thank Gregory Orf, whose cheerful personality and keen mind made the workplace fun and stimulating.

I am grateful to our collaborators in Tel Aviv University – Ifatch Yacoby, Yuval Milrad, Marina Kozuleva, and others, for being great hosts and expanding my thinking both scientifically and culturally.

I owe a great deal of gratitude to Paul King, David Mulder, Jacob Artz and other members of photobiology group at NREL for supporting my internship proposal, giving advice and allowing me the experience of top-notch research facility.

I thank former undergraduate students who helped me with this project: Alec Smith, Imran Hussain, and Taryn O'Boyle.

I am thankful to Anne Jones for helping me with my research: from a word of advice to assisting in collaboration.

I am also thankful to Yuval Mazor for being on my committee and providing valuable feedback.

I thank the School of Molecular Sciences and Arizona State University for providing this opportunity to learn from the best.

Finally, I thank National Science Foundation for financial support of the project.

TABLE OF CONTENTS

APPENDIX Page

LIST OF TABLES

LIST OF FIGURES

LIST OF ABBREVIATIONS

ADP	Adenosine Diphosphate
ATP	Adenosine Triphosphate
CAM	Chloramphenicol
CBB	Calvin-Benson-Bassham (Cycle)
Chl	Chlorophyll
CR	Charge Recombination
DBMIB	Dibromothymoquinone
DCMU	3-(3,4-dichlorophenyl)-1,1-dimethylurea
EDTA	Ethylenediamine Tetraacetate
Fd	Ferredoxin
Fld	Flavodoxin
FNR	Ferredoxin-NADP(+)-reductase
GA	Glycolaldehyde
H_2	Molecular Hydrogen
HDM	Hard-docking Model
LEF	Linear Electron Flow
MIMS	Membrane Inlet Mass Spectrometry
MV	Methyl Viologen
NADP	Nicotineamide Adenine Dinucleotide Phosphate

Ni-IDA	Nickel Iminodiacetic Acid
PAR	Photosynthetically Active Radiation
PBR	Photobioreactor
PCR	Polymerase Chain Reaction
PETC	Photosynthetic Electron Transport Chain
pLDDT	Predicted Local Distance Difference Test
PSI	Photosystem I
PSII	Photosystem II
RC	Reaction Center
RMSD	Root-mean-square Deviation
RMVA	Reduced Methyl Viologen Assay
SUF	Sulfur Utilization Factor
TAP	Tris Acetate Phosphate
TBP	Tris Bicarbonate Phosphate
β-DDM	*n*-dodecyl-β-D-maltoside

CHAPTER 1

INTRODUCTION: OXYGENIC PHOTOSYNTHESIS AND HYDROGEN METABOLISM IN GREEN MICROALGA *CHLAMYDOMONAS REINHARDTII*; SUMMARY AND SCOPE OF THE DISSERTATION

Andrey Kanygin

School of Molecular Sciences

Arizona State University, Tempe, AZ 85287

Motivation

Ongoing efforts to mitigate climate change effected by human activity require radical a shift from the way energy is extracted and stored. In 2019, the global primary energy demand was 14.41 Gtoe (Giga tonnes of oil equivalent) with more than 80% coming from fossil fuels [1]. This is approximately 600 EJ a year (or ~19 TW), with projected yearly increases of ~2-4 % depending on the GDP (gross domestic product) growth. The sun is the most abundant energy source on Earth with about ~100 PW reaching the surface on average [2]; thus, it exceeds the current global energy demand by more than 5000 times. However, the conversion of sunlight into electricity alone will not produce a desirable net zero (or low carbon) emission economy, as energy storage molecules would still be required where electricity availability or usage is limited. Currently, hydrogen is considered as a clean energy carrier alternative to fossil fuels, yet ~95% of industrially produced hydrogen is made from steam reformation of natural gas [3]. Photosynthesis is a nature's way of efficiently capturing and converting sunlight energy into chemical bonds in phototrophic organisms [4]. A fraction of photosynthetic microorganisms (including some microalgae) has been shown to also have hydrogen metabolism that is connected to photosynthesis [5,6], yet the coupling of photosynthesis to photo-production of H_2 is transient [7]. The research presented in this dissertation addresses the question of how to couple oxygenic photosynthesis to hydrogen production (and on a more fundamental level – how to rewire photosynthesis for novel redox chemistries) in a more efficient manner by re-engineering type I heterodimeric reaction center (PS I) in a model green microalgae *Chlamydomonas reinhardtii*; what effects of such engineering feat have on photosynthetic electron transport chain (PETC) and algal metabolism in general and how modern modeling tools may help improving stability of the constructs.

Oxygenic photosynthesis

In oxygenic photosynthesis, there are 4 integral membrane protein complexes: photosystem II (PS II), cytochrome *b6f,* photosystem I (PS I), and F-ATP synthase that catalyze light reactions of photosynthesis that lead to production of ATP and NADPH[8]. Reaction centers

(RC) are pigment-protein complexes where light-driven charge separation occurs resulting in electrochemical gradient across the membrane. RCs are classified on type I and type II based on the terminal electron acceptor cofactor. In type I, the iron sulfur cluster serves the role of terminal electron acceptor and in type II – a quinone [9]. Terminal acceptor of PS I (type I RC) is much more reducing (E_m~ -500 mV) than the plastoquinone (E_m ~ +100-0 mV) of PS II (type II RC) [10]. This explains why PS I is required to make NADPH ($E_m^{o'}$=-320 mV) for carbon fixation in the light or under certain conditions - proton reduction to hydrogen ($E_m^{o'}$=-414 mV) [11]. NADPH and ATP produced by the light reactions must be consumed in the dark reactions of photosynthesis (Calvin-Benson-Bassham cycle), so that $NADP^+$ and ADP can be reused and no photodamage occurs [12].

Linear electron flow (LEF).

When energized electrons from water oxidation traverse electron transport chain and end up reducing $NADP^+$ to NADPH that is ultimately used in carbon fixation, the pathway is called linear electron flow (see **figure 1-1**). It takes 2 stable charge separation events at PS II to reduce the quinone to quinol molecule at Q_B site, that then diffuses out in the membrane joining the plastoquinone pool. Cytochrome *b6f* connects plastoquinol pool to plastocyanin (soluble protein on the luminal side) and pumps extra protons to the lumen via Q-cycle [13]. Plastocyanin acts as an electron donor to PS I, which upon excitation with light and stable charge separation, reduces a ferredoxin (Fd) molecule on the stromal (acceptor) side. Two Fd molecules reduce $NADP^+$ to NADPH at ferredoxin-NADP reductase (FNR). Overall equation for linear electron flow is shown below:

$$2\ H_2O + 8\ h\nu + 8\ H^+_{stroma} \rightarrow O_2 + 12\ H^+_{lumen} + 4\ e^- \qquad \text{(equation 1)}$$

ATP synthase dissipates proton motive force across thylakoid membrane with the hydrophobic domain F_0 acting as a proton turbine. Efficiency of the enzyme depends on the number of the c subunits in the F_0 domain. *Chlamydomonas reinhardtii* has 13 c subunits, so it takes 13 protons for a complete rotation of oligomeric c-ring and consequently generation of 3 ATP [14]. This means that proton gradient generated in LEF produces about 2.77 ATP. Calvin-Benson-Bassham

(CBB) cycle requires 3 ATP and 2 NADPH for fixing 1 CO_2 molecule [15]. Cyclic electron flow around PS I and noncyclic pathways to alternative electron acceptors help generate additional ATP and prevent photoinhibition.

Cyclic electron flow (CEF).

CEF can be defined as a return of the reductant from the acceptor side of PS I to the donor side that is accompanied by proton gradient build up across thylakoid membrane [16,17]. The exact mechanism of CEF is not completely understood and shares many partners with LEF (see **Figure 1-2**). Reduced Fd can return electrons via PGRL1/PGR5 mediated pathway presumably directly reducing plastoquinone at Q_i site (blocked by Antimycin A) of cyt *b6f* [18], or via pathway involving NADPH and Nda2 (type 2 NAD(P)H:plastoquinone oxidoreductase) [19,20]. Irrespective of the route, CEF is triggered by overreduction of the stroma (Fd) [21], which is followed by increases in proton gradient across thylakoid membrane. Consequences of the proton gradient increase are 2-pronged. First, it increases ATP production, balancing ATP for optimal CO_2 fixation and thereby alleviating imbalance in the stroma (as NADPH gets oxidized in CBB). Second, acidification of the lumen increases nonphotochemical quenching at both photosystems [22] and downregulates electron transfer through cyt *b6f* [23,24].

Pseudocyclic electron flow

Under aerobic conditions, excess of stromal reductant can be oxidized by molecular oxygen to water via several pathways, thusly having net effect of generating proton motive force as electrons coming from water oxidation (PS II) complete a pseudo cycle. The major pathway involves flavodiiron proteins FlvA and FlvB (working presumably as a heterodimer) [25,26] (see **figure 1-3**). Maximal rate of O_2 uptake by FlvA/FlvB was measured in *Chlamydomonas reinhardtii* strain to be ~45 µmol h^{-1} (mg of Chl)$^{-1}$ or 22.5 e^{-1} s^{-1} PSI^{-1} [27]. Although the electron donor to FlvA/FlvB has long been presumed to be NADH/NADPH, it is not entirely settled matter and other players such as Fd and even terminal acceptors of PS I (F_B) are considered [28]**.**

Another pathway of pseudocyclic electron flow involve the activity of plastid terminal oxidases (and the major player – PTOX2 – showing rate of O_2 reduction at 5 e^{-1} s^{-1} PSI^{-1} [29]). PTOX associated pathway is also known as chlororespiration and it is crucial to maintaining redox poise of plastoquinone pool. Upregulation of the chlororespiratory pathway occur under adverse conditions such as nutrient starvation [30]. It is estimated to be ~4 times less active than flavodiiron-mediated pathway in wild type algae under nutrient replete conditions [27].

Mehler reaction and Mehler-like reactions in chloroplast occur when oxygen is directly reduced at the acceptor side of PS I to superoxide radical that is quickly turned over by superoxide dismutase and ascorbate peroxidase to a final product – water [31]. Potential formation of reactive oxygen species (superoxide anion, hydroxy radicals, hydrogen peroxide, etc.) can result in photoinhibition of PS I and/or downregulation of CBB [32], In *Chlamydomonas reinhardtii*, it was shown that phylloquinone of the A-branch is the primary site of Mehler reaction [33].

Hydrogenases

Chlamydomonas reinhardtii possesses two nuclear encoded genes that express chloroplast stroma targeted proteins HydA1 [34] and HydA2 [35]. Upon insertion of the catalytic H-cluster by maturation factors HydEF and HydG [36,37], the holoenzymes catalyze reversible proton reduction (see **figure 1-4**):

$$2\ Fd_{red} + 2\ H^+ \rightleftarrows H_2 + 2\ Fd_{ox} \qquad (\text{equation } 2)$$

The function of hydrogenases have been long thought as the “safety valve” for stromal reductant under anoxia, that is when oxygen is not available to drive pseudocyclic electron flow to generate proton gradient (ATP) [38]. Recently, their role was more generalized to maintaining redox poise of the NADPH pool as it has been shown they can also uptake hydrogen and reduce $NADP^+$ *in vivo* [39]. The HydA1 has been known as a more physiologically active hydrogenase [40,41]. A recent study of HydA2 (in comparison to HydA1) revealed not only higher specific

activity of HydA1 towards hydrogen production (with physiological and artificial electron donors), but also higher affinity for photosynthetic ferredoxin 1 (for HydA1 K_m = 23 ± 0.5 μM, HydA2 K_m = 38 ±10 μM). The catalytic bias of HydA2 towards H_2 uptake at physiological pH is about 2 times higher than for HydA1 (1.63 at pH 7.0) [42].

Catalytic cluster of algal hydrogenases is extremely oxygen sensitive (e.g., in vitro 10 ppm O_2 exposure for 2 hours reduce specific activity by 98%). The fate of the H-cluster after oxygen encounter depends on the redox state and ultimately result in degradation [43,44].

Interplay between reduced carbon sources and PETC

Carbon metabolism is complex and flexible in green microalgae. It provides long-term storage (in the form of starch) for reductant generated in the light due to activity of CBB cycle, whereas in the dark starch breakdown followed by glycolysis generates NADPH and ATP [45]. Under aerobic conditions, glycolytic products at the level of triose phosphates can be shuttled out of chloroplast and enter tricarboxylic acid cycle and oxidative phosphorylation in mitochondria for maximum yield of ATP. Under anaerobic conditions, glycolytic products enter fermentative pathways that are of mixed acid type (with formate, acetate, and ethanol as products in ~ 2.07:1.07:0.91 ratio) [46] resulting in additional ATP production and recycling NADPH. Pyruvate ferredoxin oxidoreductase [47] catalyzes ferredoxin reduction that is connected to hydrogen production in the dark, while producing acetyl-CoA and carbon dioxide. Glycolytic NADPH is oxidized by Nda2 dehydrogenase that in turn reduces plastoquionone pool [48,49] .

Chlamydomonas reinhardtii is facultative phototroph and can grow on acetate as the sole carbon source without losing photosynthetic apparatus in the dark [50]. Acetate uptake requires ~2 ATP for production of Acetyl-CoA, that can either enter mitochondria for ATP generation by oxidative phosphorylation under aerobic conditions or glyoxylate cycle in the cytoplasm that would make succinate for anabolic pathways [45]. ATP requirement for acetate uptake is

translated into strong light dependance [51] that would generate extra ATP via increased cyclic electron flow [49].

Biological hydrogen production in *Chlamydomonas reinhardtii*

Hydrogenases convert excess of reductant (under anoxia) in the form of molecular hydrogen that can later be recaptured depending on the physiological need of the cells [39]. Overall hydrogen production is a result of the interplay of electron sources and electron sinks in cell [52]. The immediate sources of reductant could be sorted out on light-independent and light-dependent. Water oxidation by PS II provides the primary source of electrons under nutrient replete conditions for high rates of hydrogen evolution in microalgae [53] (see **figure 1-5**). Overall equation for linear electron flow (equation 1) changes as follows:

$$2\ H_2O + 8\ hv + 8\ H^+_{stroma} \rightarrow O_2 + 12\ H^+_{lumen} + 2\ H_2 \qquad \text{(equation 3)}$$

Under continuous light the upregulation of CBB cycle activity results in carbon fixation outcompeting hydrogen production, followed by oxygen accumulation and inactivation of the catalytic site of hydrogenase [54].

Summary and Scope of the Dissertation

To overcome competition for electrons with other pathways, this dissertation focuses on the fusion of hydrogenase domain with photosystem I in vivo, thereby making a new kind of type I reaction center where protons could serve as a final electron acceptor under anaerobiosis. Under aerobic conditions, however, it seems to function as a classical type I RC with reduced affinity for ferredoxin/flavodoxin. In chapter 2, a photosystem I chimera with the endogenous hydrogenase-2 domain is described with implications on algal metabolism and hydrogen evolution in vivo. Chapter 3 describes photosystem I chimera with endogenous hydrogenase-1 domain that can accumulate 5 times higher than PSI-HydA2 construct. Chapter 4 addresses a photosystem I chimera with *Megasphaera elsdenii* hydrogenase domain, which was supposed to be slightly

more oxygen resistant. Chapter 5 addresses the novel modeling tool - Alphafold2 (created by DeepMind at Google) – that is capable of folding chimeric protein sequences generating plausible models. A retrospective account on the generated chimeras is given and potential in silico design algorithm is proposed that could help making chimeras more stable.

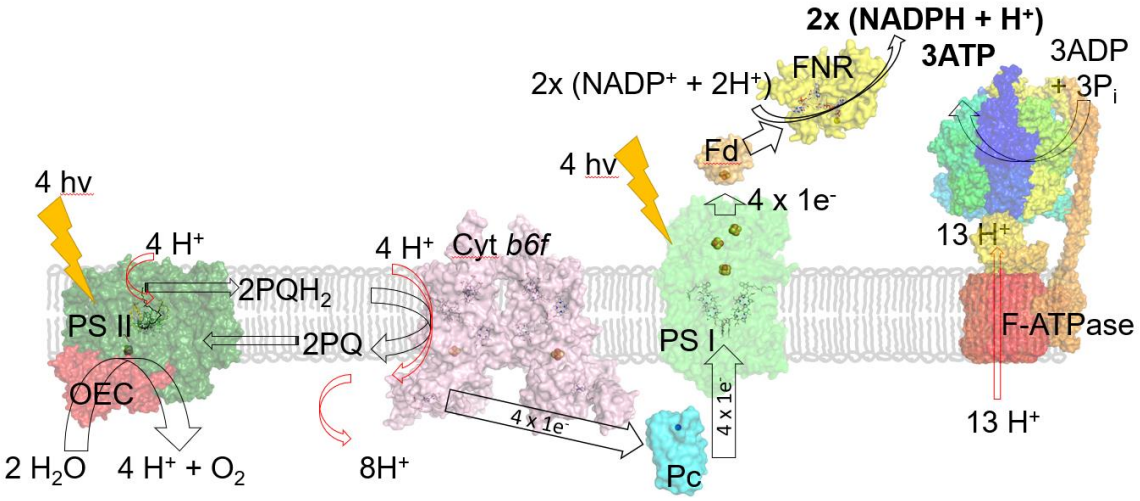

Figure 1-1. Linear electron flow in *Chlamydomonas reinhardtii*. 4 photons are required to oxidase water at OEC (oxygen evolving complex) of PS II and produce $4H^+$ (in the lumen), molecular oxygen, and 2 quinol molecules, which are in turn release additional 8 H^+ via Q-cycle at cyt *b6f*. Another 4 photons are needed to reduce 4 Fd, that produced 2 molecules of NADPH.

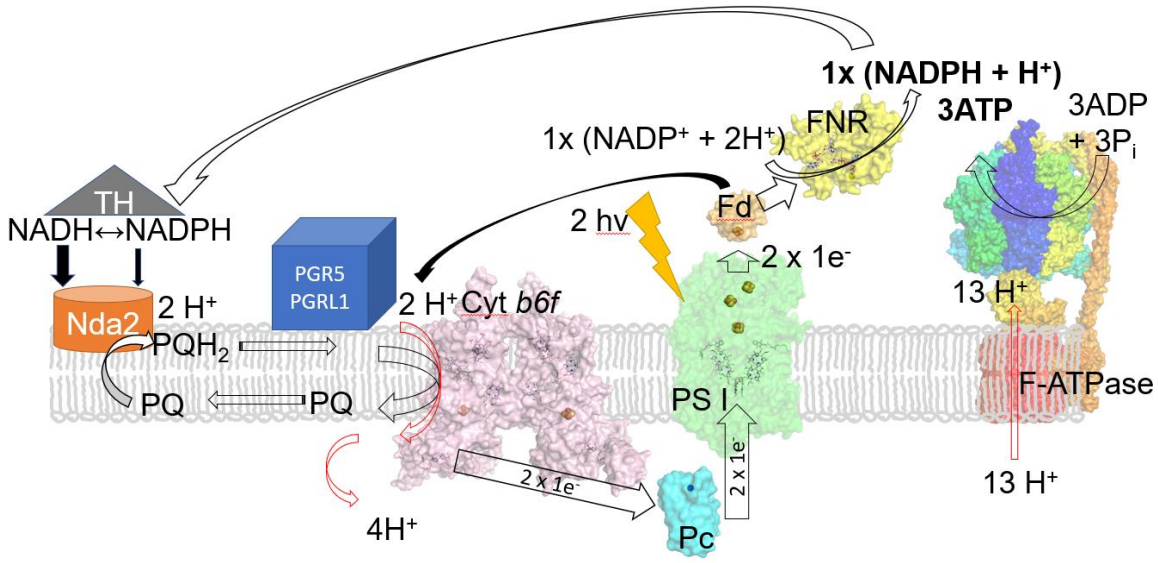

Figure 1-2. Cyclic electron flow in *Chlamydomonas reinhardtii*. Antimycin A-sensitive pathway involves Fd, PGR5/PGRL1 and cyt *b6f*. Transhydrogenase may facilitate plastoquinone pool reduction by converting NADPH to NADH, that has higher affinity for Nda2.

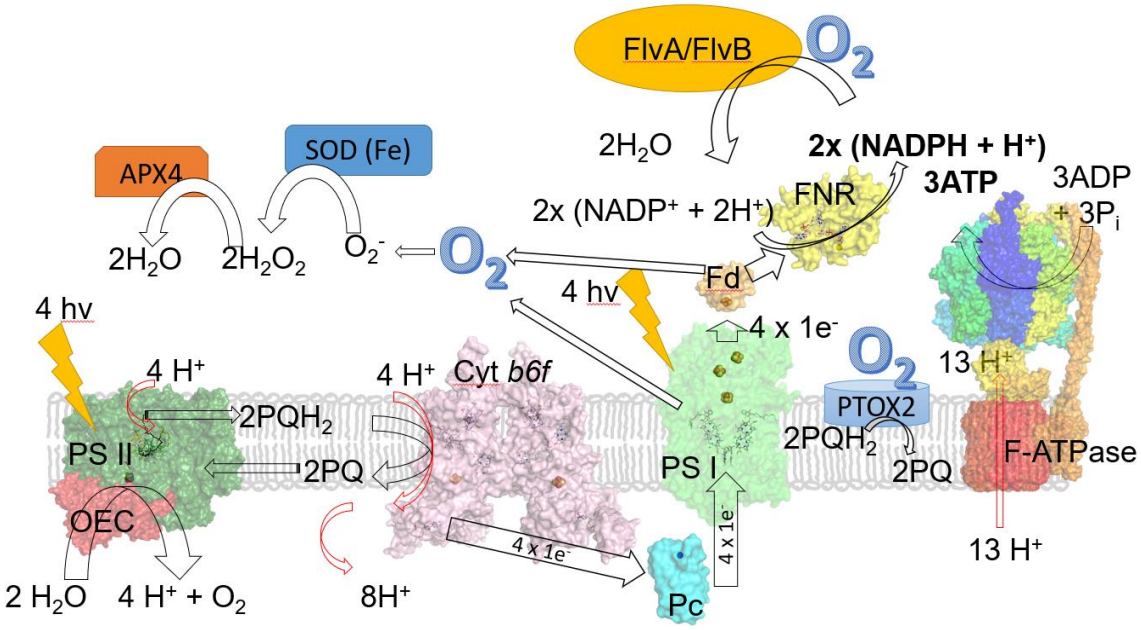

Figure 1-3. Water-water cycles in *Chlamydomonas reinhardtii* chloroplast. Flavodiiron proteins (FlvA and FlvB) are the major route for recycling NADPH under aerobic conditions and when CBB cycle is not active. Plastid terminal oxidase 2 (PTOX2) maintains the redox poise of the plastoquinone pool. Mehler and Mehler-like reactions are relatively small (~10%) fraction of total water-water cycles.

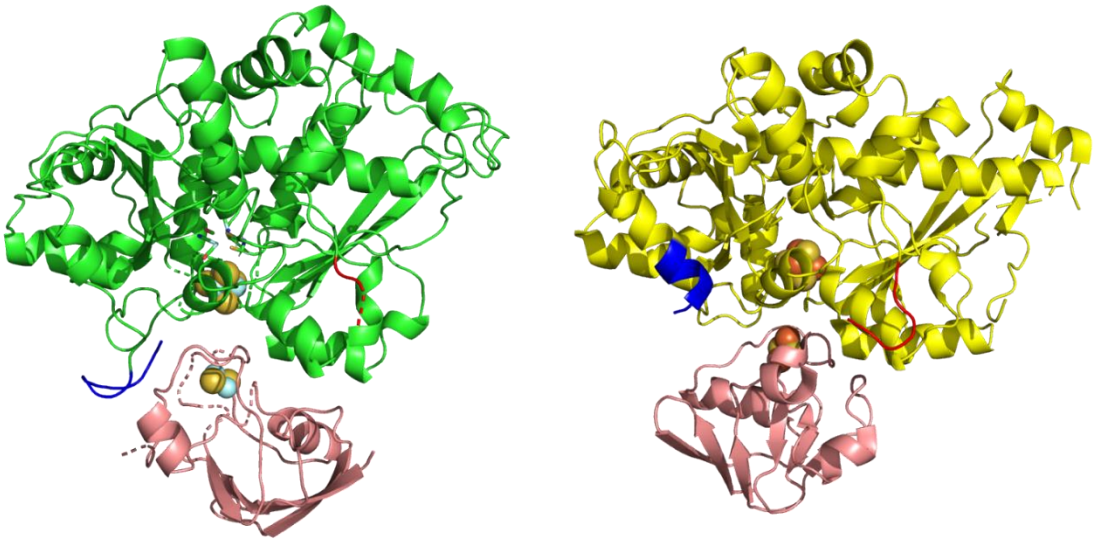

Figure 1-4. A model of ferredoxin 1 (salmon pink) docking to HydA2 (green cartoon) as described in Chang et al [55] and HydA1 (yellow) as described in Rumpel et al [56] (PDB ID: 2N0S). Hydrogenase domains were aligned in PyMOL. N-termini are colored blue, while C-termini – red.

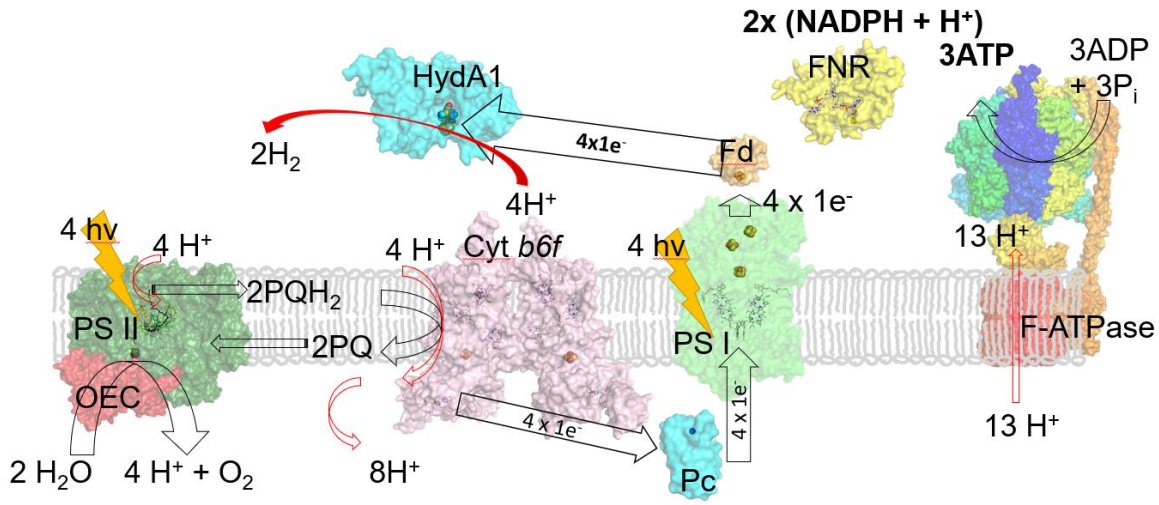

Figure 1-5. Linear electron flow to alternative electron acceptors – protons – reduced at H-cluster of hydrogenase under anaerobic conditions.

References

[1] Energy Technology Perspectives 2020. OECD; 2020. https://doi.org/10.1787/ab43a9a5-en.

[2] World Energy Council. Energy Resources: Solar. World Energy Counc 2013 World Energy Resour Sol 2013:1–28.

[3] Veeravalli SS, Shanmugam SR, Ray S, Lalman JA, Biswas N. Biohydrogen Production From Renewable Resources. In: Hosseini M, editor. Adv. Bioprocess. Altern. Fuels, Biobased Chem. Bioprod., Cambridge, UK: Woodhead Publishing; 2019, p. 289–312. https://doi.org/10.1016/B978-0-12-817941-3.00015-2.

[4] Barber J. Photosynthetic energy conversion: natural and artificial. Chem Soc Rev 2009;38:185–96. https://doi.org/10.1039/B802262N.

[5] Stuart TS, Gaffron H. The Gas Exchange of Hydrogen-adapted Algae as Followed by Mass Spectrometry. Plant Physiol 1972;50:136–40. https://doi.org/10.1104/pp.50.1.136.

[6] Gaffron H. Carbon Dioxide Reduction with Molecular Hydrogen in Green Algae. Am J Bot 1940;27:273. https://doi.org/10.2307/2436697.

[7] Cournac L, Mus F, Bernard L, Guedeney G, Vignais PM, Peltier G. Limiting steps of hydrogen production in *Chlamydomonas reinhardtii* and *Synechocystis* PCC 6803 as analysed by light-induced gas exchange transients. Int J Hydrogen Energy 2002;27:1229–37. https://doi.org/10.1016/S0360-3199(02)00105-2.

[8] Nelson N, Ben-Shem A. The complex architecture of oxygenic photosynthesis. Nat Rev Mol Cell Biol 2004;5:971.

[9] Allen JP, Williams JC. Photosynthetic reaction centers. FEBS Lett 1998;438:5–9. https://doi.org/10.1016/S0014-5793(98)01245-9.

[10] Blankenship RE, Prince RC. Excited-state redox potentials and the Z scheme of photosynthesis. Trends Biochem Sci 1985;10:382–3. https://doi.org/10.1016/0968-0004(85)90059-3.

[11] Redding K, Cournac L, Vassiliev IR, Golbeck JH, Peltier G, Rochaix J-D. Photosystem I Is Indispensable for Photoautotrophic Growth, CO_2 Fixation, and H_2 Photoproduction in *Chlamydomonas reinhardtii*. J Biol Chem 1999;274:10466–73. https://doi.org/10.1074/jbc.274.15.10466.

[12] Burlacot, Peltier, Li-Beisson. Subcellular Energetics and Carbon Storage in *Chlamydomonas*. Cells 2019;8:1154. https://doi.org/10.3390/cells8101154.

[13] Stroebel D, Choquet Y, Popot J-L, Picot D. An atypical haem in the cytochrome *b6f* complex. Nature 2003;426:413–8. https://doi.org/10.1038/nature02155.

[14] Meyer zu Tittingdorf JMW, Rexroth S, Schäfer E, Schlichting R, Giersch C, Dencher NA, et al. The stoichiometry of the chloroplast ATP synthase oligomer III in *Chlamydomonas reinhardtii* is not affected by the metabolic state. Biochim Biophys Acta - Bioenerg

2004;1659:92–9. https://doi.org/10.1016/j.bbabio.2004.08.008.

[15] Sharkey TD. Discovery of the canonical Calvin–Benson cycle. Photosynth Res 2019;140:235–52. https://doi.org/10.1007/s11120-018-0600-2.

[16] Nawrocki WJ, Bailleul B, Picot D, Cardol P, Rappaport F, Wollman F-A, et al. The mechanism of cyclic electron flow. Biochim Biophys Acta - Bioenerg 2019;1860:433–8. https://doi.org/10.1016/j.bbabio.2018.12.005.

[17] Alric J. Cyclic electron flow around photosystem I in unicellular green algae. Photosynth Res 2010;106:47–56. https://doi.org/10.1007/s11120-010-9566-4.

[18] Buchert F, Scholz M, Hippler M. Electron transfer via cytochrome b_6f complex displays sensitivity to antimycin A upon STT7 kinase activation. Biochem J 2022;479:111–27. https://doi.org/10.1042/BCJ20210802.

[19] Desplats C, Mus F, Cuiné S, Billon E, Cournac L, Peltier G. Characterization of Nda2, a Plastoquinone-reducing Type II NAD(P)H Dehydrogenase in *Chlamydomonas* Chloroplasts. J Biol Chem 2009;284:4148–57. https://doi.org/10.1074/jbc.M804546200.

[20] Peltier G, Aro E-M, Shikanai T. NDH-1 and NDH-2 Plastoquinone Reductases in Oxygenic Photosynthesis. Annu Rev Plant Biol 2016;67:55–80. https://doi.org/10.1146/annurev-arplant-043014-114752.

[21] Alric J, Lavergne J, Rappaport F. Redox and ATP control of photosynthetic cyclic electron flow in *Chlamydomonas reinhardtii* (I) aerobic conditions. Biochim Biophys Acta - Bioenerg 2010;1797:44–51. https://doi.org/10.1016/j.bbabio.2009.07.009.

[22] Girolomoni L, Cazzaniga S, Pinnola A, Perozeni F, Ballottari M, Bassi R. LHCSR3 is a nonphotochemical quencher of both photosystems in *Chlamydomonas reinhardtii*. Proc Natl Acad Sci 2019;116:4212–7. https://doi.org/10.1073/pnas.1809812116.

[23] Alric J, Johnson X. Alternative electron transport pathways in photosynthesis: a confluence of regulation. Curr Opin Plant Biol 2017;37:78–86. https://doi.org/10.1016/j.pbi.2017.03.014.

[24] Malone LA, Proctor MS, Hitchcock A, Hunter CN, Johnson MP. Cytochrome *b6f* – Orchestrator of photosynthetic electron transfer. Biochim Biophys Acta - Bioenerg 2021;1862:148380. https://doi.org/10.1016/j.bbabio.2021.148380.

[25] Chaux F, Burlacot A, Mekhalfi M, Auroy P, Blangy S, Richaud P, et al. Flavodiiron Proteins Promote Fast and Transient O_2 Photoreduction in *Chlamydomonas*. Plant Physiol 2017;174:1825 LP – 1836. https://doi.org/10.1104/pp.17.00421.

[26] Burlacot A, Sawyer A, Cuiné S, Auroy-Tarrago P, Blangy S, Happe T, et al. Flavodiiron-Mediated O_2 Photoreduction Links H_2 Production with CO_2 Fixation during the Anaerobic Induction of Photosynthesis. Plant Physiol 2018;177:1639 LP – 1649. https://doi.org/10.1104/pp.18.00721.

[27] Saroussi S, Karns DAJ, Thomas DC, Bloszies C, Fiehn O, Posewitz MC, et al. Alternative outlets for sustaining photosynthetic electron transport during dark-to-light transitions. Proc Natl Acad Sci 2019;116:11518–27. https://doi.org/10.1073/pnas.1903185116.

[28] Nikkanen L, Solymosi D, Jokel M, Allahverdiyeva Y. Regulatory electron transport pathways of photosynthesis in cyanobacteria and microalgae: Recent advances and biotechnological prospects. Physiol Plant 2021;173:514–25. https://doi.org/10.1111/ppl.13404.

[29] Houille-Vernes L, Rappaport F, Wollman F-A, Alric J, Johnson X. Plastid terminal oxidase 2 (PTOX2) is the major oxidase involved in chlororespiration in *Chlamydomonas*. Proc Natl Acad Sci 2011;108:20820–5. https://doi.org/10.1073/pnas.1110518109.

[30] Saroussi SI, Wittkopp TM, Grossman AR. The Type II NADPH Dehydrogenase Facilitates Cyclic Electron Flow, Energy-Dependent Quenching, and Chlororespiratory Metabolism during Acclimation of *Chlamydomonas reinhardtii* to Nitrogen Deprivation. Plant Physiol 2016;170:1975–88. https://doi.org/10.1104/pp.15.02014.

[31] Asada K. The water–water cycle as alternative photon and electron sinks. Philos Trans R Soc London Ser B Biol Sci 2000;355:1419–31. https://doi.org/10.1098/rstb.2000.0703.

[32] Gurrieri L, Fermani S, Zaffagnini M, Sparla F, Trost P. Calvin–Benson cycle regulation is getting complex. Trends Plant Sci 2021;26:898–912. https://doi.org/10.1016/j.tplants.2021.03.008.

[33] Kozuleva M, Petrova A, Milrad Y, Semenov A, Ivanov B, Redding KE, et al. Phylloquinone is the principal Mehler reaction site within photosystem I in high light. Plant Physiol 2021;186:1848–58. https://doi.org/10.1093/plphys/kiab221.

[34] Happe T, Kaminski A. Differential regulation of the Fe-hydrogenase during anaerobic adaptation in the green alga *Chlamydomonas reinhardtii*. Eur J Biochem 2002;269:1022–32. https://doi.org/10.1046/j.0014-2956.2001.02743.x.

[35] Forestier M, King P, Zhang L, Posewitz M, Schwarzer S, Happe T, et al. Expression of two [Fe]-hydrogenases in *Chlamydomonas reinhardtii* under anaerobic conditions. Eur J Biochem 2003;270:2750–8. https://doi.org/10.1046/j.1432-1033.2003.03656.

[36] Posewitz MC, King PW, Smolinski SL, Zhang L, Seibert M, Ghirardi ML. Discovery of Two Novel Radical S -Adenosylmethionine Proteins Required for the Assembly of an Active [Fe] Hydrogenase. J Biol Chem 2004;279:25711–20. https://doi.org/10.1074/jbc.M403206200.

[37] Britt RD, Tao L, Rao G, Chen N, Wang L-P. Proposed Mechanism for the Biosynthesis of the [FeFe] Hydrogenase H-Cluster: Central Roles for the Radical SAM Enzymes HydG and HydE. ACS Bio Med Chem Au 2022;2:11–21. https://doi.org/10.1021/acsbiomedchemau.1c00035.

[38] Ghysels B, Godaux D, Matagne RF, Cardol P, Franck F. Function of the Chloroplast Hydrogenase in the Microalga *Chlamydomonas*: The Role of Hydrogenase and State Transitions during Photosynthetic Activation in Anaerobiosis. PLoS One 2013;8:e64161. https://doi.org/10.1371/journal.pone.0064161.

[39] Milrad Y, Schweitzer S, Feldman Y, Yacoby I. Bi-directional electron transfer between H_2 and NADPH mitigates light fluctuation responses in green algae. Plant Physiol 2021;186:168–79. https://doi.org/10.1093/plphys/kiab051.

[40] Meuser JE, D'Adamo S, Jinkerson RE, Mus F, Yang W, Ghirardi ML, et al. Genetic disruption of both *Chlamydomonas reinhardtii* [FeFe]-hydrogenases: Insight into the role of HYDA2 in H_2 production. Biochem Biophys Res Commun 2012;417:704–9. https://doi.org/10.1016/j.bbrc.2011.12.002.

[41] Godman JE, Molnár A, Baulcombe DC, Balk J. RNA silencing of hydrogenase(-like) genes and investigation of their physiological roles in the green alga *Chlamydomonas reinhardtii*. Biochem J 2010;431:345–52. https://doi.org/10.1042/BJ20100932.

[42] Engelbrecht V, Liedtke K, Rutz A, Yadav S, Günzel A, Happe T. One isoform for one task? The second hydrogenase of *Chlamydomonas reinhardtii* prefers hydrogen uptake. Int J Hydrogen Energy 2021;46:7165–75. https://doi.org/10.1016/j.ijhydene.2020.11.231.

[43] Swanson KD, Ratzloff MW, Mulder DW, Artz JH, Ghose S, Hoffman A, et al. [FeFe]-Hydrogenase Oxygen Inactivation Is Initiated at the H Cluster 2Fe Subcluster. J Am Chem Soc 2015;137:1809–16. https://doi.org/10.1021/ja510169s.

[44] Kubas A, Orain C, De Sancho D, Saujet L, Sensi M, Gauquelin C, et al. Mechanism of O_2 diffusion and reduction in FeFe hydrogenases. Nat Chem 2017;9:88–95. https://doi.org/10.1038/nchem.2592.

[45] Johnson X, Alric J. Central Carbon Metabolism and Electron Transport in *Chlamydomonas reinhardtii*: Metabolic Constraints for Carbon Partitioning between Oil and Starch. Eukaryot Cell 2013;12:776–93. https://doi.org/10.1128/EC.00318-12.

[46] Gfeller RP, Gibbs M. Fermentative Metabolism of *Chlamydomonas reinhardtii*. Plant Physiol 1984;75:212–8. https://doi.org/10.1104/pp.75.1.212.

[47] Noth J, Krawietz D, Hemschemeier A, Happe T. Pyruvate:Ferredoxin Oxidoreductase Is Coupled to Light-independent Hydrogen Production in *Chlamydomonas reinhardtii*. J Biol Chem 2013;288:4368–77. https://doi.org/10.1074/jbc.M112.429985.

[48] Gfeller RP, Gibbs M. Fermentative Metabolism of *Chlamydomonas reinhardtii*. Plant Physiol 1985;77:509–11. https://doi.org/10.1104/pp.77.2.509.

[49] Johnson X, Alric J. Interaction between Starch Breakdown, Acetate Assimilation, and Photosynthetic Cyclic Electron Flow in *Chlamydomonas reinhardtii*. J Biol Chem 2012;287:26445–52. https://doi.org/10.1074/jbc.M112.370205.

[50] Harris EH. *Chlamydomonas* as a Model Organism. Annu Rev Plant Physiol Plant Mol Biol 2001;52:363–406. https://doi.org/10.1146/annurev.arplant.52.1.363.

[51] Gibbs M, Gfeller RP, Chen C. Fermentative Metabolism of *Chlamydomonas reinhardii*. Plant Physiol 1986;82:160–6. https://doi.org/10.1104/pp.82.1.160.

[52] Hemschemeier A, Fouchard S, Cournac L, Peltier G, Happe T. Hydrogen production by *Chlamydomonas reinhardtii*: an elaborate interplay of electron sources and sinks. Planta 2008;227:397–407. https://doi.org/10.1007/s00425-007-0626-8.

[53] Kosourov S, Nagy V, Shevela D, Jokel M, Messinger J, Allahverdiyeva Y. Water oxidation by photosystem II is the primary source of electrons for sustained H_2 photoproduction in nutrient-replete green algae. Proc Natl Acad Sci 2020;117:29629–36. https://doi.org/10.1073/pnas.2009210117.

[54] Milrad Y, Schweitzer S, Feldman Y, Yacoby I. Green Algal Hydrogenase Activity Is Outcompeted by Carbon Fixation before Inactivation by Oxygen Takes Place. Plant Physiol 2018;177:918–26. https://doi.org/10.1104/pp.18.00229.

[55] Chang CH, King PW, Ghirardi ML, Kim K. Atomic Resolution Modeling of the Ferredoxin:[FeFe] Hydrogenase Complex from *Chlamydomonas reinhardtii*. Biophys J 2007;93:3034–45. https://doi.org/10.1529/biophysj.107.108589.

[56] Rumpel S, Siebel JF, Diallo M, Farès C, Reijerse EJ, Lubitz W. Structural Insight into the Complex of Ferredoxin and [FeFe] Hydrogenase from *Chlamydomonas reinhardtii*. ChemBioChem 2015;16:1663–9. https://doi.org/10.1002/cbic.201500130.

CHAPTER 2

REWIRING PHOTOSYNTHESIS: A PHOTOSYSTEM I-HYDROGENASE CHIMERA THAT MAKES H_2 IN VIVO

Andrey Kanygin[a], Yuval Milrad[b], Chandrasekhar Thummala[a,c], Kiera Reifschneider[a†], Patricia Baker[a], Pini Marco[b], Iftach Yacoby[b*] and Kevin E. Redding[a*]

[a] *School ofMolecular Sciences and Center for Bioenergy & Photosynthesis, Arizona State University, Tempe, Arizona, USA. E-mail: kredding@asu.edu*

[b] *School ofPlant Sciences and Food Security, Tel Aviv University, Tel Aviv, Israel. E-mail: Iftachy@tauex.tau.ac.il*

[c] *Department ofEnvironmental Science, Yogi Vemana University, Kadapa, Andhra Pradesh, India*

[‡] *Current address: 3582 AB Utrecht, Netherlands.*

Reproduced with permission from:

Kanygin A, Milrad Y, Thummala C, Reifschneider K, Baker P, Marco P, et al. Rewiring photosynthesis: a photosystem I-hydrogenase chimera that makes H_2 *in vivo*. Energy Environ Sci 2020;13:2903–14. https://doi.org/10.1039/C9EE03859K

Harnessing the power of photosynthesis to catalyze novel light-driven redox chemistry requires a way to intercept electron flow directly from the photosynthetic electron transport chain (PETC). As a proof of concept, an in vivo fusion of photosystem I (PSI) and algal hydrogenase was created by insertion of the HydA sequence into the PsaC subunit. The PSI and hydrogenase portions are co-assembled and active in vivo, effectively creating a new photosystem. Cells expressing only the PSI-hydrogenase chimera make hydrogen at high rates in a light-dependent fashion for several days. In these engineered cells, photosynthetic electron flow is directed away from CO_2 fixation and towards proton reduction, demonstrating the possibility of driving novel redox chemistries using electrons from water splitting and the photosynthetic electron transport chain.

Broader context

Re-engineering fundamental processes in photosynthetic microorganisms offers a cheap and renewable platform for creating bio-factories capable of driving difficult redox transformations, powered only by the sun and using water as the electron source. To maximize the usefulness of such engineered systems, we require a way to intercept intracellular electron flow at the most reductive potential. We have taken the approach of positioning redox enzymes to directly capture electrons from photosystem I (PSI) before they enter the general cellular pool. In this paper, we describe a functional fusion of PSI with the hydrogenase enzyme to re-direct electrons from carbon fixation to proton reduction. This results in a large fraction of the electrons from water oxidation by photosystem II being used to make dihydrogen. Perhaps most importantly, we have identified a site in PSI where redox enzymes can be attached to intercept electrons from the photosynthetic electron transport chain.

Introduction

Conversion of algal cells into solar-powered bio-factories generating high-energy product molecules is a promising avenue for addressing the ever-increasing global energy demand, due to its environmental friendliness and cheap replication. Hydrogen (H_2) is an attractive target

product for several reasons. It is an important commodity with over 60 million tons produced globally, but ~95% of it is produced from steam reformation of fossil fuels, thus contributing to the rise of atmospheric CO_2 [1]. The [FeFe] hydrogenase enzyme catalyzes the rapid and reversible reduction of protons ($2\ H^+ + 2\ e^- \leftrightarrows H_2$). The active site of the enzyme is a metallic cofactor that is O_2-sensitive and must be inserted by maturation factors [2]. These characteristics are shared with many important redox enzymes, making hydrogenase an ideal test case for synthetic biology manipulations.

In the thylakoid membranes of the chloroplast, the photosynthetic electron transport chain (PETC) performs light-driven electron transport from water to ferredoxin (Fd) and pumps protons across the membrane, ultimately providing metabolic energy (ATP) and low-potential reductant (NADPH) to drive CO_2 fixation by the Calvin-Benson-Bassham (CBB) cycle (**figure 2-1A**) [3]. Algal hydrogenases are particularly attractive as producers of a solar fuel due to their structural simplicity (e.g., a single catalytic domain) [4] and ability to couple sunlight to hydrogen production by using reducing equivalents from the PETC. The active site of the enzyme consists of a [4Fe-4S] cluster coupled to a di-iron subsite containing CO and CN^- ligands; insertion of the latter requires three maturase proteins [5]. Algal hydrogenases normally function to dispose of excess reductant under anoxic conditions, to facilitate fermentative processes in the dark or the initiation of photosynthetic linear electron flow during dark-to-light transitions [6]. Despite various attempts to improve hydrogen production in green algae, it has not yet become economically feasible due primarily to two major issues: inactivation of the hydrogenase by oxygen and competition for reductant with other processes [7,8].

It has recently been shown that algal hydrogenases compete poorly for reduced Fd [9]. The primary competitor, Fd:$NADP^+$ oxidoreductase (FNR), not only has a cellular abundance ~70 times that of hydrogenase [10], but it also has a higher affinity for Fd (K_m = 0.8-2.6 μM) [11,12] than does hydrogenase (K_m = 3.4-35 μM) [13–15]. As the estimated Fd concentration in the

chloroplast is ~120 μM[1], both enzymes should be operating near saturation when the Fd pool is mostly reduced. Thus, the competition between them should be largely dependent on the concentrations and k_{cat} values of the respective enzymes, and one would predict that roughly 14 times as many electrons would be used to reduce $NADP^+$ via FNR than to reduce protons via hydrogenase[1]. Thus, it is unsurprising that H_2 production in algae decreases upon activation of the CBB cycle [16,17].

In order to circumvent this problem, we sought a way to divert electrons from the PETC towards H_2 production. PSI is the ideal choice for the diversion point for several reasons. The terminal cofactors of PSI are at a very low potential (-450/-490 mV vs. SHE) [18], thus maximizing the driving force of the engineered redox chemistry. In addition, allowing electrons originating from water oxidation by PSII to transit the PETC maximizes the proton pumping carried out by the PETC, and thereby ATP production by the thylakoid, thus maintaining viability of the cellular bio-factory. Diversion at an earlier point would diminish this advantage, while diversion after PSI would be much less effective – once electrons enter the Fd and NADPH pools, many metabolic processes can draw upon them.

Using a unicellular green alga (*Chlamydomonas reinhardtii*) as an experimental system, we made an in vivo fusion of PSI and the [FeFe] hydrogenase expressed by the organism (see **figure 2-1B**). While the structural gene for this hydrogenase is in the nuclear genome [19] and the core photosystem components are chloroplast encoded, it has been shown that active hydrogenase can be made from a gene transplanted into the chloroplast chromosome [20,21]. We show that photosynthetic flow in the re-engineered chloroplast is diverted from CO_2 fixation to proton reduction and results in sustained biohydrogen production.

[1] Values were derived using these parameters: k_{cat}(HydA1)= 450 s^{-1} [14]; k_{cat}(FNR)= 90 s^{-1} [12]; Fd concentration in spinach chloroplast is 4.4 nmol/(μmol of Chl)[60]; each TAP-grown *C. reinhardtii* cell contains 1 chloroplast with a volume of 130 μm^3 [61] and 3.5 fmol Chl [62].

Experimental

Chimeric protein design and homology modeling

The site of insertion of the hydrogenase domain corresponds to residues 32-36 (DGCKA) of *C. reinhardtii* PsaC. Residue Asp32 was replaced with Gly for additional flexibility and residues Cys34 and Lys35 were replaced with "trimmed" HydA2 sequence, such that PsaC-Gly33 was connected directly to the N-terminus of mature HydA2 (Ala63) and the C-terminus of HydA2 (Gly500) was connected to PsaC-Ala36 (see **figure 2-2**). Trimming of the *HYDA2* sequence consisted of removal of the transit peptide from the N-terminus (first 62 residues) and the last 5 residues (which are not conserved) from the C-terminus.

To model the structure of PSI-HydA, the protein structure prediction webtool Phyre2 [22] (intensive algorithm) was used to model individual subunits of *C. reinhardtii* PSI (PsaA, PsaB, PsaC, PsaD, PsaE and PsaF) and HydA2, based on the sequences of the polypeptides from protein data bank. Following removal of residues D32-K35 of PsaC in Pymol, the docking of HydA2 was performed using the ClusPro2 [23] server with distance restraints of 10 Å, corresponding to the amino acid residues involved in the junctions in the chimeric protein (Trp31 of PsaC to the N-terminal Gly of the modified HydA2 and the C-terminal Gly of the modified HydA2 to Ala36 of PsaC). The most plausible model based on ClusPro2's energy minimization algorithm was chosen and, after formation of two peptide bonds between PsaC and HydA2, the connecting loops were allowed to relax, using the ModLoop server [24]. PsaD and then PsaE were then docked to the PsaC-HydA2 chimera with ClusPro2 as well.

Generation of cells expressing PSI-hydrogenase

The *psaC-hydA2* fusion sequence (see **figure 2-2**) was synthesized by Genscript (Piscataway, NJ USA) and inserted via flanking *Nde*I and *Bgl*II sites into the pBS-EP5.8 *aadA* vector [25] digested with *Nde*I and *Bgl*II. The resulting pAK10G plasmid neatly replaces the *psaC* gene with the designed *psaC-hydA2* fusion gene. This plasmid was introduced into the *hydA* [26] and PBC4-2 strains of *C. reinhardtii* by particle-mediated transformation. The latter strain

combines two mutations in the chloroplast genome: deletion of *psaC* [27] and the hexahistidine-tagged *psaA* exon 1 [28]. The transformants were initially selected on TAP plates with 100 mg/L spectinomycin in the dark. Individual colonies were passaged alternately on plates containing 100 mg/L streptomycin or 300 mg/L spectinomycin in the dark and colony purified until they became homoplasmic, as determined by PCR (see method below). The amplified PCR products were verified by Sanger sequencing to ensure that no mutations in the introduced *psaC-hydA2* gene had arisen during the process. The same transformation and verification steps were performed on the strain expressing a hexahistidine-tagged (H_6) version of PSI [29].

PCR analysis of algal transformants

PsaC-HydA2 detection PCR was performed with flanking primers (PsaC5': TAATATGGAGATGACATATTTAG and PsaC3': GATCTCACCAAGATACTCCC) as well as with gene-specific primers (PsaC5'int: TCAATGTGTACGTGCTTGTCC and PsaC3'int: ACAACGTTTGCAACCTACACA) on 100 ng of genomic DNA using MeanGreen 2x Taq DNA polymerase master mix (Syzygy Biotech). Reactions (50 µL) were cycled 35 times (95 °C for 15 s, 51 °C for 15 s, 72 °C for 90 s) using initial primer concentrations of 0.5 µM. To determine the limits of detection of the PCR for the *psaC* gene, test PCR templates were generated by diluting genomic DNA from the *hydA* strain (containing *psaC*) into genomic DNA from the ***psaCΔ*** mutant (lacking *psaC*)[27] at the same concentration, in order to emulate conditions of heteroplasmy (10%, 1% *psaC*) and homoplasmy (100%, 0% *psaC*).

Growth conditions

Unless otherwise specified, algae were grown in liquid Tris-acetate-phosphate (TAP) medium with revised mineral nutrient supplement [30] in Erlenmeyer baffled cell culture flasks under low ambient light conditions (~5 µmol photons m^{-2} s^{-1} PAR) with agitation (150 rpm). Larger cultures (1 L and greater) were grown with continuous stirring and sparging with sterile filtered air. For autotrophic growth, Tris-bicarbonate phosphate (TBP) medium was prepared by substituting 25 mM sodium bicarbonate (pH 7.0) for acetate (~16.6 mM) in the medium.

An FMT-150 (Photon Systems International, Brno, Czech Republic) photobioreactor (PBR) system equipped with pH and Clark-type O_2 electrodes was used to obtain growth curves at constant temperature (24 °C). Starter cultures were pre-grown in TAP and washed twice with TBP. Cells were resuspended in TBP to a final OD_{680} of 0.1. At the beginning of each run, the photobioreactor vessel was sparged with N_2 for ~1 hour. Afterwards, the cultures were sealed and stirred for the duration of the experiment.

Chlorophyll (Chl) measurement

Concentrations of Chl *a* and *b* were determined as described in Porra et al [31].

Thylakoid and PSI preparation

Thylakoid membranes were prepared as previously described [25], with minor modifications outlined below. Cells were grown in 4-L flasks and centrifuged at 3500 x *g* at 4 °C for 10 min. The pellet was washed with H1 buffer (25 mM HEPES-KOH, 5 mM $MgCl_2$, 0.3 M sucrose, pH 7.5), flash-frozen in liquid nitrogen, and stored at –80 °C. Subsequent steps were performed in the dark and samples were kept at 4 °C. Cells were resuspended at 2-4 $x10^8$ cells mL^{-1} in H1 containing 1 mM phenylmethane sulfonyl fluoride to inhibit proteolysis. Cell breakage was accomplished with a French Press (Aminco) at ~1.7 tons pressure. Unbroken cells were pelleted by centrifugation at 2000 *x g* for 1 min, and the supernatant was centrifuged at 20000 *x g* for 10 min. The pelleted membranes were washed in 50 mL of H2 buffer (5 mM HEPES-KOH, 10 mM EDTA, 0.3 M sucrose pH 7.5) and resuspended in H3 buffer (5 mM HEPES-KOH, 10 mM EDTA, 1.8 M sucrose, pH 7.5). A discontinuous sucrose gradient was prepared using H3 buffer containing suspended thylakoid membranes, which was in turn overlaid with 1.3 M sucrose and 0.5 M sucrose solutions. After 1 hour of centrifugation in an SW-28 rotor at 25,000 rpm, the upper green band (0.5/1.3 M interface) was collected and washed with 3x volume of H6 buffer (5 mM HEPES-KOH, 10 mM EDTA pH 7.5). Purified thylakoids were concentrated by centrifugation (90,000 x *g* for 30 min) and resuspended in H6 + 20% glycerol and were either stored at 200 K after flash-freezing in liquid N_2 or solubilized for PSI purification.

PSI particles were purified from thylakoid membranes on sucrose gradients after solubilization with β-dodecyl maltoside (β-DDM), as described in Li et al [29]. Purification of hexahistidine-tagged PSI was performed as described previously [28], except that a Ni(II)-iminodiacetic acid (IDA) resin (G-biosciences, St. Louis, MO U.S.A.) was used.

Anoxic PSI-HydA2 isolation

Twelve liters of cells grown aerobically in TAP to mid-log phase were harvested and resuspended in fresh TAP to ~200-300 µg/mL of total Chl and sparged with Ar for ~ 4 h. After this point, all preparation steps were done in an anaerobic glovebox (Coy) filled with a 5% H_2/95% N_2 gas mixture. Sodium dithionite was added to 2mM final concentration and 5-mL aliquots were pelleted and stored in liquid nitrogen. Once thawed, each pellet was resuspended in breaking buffer (0.1 M Tris•HCl, pH 8.0), 10 mM EDTA•KOH, 1 mM PMSF and 2 mM $Na_2S_2O_4$) in a total volume of 30 mL. Cell lysis was accomplished using a Branson sonifier S-450 operated at amplitude 3, 50% duty cycle for a total of 6 min (2 minutes sonication followed by 2 min waiting) on chilled beads (-20 to -10 ^oC) to achieve complete cell lysis. Crude thylakoids were pelleted (208,000 xg, 15 min, 4 ^oC), and resuspended in solubilization buffer (25 mM Tricine•KOH, pH 8.0, 300 mM KCl, 10% glycerol) containing 2 mM sodium dithionite. Solubilization and IMAC purification steps were done as described above with the exception of using Ni-Penta^{TM} resin (Marvelgent Biosciences), Tricine•KOH buffer (pH 8.1) and 200 mM imidazole for elution. Purified PSI was stored in 25 mM Tricine•KOH (pH 8.1), 300 mM KCl, 10 % glycerol, 0.03 % β-DM. Aliquots were flash frozen and stored in liquid nitrogen.

Laser-flash spectroscopy

Samples of thylakoid membranes (60 µg Chl mL^{-1} in 5 mM HEPES•KOH, pH 7.5) or PSI particles (6 µg Chl mL^{-1} in 5 mM Tricine•KOH pH 8.0, 0.03 % β-DDM) were diluted and mixed with the same buffer containing 10 mM sodium ascorbate in the dark. A JTS-10 (Bio-Logic) kinetic spectrophotometer was used to monitor absorbance changes at 696 nm. Excitation was

provided by a frequency-doubled Nd/YAG laser (532 nm) generating ~6-ns pulses (~25 mJ per pulse).

A saturating laser flash was used to create the $P_{700}^{+}(F_A/F_B)^{-}$ charge-separated state, which occurs in <1 µs.[32] Absorbance changes at 696 nm were monitored with dim 10-µs flashes before and after the laser flash (starting 250 µs after the flash) to monitor creation and decay of P_{700}^{+}. To eliminate actinic effects of the probing light and electronic artifact due to changing data collection rates, a background transient (with the laser shutter closed) was subtracted. The decay of P_{700}^{+} was fit to a sum of 2-6 exponential decay components using the Levenberg-Marquardt iteration algorithm.

Anaerobic adaptation

To allow activation of the hydrogenase enzyme, cells were harvested in early/mid-logarithmic phase (2-6 µg Chl mL^{-1}) by centrifugation (3500 *x g* for 5 min) and resuspended in fresh TAP medium at ~1-2 µg Chl mL^{-1} (for in vivo H_2 measurements). Ten mL of the cell suspension was placed in a 25-mL clear glass bottle sealed with stoppers, wrapped in aluminum foil and bubbled with argon (flow rate 10-15 mL min^{-1}) for 90 min in the dark, unless otherwise indicated, prior to the start of the H_2 production period. Once sparging was terminated, cells were agitated on a shaker at 160 rpm.

In vitro hydrogenase activity

Cells were centrifuged and resuspended at ~30 µg Chl mL^{-1} in anaerobic adaptation buffer (50 mM potassium phosphate pH 7.2, 3 mM $MgCl_2$) and sparged with water-saturated argon for variable times in the dark in the initial experiments; the standard time was 90 min thereafter. For each reaction, 1 mL of reaction buffer (100 mM Tris•HCl, pH 7.3, 1 M NaCl, 10 mM methyl viologen, 0.2% Triton X-100) was mixed with 0.2 mL of 100 mM $Na_2S_2O_4$ (dissolved in 30 mM NaOH) in an anoxic glovebox (Coy) and sealed; the headspace of the vial was sparged with argon for 20 min to remove any residual H_2 from the glovebox gas and warmed to 37 °C prior to injection of 100 µL of cell suspension into the reaction mixture. The vial was mixed well,

temperature was maintained at 37 °C with mild shaking, and aliquots of the headspace gas were removed at intervals and analyzed by gas chromatography (see below).

Gas chromatography (GC) measurements

A model SRI 310 GC equipped with a thermal conductivity detector (TCD) and molecular sieve (13X or 5A) was used for all gas measurements. A sample (80 µL) of the headspace gas was removed with a 1710RN airtight Hamilton 100-µL syringe (that had been flushed with argon) and injected into the GC. A 1% H_2/99% N_2 gas mixture (Supelco) was used to create a standard curve for H_2, and air was used as a standard for O_2 and N_2. The O_2:N_2 ratio was used to monitor for air contamination during sampling, as the headspace of all samples was primarily Ar.

Immunoblotting

Polypeptide separation and immunoblotting was performed as described previously [20]. Isolated PSI^{H6} or PSI-$HydA^{H6}$ were loaded on the basis of P_{700} photobleaching activity (see below): 1.6 pmol of P_{700} for detection of small polypeptides (PsaC, PsaD, PsaC-HydA2) or 0.4 pmol of P_{700} for detection of larger polypeptides (PsaA).

Membrane inlet mass spectrometry (MIMS) measurements

Cells grown to early log phase were spun down and resuspended to 15 µg Chl mL^{-1} in a total volume of 5 mL in TAP or TP medium (with or without acetate, respectively); 50 mM HEPES (pH 7.2) and 2 mM $NaHCO_3$ were included to maintain pH and CO_2 levels. Cells were loaded into a closed temperature-controlled (24.5° C) and stirred MIMS cuvette. Anaerobiosis was achieved in approximately 1 hour due to respiration in the dark; relevant gas masses were monitored continuously. After approximately 1 h, cells were exposed to various intensities of red light (635 nm via the actinic module of the DUAL-PAM 100 from Heinz Walz GmbH) for 2 min interspersed with 2 min darkness. Rates were calculated from the slope of the best linear fit over a 1-min period. H_2 and O_2 analysis was done by MIMS [33]. Enforced anaerobiosis with glucose oxidase and glycolaldehyde treatment were performed as described previously [16].

Light-to-hydrogen conversion efficiency

PAR was determined with Li-COR photon counter equipped with quantum sensor (LI-190R). Efficiency calculations were performed as previously described [17] with slight modifications.

$$\eta(\%) = \frac{\left(\Delta G° - RT \ln \frac{P°}{P}\right) v_{H2}}{E_i A t} 100$$

, where $\Delta G°$ is the standard Gibbs free energy for water oxidation (237.2 kJ mol^{-1} at 25 ℃ and 1 atm), R is the universal gas constant, T is absolute temperature (K), $P°$ and P are the hydrogen partial pressures (standard and observed, respectively), v_{H2} = amount of H_2 produced (mol), E_i = energy of the incident light (J m^{-2} s^{-1}), A = illuminated surface area (m^2), t = duration of illumination (s). Energy for the incident light was calculated using the Planck-Einstein relation for red light at 630 nm.

Dissolved O_2 measurements in vivo

Dissolved O_2 was monitored with a Firesting O_2 optical oxygen meter (PyroScience). Cells were washed with either fresh TAP or TBP twice, then resuspended at approximately 5 µg Chl ml^{-1}. They were dark adapted and sparged with filtered water-saturated air for 10 min before the run. Each run made use of 2 ml of cell suspension stirred continuously in a 5-ml cuvette. For light-dependent O_2 evolution rates, the dark O_2 consumption rate (the average of rates in the dark just before and after illumination) was subtracted from the net evolution rate in the light. For maximal O_2 evolution rates, the cell suspensions (in TBP) were subjected to a 5 min dark period in the presence of 0.2 mM Phenyl-p-benzoquinone (PPBQ) (Acros Organics), followed by 5 min of high red light (~2300 µmol photons m^{-2} s^{-1}) and 5 min of darkness.

$NADP^+$ photoreduction assay

The reaction mixture (2 mL) consisted of 10 mM sodium ascorbate (Sigma), 17 µM plastocyanin (Pc: prepared in-house from a recombinant source as described in ref. [34]), 3 µM ferredoxin (Fd: prepared in-house from a recombinant source as previously described [35]), 0.2

µM FNR (prepared in-house from a recombinant source as previously described [35]), 2.5 mM $NADP^+$ disodium salt (Roche), and 27 nM PSI in reaction buffer (50 mM Tris-HCl, pH 7.4, 3.35 mg mL^{-1} BSA, 10 mM $MgCl_2$, 200 mg mL^{-1} sucrose, 0.03% ß-DDM). The concentrations of Pc, Fd, and FNR were optimized for maximal reaction rates with WT PSI. Each sample was mixed in a 3-mL quartz cuvette with a stir bar for 3 minutes. All preparatory steps were done in the dark. The reference cuvette contained all components except PSI. Absorbance at 340 nm was measured with a Perkin Elmer Lambda35 double-beam spectrophotometer. Band pass filters (340 nm, 27nm FWHM, Omega Optical) were placed before the detectors to block actinic light. A red LED light source (630 nm, 300 µmol photons m^{-2} s^{-1}) was assembled on top of the cuvette and controlled manually. A technical replicate consisted of a "dark" run of 3 minutes using a data collection frequency of 6 Hz, followed by 3 min of data collected with the actinic light on. The data were analyzed for each run separately; each "dark" slope was subtracted from the following "light" slope to obtain a light-dependent rate before averaging. The dark rates never exceeded 11% of the light rates. An initial rate was determined from the slope of the line (linear fit with the instrumental weighting of error) to the first 9 points of each averaged data set using Beer's law and the extinction coefficient for NADPH at 340 nm (6.22 mM^{-1} cm^{-1}) with a path length of 1 cm.

Flavodoxin photoreduction assay

Recombinant *Synechococcus* sp. PCC7002 flavodoxin was prepared as previously described.[36] The reaction mixture consisted of ~100 nM PSI particles in 25 mM Tricine-KOH (pH 8), 50 mM $MgCl_2$, 20 mM KCl, 0.03 % ß-DDM, 5 mM sodium ascorbate, 5 µM Pc, and 5 µM flavodoxin. All preparation steps were performed in the dark. Accumulation of flavodoxin semiquinone was monitored with a JTS-10 kinetic spectrometer (Bio-Logic) using 10-µs flashes centered at 573 nm (6 nm full width at half maximum). Actinic light consisted of 250-ms LED pulses at 630 nm (3000 µmol m^{-2} s^{-1}), with the probe flash occurring 50 ms after the actinic pulse ceased, allowing time for any rapid decay processes to be complete. (This 250-ms/50-ms duty cycle was factored in the rate calculations.) An extinction coefficient of 5100 M^{-1} cm^{-1} for the flavosemiquinone-minus-flavin difference at 573 nm was used, based on the published difference

spectrum of *Synechococcus* sp. PCC7002 flavodoxin. [37] The slow baseline drift in the dark was subtracted from the rate in the light to yield the light-dependent rate.

O_2 uptake assay

Reaction mixtures were prepared as in the flavodoxin photoreduction experiment, except that 2,6-dichlorophenol indophenol (0.2 mM) was used as mediator instead of Pc, and flavodoxin was not added. Dissolved O_2 was measured with a Clark-type electrode. Each sample was mixed in the dark to saturate with air. Data was collected with 1 Hz frequency for 1 minute in the dark, followed by 2 minutes under saturating illumination from a white LED (1200 µmol m^{-2} s^{-1} of PAR). Rates of O_2 consumption/production in the light were calculated for each replicate (n=3) via linear regression of 10-s intervals. The dark rate for each replicate was calculated from the last 2 minutes of the 3 min dark run of the sample before illumination commenced. This dark rate was subtracted from the light rate to determine the light-dependent rate, which was normalized to the amount of photobleachable P_{700}. The dark rate never exceeded 18% of the corresponding light rate. After data collection, the Chl content of each sample was measured to ensure consistency between replicates.

In vivo P_{700} photobleaching and fluorescence measurements

Cells were collected during early log phase, centrifuged (3500 *x g* for 5 min) and resuspended to a Chl concentration of 33 µg mL^{-1} (P_{700}) or ~9 µg mL^{-1} (fluorescence) in 20% Ficoll™ PM400 (GE Healthcare), 10 mM sodium phosphate (pH 7.2). P_{700} bleaching and recovery was performed essentially as previously described.[38] Absorbance changes at 695 nm were measured with the JTS-10 spectrometer. For P_{700} photobleaching, actinic light (630 nm) was briefly (200 µs) switched off for each 10-µs detection measurement during the 10-s illumination period, followed by the dark decay.

For fluorescence, cells were dark adapted for 5 min before taking each measurement. (During dark periods, samples were sparged with air to prevent development of anoxia.) Fluorescence emission from Chl was measured with the JTS-10 Fluo59 accessory. A saturating

pulse (80 ms, 8 mmol photons m^{-2} s^{-1}, 520 nm) was used to obtain F_{max}, measured 170 µs after the pulse. The steady-state fluorescence parameter (F_s) was measured after 2 minutes of illumination (520 nm) with actinic light of variable intensities. Quantum yields of PS II ($\Phi_{(II)}$) were calculated as described.[39]

Long term H_2 production in a photobioreactor (PBR)

Cells were grown in 4 L TAP under ambient room light (~5 µmol m^{-2} s^{-1} photosynthetically active radiation (PAR)) with constant air-sparging and stirring. They were harvested in the mid log-phase, resuspended in ~500 mL fresh TAP to OD_{735} ≈ 0.7 (corresponding to ~30 µg/mL of Chl) and transferred to the 400-mL PBR vessel. Once in the FMT150 PBR (see above), the culture was continuously sparged with Ar at 80 mL min^{-1}, controlled at the influx and monitored at the efflux by mass flow controllers (MC-500SCCM-D/5M, Alicat Scientific, USA). After 2 h of anaerobic adaptation in the dark, the culture was illuminated continuously with white light at 600 µmol photons m^{-2} s^{-1} PAR. Sterile argon was hydrated by bubbling through water and then through the sterile TAP media, before it entered the PBR vessel. The PBR was operated in turbidostat mode with OD_{735} set to remain between 0.60 and 0.65; Ar-sparged sterile TAP was used to dilute the culture, which was constantly stirred. The PBR gas efflux was passed through a 500-mL trap flask (to retain excess culture) before passing out and through the monitoring mass flow controller. A rubber septum mounted atop the trap flask allowed probing of the efflux gas with an air-tight syringe (100 µL, Hamilton), followed by injection of the sample into the GC-TCD, as in the experimental section.

Results and discussion

Chimeric protein design and creation

Based on the crystal structure of cyanobacterial PSI (1JB0) [40] and a homology model of HydA2 [41], we selected the turn of a β-hairpin over the terminal F_B cluster in PsaC as the optimal insertion point for the hydrogenase domain. The entire sequence of the mature HydA2

hydrogenase from *C. reinhardtii* was inserted into this site as an in-frame fusion that would effectively split PsaC into two polypeptide segments. (See **Experimental** for details and **figure 2-2** for exact sequence of the chimeric polypeptide). The N- and C-termini of HydA2 are in close proximity,[41] in principle allowing this type of chimeric polypeptide to fold as two domains, with the HydA domain presumably folding first, allowing the two PsaC fragments to fold together. According to our modeling studies, this design would place the [4Fe-4S] cluster of HydA2 relatively close to the F_B cluster of PSI (14.8 Å edge-to-edge distance, see **Experimental** for details). The fusion gene and protein are henceforth referred to as *psaC-hydA2* and PsaC-HydA2, respectively. When co-assembled with PSI, the chimeric protein is called "PSI-HydA" (see **figure 2-1C** for a model).

The *psaC-hydA2* gene was introduced into the chloroplast genome by particle-mediated gene transfer using flanking sequences to direct homologous recombination such that it would replace the endogenous *psaC* gene.[25] Serial cloning under selective conditions was maintained until a homoplasmic state was achieved (*i.e.*, all copies of *psaC* replaced by *psaC-hydA2*), as verified by PCR (**figure 2-3**). The amplified PCR products were sequenced to ensure that no mutations in the chimeric gene had arisen during the process. The *psaC-hydA2* gene was introduced into two strains: a *hydA1-1 hydA2-1* mutant lacking endogenous hydrogenases[26] as well a strain expressing a hexahistidine-tagged (H_6) version of PsaA, a core subunit of PSI.[28] Note that in the former, PSI-HydA is the only significant contributor to hydrogen production; in both strains, WT PSI is replaced by PSI-HydA. For brevity, the congenic D66 control strain is referred to as wild-type (WT), the *hydA1-1 hydA2-1* strain is called *hydA*, and the *hydA1-1 hydA2-1*[*psaC-hydA2*] transformant is referred to as ΨH1. The stains expressing H_6-tagged PSI are called WT^{H6} (with normal PsaC) or $ΨH1^{H6}$ (with PsaC-HydA2).

Subunit composition of PSI-HydA chimera

PSI and PSI-HydA were each purified from WT^{H6} and $ΨH1^{H6}$ via immobilized metal affinity chromatography.[28] Purified complexes were denatured with SDS and equivalent amounts of PSI were analyzed by immunoblotting with antibodies against PSI subunits and

hydrogenase, to assess the subunit composition of the complexes. The anti-PsaC antibody recognized a ~9-kDa polypeptide in WT PSI (**figure 2-4 A, left**), consistent with its predicted size (8.8 kDa). This polypeptide was not observed in the PSI-HydA complex; instead, a new ~52-kDa polypeptide was seen, similar to the predicted size of the PsaC-HydA2 polypeptide (56 kDa). Probing with anti-HydA antibodies revealed a polypeptide of the same size in PSI-HydA complexes, but not in WT PSI (**figure 2-4 A, right**). Thus, PSI complexes in this strain incorporate PsaC-HydA2 rather than PsaC.

Roughly equal amounts of PsaA were detected in PSI and PSI-HydA (1.0:1.1; **figure 2-4 B**) when the lanes were loaded on the basis of equal photochemical activity (see **figure 2-5 A**), implying that >90% of the PSI-HydA in the ΨH1 cells is photochemically active. We would not expect any unassembled PsaA polypeptide to be present, as it has been shown that the quality control system of the chloroplast keeps the level of unassembled subunits of PSI or other multi-subunit complexes very low.[42]

Based on the structure of cyanobacterial PSI,[40] as well as mutagenesis[43] and modeling[44] studies, it is thought that the Fd-docking site of PSI is formed by PsaC in concert with PsaD. The structure of PSI reveals an intimate interaction between PsaC and a long C-terminal extension of PsaD, and the addition of the HydA domain in the fusion had the potential to interrupt this interaction and prohibit assembly of PsaD into the complex. However, we found that the level of PsaD in the purified PSI complexes was similar in both preparations (**figure 2-6**), consistent with our model of PSI-HydA (**figure 2-1 C**).

Activities of the PSI-HydA chimera in vitro

Laser-flash spectroscopy experiments were performed to assess the photochemical activity of the PSI portion of the PSI-HydA chimera. P_{700} is a pair of Chl *a* molecules serving as the primary electron donor in PSI. Excitation of PSI produces a charge-separated state in which P_{700} is oxidized (P_{700}^{+}) and the terminal acceptor is reduced. In the absence of an electron acceptor, the rate of charge recombination is characteristic of the charge-separated state; for example, charge recombination of $P_{700}^{+}(F_A/F_B)^{-}$ occurs in 40-200 ms, but is >50 times faster from

the prior charge-separated state ($P_{700}^{+}F_X^{-}$).[18] In the absence of the PsaC subunit, the PsaA/PsaB heterodimer is degraded and does not accumulate in *C. reinhardtii*.[45] Therefore, the level of photoactive PSI can be used to assess the ability of PsaC-HydA to assemble with and stabilize the PSI core. The amount of photo-bleachable P_{700} in thylakoid membranes isolated from ΨH1 was ~15% that of WT (**figure 2-5 A**). The lowered accumulation of PSI-HydA was not unexpected, given that point mutations of single residues in PSI can result in more drastic effects.[25] The kinetics of fast P_{700}^{+} decay (**figure 2-5 A inset**) are very similar in PSI and PSI-HydA, indicating that the F_A and F_B clusters must be properly assembled within the PsaC domain of the chimeric protein (**Table 2-1**). Oxygen can readily accept electrons from PSI effectively quenching back reactions with longer lifetimes and contributing to overall "electron escape" that must be replenished by an exogenous electron donor (*i.e.*, ascorbate). In order to get a better understanding of charge recombination kinetics in the PSI-HydA2 chimera, we anoxically prepared PSI complexes from anaerobically adapted WT^{H6} and $ΨH1^{H6}$ cultures. As seen in **figure 2-7 A**, electron escape is reduced in both preparations to ~24% (**figure 2-7 B**), and there is the typical biphasic kinetics of charge recombination from the $P_{700}^{+}(F_A/F_B)^{-}$ state in the 40-200 ms time range. In the PSI-HydA2 chimera, there are 3 new kinetic phases. The fastest two represent charge recombination of the $P_{700}^{+}F_X^{-}$ state, and together represent ~12% of the total decay, indicating that the association of PsaC-HydA2 with PSI may be weaker than PsaC and some of it dissociates during purification. There is also a new component with a lifetime of 550-600 ms, representing ~9% of the total decay. We tentatively assign this to charge recombination from the FeS cluster of the HydA2 domain.

The HydEF/G maturases are required for insertion of the di-iron site into the HydA domain after assembly of the [4Fe-4S] cluster by the chloroplast SUF machinery[46], and it was unclear if the maturases would be able to access the HydA domain in the new chimeric context. The hydrogenase activity of cells expressing PSI-HydA was assessed in detergent-permeabilized cells with reduced methyl viologen (MV) as electron donor. We found that maximal hydrogenase activity was attained within 1.5 hours after a shift to anaerobiosis, similar to what was shown for

WT hydrogenases in *C. reinhardtii.* [15] (**figure 2-5 B**). The parental *hydA* strain exhibited a very slow rate of H_2 production (~4.1 ± 0.2 µmol h^{-1} (mg Chl)$^{-1}$), as expected, while the WT rate was 770 ± 50 µmol h^{-1} (mg Chl)$^{-1}$). The H_2 production rate in permeabilized ΨH1 cells was linear with time over the 20-min time course, similar to the permeabilized WT cells, indicating that the hydrogenase domain in PSI-HydA was not unstable (**figure 2-5 B inset**). They produced H_2 at a rate of ~380 ± 80 µmol h^{-1} (mg Chl)$^{-1}$. Since the hydrogenase activity in the parental strain is ~1% of this, nearly all of the H_2 produced by the ΨH1 cells can be attributed to the PSI-HydA chimera. Using the extinction coefficient of P_{700},[47] we estimate the amount of PSI-HydA in the ΨH1 strain as 1 per 5650 Chl. If each PSI-HydA had an active hydrogenase, the turnover frequency for PSI-HydA would be ~530 ± 110 H_2 s^{-1}. This number is comparable with the reported specific activity of HydA1 using a similar assay (380 ± 97 µmol H_2 min^{-1} mg^{-1}),[10] which is equivalent to a turnover frequency of ~300 H_2 s^{-1}. Thus, it seems likely that all of the HydA domains in the PSI-HydA chimeric complexes are fully active after the anaerobic induction period.

Addition of the large HydA domain to PsaC was expected to block its access to electron acceptors such as Fd. This was tested *in vitro* by assaying the purified protein for light-dependent reduction of low-potential electron acceptors in the presence of ascorbate, a high-potential electron donor. The PSI-HydA chimera exhibited a ~9-fold drop in light-driven reduction of cyanobacterial flavodoxin (**figure 2-8 A**). This protein replaces Fd in cyanobacteria grown in low iron, and has been shown to bind to both cyanobacterial and algal PSI in the same mode as Fd.[48] In contrast, the ability of PSI-HydA to reduce algal Fd (in a coupled assay) was reduced by only 50% (**figure 2-8 B**). Photoreduction of O_2 to superoxide (*i.e.*, Mehler reaction) was ~2-fold *higher* in PSI-HydA (**figure 2-8 C**), proving that overall electron flow was not compromised by addition of the HydA domain. These assays were performed in air, where the di-iron site would be inactivated (*i.e.*, no competition with proton reduction), but the [4Fe-4S] cluster should still be present in the HydA domain.[4] Both algal Fd and cyanobacterial flavodoxin bind the same site on PsaC involving Lys35,[49,50] which is absent in PSI-HydA; thus, one would expect both proteins to have lost their high-affinity binding site on PSI. An explanation for the difference between their

behavior with PSI-HydA is that it is the HydA domain that reduces them, rather than PsaC. The algal hydrogenase is reversible; the HydA domain binds Fd, oxidizing it when producing H_2, and reducing it when oxidizing H_2.[16] Access to the Fd-binding site of HydA2 is not expected to be blocked in the PSI-HydA chimera. Thus, Fd reduction by PSI-HydA likely proceeds via the HydA [4Fe-4S] cluster to Fd bound to its interaction site on HydA. The algal HydA domain would not be expected to interact with cyanobacterial flavodoxin, explaining the much lower photoreduction rate with this electron acceptor. The higher O_2 photoreduction rate of PSI-HydA may reflect a higher rate of O_2 reduction from the HydA [4Fe-4S] cluster than from the F_A/F_B clusters of PsaC.

Production of H_2 and O_2 in vivo

The ability of the hydrogenase domain in PSI-HydA to carry out H_2 production during dark fermentative conditions, in which Fd is largely reduced by pyruvate:Fd oxidoreductase,[51] was assessed by gas chromatography using a thermal conductivity detector (GC-TCD). Slow accumulation of H_2 in the headspace was observed in the cultures incubated in the dark (**figure 2-9 A**). Hydrogen did not accumulate to detectable levels in the *hydA* culture until after 6 h and the rate was extremely low thereafter (8 ± 5 nmol H_2 h^{-1} (mg Chl)$^{-1}$). The rate of H_2 production by ΨH1 was roughly 60% of the WT rate [330 ± 10 nmol H_2 h^{-1} (mg Chl)$^{-1}$ vs 507 ± 30 nmol H_2 h^{-1} (mg Chl)$^{-1}$] and remained fairly constant throughout the 6-hour experiment (see **figure 2-9 A**). This ratio of activities is similar to the ratio of maximal H_2 production rate measured in these cells (**figure 2-5 B**), indicating that the HydA2 domain in the PSI-HydA chimera is fully able to accept electrons via its normal physiological donor (Fd), consistent with the conclusion above that the HydA2 domain of the PSI-HydA chimera can bind and reduce Fd.

Illumination of the anoxic WT culture resulted in transient H_2 production, as observed previously.[16,52] The average rate was 28 ± 8 μmol H_2 h^{-1} (mg Chl)$^{-1}$ during the first hour, but rapidly dropped to negligible levels thereafter (**figure 2-9 B**). The *hydA* strain did not make any detectable H_2. In contrast, ΨH1 produced H_2 continuously for 6 h, with an initial rate of ~25 ± 6 μmol H_2 h^{-1} (mg Chl)$^{-1}$ in the first hour and an average rate of 21 ± 6 μmol H_2 h^{-1} (mg Chl)$^{-1}$ over the entire time course.

Like many redox enzymes catalyzing low-potential redox reactions, the algal hydrogenase is inactivated by O_2. One of the reasons for sustained H_2 production by ΨH1 is that O_2 does not accumulate in the sealed culture, unlike WT or *hydA* (**figure 2-10**). To test the hypothesis that the ΨH1 strain consumes O_2 faster than it is produced, we measured net O_2 rise/fall in aerobic cultures. The compensation point is the light intensity at which O_2 production by PSII is matched by O_2 consumption. Even up to the brightest light used, the ΨH1 culture with acetate never reached this point, while the culture lacking acetate required a light intensity ~5 times that of the parental strain to reach compensation. Acetate decreases net O_2 evolution via its effects on photosynthesis and mitochondrial respiration.[53] Light-dependent net O_2 evolution rates were ~35% lower in ΨH1 compared to the parental strain (**figure 2-11**). This could stem from either higher respiration rates or lower photosynthesis rates. In fact, we did not observe higher dark respiration rates in ΨH1 (**figure 2-11 A**). Lower rates of water oxidation could be due to either lower PSII activity or to limitations in electron flow downstream of PSII. We found that addition of phenyl-1,4-benzoquinone (PPBQ) as an artificial PSII electron acceptor resulted in similar light-dependent O_2 evolution rates in the two strains (**figure 2-11 B**), consistent with the latter hypothesis. Additionally, the quantum yield of PSII drops to low values at fairly low light intensities in the light saturation curve (**figure 2-11 C**), consistent with a highly reduced plastoquinone pool and a limitation in downstream electron flow. This is almost certainly due to the PSI-HydA chimera, whose abundance is ~7-fold lower than WT PSI. Thus, it appears that the bottleneck induced by lowered accumulation of the chimeric protein had the effect of constraining PSII O_2 evolution activity such that respiration and other O_2-consuming processes could keep up with it. While this was an *unintended* consequence of the PSI-HydA design, it resulted in preserving hydrogenase activity for sustained H_2 production. However, as many other redox enzymes are sensitive to O_2 and lowered abundance of chimeric proteins is a likely occurrence, this actually bodes well for the approach of fusing such enzymes to PSI.

To quantify the instantaneous rates of H_2 and O_2 production by the algal cells, an online membrane inlet mass spectrometry (MIMS) technique was used to measure dissolved gasses

during short illumination times (<2 min). The ΨH1 cells exhibited a significantly higher H_2 evolution than WT at photon fluxes above ~300 µmol m^{-2} s^{-1} and did not saturate until over ~1000 µmol photons m^{-2} s^{-1} (**figure 2-12 A**). In stark contrast, H_2 production by WT cells saturated at lower light intensities (~100 µmol photons m^{-2} s^{-1}) with a maximum rate of 11 ± 4 µmol H_2 h^{-1} (mg Chl)$^{-1}$, regardless of the presence of acetate. There was no detectable H_2 production by *hydA* cells. For ΨH1 cells, the highest observed rates were 76 ± 11 or 49 ± 6 µmol H_2 h^{-1} (mg Chl)$^{-1}$ in media with or without acetate, respectively. To eliminate the effect of O_2 inhibition on hydrogenase activity, we added glucose, glucose oxidase, and catalase to the medium to scavenge O_2.[16] With saturating light, the highest observed rate was 90 ± 5 µmol H_2 h^{-1} (mg Chl)$^{-1}$, representing a ~20% improvement (**figure 2-12 C**). Fitting of the data to a hyperbolic curve allowed us to estimate V_{max} to be 120 µmol H_2 h^{-1} (mg Chl)$^{-1}$ with half-saturation at 340 µmol photons m^{-2} s^{-1}. (In order to compare this maximal rate to those of chemotrophs or abiotic materials, it is equivalent to 2.7 mmol H_2 h^{-1} per g dry weight of cells.) To put this in context, such a strain could perform well even on a cloudy day (~600 µmol m^{-2} s^{-1}) and still reach saturation on a sunny day (≥2000 µmol m^{-2} s^{-1}).[54] Although the algal [FeFe] hydrogenase is known to be irreversibly inhibited by O_2 in a matter of seconds[55] and PSII is producing O_2 in the same membrane, O_2 scavenging only improved H_2 production in the ΨH1 culture by 20%. This demonstrates that keeping the enzyme in its cellular context allows maintenance of its activity for much longer periods than might be expected.

We now turn to the possible sinks in ΨH1 cells for electrons from PSII. A major motivation for our design was to intercept electrons from the PETC before they reached the Fd pool. However, we know from the experiments described above that there is a possibility of electron 'leakage' to Fd from the HydA domain in PSI-HydA. To test the impact of competition with CO_2 fixation, we used a phosphoribulokinase inhibitor (glycolaldehyde) to block the CBB cycle.[56] In the WT culture, the H_2 evolution rate quickly dropped after ~1 minute, decreasing over 10-fold from the peak rate within 5 minutes (**figure 2-12 D**). This drop was largely due to the activation of the CBB cycle, as addition of glycolaldehyde resulted in a much lower drop (~50%)

in H_2 evolution, which persisted during the experiment (10 min), as previously reported.[16] In contrast, the ΨH1 culture exhibited very stable H_2 production rates over the time course, and a ~20% *decrease* in H_2 evolution rate was seen after addition of glycolaldehyde. Nevertheless, we found that the ΨH1 strain was able to grow photoautotrophically, albeit much more slowly than strains containing WT PSI, and only if the culture was first rendered anoxic (**figure 2-13**). These results are consistent with the hypothesis that PSI-HydA reduces Fd in vivo poorly, and directs *most*, but not all, of the electrons from the PETC to proton reduction. We also found that cyclic electron flow around PSI was negligible in ΨH1 cells (**figure 2-14**), consistent with this idea. Thus, both linear and cyclic electron transport pathways are strongly affected in ΨH1 cells, demonstrating that photosynthetic electron flow has effectively been redirected in these cells by replacement of PSI with PSI-HydA. When one considers that the amount of PSI is ~7-fold lower (**figure 2-5 A**) and the total amount of hydrogenase activity is ~2-fold lower (**figure 2-5 B**) in the ΨH1 strain compared to WT, and yet the instantaneous light-saturated H_2 production rate is almost 7-fold higher in this strain, it is difficult to imagine how this could be, unless electrons from PSI were being directly fed to the hydrogenase active site, as intended by the chimeric protein design.

We tested the utility of this system for long-term H_2 production. After anoxia was imposed in a sealed bottle, the culture produced H_2 continuously for 5 days at an average rate of 14.0 ± 1.7 µmol H_2 h^{-1} (mg Chl)$^{-1}$ (**figure 2-15 A**). A similar experiment was run without imposing anoxia, and within 2 days the ΨH1 culture had become hypoxic (~4% O_2 in the headspace) and started producing H_2 (**figure 2-15 B**). We also set up long-term experiments using a PBR in turbidostat mode, which was flushed continuously with argon. Hydrogen was monitored in the efflux gas, allowing calculation of the rate of H_2 production by the culture. Cultures were maintained at high density (~ 30 mg Chl L^{-1}) under continuous illumination (600 µmol photons m^{-2} s^{-1}). The continuous production rate was 86.6 ± 2.4 mL H_2 d^{-1} per L culture (n=3). These rates, whether in sealed bottles or in a PBR, are at least comparable to rates reported in this species using the endogenous hydrogenases in concert with other methods to lower steady-state O_2 levels and/or

direct electrons to H_2 production.[8] In order to compare this rate to H_2 production rates using chemotrophs or abiotic materials, we normalized to dry weight of cells rather than Chl to obtain a rate of 164 ± 5 mL H_2 d^{-1} g^{-1}. The light-to-hydrogen conversion efficiency of ΨH1 cultures reached 1.75% under the best conditions (*i.e.*, short term with acetate and enforced anoxia, using 6.65 W m^{-2} of 630-nm photons), which is just over 10% of the theoretical maximum. While this is encouraging, we are still far from realizing the full potential of the system on a long-term basis.

It is somewhat surprising that marrying two very different proteins resulted in such an active chimeric protein. Using the maximal rate estimated from the MIMS experiment, and taking into account the PSI-HydA cellular abundance, one arrives at a H_2 production rate of ~170 H_2 s^{-1} for each PSI-HydA (*i.e.*, ~340 electrons s^{-1}). This is in line with previously reported electron throughput rates for PSI.[57] It also compares favorably with the PSI-hydrogenase assembly created *in vitro* that is currently the best *in vitro* H_2 photoproduction device (~50 H_2 s^{-1}).[58] In both cases, the overall throughput is likely limited by electron donation to P_{700}. The PSI-HydA chimera may have an advantage, as algal Pc can reduce P_{700} in <50 µs.[59] Based on these calculations, we conclude that the PSI-HydA chimera reported here is actually a very efficient light-driven proton photoreduction machine, capable of producing a dihydrogen every ~6 ms in vivo.

It is important to consider that the addition of the hydrogenase domain to PSI has created a photosystem that is fundamentally different from PSI, which is a type I reaction center that oxidizes and reduces 1-electron carriers. The PSI-HydA chimera requires 2 electrons to produce 1 H_2. Thus, it first needs to accumulate one electron on the HydA domain; after re-reduction of P_{700}^+ by plastocyanin and excitation of the reaction center, a second electron will be sent to the hydrogenase active site (see **figure 2-1 C**), resulting in reduction of 2 protons to a dihydrogen molecule. This is more akin to the action of a type II photochemical reaction center, which accumulates 2 electrons to reduce a quinone to quinol (also consuming 2 protons), although in this case the product is a *gaseous* molecule. Thus, it is not an overstatement to say that we have created a novel photochemical reaction center by fusing hydrogenase to PSI. It is also important

to consider the competition between reduction of Fd (requiring 1 electron) and protons (requiring 2 electrons). The longer the delay between the first and second electron arriving at the H-cluster, the more time that Fd has to bind to the HydA domain and “steal” the electron. This almost certainly explains the very high light flux required to saturate H_2 production in vivo in the ΨH1 cultures (**figure 2-12 A**), as higher light intensities result in shorter delays between consecutive excitations of PSI-HydA. Thus, as such a culture went through a day-night cycle, it would be biased towards Fd reduction at the beginning and end of the day, allowing it to fulfill basic physiological needs, but be biased towards H_2 production in the middle of the day, storing some of the energy of the extra photons as molecular hydrogen.

Future efforts to increase H_2 production with this system will focus on use of more O_2-tolerant hydrogenases. This would in turn allow use of PSI-HydA chimeras that accumulated to higher levels. While that would increase H_2 production, it would allow more O_2 production. However, as long as the steady-state level of O_2 present in the flow PBR system were not higher than the tolerance of the hydrogenase domain, the system should be able to produce H_2 continuously at a rate significantly higher than reported here. It should also be possible to modulate the partitioning of electrons between reduction of Fd and protons by modifying the Fd binding site of the HydA domain.

Conclusions

Use of the PSI-HydA chimera offers at least 4 advantages: (1) it constitutively expresses the chimeric protein; (2) it directs the majority of electrons from water oxidation to H_2 production; (3) it constrains O_2 evolution from PSII, preserving hydrogenase activity for sustained H_2 production over many days, obviating the need to use nutrient deprivation, PSII inhibitors or mutations; and (4) it preserves the proton pumping and ATP production carried out by the PETC, thus maintaining cell viability. By rewiring photosynthesis to deliver electrons from PSI directly to hydrogenase – thus cutting out the Fd ‘middleman’ – one is no longer at the mercy of cellular metabolic networks. With the system entirely encoded by the algal chloroplast genome, the use of directed evolution techniques to improve the system also becomes possible. Perhaps more

important than this particular example, however, is the discovery of a site in PSI that allows in-frame fusion of a protein to intercept electrons from PSI. The F_A/F_B clusters of PSI are at a lower reduction potential than any soluble electron carrier in the cell (*e.g.*, Fd, NADPH, thioredoxin). This opens the ability to drive novel redox chemistries not native to plants and algae at high flux by using a large fraction of the electrons from water-splitting and the PETC.

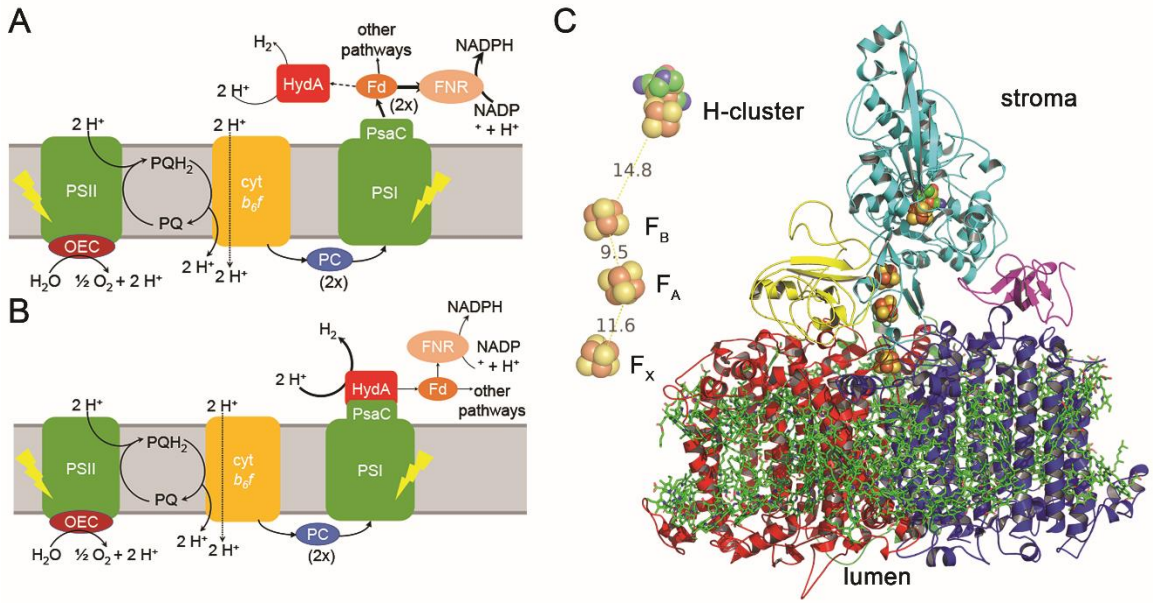

Figure 2-1. The photosynthetic electron transport chain (PETC) in WT cells (A), the proposed system (B), and a model of PSI-HydA (C). (A) The PETC in the thylakoid membrane drives linear electron flow, with water being oxidized by the oxygen evolving complex (OEC) of PSII and Fd being reduced by PSI, accompanied by formation of proton motive force. Two electrons will exit the PETC for each H2O oxidized. Under most conditions, NADPH is the major product, made by FNR. H2 is a minor and/or transient product under anoxic conditions. (B) In the system described here, hydrogenase (HydA) is directly attached to PSI, which should direct most electrons to H2 production at the expense of Fd reduction. (C) A model of PSI core subunits (PsaA – red, PsaB – blue) as ribbon diagrams, with PsaC–HydA2 (cyan), PsaD (yellow) and PsaE (magenta). Antenna pigments (chlorophyll (Chl) a and b-carotenes) are shown as green stick models, while FeS clusters and the H-cluster are shown as space-filling models. The predicted edge-to-edge distances between the inorganic substituents of the FeS clusters and the H-cluster (in Å) are shown to the left of the model.

MAHIVKIYDTCIGCTQCVRACPLDVLEMVPWGGATATDAVPHWKLALEELDKPKDGGRK
VLIAQVAPAVRVAIAESFGLAPGAVSPGKLATGLRALGFDQVFDTLFAADLTIMEEGTELL
HRLKEHLEAHPHSDEPLPMFTSCCPGWVAMMEKSYPELIPFVSSCKSPQMMMGAMVKT
YLSEKQGIPAKDIVMVSVMPCVRKQGEADREWFCVSEPGVRDVDHVITTAELGNIFKER
GINLPELPDSDWDQPLGLGSGAGVLFGTTGGVMEAALRTAYEIVTKEPLPRLNLSEVRGL
DGIKEASVTLVPAPGSKFAELVAERLAHKVEEAAAAEAAAAVEGAVKPPIAYDGGQGFST
DDGKGGLKLRVAVANGLGNAKKLIGKMVSGEAKYDFVEIMACPAGCVGGGGQPRSTDK
QITQKRQAALYDLDERNTLRRSHENEAVNQLYKEFLGEPLSHRAHELLHTHYVPGGASQ
MASAPRTEDCVGCKRCETACPTDFLSVRVYLGSESTRSMGLSY

Figure 2-2. Coding sequence of the PsaC-HydA2 fusion polypeptide. Highlighted residues indicate the PsaC fragments (green), N-terminal junction (cyan), and C-terminal junction (red). The red highlighted Ala residue is shared between the HydA2 and PsaC sequences.

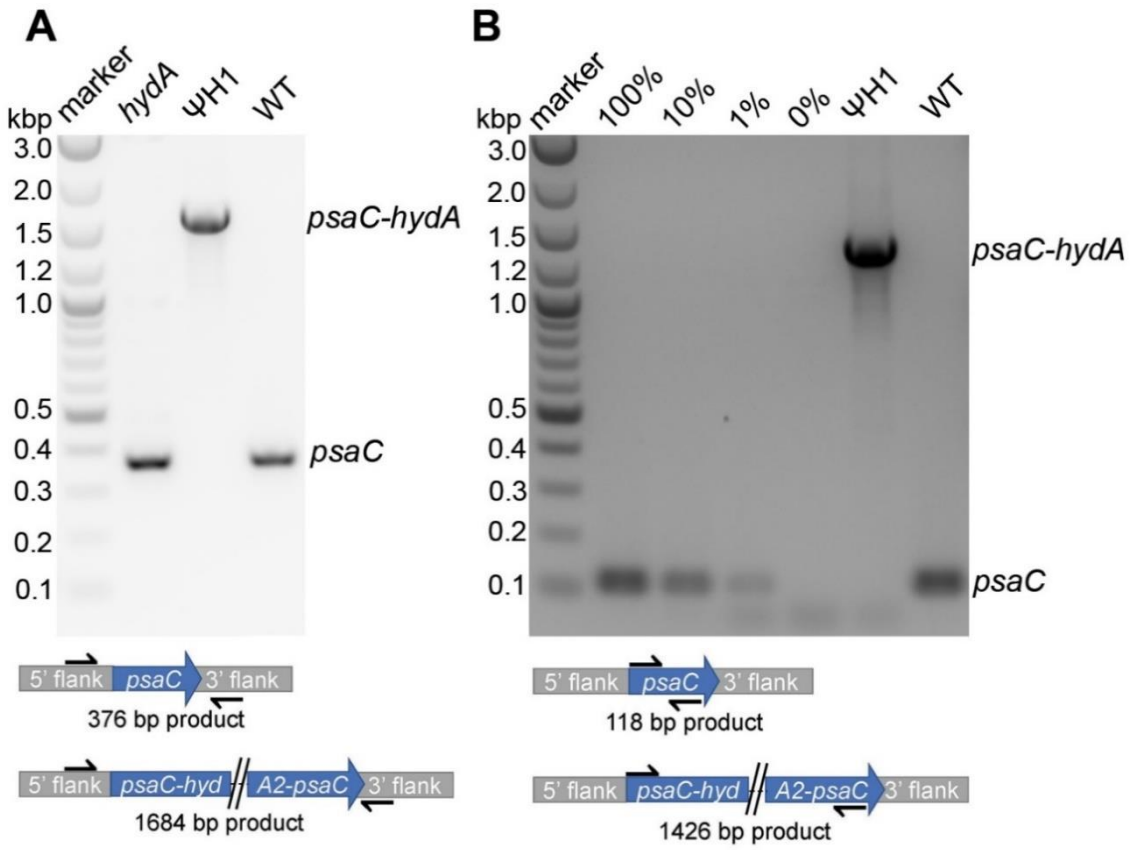

Figure 2-3. Agarose gel of PCR amplification of *C. reinhardtii* genomic DNA from parental (*hydA*), chimera-expressing (ΨH1) and WT strains with locus-specific (A) and gene-specific primers (B) A**:** *psaC* detection PCR with primers annealing to flanking sequences and corresponding cartoon showing primer locations and amplicon sizes using *psaC* or *psaC-hydA2* as the template. B**:** Homoplasmy detection PCR with gene-specific primers and corresponding cartoon with primer locations and amplicon sizes. Percentages indicate the abundance of the wild type genomic DNA (containing *psaC* gene) that had been diluted into the genomic DNA of the ***psaCΔ*** strain at the same DNA concentration (i.e., total genomic DNA was kept at 100 ng/reaction). PCR amplicons were resolved on 1% agarose gel and stained with ethidium bromide. A 2-log DNA marker (NEB) was used for size approximation; sizes in kbp are indicated to the left of the gel images.

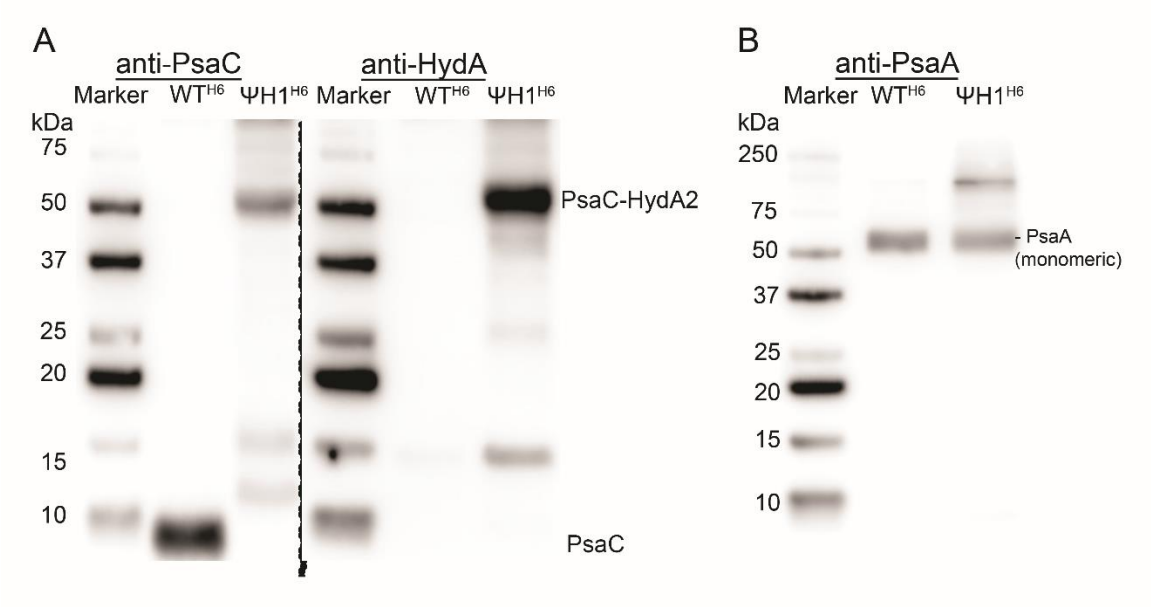

Figure 2-4. Immunoblots of isolated PSI and PSI-HydA from WT^{H6} or $\Psi H1^{H6}$, demonstrating assembly of PsaC–HydA2 into PSI-HydA. Equimolar amounts of PSI and PSI-HydA were probed with α-PsaC (A, left), α-HydA (A, right), or α-PsaA (B) antibodies. Sizes of marker polypeptides are indicated to the left. Integration of α-PsaA cross-reactive bands gave a ratio of 1.00 : 1.09 (WT : chimera).

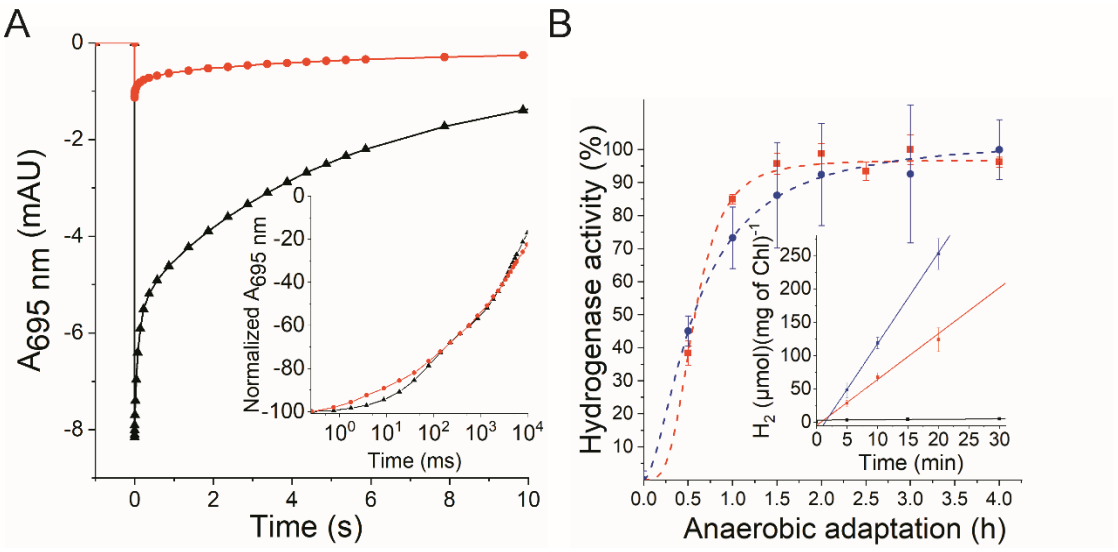

Figure 2-5. In vitro characterization of the PSI-hydrogenase chimera. (A) Transients of flash-induced P_{700} photobleaching and recovery in thylakoid membranes (60 mg Chl) isolated from *hydA* (black) and ΨH1 (red) cells that had been grown aerobically. The inset displays transients normalized to the maximal bleaching and using a log time scale. (B) Hydrogenase activity (expressed as % of maximal activity attained) assayed with reduced MV on whole cells, as a function of the anaerobic adaptation period. Inset: *In vitro* H_2 production with dithionite/MV in detergent-permeabilized *hydA* (black), WT (blue), and ΨH1 (red) cells after 1.5 h anaerobic induction. Error bars represent standard error (n = 3).

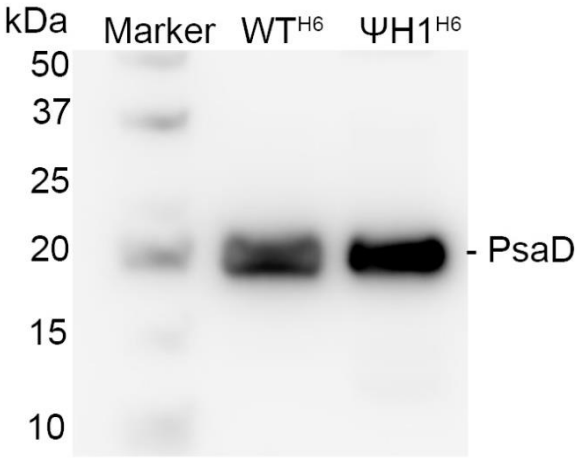

Figure 2-6. Immunoblot of isolated PSI particles using anti-PsaD antibodies. Samples were loaded on equal P_{700}, as in Figure 2-4. Integration of the anti- PsaD cross-reactive bands gave a ratio of 1.00:1.02 (PSI : PSI-HydA).

A

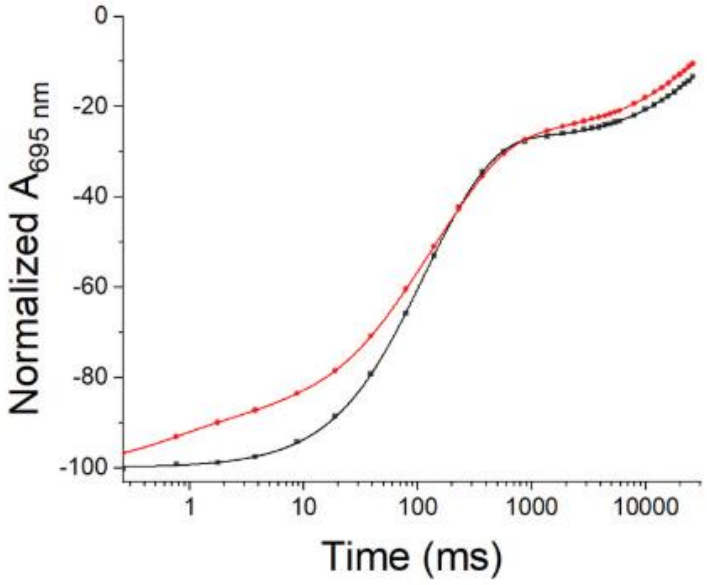

B

Assignment of phase	Time constant ± SE, ms (relative amplitude, %)	
	PSI^{H6}	**PSI^{H6}-HydA2**
CR of $P_{700}^{+}F_X^{-}$	N/A	0.56 ± 0.10 (7.3) 3.0 ± 0.6 (4.6)
CR of $P_{700}^{+}(F_AF_B)^{-}$	63 ± 4 (28.1) 204 ± 7 (44.5)	45 ± 3 (17.5) 192 ± 15 (35.8)
CR of $P_{700}^{+}F_H^{-}$	N/A	570 ± 81 (9.1)
ascorbate	30,000 ± 2750 (24.1)	25,500 ± 1060 (23.9)
Non-decaying	– (3.3)	– (1.8)
R^2	0.9999	0.9999

Figure 2-7. Spectroscopic characterization of anoxically prepared PSI^{H6} and PSI^{H6}-HydA2 particles that were loaded into a sealed cuvette in an anaerobic glovebox to eliminate O_2 from the environment. (A) Normalized transients (n=3, technical replicates) of P_{700}^{+} recovery upon laser flash-induced bleaching in anoxically prepared PSI particles: WT^{H6} (black, 74 fmol of P_{700}^{+}) and PSI^{H6}-HydA2 (red, 71 fmol of P_{700}^{+}). Solid lines represent fit to a multi-exponential decay, using the time constants and relative amplitudes reported in panel B. CR = charge recombination, F_H = [4Fe-4S] cluster of HydA2 domain.

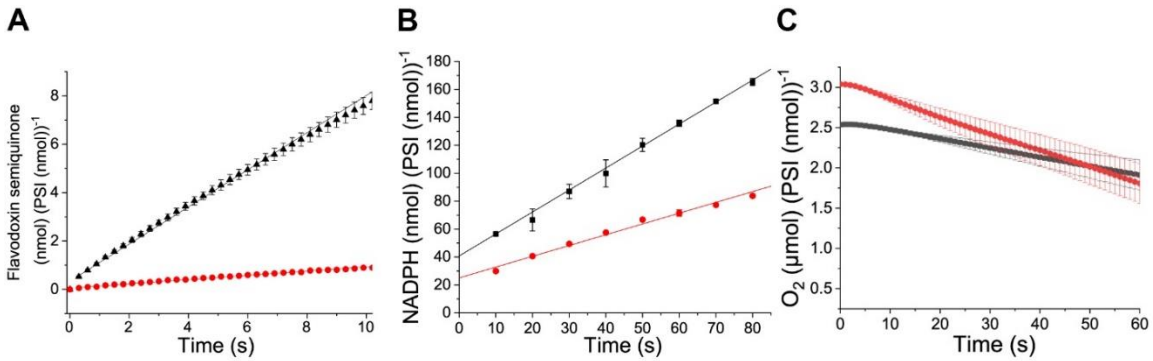

Figure 2-8. In vitro PSI activity measured by photoreduction of flavodoxin (A), $NADP^+$ (B) and O_2 (C). (A) Flavodoxin photoreduction with purified PSI [black=hydA, red=ΨH1] (normalized to 1 nmol of PSI) under saturating light conditions. Turnover rates are 0.77 s^{-1} (hydA) and 0.088 s^{-1}(ΨH1). (B) Assays contained equal amounts of PSI (54 nM) [black=WTH6, red=$\Psi H1^{H6}$] with an excess of ferredoxin (3 µM), FNR (0.2 µM), and $NADP^+$ (2.5 mM). Illumination (300 µmol of red photons m^{-2} s^{-1}) of cuvette commenced at t = 0. Lines represent a linear fit of the data. Rates thus obtained are 1.57 ± 0.01 and 0.77 ± 0.04 NADPH s^{-1} per PSI for WT and PSI-HydA, respectively. (C) O_2 reduction rates measured with a Clark-type electrode. The O_2 uptake rates were normalized to the amount of P_{700}. Maximal light-dependent rates were 12.7 ± 1.6 and 26.4 ± 4.8 O_2 s^{-1} per PSI for WT and PSI-HydA, respectively. Error bars represent SE (n=3).

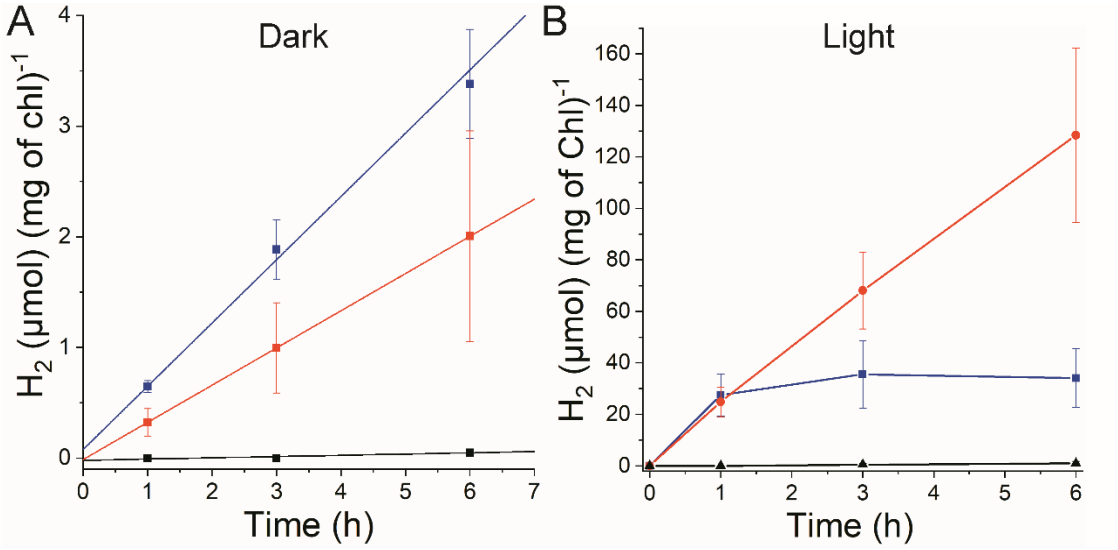

Figure 2-9. Accumulated H_2 in the headspace of sealed bottles produced by WT (blue), *hydA* (black), or ΨH1 (red) cultures in dark (A) or light (B, 200 µmol photons m^{-2} s^{-1}), as measured by GC-TCD (n = 3). Values are normalized to the initial Chl content of the cultures. Please note the different scales.

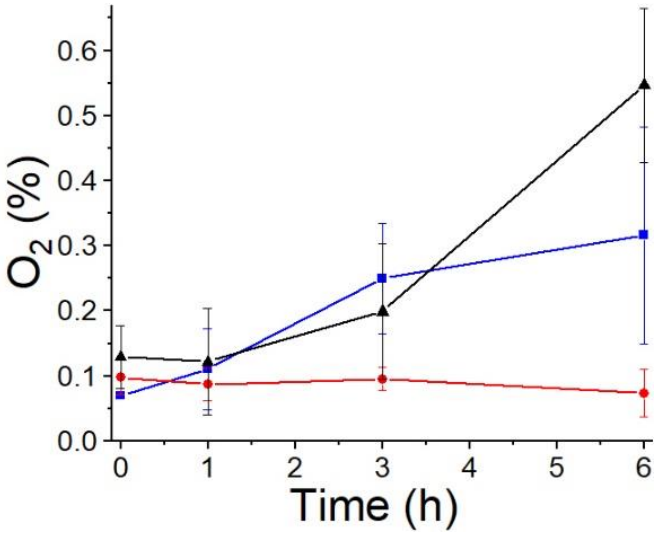

Figure 2-10. Accumulation of O_2, as measured by GC-TCD, in the headspace of sealed bottles containing cultures of WT (blue), *hydA* (black), and ΨH1 (red). Illumination intensity was 200 µmol photons m^{-2} s^{-1}. Experiment is the same one as shown in Figure 2-9 B.

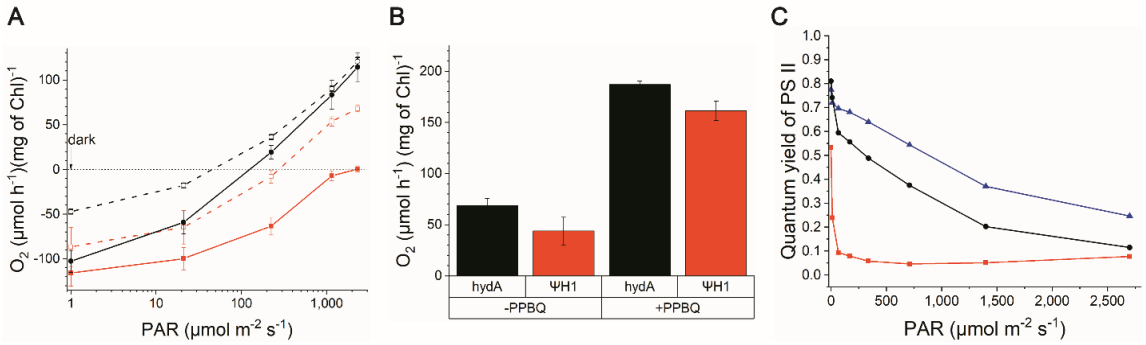

Figure 2-11. Rates of dissolved O_2 consumption/production and quantum yield of PSII. A: Net O_2 production rates under red LED illumination in aerobic cultures of *hydA* (black, circles) or ΨH1 (red, squares) in media with (solid lines and symbols) or without (dashed lines, hollow symbols) acetate. Data at 1 PAR correspond to the dark sample for graphing purpose. B: Light-dependent O_2 evolution rates under ~2300 µmol m^{-2} s^{-1} of red light in cultures containing bicarbonate, with or without addition of 0.2 mM PPBQ. In all instances, cells were grown in medium containing acetate and then resuspended in fresh medium containing bicarbonate instead of acetate as a carbon source before being placed into the measuring cuvette. Cells were stirred and occasionally bubbled with air to maintain them in an aerobic state before dissolved O_2 was measured with an optical sensor. Error bars represent standard error (n=3). C: Quantum yield of PSII in WT (blue), *hydA* (black) and ΨH1 (red) strains under various illumination intensities. Cells were aerobically resuspended in 20% Ficoll buffer (Tris-phosphate, pH 7.0) and kept aerobic throughout the experiment.

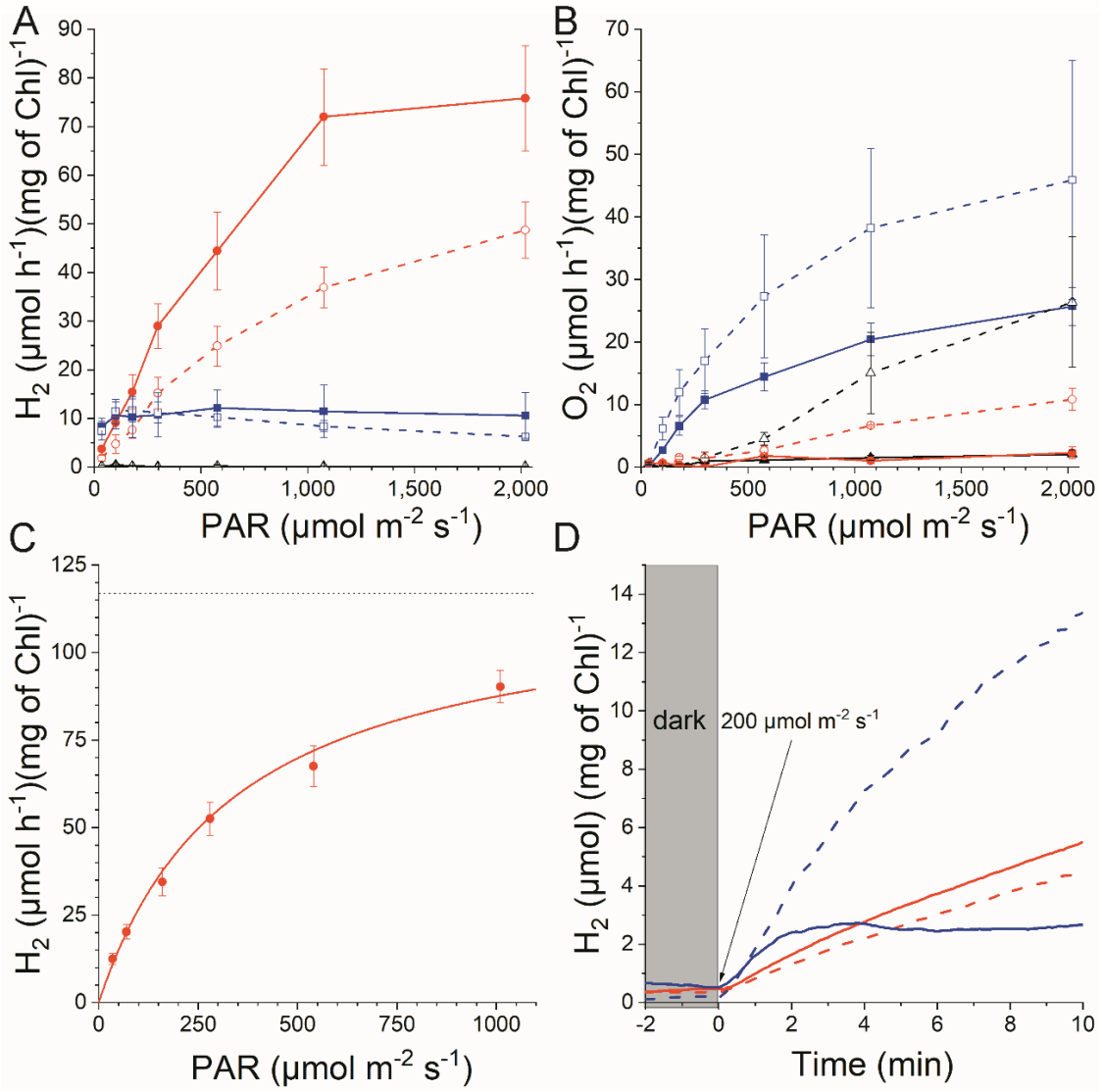

Figure 2-12. Membrane inlet mass spectrometry (MIMS) data. Rates of H_2 (A) or O_2 (B) production in cultures of WT (blue), *hydA* (black), and ΨH1 (red) under indicated light intensities in media containing acetate (solid symbols/lines) or lacking acetate (hollow symbols/dashed lines). Rates were determined as the slope of concentration change over 1 min of time. (C) Effect of enforced anoxia using glucose oxidase/catalase on H_2 evolution rate in an anaerobically adapted ΨH1 culture with acetate. Light-saturation data were fitted to a hyperbolic curve with Vmax (dotted line) ~ 120 µmol of H_2 h^{-1} (mg of Chl)$^{-1}$. Error bars in (A)–(C) represent standard error of the mean (biological replicates, n = 3). (D) Instantaneous H_2 production normalized to Chl under enforced anoxia of ΨH1 (red) or WT (blue) cultures with (dashed lines) or without (solid lines) 60 mM glycolaldehyde under continuous 200 µmol m^{-2} s^{-1} red light (average of 3 biological replicates).

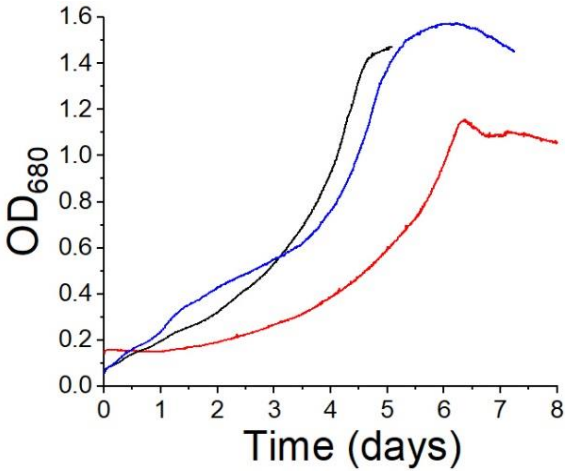

Figure 2-13. Photoautotrophic growth of *hydA* (black), WT (blue), and ΨH1 (red) cultures in a closed photobioreactor in TBP medium containing bicarbonate as the sole carbon source. Growth was monitored at 680 nm. The cultures were sparged in the dark with N_2 for 1 h prior to growth under illumination (340 µmol photons m^{-2} s^{-1}).

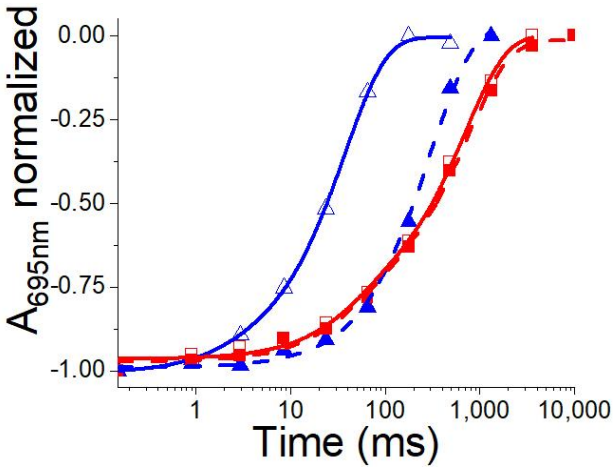

Figure 2-14. Cyclic electron flow measured in WT and ΨH1 cells. Normalized P_{700}^{+} decay transients after 10 s of strong illumination (940 µmol photons m^{-2} s^{-1}) in fully aerobic cultures of WT (blue triangles) and ΨH1 (red squares), to which had been added 20 µM DCMU (empty symbol/solid line), or 20 µM DCMU + 20 µM 2,5-dibromo-3-methyl-6-isopropylbenzoquinone (DBMIB; filled symbol/dashed line). The level of P_{700} photobleaching is normalized to the maximal level, and is plotted on a log time scale. Note that the rate of P_{700}^{+} reduction in the absence of PSII (with DCMU) is much slower in ΨH1 than in the WT cells and is unaffected by inhibition of cytochrome b_6f (with DBMIB), unlike the WT cells. Taken together, this indicates that cyclic electron flow is negligible in ΨH1 cells.

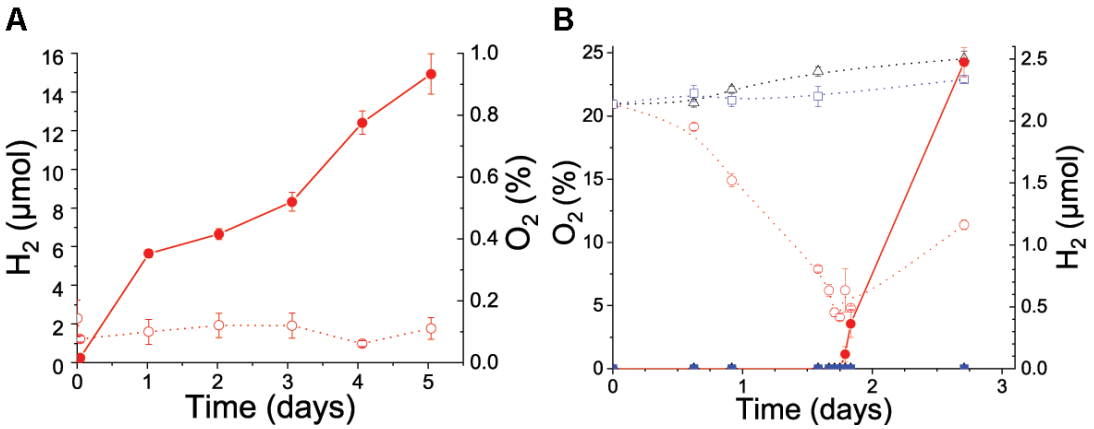

Figure 2-15. Long-term measurements of H_2 (solid symbols and lines) and O_2 (hollow symbols, dotted lines) produced by 10-mL cultures in sealed 25-mL bottles with (**A**) or without (B) prior imposition of anoxia via argon-sparging. ΨH1 (red), *hydA* (black) or WT (blue) cultures resuspended at ~1 µg/mL of Chl in fresh TAP were exposed to white light (~200 µmol m^{-2} s^{-1} PAR) and the headspace (15 mL) was sampled at the indicated times, followed by analysis via GC-TCD. Error bars represent SE (n=3).

parameter	PSI	PSI-hydrogenase	Comments
τ_1	91 ± 5.6 ms	79 ± 12	Decay constant of fast phase (ms)
A_1	33 ± 0.7 %	30 ± 1.5 %	Amplitude of fast phase (% of total)
τ_2	5500 ± 150 ms	4500 ± 290	Decay constant of slow phase (ms)
A_2	60 ± 0.6 %	51 ± 1.3 %	Amplitude of slow phase (% of total)
A_0	6 ± 0.4 %	15 ± 0.8 %	Non-decaying fraction (% of total)
R^2	0.9993	0.9961	Coefficient of determination

Table 2-1. Bi-exponential fitting parameters of P_{700}^+ decay curves *in vitro* shown in fugure 2-5 A. Function: $A(t) = A_0 + A_1 \exp(-x/t_1) + A_2 \exp(-x/t_2)$. Fast recovery phase parameters τ_1 and A_1 are likely due to charge recombination from P_{700}^+ (F_A/F_B^-) while τ_2 and A_2 result from a slow reduction of P_{700}^+ by ascorbate.

References

[1] Veeravalli SS, Shanmugam SR, Ray S, Lalman JA, Biswas N. Biohydrogen Production From Renewable Resources. In: Hosseini M, editor. Adv. Bioprocess. Altern. Fuels, Biobased Chem. Bioprod., Cambridge, UK: Woodhead Publishing; 2019, p. 289–312. https://doi.org/10.1016/B978-0-12-817941-3.00015-2.

[2] Swanson KD, Ratzloff MW, Mulder DW, Artz JH, Ghose S, Hoffman A, et al. [FeFe]-Hydrogenase Oxygen Inactivation Is Initiated at the H Cluster 2Fe Subcluster. J Am Chem Soc 2015;137:1809–16. https://doi.org/10.1021/ja510169s.

[3] Nelson N, Ben-Shem A. The complex architecture of oxygenic photosynthesis. Nat Rev Mol Cell Biol 2004;5:971.

[4] Mulder DW, Boyd ES, Sarma R, Lange RK, Endrizzi JA, Broderick JB, et al. Stepwise [FeFe]-hydrogenase H-cluster assembly revealed in the structure of $HydA^{\Delta EFG}$. Nature 2010;465:248–51. https://doi.org/10.1038/nature08993.

[5] Posewitz MC, King PW, Smolinski SL, Zhang L, Seibert M, Ghirardi ML. Discovery of Two Novel Radical S -Adenosylmethionine Proteins Required for the Assembly of an Active [Fe] Hydrogenase. J Biol Chem 2004;279:25711–20. https://doi.org/10.1074/jbc.M403206200.

[6] Ghysels B, Godaux D, Matagne RF, Cardol P, Franck F. Function of the Chloroplast Hydrogenase in the Microalga *Chlamydomonas*: The Role of Hydrogenase and State Transitions during Photosynthetic Activation in Anaerobiosis. PLoS One 2013;8:e64161. https://doi.org/10.1371/journal.pone.0064161.

[7] Torzillo G, Scoma A, Faraloni C, Giannelli L. Advances in the biotechnology of hydrogen production with the microalga *Chlamydomonas reinhardtii*. Crit Rev Biotechnol 2015;35:485–96. https://doi.org/10.3109/07388551.2014.900734.

[8] Tóth SZ, Yacoby I. Paradigm Shift in Algal H_2 Production: Bypassing Competitive Processes. Trends Biotechnol 2019;37:1159–63. https://doi.org/10.1016/j.tibtech.2019.05.001.

[9] Yacoby I, Pochekailov S, Toporik H, Ghirardi ML, King PW, Zhang S. Photosynthetic electron partitioning between [FeFe]-hydrogenase and ferredoxin: $NADP^+$-oxidoreductase (FNR) enzymes in vitro. Proc Natl Acad Sci 2011;108:9396–401.

[10] Nikolova D, Heilmann C, Hawat S, Gäbelein P, Hippler M. Absolute quantification of selected photosynthetic electron transfer proteins in *Chlamydomonas reinhardtii* in the presence and absence of oxygen. Photosynth Res 2018;137:281–93. https://doi.org/10.1007/s11120-018-0502-3.

[11] Decottignies P, Lemarechal P, Jacquot JP, Schmitter JM, Gadal P. Primary Structure and Post-translational Modification of Ferredoxin-NADP Reductase from *Chlamydomonas reinhardtii*. Arch Biochem Biophys 1995;316:249–59. https://doi.org/https://doi.org/10.1006/abbi.1995.1035.

[12] Decottignies P, Flesch V, Gérard-Hirne C, Le Maréchal P. Role of positively charged residues in *Chlamydomonas reinhardtii* ferredoxin-$NADP^+$-reductase. Plant Physiol Biochem 2003;41:637–42. https://doi.org/10.1016/S0981-9428(03)00061-5.

[13] Winkler M, Kuhlgert S, Hippler M, Happe T. Characterization of the Key Step for Light-driven Hydrogen Evolution in Green Algae. J Biol Chem 2009;284:36620–7. https://doi.org/10.1074/jbc.M109.053496.

[14] von Abendroth G, Stripp S, Silakov A, Croux C, Soucaille P, Girbal L, et al. Optimized over-expression of [FeFe] hydrogenases with high specific activity in *Clostridium acetobutylicum*. Int J Hydrogen Energy 2008;33:6076–81. https://doi.org/10.1016/j.ijhydene.2008.07.122.

[15] HAPPE T, NABER JD. Isolation, characterization and N-terminal amino acid sequence of hydrogenase from the green alga *Chlamydomonas reinhardtii*. Eur J Biochem 1993;214:475–81. https://doi.org/10.1111/j.1432-1033.1993.tb17944.x.

[16] Milrad Y, Schweitzer S, Feldman Y, Yacoby I. Green Algal Hydrogenase Activity Is Outcompeted by Carbon Fixation before Inactivation by Oxygen Takes Place. Plant Physiol 2018;177:918–26. https://doi.org/10.1104/pp.18.00229.

[17] Kosourov S, Jokel M, Aro E-M, Allahverdiyeva Y. A new approach for sustained and efficient H_2 photoproduction by *Chlamydomonas reinhardtii*. Energy Environ Sci 2018;11:1431–6. https://doi.org/10.1039/C8EE00054A.

[18] Brettel K. Electron transfer and arrangement of the redox cofactors in photosystem I. Biochim Biophys Acta - Bioenerg 1997;1318:322–73. https://doi.org/10.1016/S0005-2728(96)00112-0.

[19] Forestier M, King P, Zhang L, Posewitz M, Schwarzer S, Happe T, et al. Expression of two [Fe]-hydrogenases in *Chlamydomonas reinhardtii* under anaerobic conditions. Eur J Biochem 2003;270:2750–8. https://doi.org/10.1046/j.1432-1033.2003.03656.

[20] Reifschneider-Wegner K, Kanygin A, Redding KE. Expression of the [FeFe] hydrogenase in the chloroplast of *Chlamydomonas reinhardtii*. Int J Hydrogen Energy 2014;39:3657–65. https://doi.org/10.1016/j.ijhydene.2013.12.157.

[21] Sawyer A, Bai Y, Lu Y, Hemschemeier A, Happe T. Compartmentalisation of [FeFe]-hydrogenase maturation in *Chlamydomonas reinhardtii*. Plant J 2017;90:1134–43. https://doi.org/10.1111/tpj.13535.

[22] Kelley LA, Mezulis S, Yates CM, Wass MN, Sternberg MJE. The Phyre2 web portal for protein modeling, prediction and analysis. Nat Protoc 2015;10:845–58. https://doi.org/10.1038/nprot.2015.053.

[23] Kozakov D, Hall DR, Xia B, Porter KA, Padhorny D, Yueh C, et al. The ClusPro web server for protein–protein docking. Nat Protoc 2017;12:255. https://doi.org/10.1038/nprot.2016.169.

[24] Fiser A, Do RKG, Šali A. Modeling of loops in protein structures. Protein Sci 2000;9:1753–73. https://doi.org/10.1110/ps.9.9.1753.

[25] Fischer N, Sétif P, Rochaix JD. Targeted Mutations in the *psaC* Gene of *Chlamydomonas reinhardtii*: Preferential Reduction of F_B at Low Temperature Is Not Accompanied by Altered Electron Flow from Photosystem I to Ferredoxin. Biochemistry 1997;36:93–102. https://doi.org/10.1021/bi962244v.

[26] Meuser JE, D'Adamo S, Jinkerson RE, Mus F, Yang W, Ghirardi ML, et al. Genetic disruption of both *Chlamydomonas reinhardtii* [FeFe]-hydrogenases: Insight into the role of HYDA2 in H_2 production. Biochem Biophys Res Commun 2012;417:704–9. https://doi.org/10.1016/j.bbrc.2011.12.002.

[27] Fischer N, Stampacchia O, Redding K, Rochaix J-D. Selectable marker recycling in the chloroplast. Mol Gen Genet MGG 1996;251:373–80.

[28] Gulis G, Narasimhulu K V, Fox LN, Redding KE. Purification of His_6-tagged Photosystem I from *Chlamydomonas reinhardtii*. Photosynth Res 2008;96:51–60. https://doi.org/10.1007/s11120-007-9283-9.

[29] Li Y, Lucas M-G, Konovalova T, Abbott B, MacMillan F, Petrenko A, et al. Mutation of the Putative Hydrogen-Bond Donor to P_{700} of Photosystem I. Biochemistry 2004;43:12634–47. https://doi.org/10.1021/bi036329p.

[30] Kropat J, Hong-Hermesdorf A, Casero D, Ent P, Castruita M, Pellegrini M, et al. A revised mineral nutrient supplement increases biomass and growth rate in *Chlamydomonas reinhardtii*. Plant J 2011;66:770–80. https://doi.org/10.1111/j.1365-313X.2011.04537.x.

[31] Porra RJ, Thompson WA, Kriedemann PE. Determination of accurate extinction coefficients and simultaneous equations for assaying chlorophylls a and b extracted with four different solvents: verification of the concentration of chlorophyll standards by atomic absorption spectroscopy. Biochim Biophys Acta - Bioenerg 1989;975:384–94. https://doi.org/10.1016/S0005-2728(89)80347-0.

[32] Byrdin M, Santabarbara S, Gu F, Fairclough W V, Heathcote P, Redding K, et al. Assignment of a kinetic component to electron transfer between iron–sulfur clusters F_X and $F_{A/B}$ of Photosystem I. Biochim Biophys Acta - Bioenerg 2006;1757:1529–38. https://doi.org/10.1016/j.bbabio.2006.06.016.

[33] Liran O, Semyatich R, Milrad Y, Eilenberg H, Weiner I, Yacoby I. Microoxic Niches within the Thylakoid Stroma of Air-Grown *Chlamydomonas reinhardtii* Protect [FeFe]-Hydrogenase and Support Hydrogen Production under Fully Aerobic Environment. Plant Physiol 2016;172:264 LP – 271. https://doi.org/10.1104/pp.16.01063.

[34] Kuhlgert S, Drepper F, Fufezan C, Sommer F, Hippler M. Residues PsaB Asp612 and PsaB Glu613 of Photosystem I Confer pH-Dependent Binding of Plastocyanin and Cytochrome c_6. Biochemistry 2012;51:7297–303. https://doi.org/10.1021/bi300898j.

[35] Marco P, Kozuleva M, Eilenberg H, Mazor Y, Gimeson P, Kanygin A, et al. Binding of ferredoxin to algal photosystem I involves a single binding site and is composed of two thermodynamically distinct events. Biochim Biophys Acta - Bioenerg 2018;1859:234–43. https://doi.org/10.1016/j.bbabio.2018.01.001.

[36] Zhao J, Li R, Bryant DA. Measurement of Photosystem I Activity with Photoreduction of Recombinant Flavodoxin. Anal Biochem 1998;264:263–70. https://doi.org/10.1006/abio.1998.2845.

[37] Meimberg K, Mühlenhoff U. Laser-flash absorption spectroscopy study of the competition between ferredoxin and flavodoxin photoreduction by Photosystem I in *Synechococcus* sp. PCC 7002: Evidence for a strong preference for ferredoxin. Photosynth Res 1999;61:253–67. https://doi.org/10.1023/A:1006308729990.

[38] Alric J, Lavergne J, Rappaport F. Redox and ATP control of photosynthetic cyclic electron flow in *Chlamydomonas reinhardtii* (I) aerobic conditions. Biochim Biophys Acta - Bioenerg 2010;1797:44–51. https://doi.org/10.1016/j.bbabio.2009.07.009.

[39] Genty B, Briantais J-M, Baker NR. The relationship between the quantum yield of photosynthetic electron transport and quenching of chlorophyll fluorescence. Biochim Biophys Acta - Gen Subj 1989;990:87–92. https://doi.org/10.1016/S0304-4165(89)80016-9.

[40] Jordan P, Fromme P, Witt HT, Klukas O, others. Three-dimensional structure of cyanobacterial photosystem I at 2.5 angstrom resolution. Nature 2001;411:909.

[41] Chang CH, King PW, Ghirardi ML, Kim K. Atomic Resolution Modeling of the Ferredoxin:[FeFe] Hydrogenase Complex from *Chlamydomonas reinhardtii*. Biophys J 2007;93:3034–45. https://doi.org/10.1529/biophysj.107.108589.

[42] Ostersetzer O, Adam Z. Light-stimulated degradation of an unassembled Rieske FeS protein by a thylakoid-bound protease: the possible role of the FtsH protease. Plant Cell 1997;9:957–65.

[43] Sétif P, Fischer N, Lagoutte B, Bottin H, Rochaix JD. The ferredoxin docking site of photosystem I. Biochim Biophys Acta - Bioenerg 2002;1555:204–9. https://doi.org/10.1016/S0005-2728(02)00279-7.

[44] Cashman DJ, Zhu T, Simmerman RF, Scott C, Bruce BD, Baudry J. Molecular interactions between photosystem I and ferredoxin: an integrated energy frustration and experimental model. J Mol Recognit 2014;27:597–608. https://doi.org/10.1002/jmr.2384.

[45] Takahashi Y, Goldschmidt-Clermont M, Soen SY, Franzén LG, Rochaix JD, Franzen LG, et al. Directed chloroplast transformation in *Chlamydomonas reinhardtii*: insertional inactivation of the *psaC* gene encoding the iron sulfur protein destabilizes photosystem I. EMBO J 1991;10:2033.

[46] Shepard EM, Mus F, Betz JN, Byer AS, Duffus BR, Peters JW, et al. [FeFe]-Hydrogenase Maturation. Biochemistry 2014;53:4090–104. https://doi.org/10.1021/bi500210x.

[47] Witt H, Bordignon E, Carbonera D, Dekker JP, Karapetyan N, Teutloff C, et al. Species-specific differences of the spectroscopic properties of P700: analysis of the influence of non-conserved amino acid residues by site-directed mutagenesis of photosystem I from *Chlamydomonas reinhardtii*. J Biol Chem 2003;278:46760–71. https://doi.org/10.1074/jbc.M304776200.

[48] Sétif P. Ferredoxin and flavodoxin reduction by photosystem I. Biochim Biophys Acta - Bioenerg 2001;1507:161–79. https://doi.org/https://doi.org/10.1016/S0005-2728(01)00205-5.

[49] Fischer N. The PsaC subunit of photosystem I provides an essential lysine residue for fast electron transfer to ferredoxin. EMBO J 1998;17:849–58. https://doi.org/10.1093/emboj/17.4.849.

[50] Meimberg K, Fischer N, Rochaix J-D, Mühlenhoff U. Lys35 of PsaC is required for the efficient photoreduction of flavodoxin by photosystem I from *Chlamydomonas reinhardtii*. Eur J Biochem 1999;263:137–44. https://doi.org/10.1046/j.1432-1327.1999.00474.x.

[51] Noth J, Krawietz D, Hemschemeier A, Happe T. Pyruvate:Ferredoxin Oxidoreductase Is Coupled to Light-independent Hydrogen Production in *Chlamydomonas reinhardtii*. J Biol Chem 2013;288:4368–77. https://doi.org/10.1074/jbc.M112.429985.

[52] Ben-Zvi O, Dafni E, Feldman Y, Yacoby I. Re-routing photosynthetic energy for continuous hydrogen production in vivo. Biotechnol Biofuels 2019;12:266. https://doi.org/10.1186/s13068-019-1608-3.

[53] Chapman SP, Paget CM, Johnson GN, Schwartz J-M. Flux balance analysis reveals acetate metabolism modulates cyclic electron flow and alternative glycolytic pathways in *Chlamydomonas reinhardtii*. Front Plant Sci 2015;6:474. https://doi.org/10.3389/fpls.2015.00474.

[54] Wang L, Gong W, Lin A, Hu B. Analysis of photosynthetically active radiation under various sky conditions in Wuhan, Central China. Int J Biometeorol 2014;58:1711–20. https://doi.org/10.1007/s00484-013-0775-3.

[55] Erbes DL, King D, Gibbs M. Inactivation of Hydrogenase in Cell-free Extracts and Whole Cells of *Chlamydomonas reinhardi* by Oxygen. Plant Physiol 1979;63:1138 LP – 1142. https://doi.org/10.1104/pp.63.6.1138.

[56] Sicher RC. Glycolaldehyde Inhibition of Photosynthetic Carbon Assimilation by Isolated Chloroplasts and Protoplasts. In: Sybesma C, editor. Adv. Photosynth. Res. Proc. VIth Int. Congr. Photosynth. Brussels, Belgium, August 1--6, 1983, Dordrecht: Springer Netherlands; 1984, p. 413–6. https://doi.org/10.1007/978-94-017-4973-2_94.

[57] Takahashi H, Clowez S, Wollman F-A, Vallon O, Rappaport F. Cyclic electron flow is redox-controlled but independent of state transition. Nat Commun 2013;4:1954.

[58] Lubner CE, Applegate a. M, Knorzer P, Ganago a., Bryant D a., Happe T, et al. Solar hydrogen-producing bionanodevice outperforms natural photosynthesis. Proc Natl Acad Sci 2011;108:20988–91. https://doi.org/10.1073/pnas.1114660108.

[59] Santabarbara S, Redding KE, Rappaport F. Temperature Dependence of the Reduction of P_{700}^{+} by Tightly Bound Plastocyanin in Vivo. Biochemistry 2009;48:10457–66. https://doi.org/10.1021/bi901052c.

[60] BOHME H. Quantitative Determination of Ferredoxin, Ferredoxin-$NADP^{+}$ Reductase and Plastocyanin in Spinach Chloroplasts. Eur J Biochem 1978;83:137–41. https://doi.org/10.1111/j.1432-1033.1978.tb12077.x.

[61] Weiß D, Schneider G, Niemann B, Guttmann P, Rudolph D, Schmahl G. Computed tomography of cryogenic biological specimens based on X-ray microscopic images. Ultramicroscopy 2000;84:185–97. https://doi.org/10.1016/S0304-3991(00)00034-6.

[62] Polle JEW, Benemann JR, Tanaka A, Melis A. Photosynthetic apparatus organization and function in the wild type and a chlorophyll *b* -less mutant of *Chlamydomonas reinhardtii* . Dependence on carbon source. Planta 2000;211:335–44. https://doi.org/10.1007/s004250000279.

CHAPTER 3

INTERPLAY BETWEEN HYDROGEN PRODUCTION AND PHOTOSYNTHESIS IN A GREEN ALGA EXPRESSING AN ACTIVE PHOTOSYSTEM I-HYDROGENASE CHIMERA

Andrey Kanygin[a], Alec Smith[a], Valéria Nagy[b], Szilvia Z. Tóth[b], and Kevin E. Redding[a*]

[a] School of Molecular Sciences, Center for Bioenergy & Photosynthesis, Box 871604 Arizona State University Tempe, Arizona 85287-1604

[b] Institute of Plant Biology, Biological Research Centre, Szeged, Temesvári krt. 62, H-6726 Szeged, Hungary

Reproduced with permission from:

Kanygin A, Smith A, Nagy V, Tóth SZ, Redding KE. Interplay between hydrogen production and photosynthesis in a green alga expressing an active photosystem I-hydrogenase chimera. Int J Hydrogen Energy 2022;47:21969–83. https://doi.org/10.1016/j.ijhydene.2022.03.096.

Abstract

We have previously created and expressed a chimeric polypeptide joining the PsaC subunit of Photosystem I (PSI) to the HydA2 hydrogenase of *Chlamydomonas reinhardtii* and demonstrated that it assembles into the PSI complex and feeds electrons directly to the hydrogenase domain, allowing for prolonged photobiological hydrogen production. Here we describe a new PSI-hydrogenase chimera using HydA1, the more abundant and physiologically active endogenous hydrogenase of this alga. When the PsaC-HydA1 polypeptide was expressed in a *C. reinhardtii* strain lacking endogenous hydrogenases, it was assembled into active PSI-HydA1 complexes that were accumulated at a level ~75% that of PSI, which is ~5 times higher than the PSI-HydA2 chimera. Hydrogen production by the chimera could be restored after complete inactivation by oxygen without requiring new synthesis of PSI or the PsaC-HydA1 polypeptide, demonstrating that the complex could be repaired *in vivo*. The PSI-HydA1 chimera reduces ferredoxin *in vivo* to such an extent that it can drive the Calvin-Benson-Bassham cycle, leading to high O_2 production rates, and eventually resulting in inactivation of the hydrogenase; use of media that drastically diminished CO_2 fixation and an O_2-scavenging material allowed H_2 production for at least 4 days.

Introduction

Sunlight is an abundant and sustainable, yet dilute, source of energy that requires conversion into useful forms for societal utilization [1]. Photosynthetic biohydrogen is one of the venues for a potentially inexpensive carbon-neutral fuel that relies on solar-driven production by living organisms [2–4]. Unfortunately, progress towards achieving a cost-effective biological H_2 production technology has so far been lackluster [5]. More radical approaches are, therefore, required to make significant progress. We have taken the approach of linking the H_2 production enzyme directly to the photosynthetic machinery.

During photosynthesis, light energy is captured and converted into chemical bond

energy. In oxygenic photosynthesis, photosystem (PS) II and I are excited by light, producing stable charge separation resulting in reduction of plastoquinone and ferredoxin (Fd), respectively. Plastoquinol participates in the Q-cycle at cytochrome *b6f*, passes on reductant for PSI and contributes to generation of proton motive force across thylakoid membrane (along with oxygen-evolving complex of PSII). Fd-$NADP^+$ reductase (FNR) reduces $NADP^+$ using the electrons from two reduced ferredoxins. The proton electrochemical gradient generated by the process is used by ATP synthase to drive phosphorylation of ADP to ATP. The assimilation of a CO_2 molecule by the Calvin-Benson-Bassham (CBB) cycle consumes 3 ATP and 2 NADPH [6]. While linear electron flow (LEF) generates both NADPH and ATP, as well as O_2 as a byproduct, LEF alone is insufficient to satisfy cellular ATP needs. Cyclic electron flow around PSI [7], as well as electron flow to alternative electron acceptors (e.g., protons, O_2), have evolved as mechanisms to increase the ATP/NADPH ratio.

The [FeFe]-class of hydrogenases are metalloenzymes catalyzing reversible proton reduction[8] and typically interact with Fd as electron carrier[9,10] Under anoxia, hydrogenase can be used to get rid of excess electrons, which is especially important when the proton gradient is insufficient to drive ATP synthase (e.g., just after a dark-light transition). Thus, some microalgae (including *C. reinhardtii*) are capable of photosynthetic H_2 production for brief periods of time during transitions from dark to light in anoxia [11] as an adaptive mechanism [12]. The transient nature of H_2 evolution is dictated by competition for reductant with other metabolic processes such as carbon fixation [13,14], flavodiiron-mediated O_2 photoreduction [15], cyclic electron flow (CEF) and loss of activity in the presence of O_2. Under microoxic-anoxic conditions, H_2 gas represents an alternative pool of reductant for algae possessing hydrogenases and can be used to fix CO_2 in the light or reduce O_2 (as long as O_2 is <1% by volume) [16,17]. Recently, a link between H_2 oxidation and $NADP^+$ reduction was experimentally demonstrated in *Chlamydomonas* [18], indicating the importance of hydrogenases for maintenance of the $NADP^+$ pool redox state under anoxia.

For algal hydrogenase to become active, the H-cluster needs to be inserted into apoprotein. First, the cubane [4Fe-4S] cluster is delivered by the sulfur utilization factor (SUF) machinery, followed up by insertion of the diiron site with the help of the maturation factors HydE, HydF and HydG [19–22]. The H-cluster is inactivated by O_2 at the diiron site. Depending on the H-cluster redox state [23], the inactivation can be reversible or irreversible. In case of irreversible inactivation, the diiron site departs first [24]. Further damage to the iron sulfur cluster can take place [25] or the diiron site may be reinserted by maturases.

Most successful approaches to photobiohydrogen production directly or indirectly involve decreasing the activity of the major electron sink for photosynthesis – the CBB cycle – via diversion of reductant/ATP/substrate. As an example of the direct approach, the Rubisco mutant (RbcS-Y67A) [26] showed 10-15 fold increased H_2 production compared to the wild-type under the same conditions. The increased H_2 production was coupled with abolished net O_2 evolution, even under S-replete, acetate-supplemented conditions using low-to-medium irradiation. Although promising results for H_2 production were shown, such impairment of the CBB has negative repercussions for PSII levels, cell growth and viability. Indirect approaches modulating CBB cycle activity include sulfur deprivation to lower PSII activity [27], downregulation of FNR [28], pulsed light [29], depriving the cultures of CO_2 and acetate [30], and various hydrogenase chimeras (e.g., Fd-hydrogenase [31–33], PSI-hydrogenase [34]). Our previous PSI-HydA2 chimera only accumulated to ~10-15% of the WT PSI level and directed most electrons to proton reduction, while CBB cycle activity remained dormant. Here we describe use of the PSI-HydA1 chimera in an attempt to improve biohydrogen production.

Materials and methods

Design of PsaC-HydA1 chimera

A complete annotated protein sequence of PsaC-HydA1 is shown in **figure 3-1**. The insertion site of the hydrogenase domain and modifications to PsaC protein sequence were the

same as previously described[34], as outlined below. The sequence of HydA1 was modified in the following ways: (1) the transit peptide (first 56 amino acids [35]) was removed; (2) the remaining unstructured region (AAPAAEAPLS) leading up to the first α-helix H67-L75 was replaced with the sequence used in the *psaC-hydA2* construct (**figure 3-1**, highlighted in magenta); (3) the last eight (non-conserved) amino acids of HydA1 were also removed (**figure 3-2**). Residues 32-35 of PsaC corresponding to the short loop of a β-hairpin were removed and the modified HydA1 sequence was inserted in their place. The N-terminus of HydA1 was linked to PsaC-Trp31 via 2 glycine residues, while the C-terminus (Gly489) was linked to PsaC-Ala36. Sequence alignments show a close match to the design of the PsaC-HydA2 construct (**figure 3-3**).

For modeling the PsaC-HydA1 chimera, the crystal structure of HydA1 (3LX4 [36]) was used as the ligand and PsaA, PsaB, PsaC (D32-K35 residues removed) and PsaF subunits of *C. reinhardtii* PSI (6JO5[37]) were used as a receptor in docking with ClusPro2. Unstructured terminal residues (6 N-terminal residues only) were removed from the ligand by the ClusPro2 algorithm prior to docking. Also, distance restraints of 1-25 Å were placed between the outermost cysteine of the F_B iron-sulfur cluster (Cys14) and the outermost cysteines of the H-cluster: cysteines 185 or 377 in 3LX4 (corresponding to cysteines 199 or 391 in PsaC-HydA1, respectively). The most plausible model was chosen based on the ClusPro2 energy minimization algorithm. Linking regions between PsaC and HydA1 domains were modeled with the help of the Robetta web server by uploading docked coordinates into their comparative modeling option[38]. The PsaD subunit (6IJJ, chain D) was aligned as in native PSI. PyMOL[39] was used for generation of final images as well as structure alignments.

For modeling ferredoxin docking to the PSI-HydA1 chimera, Fd 1 (PDB ID 2N0S)[40] was used as the ligand and PsaA, PsaB, PsaC-HydA1, PsaD, and PsaF of our model as receptor in ClusPro2 server. A single distance restraint of 2-20 Å between Cys42 of ferredoxin and Cys391 of PsaC-HydA1 was used.

Generation of algal mutants bearing chimeric photosystem I-hydrogenase

All transformations were carried out in the *hydA* strain (*mt- hydA1-1, hydA2-1*)[41] that lacks both endogenous hydrogenases via DNA-coated particle bombardment as previously described[34].

PCR for homoplasmy confirmation

PsaC-HydA1 homoplasmy was tested by PCR using flanking primers (PsaC5': TAATATGGAGATGACATATTTAG and PsaC3': GATCTCACCAAGATACTCCC) on 100 ng of genomic DNA as previously described[34], with minor modifications. The detection limit for *psaC* was tested by making a series of dilutions of genomic DNA of parental strain (containing *psaC* gene) into ΨH2 genomic DNA (containing *psaC-HydA2* gene) [34].

Growth conditions

Algae were routinely grown on Tris-acetate-phosphate (TAP) medium with revised mineral nutrient supplement [42] as previously described [34].

For growth assays on plates, 10 µL (~10^4 cells) cells resuspended in the same medium as the corresponding agar plate were spotted onto the plate and left to dry for 10 min. Then, plates were either sealed with parafilm to prevent further drying or placed in an anaerobic pouch (for high CO_2/anoxic conditions). TAP or TBP (Tris-bicarbonate phosphate) plates containing 1.4 % agar were used. TBP containing plates were prepared by replacing acetate (16.6 mM) with sodium bicarbonate (25 mM, pH 7.0). Growth assays were performed under continuous white fluorescent light (70 µmol m^{-2} s^{-1}). Plates were photographed on the second and seventh days of growth.

Chlorophyll (Chl) measurement

Chl *a+b* concentrations were determined in 80% acetone by the method of Porra et al. [43]

Thylakoids and PSI preparation

Cells were grown in TAP in 4 L flasks with aeration and stirring under ambient room light (<5 µmol m^2 s^{-1} white fluorescent) to mid-to-late log phase. Thylakoids were prepared as previously described[44] with minor modifications. Cells were harvested at 3500 x *g* at 4 ^oC for 10 min. The pellet was washed with buffer H1 (25 mM HEPES-KOH, 5 mM $MgCl_2$, 0.3 M sucrose, pH 7.5), flash-frozen in liquid nitrogen and stored at -80 ^oC. Further steps were done in the dark. Cells resuspended in H1+ 1mM phenylmethane sulfonyl fluoride to ~ 4 x 10^8 cells ml^{-1} were broken by French press using ~1.7 tons of pressure or Branson Sonifier S-450 using amplitude 3 (50 % duty cycle) for 2 min ON followed by 2 min OFF and repeated 3 times under temperature control (4 ^oC). The membranes were pelleted at 20000 x *g* for 10 min and washed with buffer H2 (5 mM HEPES-KOH, 10 mM EDTA, 0.3 M sucrose, pH 7.5). The washed pellet was resuspended in buffer H3 (5 mM HEPES-KOH, 10 mM EDTA, 1.8 M sucrose, pH 7.5) and overlaid with buffer H4 (1.3 M sucrose) and H5 (0.5 M sucrose) in a gradient tube. After 1 h of centrifugation (SW-28 rotor at 112400 x *g*) the upper green band formed between 0.5 M and 1.3 M sucrose layers was pooled with the lower band (1.3 M/1.8M sucrose). Purified membranes were centrifuged (90000 x *g* for 30 min) and resuspended in H6 (5 mM HEPES-KOH, 10 mM EDTA, pH 7.5) + 20% glycerol for storage at -80 ^oC.

Membranes (~800 µg ml^{-1}) were solubilized with 1% n-dodecyl-β-D-maltoside (β-DDM) for 1 hour. Unsolubilized material was pelleted at 41000 x *g* for 15 min. The solubilized membranes were loaded on continuous sucrose gradient prepared by freeze-thaw method as described in [45]

Anoxic PSI-HydA1 isolation

This was performed as previously described for PSI-HydA2[34]. Since PSI was not tagged, we used the sucrose gradient protocol described above for anoxic PSI isolation (adding ~ 2 mM sodium dithionite at every step).

Laser-flash spectroscopy

Our experimental setup was very similar to what is described in[34]. Thylakoids (~60 µg *Chl* mL^{-1} in 25 mM HEPES-KOH, pH 7.5, 5 mM sodium ascorbate) or PSI particles (~6 µg *Chl* mL^{-1} in 25 mM tricine-KOH, 300 mM KCl pH 8.0, 10% glycerol, 0.03 % β-DDM, 5 mM sodium ascorbate) were kept on ice in the dark before measurements. Absorbance changes at 696 nm were triggered by a single-turnover saturating (6 ns, ~20 mJ) flash generated by a frequency-doubled Nd/YAG laser (532 nm) and monitored with weak LED pulses (10 µs) using a JTS-10 (Bio-Logic) kinetic spectrophotometer. Background transient was collected by running the same sequence with laser shutter closed, allowing us to control for small actinic effects of probing light and electronic artifacts (due to changing collecting rates).

In vitro hydrogenase activity

This assay is similar to what was described before[34]. Cells were resuspended in TAP at ~30 µg *Chl* mL^{-1}. An aliquot of 0.2 mL of cell suspension was taken at various times during anaerobic adaptation and mixed with Ar-purged, pre-warmed (37 ^{o}C) reaction buffer (100 mM Tris-HCl, pH 7.3, 1 M NaCl, 8 mM methyl viologen, 0.2 % Triton X-100, 16 mM sodium dithionite). After 10-30 min of incubation at 37 ^{o}C with agitation, headspace of the vial was probed with gas chromatography. For inhibition with chloramphenicol (CAM), a 50 mg/mL CAM stock solution in ethanol was freshly prepared.

Gas chromatography (GC) measurements

A model SRI 310 gas chromatograph with thermal conductivity detector and 5Å molecular sieve prepacked column (91.4 cm long) was used. Gas tight syringes (1700 series) with non-coring needles were used for probing headspace.

Photoautotrophic H_2 production with O_2 absorbent

After four days of cultivation, cultures were transferred to high-salt (HS) medium (http://www.chlamycollection.org/methods/media-recipes/) and the Chl content was set to 4 - 5 µg Chl mL^{-1}. For H_2 production, 10 ml of culture processed as above was placed in 30-ml glass serum bottles and sealed with rubber septa under sterile conditions, similarly as described in[30]. An iron-salt-based, non-cytotoxic O_2 absorbent (O_2Zero-50 cc loose; Global Reach Ltd, London, UK) was used to diminish the O_2 concentration below 0.05% in the headspace [46].

Dark anaerobic incubation was performed by flushing the headspace with N_2 gas for 10 min and keeping the cultures in the dark for 3 h. Afterward, algal cultures were placed under warm white LED panels, providing ~200 µmol photons m^{-2} s^{-1}. The cultures were illuminated continuously, kept at 23 - 25 °C for 96 h, and shaken at 120 rpm.

The net amounts of H_2 were determined by collecting a 100-µl aliquot from the gas phase of the cultures with a gas-tight Hamilton syringe. These samples were injected manually into a Hewlett Packard 5890 gas chromatograph (GC) equipped with an HP-PLOT Molesieve column (30 m*0.53 mm*0.25 µm) set at 40 °C and connected to a thermal conductivity detector set at 160 ºC. The carrier gas was argon, linear velocity 115 cm s^{-1}. After gas sampling every 24 h, serum bottles were flushed with N_2 gas to prevent H_2 accumulation above 5% in the gas phase [47].

Western blotting

Immunoblots were performed as described in[34]. Solubilized thylakoids were loaded on

the basis of the same P_{700}^{+} photobleaching (1.41 pmol) or the same Chl (2 µg) amounts.

Membrane inlet mass spectrometry (MIMS) measurements of H_2, O_2 and CO_2 in vivo

Cells were washed once with TP media, then resuspended in either TP or TAP media to 15 µg/mL of total Chl. Anaerobic adaption was done in 25-mL Wheaton glass bottles covered with aluminum foil. Cell suspensions were sparged with either Ar or N_2 at 100 mL min^{-1} for 10 min, followed up by at least 3 hours of agitation in the dark. Five mL of suspended cells were injected into a continuously purged (500 mL min^{-1} N_2) custom-built glass cuvette (5 mL) with 4 ports on top. The cuvette was maintained at 24 °C and stirred using a Peltier temperature programmer (PTP-1 by Perkin Elmer). Red LED lights (Hansatech instruments) of various intensity were used to illuminate the cuvette.

A QMG 220 M1 Prisma Plus compact mass spectrometer (Pfeiffer vacuum) equipped with gas-tight ion source was connected to a home-built membrane inlet system. The system was made of ¼" (6.35 mm) OD stainless steel tubing (0.035" (0.889 mm) (wall thickness) that included a loop as a cold trap, a port connected to a pressure gauge, an external vacuum line port and a 1/16" (1.5875 mm) OD stainless steel probe with mounted membrane inlet at the end. Membrane inlet consisted of 7-mm long silicon-based polymer tube supported by rings on the inside and ended with 5 mm long silicone rubber tapered plug. A mixture of dry ice and ethanol was used in the cold trap for all experiments.

Ion currents (*m/z* 2, *m/z* 32, *m/z* 44) were collected with a 0.5-s dwelling time and used for H_2, O_2 and CO_2 determination, respectively. Standards were made by sparging cell-free buffers either with a 1% H_2 (balance N_2) standard (Matheson) or air at the known pressure until equilibrium was reached. Rates of gas consumption by the mass spectrometer were calculated after sparging cell free buffers with a standard gas or air as described elsewhere [48].

In vivo dissolved O_2 measurements with FireSting-O_2.

Cells were grown on TAP to mid-to-late log phase. Then, they were resuspended in TAP+25 mM sodium bicarbonate (freshly made) to ~20 (µg of Chl) mL^{-1} and briefly sparged with air to saturate with O_2. Once placed in the cuvette with continuous stirring, O_2 concentration was monitored with FireSting-O_2 (PyroScience GmbH, Aachen, Germany) probe for dark respiration (5 min) followed by 5 min of continuous red light (~1435 µmol PAR m^{-2} s^{-1}). Gross rate of oxygen change was calculated as Light (net) minus dark rates.

In vivo P_{700}^+ recovery measurements and Chl fluorescence measurements

Cells were collected during early log phase, centrifuged (3500 *x g* for 5 min) and resuspended in 10 mM sodium phosphate (pH 7.0), 2 mM sodium bicarbonate and 20% Ficoll™ PM400 (GE Healthcare) to ~30 µg/mL Chl (P_{700}^+) or ~9 µg Chl mL^{-1} (for Chl fluorescence measurements). Cells were dark adapted for 5 min before taking each measurement. During dark periods, samples were briefly sparged with air to prevent development of anoxia. P_{700}^+ signal was measured via JTS-10 as previously described[34]. Fluorescence emission from Chl was measured with the JTS-10 Fluo59 accessory. A saturating pulse (80 ms, 8 mmol photons m^{-2} s^{-1}, 520 nm) was used to obtain F_{max}, measured 170 µs after the pulse. The steady-state fluorescence parameter (F_s) was measured after 2 minutes of illumination (520 nm) with actinic light of variable intensity. Quantum yields of PS II ($\Phi_{(II)}$) were calculated as described [49].

Flavodoxin photoreduction in vitro

Recombinant flavodoxin (*Synechococcus sp* PCC7002) was prepared as described in [50] The experiment with PSI-HydA1 was performed at the same time as PSI-HydA2 [34], therefore, the same wild type PSI control (prepared from the parental -hydA strain) is shown here. Each reaction contained ~100 nM PSI in 25 mM Tricine-KOH (pH 8), 50 mM $MgCl_2$, 20 mM KCl, 0.03% β-DDM, 5 mM sodium ascorbate, 5 µM plastocyanin (prepared in-house form a

recombinant source)[51] and 5 µM flavodoxin. Reaction mixtures were set up in the dark. Flavodoxin semiquinone was monitored with JTS-10 kinetic spectrometer (Bio-Logic) using 10-µs flashes at 573 nm (6 nm full width at half maximum). A 250-ms actinic LED pulse at 630 nm (3000 µmol photons m^{-2} s^{-1}) was followed by a delayed (50-ms) detection pulse. The dark periods (50-ms out of 300 ms) was factored in the final rate calculations. Semiquinone-minus-flavin difference at 573 nm extinction coefficient (5100 M^{-1} cm^{-1} was used based on published difference spectrum [52]. Baseline correction for the illuminated sample was done using preceding dark sampling for obtaining light-dependent rate.

Results

Chimeric protein design and expression

Based on our previous work with the PsaC-HydA2 chimera and the close similarity of the two endogenous hydrogenases of *C. reinhardtii*, we designed a PsaC-HydA1 construct that has 78 % identity and 88 % similarity to the PsaC-HydA2 chimera (**figure 3-3**). We used the same principles as we had used before (e.g., PsaC and HydA domains should be able to fold, distance between F_B and H-cluster should be close enough for electron transfer) to come up with a plausible model of the chimeric photosystem I-hydrogenase (**figure 3-4**).

The *psaC-hydA1* gene was introduced into the chloroplast genome of the *hydA1-1 hydA2-1* strain via biolistic transformation followed up by homologous recombination, as previously described for the *psaC-hydA2* gene [34]. After several passages on selective plates containing acetate in the dark, transformants were screened for homoplasmy (i.e., all copies of the chloroplast genome contained *psaC-hydA1* in place of *psaC*; see **figure 3-5**). Sequencing of PCR products verified proper gene insertion and lack of unintended mutations. For brevity, the *hydA1-1 hydA2-1* strain will be referred to as *hydA*, and the *psaC-hydA1* transformant will be called ΨH2.

Expression of PsaC-HydA1 was verified by immunoblots using solubilized thylakoid membranes prepared from aerobically grown cells. We measured the amount of photoactive PSI in WT and ΨH2 thylakoids (as described below) and loaded equal amounts of PSI reaction centers, as determined based on the amount of $P700^+$. When probed with anti-PsaC antibodies (**figure 3-6 A**), a band of ~10 kDa was visualized in the parental *hydA* strain ("WT" in **figure 3-6**), as expected for PsaC. In the ΨH2 strain, a band of ~50 kDa was seen, which is similar in size to the predicted PsaC-HydA1 chimeric polypeptide (54.8 kDa). No 10-kDa cross-reactive band was seen in ΨH2 thylakoids. When probed with anti-HydA antibodies (**figure 3-6 A**), there were no bands detected in the WT sample, as expected, because hydrogenase does not bind to thylakoids. A ~50-kDa band was detected in the ΨH2 sample, indicating that PsaC-HydA1 was expressed in the mutant and assembled into PSI complexes. When solubilized thylakoids were loaded on the basis of equal Chl and probed with anti-PsaA antibodies, we found that the amount of PsaA in membrane from the ΨH2 strain was ~ 2/3 that of the WT strain (**figure 3-6 B**). The presence of the PsaD subunit in the PSI-HydA1 complex was confirmed by immunoblots of solubilized ΨH2 thylakoids (**figure 3-7**).

Spectroscopic characterization of the PSI-HydA1 chimera

The light-driven generation of a stable charge-separated state in PSI can only be achieved if all core subunits carrying electron transfer cofactors are functional and properly assembled into the PSI complex. Since we replaced the PsaC subunit, which coordinates the terminal iron sulfur clusters of PSI, with the PsaC-HydA1 fusion polypeptide, we wanted to see if these FeS clusters were still present and whether we could detect the additional iron sulfur cluster within the H-cluster of hydrogenase.

Thylakoid membranes prepared from aerobically grown cultures were used as samples in a P_{700} photobleaching experiment, which detects the amount of photoactive PSI due to reversible oxidation of P_{700}. The amplitude of the P_{700}^+ signal from ΨH2 thylakoids after a saturating laser

flash was ~76% of the parental strain (**figure 3-8**). The dark recovery kinetics (**figure 3-8 A** inset) could be modeled with a 2-component exponential decay function. The faster component exhibited the characteristic time constant due to charge recombination from $(F_AF_B)^-/P_{700}^+$ (123 ± 9 ms, see **table 3-1**). This demonstrates that the PsaC-HydA1 chimeric polypeptide must be co-assembled with PSI. The slow phase (>3 s) is assigned to slow re-reduction of P_{700}^+ by ascorbate present in the medium in those PSI complexes from which the electron on the Fe-S clusters has escaped to O_2 (or other acceptors).

The presence of exogenous electron acceptors can complicate analysis of charge recombination kinetics. To remove O_2 as a potential electron acceptor, we anaerobically adapted ΨH2 cells and isolated the PSI-HydA1 complex anoxically. Another PSI-HydA1 preparation was accomplished without anaerobic adaptation and in the presence of air as a control. P_{700}^+ recovery kinetics of anoxic and oxic PSI-HydA1 after a single saturating laser flash are presented in **figure 3-8 B**. Decay of P_{700}^+ in the oxic preparation could be best described by 3 exponential decay components, with a dominant slow phase (~65% amplitude) and 2 fast components (42 and 183 ms) having similar amplitudes (19-20%) (**table 3-2**). Fitting of the decay of P_{700}^+ in the anoxic preparation, however, required a fourth component. The amplitude of the slow phase was significantly reduced, consistent with the absence of O_2. Two fast decay components with time constants of 29 ms and 86 ms (and amplitudes of 28% and 40%, respectively) were assigned to charge recombination from $P_{700}^+(F_AF_B)^-$. A novel decay component with a time constant of 270 ± 34 ms and amplitude of 14 % was also seen. This is provisionally assigned to charge recombination from the $P_{700}^+F_H^-$ state, indicating that electron transfer from the PsaC domain to the hydrogenase domain occurs upon excitation in at least some of the chimeric PSI-HydA1 complexes. It is noteworthy that WT PSI prepared anoxically lacks such a component.[34]

PSI-HydA1 activity in permeabilized cells with artificial electron donor

The HydEF and HydG maturases are necessary for insertion of the unique diiron site,

completing H-cluster assembly of the [FeFe]-hydrogenase [22]. The ΨH2 strain accumulates about 5 times as much photoactive PSI-HydA as the PSI-HydA2 chimera in the ΨH1 mutant. It was thus important to determine the time necessary for maturation of all the PSI-HydA1 chimera, as it might be longer in the ΨH2 strain if the maturases are limiting. The activity of hydrogenase can be assayed in detergent-permeabilized cells using reduced methyl viologen as electron donor. We performed this assay to determine the maximal hydrogenase activity in cells after anaerobic adaptation for various amounts of time (**figure 3-9, table 3-3**). We found that 3 hours of anaerobic adaptation is sufficient to reach a plateau. There was only ~11 % increase in the rate of H_2 production between 3 and 4 hours of anaerobic induction. We noted that longer anaerobic adaptations resulted in somewhat decreased activities. Using a ratio of 1100 Chl to P_{700} obtained spectroscopically with thylakoids, we estimate the turnover rate of the PSI-HydA1 chimera as 219 ± 15 H_2 s^{-1} in this assay. Based on a similar assay on whole cells, the specific activity of HydA1 was reported as 382 ± 97 µmol H_2 $(min)^{-1}$ mg^{-1}, equivalent to a turnover number of ~306 ± 77 H_2 s^{-1}[53]. Thus, if all of the PSI-HydA1 complexes are enzymatically active, the activity of the HydA1 domain is roughly 72% that of the free enzyme.

Like the PsaC polypeptide, the PsaC-HydA1 chimeric polypeptide is constitutively expressed in the chloroplast. In contrast, the HydA1 product is increased in anoxia by at least 6-fold[53]. This provided an opportunity to use the methyl viologen assay to test the ability of the maturases to activate the apoHydA1 in the context of the PSI-HydA1 chimeric complex. Chloramphenicol (CAM), an inhibitor of translation in the chloroplast[54], was added to cells immediately before anaerobic adaptation to block further synthesis of PSI-HydA1. (The PsaA, PsaB, and PsaC-HydA1 core subunits are all made by chloroplast ribosomes, so this will block synthesis of these subunits during the time when maturases become active.) After 4 h of anaerobic adaptation, the amount of hydrogenase activity was >90% of the control activity observed without CAM treatment (**figure 3-9**, compare red to black). Thus, we conclude that (1) degradation of the PsaC-HydA1 chimera is relatively slow, and (2) the maturases were able to activate apo-PsaC-HydA1 that had been synthesized before the shift to anoxia.

To test the ability of the maturase system to re-activate hydrogenase that had been inactivated by exposure to O_2, we took control cells that had undergone 4 hours of anaerobic adaptation (in the absence of CAM) and bubbled them with air for 5 minutes. This was sufficient to abolish all the hydrogenase activity, as verified by the assay. CAM was added immediately prior to sparging with air to prevent synthesis of new PsaC-HydA1. After a subsequent 4-h anaerobic adaptation, more than 60% of the hydrogenase activity was recovered, indicating that the algal maturases are capable of re-activating hydrogenase in more than half of the active sites previously inactivated by O_2 (**figure 3-9**, compare blue to black).

Hydrogen production in vivo

We first examined the chimera's ability to carry out H_2 production *in vivo* in the dark. For H_2 production to take place, the electron donor (reduced Fd) must transiently bind to PsaC-HydA1 and transfer an electron to one of the iron-sulfur clusters, ultimately arriving at the H-cluster; this must happen twice for each H_2 produced. Since our previously published ΨH1 mutant (PSI-HydA2 chimera)[34] could generate H_2 in the dark, it was of interest to test the ability of Fd to bind the PSI-HydA1 chimera *in vivo*. With GC-TCD we probed the headspace of cultures in sealed glass bottles to measure H_2 accumulation by ΨH2 (**figure 3-10 A**). The average rate was 1.13 ± 0.05 µmol H_2 h^{-1} (mg Chl)$^{-1}$ and remained linear over a 3-hour period (for maximal dark rate see **table 3-3**). For comparison, the rate in the WT parental strain expressing *HYDA1* and *HYDA2* genes (D66) was ~ 0.5 ± 0.03 µmol H_2 h^{-1} (mg Chl)$^{-1}$ over a 6-hour period [34].

We next measured H_2. In 1 hour, ΨH2 cells produced 18.4 ± 2.7 µmol H_2 (mg Chl)$^{-1}$ when supplied with acetate, which is not significantly better than without acetate (17 ± 2 µmol H_2 (mg Chl)$^{-1}$). In the presence of acetate, the amount of H_2 produced peaked at 2 h, switching to H_2 uptake afterwards. In the absence of acetate, H_2 continued to climb throughout the course of the experiment (18 h), albeit at a much smaller rate (~2.5 µmol H_2 h^{-1}(mg Chl)$^{-1}$ for 16 h). Net O_2 evolution (**figure 3-10 B**) was not significantly different in the presence or absence of acetate (2 ±

2 vs. 2.6 ± 1 μmol O_2 h^{-1} (mg Chl)$^{-1}$, respectively) in the first 3 hours. However, after overnight incubation with acetate, accumulation of O_2 in the ΨH2 culture headspace was significant (~8 %); in ΨH2 cultures without acetate, O_2 remained low (~0.1%).

It is worth mentioning that after 18 hours of illumination, ΨH2 cells in the presence of acetate grew well while ΨH2 cells without acetate hardly grew at all. The overnight growth was accompanied by H_2 consumption and O_2 production. Meanwhile, ΨH2 cells without acetate produced ~50% increase in headspace H_2 overnight, and only a marginal increase in O_2 was observed (**figure 3-10**).

Addition of 3-(3,4-dichlorophenyl)-1,1-dimethylurea (DCMU) – a potent PSII inhibitor – to cultures without acetate resulted in a ~6-fold decrease in H_2 production (**figure 3-10 A**, green symbols). No O_2 in the headspace was detected in experiments with DCMU or dark, as expected (**figure 3-10 B**).

To test whether co-produced O_2 limits the activity of the PSI-HydA1 chimera, H_2 evolution was measured in the absence and presence of O_2 absorbent in an H_2 production system making use of an O_2 absorbent that keeps O_2 concentration below 0.05% and a carbon-free media, which prevents CBB cycle activity[30]. The amount of H_2 produced in 24 h increased three-fold in the presence of O_2 absorbent (**figure 3-11**). For four consecutive days, the daily H_2 production remained the same in the absence of O_2 absorbent (~110 μmol H_2 (mg Chl)$^{-1}$ was produced in total). With O_2 absorbent, the amount of daily H_2 production diminished to some extent but remained more than two-fold higher than without the absorbent (~270 μmol H_2 (mg Chl)$^{-1}$ in total; **figure 3-11 D**). In four days the ΨH2 strain produced 1.8-fold or 2.1-fold more H_2 than the D66 control strain in the absence or presence of the O_2 absorbent, respectively (**figure 3-11 D**).

Membrane inlet mass spectrometry (MIMS) was employed to monitor ion currents as a proxy for dissolved H_2, O_2 and CO_2 concentrations. Preadapted cells were subject to increasing intermittent illumination, followed by continuous illumination, as shown in **figure 3-12**. The

maximal rate at each intensity were measured during the 2-min illumination interval, which was followed by 3 min of darkness (**figure 3-13**). Under low CO_2 conditions, the H_2 production rate saturated at about 600 µmol photons m^{-2} s^{-1} and only slightly increased at double the intensity. The rates were not very different in the presence or absence of acetate, although in the presence of acetate the rate seemed to saturate at somewhat lower intensities (see **table 3-3, figure 3-13 A**). Addition of 2 mM bicarbonate to acetate-free medium caused the light-saturated H_2 evolution rate to decrease by ~33%. Addition of 10 µM DCMU resulted in a ~10-fold drop in the H_2 evolution rate, consistent with what was observed in **figure 3-10**.

The maximal O_2 evolution rate (**figure 3-13 B**) increased with increasing light flux for cultures without acetate, reaching 5-8 µmol O_2 h^{-1} (mg Chl)$^{-1}$. In the presence of acetate, it saturated at 170 µmol photons m^{-2} s^{-1}, then dropped by ~60% with increasing light. As expected, addition of DCMU completely inhibited O_2 evolution. Under all three conditions, the ΨH2 strain did not perform net CO_2 uptake but instead evolved CO_2 under all light intensities (**figure 3-13 C**). In fact, CO_2 evolution increased with increasing light intensity, to a maximal observed rate of 8-11 µmol CO_2 h^{-1} (mg Chl)$^{-1}$; it was somewhat higher in the presence of acetate, consistent with higher respiration rates. The decrease in O_2 evolution rate coincided with an increased CO_2 evolution rate (**figure 3-13 C**) observed in the presence of acetate at higher light intensities, suggesting that the two phenomena might be related as a result of increased respiration.

Physiological consequences of replacing PSI with PSI-HydA1

The instantaneous rates of H_2 evolution measured during the first 2 min of illumination did not match well the rates observed during longer irradiances (**figure 3-10**, except for the DCMU results). The H_2 production rate started high, but quickly dropped to very low values and even became negative in the presence of acetate. This was reminiscent of the pattern often reported for wild-type algae using unmodified hydrogenases. Moreover, the fact that there was always net CO_2 production rather than consumption indicates that the CBB cycle was largely inactive under

these conditions. Lower than expected net O_2 production rates were also seen, likely due to either high initial respiration rates (see **figure 3-14**) or a bottleneck effect created by the PSI-HydA1 chimera similar to what was seen with the PSI-HydA2 construct [34]. The latter effect is supported by Chl fluorescence induction measurements (see below, **figure 3-15**).

To bridge the gaps in our understanding of the physiology of ΨH2, we monitored H_2, O_2, and CO_2 with MIMS during a 30-min period of continuous high illumination (1435 µmol red photons m^{-2} s^{-1}) using cells that had just undergone the cycles of increasing light (2 min ON, 3 min OFF) shown in **figure 3-16**. In ΨH2 cultures lacking acetate or bicarbonate, H_2 production rates exhibited high variability (**figure 3-16 A**). They reached near maximal levels (53 ± 15 µmol H_2 h^{-1} (mg Chl)$^{-1}$) in 1 minute, followed by a decline that resulted in net H_2 uptake after ~15 minutes of illumination. Oxygen evolution rates had a small initial spike (~7 ± 3 µmol h^{-1} (mg Chl)$^{-1}$) when the H_2 production rate reached its maximum, followed up by a dip (net O_2 uptake) that mirrored the simultaneous decline in H_2 and CO_2 production rates. Shortly before the switch from net H_2 production to uptake, O_2 production rates started to rise again while CO_2 rates were net negative, implying increasing activity of the CBB cycle. For reference, the dissolved CO_2 concentration in water equilibrated with air at 24 °C and atmospheric pressure is ~15 µM, which is less than what we observed under experimental conditions (**figure 3-17 A**). As the lights went out, H_2 uptake rates increased, reaching a maximum of 44 ± 16 µmol H_2 h^{-1} (mg Chl)$^{-1}$; this indicates that hydrogenase activity was mostly preserved, since the rate of H_2 uptake (presumably catalyzed by the hydrogenase domain fused to PSI) was ~80% of the maximal H_2 production rate in the light. The respiration rate in the dark reached ~35 ± 12 µmol O_2 h^{-1} (mg Chl)$^{-1}$ as CO_2 fixation switched to CO_2 evolution (~11 ± 3 µmol CO_2 h^{-1} (mg Chl)$^{-1}$). Dissolved O_2 rose to its highest level (~20 ± 6 µM) only towards the end of the illumination and is likely responsible for the partial inactivation of the hydrogenase domain (**figure 3-17 A**). Taken together, the early drop in H_2 production by ΨH2 is mainly due to activation of the CBB cycle, not to inactivation of the hydrogenase active site.

Under similar conditions (no added bicarbonate or acetate), wild type cells (D66) exhibited a sudden surge in H_2 evolution that switched to net H_2 uptake within 5 min, much earlier than the ΨH2 strain (**figure 3-16 B**). The O_2 production rate rose to 14 ± 9 µmol h^{-1} (mg Chl)$^{-1}$, followed up by a dip associated with H_2 uptake. Shortly after, CO_2 fixation commenced, reaching 5 µmol CO_2 h^{-1} (mg Chl)$^{-1}$. After 15 minutes, the net CO_2 rate approached the compensation point due to apparent substrate limitation (no exogenous bicarbonate was added to the media and CO_2 concentration decreased considerably – **figure 3-17 B**). Interestingly, after the light went out, there was still some residual hydrogenase activity, judging by a drop in H_2 in the dark corresponding to -5 µmol H_2 h^{-1} (mg Chl)$^{-1}$, which is ~7% of the maximal production rate in the light. This can be explained by a rise in O_2, up to 37 µM, inactivating most of the endogenous hydrogenase activity. The CO_2 production rate increased to about 10 µmol h^{-1}(mg Chl)$^{-1}$ and O_2 consumption briefly reached 45 µmol h^{-1} (mg Chl)$^{-1}$, as expected for respiration in the dark; note that the absolute rate of CO_2 uptake is likely underestimated due to the buffering by bicarbonate.

Under conditions of excess bicarbonate (without acetate), ΨH2 cells showed a much smaller initial surge in H_2 evolution (~35 µmol H_2 h^{-1} (mg Chl)$^{-1}$), which switched to H_2 uptake within 2 minutes of the onset of light (**figure 3-16 C**). This led to rapid depletion of the dissolved H_2 pool within 15-20 min (**figure 3-17 C**). At the same time, O_2 production rates were higher than before depletion of H_2 and continued climbing, reaching ~35-40 µmol O_2 h^{-1} (mg Chl)$^{-1}$. The onset of CO_2 fixation coincided with the decline in H_2 production rate and remained steady for the rest of the experiment. Once the light was off, there was no H_2 uptake, as there was essentially no H_2 left in the media; the O_2 uptake rate was 45 µmol h^{-1} (mg Chl)$^{-1}$ and CO_2 evolution reached ~20 µmol h^{-1} (mg Chl)$^{-1}$and then declined.

Addition of 40 mM glycol aldehyde (GA) – an inhibitor of the CBB cycle – to ΨH2 cells in the presence of bicarbonate resulted in an increased initial H_2 evolution rate of ~45 µmol h^{-1} (mg Chl)$^{-1}$ (**figure 3-16 D**). Moreover, the rate remained overall positive for the duration of illumination. Only after the light was off did it become negative (~-25 µmol H_2 h^{-1} (mg Chl)$^{-1}$). The O_2 evolution

rate spiked immediately to 15 µmol h^{-1} (mg Chl)$^{-1}$, followed by a negative dip and then approached the compensation point for the remainder of the experiment. Similarly, dissolved O_2 increased briefly to ~10 µM and quickly dropped to near zero for the rest of the illumination period (**figure 3-17 D**). After the light was off, O_2 consumption commenced but was small (~5 µmol h^{-1} (mg Chl)$^{-1}$) due to the lack of available O_2. The CO_2 production rate remained positive during the experiment, indicating that no carbon fixation was taking place, as expected.

Acetate-supplemented ΨH2 cells produced inconsistent results in the 30-min illumination MIMS experiment (see below, **figure 3-18 – 3-19**). In one trial (**figure 3-18 A-19 A**), H_2/CO_2 uptake started 9 min after illumination, while the other 2 trials showed no net H_2 uptake during first 30 min. In another run (**figure 3-18 B - 19 B**), H_2 uptake occurred only after spiking the media with 2 mM bicarbonate during the extended illumination (~2 h). In a further run, we attempted to test the hypothesis that substrate limitation (CO_2) is the reason for low activity of CBB in ΨH2. After 30 min of illumination without significant net H_2 uptake, bicarbonate was added in the dark and illumination was restarted (**figure 3-18 C – 19 C**). After a brief burst of H_2 production, H_2/CO_2 consumption followed within 4 min and continued until most of the H_2 was consumed.

On variability of CBB activation in ΨH2 with acetate in the media

Our previous observations of the ΨH1 mutant demonstrated the benefits of adding acetate to the media for H_2 production, in terms of both maximal rate and longevity. Our long-term experiments with ΨH2 did not show a clear advantage of having acetate in the media for H_2 production (**figure 3-10**), likely due to H_2 consumption during cell growth. On the other hand, initial maximal H_2 rates during light saturation indicated that H_2 production benefited from addition of acetate especially at lower light intensities (**figure 3-13 A**). To further explore this phenomenon, we extended illumination on the MIMS ΨH2 samples containing acetate and found large variability between runs (**figure 3-18 and 3-19**). In the lowest performing trial, the H_2

production rate at the light onset was only 33 μmol h^{-1} (mg Chl)$^{-1}$ and quickly dwindled followed by H_2 uptake (after 9 min of illumination) (**figure 3-18 A**). H_2 consumption coincided with an increase in the rate of carbon uptake and decreased only when H_2 concentration dropped below 10 μM (**figure 3-19 A**). At the time of H_2 depletion, the O_2 concentration started to build up (**figure 3-19 A**), which could also inactivate hydrogenase. Nevertheless, there was at least 30% hydrogenase activity remaining intact as judged by H_2 uptake after the lights were off. The O_2 production rate had a tiny spike and then remained close to zero, becoming slightly positive in the last 7 min of illumination, with O_2 reaching 6.4 μM. In the dark, O_2 uptake rose to 20 μmol h^{-1} (mg Chl)$^{-1}$ but was limited by O_2 concentration. CO_2 was produced for the first 9 min followed by uptake. Once the light was off, the CO_2 production rate jumped to ~20 μmol h^{-1} (mg Chl)$^{-1}$.

In the best performing trial (**figure 3-18 B**), ΨH2 cells had high initial H_2 production rate (60 μmol h^{-1} (mg Chl)$^{-1}$ that fell gradually to ~ 5 μmol h^{-1} (mg Chl)$^{-1}$ but never switched to net H_2 uptake during first 30 min of illumination. Net O_2 production rate was close to zero and CO_2 rate was slightly positive in the first 30 min indicating minimal CBB cycle activity. During 2 min of darkness, the H_2 uptake rate was rather small (-5 μmol h^{-1} (mg Chl)$^{-1}$), despite ~180 μM of H_2 available (**figure 3-19 B**) and O_2 uptake – non-existent (due to lack of O_2 and presence of H_2). Interestingly, a small CO_2 uptake in the dark coincided with H_2 uptake in the dark. Since 30 min illumination did not lead to high activity of CBB cycle, we decided to proceed and turn illumination back on. The H_2 production rate spiked to 15 μmol h^{-1} (mg Chl)$^{-1}$ then decreased but remained positive for the next 90 min of illumination. O_2 and CO_2 rates remained close to zero. H_2 concentration reached 192 μM, O_2 stayed less than 2 μM and CO_2 less than 41 μM. About 2 hours after onset of continuous illumination, we added bicarbonate – a substrate for Rubisco. It triggered profound changes resulting in a H_2 uptake rate of 50 μmol h^{-1} (mg Chl)$^{-1}$ and activation of CBB cycle as judged by the CO_2 uptake rate. Absence of steep raise in oxygen levels suggest that most electrons came from H_2 oxidation rather than water oxidation and/or O_2 was partially oxidized by PSI-HydA1 chimera. It is worth noting that the initial CO_2 concentration at the onset of long illumination between the worst and the best performing trial (43 μM vs 33 μM) as well as

their maximum levels (52 µM vs 42 µM) were not much different. Moreover, CO_2 concentration in cultures without acetate (**figure 3-17 A**) was much less on average (~20 µM) yet resulted in CBB activation.

In the third trial (**figure 3-18 C**), ΨH2 cells had slightly lower initial H_2 evolution rate peaking at 53 µmol h^{-1} (mg Chl)$^{-1}$ and gradually decreasing. Significant H_2 uptake did not start until the light was switched off at 30 min. Dissolved H_2 concentration started at the same level as in the best performing trial (~78 µM) but only reached to 154 µM at the end of the 30 min illumination (**figure 3-19 C**). Net O_2 rate was zero as there was no O_2 during first 30 min of illumination. CO_2 evolution rate reached to ~10 µmol h^{-1} (mg Chl)$^{-1}$ in the first 2 min just like in the previous trials, but then gradually become slightly negative after ~13 min of illumination. After spiking bicarbonate in the dark, H_2 uptake rate briefly increased to ~130 µmol h^{-1} (mg Chl)$^{-1}$, then returned to the previously observed dark rate of ~18 µmol h^{-1} (mg Chl)$^{-1}$. Once we restarted illumination, there was a quick burst of H_2 production (4 min) followed up by H_2/CO_2 uptake in the light (~ -50 µmol H_2 h^{-1} (mg Chl)$^{-1}$ and ~8 µmol CO_2 h^{-1} (mg Chl)$^{-1}$). Oxygen did not start to accumulate until most H_2 was consumed.

Cyclic electron flow (CEF) in ΨH2

CEF around PSI is an effective way to deal with ATP shortages in the light. In the typical paradigm of oxygenic photosynthesis, electrons from the acceptor side of PSI can enter the plastoquinone pool, thus forming a cycle. To test ΨH2's ability to perform CEF under fully aerobic conditions (where they cannot produce H_2), we added 10 µM DCMU to cells and then illuminated them for 10 s, after which the P_{700}^+ decay rate was measured as a proxy for CEF (**figure 3-20**). We found that the rate constant for P_{700}^+ decay in ΨH2 was 36.6 ± 4.4 s^{-1}, which is almost twice the rate of D66 (WT) strain (15.4 ± 0.4 s^{-1}). Addition of 20 µM DBMIB – an inhibitor of the Q_o site of cytochrome b_6f – resulted in low rates of decay in both strains (~2-2.5 s^{-1}).

Flavodoxin photoreduction in vitro

The hydrogenase domain of PSI-HydA1 was expected to block native electron acceptors (flavodoxin/ferredoxin) from binding to PSI. We tested this by carrying out an *in vitro* assay with purified PSI/PSI-HydA1 (~0.1 µM), plastocyanin (50-fold excess of PSI) and ascorbate (5 mM) as immediate and sacrificial electron donors to PSI, respectively, and flavodoxin (50-fold excess) as electron acceptor (**figure 3-23**). The assay was carried out under oxic conditions; therefore, we only expect the [Fe_4S_4] cluster of the H-cluster be present in the chimera. Flavodoxin reduction was mostly blocked in PSI-HydA1 (only ~13% WT rate) from the rate determined from the linear fit to the full 10-s illumination dataset. It is worth pointing out that the relative rate decrease over time was higher for the PSI-HydA1 chimera than for the WT. To study this, we applied a quadratic equation to the same dataset (which improved the goodness of fit significantly) and found that the initial rate of flavodoxin reduction (first derivative of the quadratic equation at time 0) by PSI-HydA1 was 14.2 % of the WT (0.15 s^{-1} vs 1.04 s^{-1}). The drop in the rate over time was calculated from a coefficient next to quadratic variable. To account for difference in the initial rates, we normalized the quadratic coefficients to the respective rates. The resulting normalized drop in the rate by WT and PSI-HydA1 were -0.025 s^{-1} and -0.030 s^{-1}, respectively. In other words, PSI-HydA1 normalized rate drop was ~21% higher than WT (see **table 3-4)**. This agrees with empirical slope determination at shorter time intervals from origin and consecutive relative rate determination. Since acceptor limitation (availability of oxidized flavin as opposed to semiquinone form) cannot explain this increased drop in the rate (~16 % semiquinone of the total flavin was produced by the WT PSI and only ~ 2% by the PSI-HydA1 at the end of illumination), we attribute this to the reaction with O_2 to a greater degree and subsequent destruction of [Fe_4S_4] clusters. Applying the same analysis to the previously published PSI-HydA2 data[34], we find that initial rate of flavodoxin reduction by PSI-HydA2 was 12.9% WT control, however, normalized drop in the rate was 2.7 times higher than for the PSI-HydA1 (227 % of the WT rate drop).

Effect of flavodoxin on electron escape in a single flash experiment

Another way to look at the interaction between PSI and flavodoxin is to quantitate the fraction of electrons that reduced flavin to semiquinone form after a saturating laser flash. Escaped electrons will not contribute to fast charge recombination components (<1 s) and therefore will have to be replenished by ascorbate (slow, >1 s). We used the same ingredients as in the flavodoxin reduction kinetic experiment, except for plastocyanin. To quantitate the fraction of electrons that escaped, we integrated the P_{700}^{+} normalized signal (fitted to the 4-exponential decay) with and without flavodoxin. Area difference (corresponding to electrons*ms) was scaled with the time constant corresponding to the slowest phase of P_{700}^{+} decay with flavodoxin. The experiment was performed under oxic conditions; however, we do not have reasons to believe that the levels of O_2 were significantly different between the trials. Our findings (**figure 3-22**) suggest that, although PSI-HydA1 is not as good as PSI in terms of reducing flavodoxin (47 % of WT), it is almost 3 times better than PSI-HydA2 (17 % of WT).

Discussion

Design and operational characteristics of the PSI-HydA1 chimeric protein

In this paper we applied the principles of rewiring PSI for alternative electron acceptors to produce a PsaC-HydA1 chimera capable of assembling on PSI and performing proton reduction *in vivo* using electrons extracted from water by PSII. One of the goals in our design was to explore the differences between the 2 endogenous hydrogenases of *C. reinhardtii* and how they affect the efficiency of chimeric protein assembly. Therefore, we preserved the same linking regions between the PsaC and HydA domains as we had done earlier in the PsaC-HydA2 fusion polypeptide. For the N-terminal junction (i.e., PsaC-HydA1), we used the exact same PsaC-HydA2 linking sequence (**figure 3-2, blue box**), since the HydA1 N-terminus sequence was significantly different. For the C-terminal junction (i.e., HydA1-PsaC), we decided to use the native C-terminal sequence of HydA1, as it was different in only 1 amino acid from the HydA2

sequence and did not change the predicted secondary structure of the linker (**figure 3-2, red box**).

PsaC-HydA1 and PsaC-HydA2 were introduced into the same strain lacking both endogenous hydrogenases (*hydA*). To our surprise, the PSI-HydA1 chimera could accumulate to a level ~5 times higher than the PSI-HydA2 chimera, based on both spectroscopic and immunoblotting data. Although, the turnover number of PSI-HydA1 (220 ± 15 H_2 s^{-1}) was similar to HydA1(~300 ± 80 H_2 s^{-1})[53] in RMVA, it was lower than that of the PsaC-HydA2 chimera (530 ± 110 H_2 s^{-1}) [34].

Light-driven charge separation is at the heart of photosynthetic reaction center function, providing a path to efficient conversion of electromagnetic quanta into chemical bonds. PSI is well known for a quantum yield of charge separation near unity; i.e., forward electron transfer far outcompetes charge recombination at every step under physiological conditions. With the hydrogenase appendage on the acceptor side of PSI placing the H-cluster within 15 Å of F_B (edge-to-edge, according to our model **figure 3-4**), we have extended the electron transfer chain. In pump-probe experiments, we observed charge recombination with time constants previously associated with $P_{700}^+(F_AF_B)^-$ (30-40 ms and 80-180 ms); in anoxia (i.e., absence of electron acceptors), a new component with a longer time constant (~270 ms) was seen, which we have assigned to $P_{700}^+F_H^-$ charge recombination. We suspect that this component is suppressed in the presence of O_2 due to oxidation of F_H^- by O_2 and/or destruction of the active site by O_2. Together with the evidence from the methyl viologen assay, we have ascertained that the PSI-HydA1 chimera is both photoactive and fully capable of making H_2.

In vivo characteristics of the ΨH2 mutant

The *in vivo* performance of the PSI-HydA1 chimera was first evaluated for its ability to accept electrons in the dark from the reduced Fd pool, which serves as a measure of its connection to algal metabolism. The ΨH2 mutant showed ~4 times higher H_2 evolution rate in the

dark as compared to ΨH1 mutant. This is only slightly higher than what might be expected, given the ~5-fold higher accumulation of the chimeric complex and the ~2-fold lower turnover frequency. The reversible nature of the hydrogenase enzyme (H_2 oxidation vs reduction) must hold true for PSI-HydA1 chimera as well. In addition, we can conclude that ferredoxin can bind to and deliver electrons to PSI-HydA1, despite our efforts to exclude Fd from H_2 metabolism.

Photobiological H_2 production in the ΨH2 mutant could be subdivided into 3 phases, based on activity of the major electron sinks for the PETC after the anaerobic dark-to-light transition: (1) **positive** (CBB cycle is mostly inactive, H_2 production rate reaches maximum and there is net CO_2 production); (2) **transitionary** (CBB cycle becomes somewhat active, H_2 production rate drops, and CO_2 production shifts to CO_2 uptake); (3) **negative** (CBB cycle is active, H_2 uptake rate increases, CO_2 uptake rate is high).

In the positive phase, the ΨH2 mutant performs similarly to ΨH1 in terms of the maximal rate of H_2 production and greatly outperforms the WT strain under conditions of bicarbonate excess.[34] When one compares turnover frequencies, however, the ΨH2 mutant does not look so good. The in vivo maximal rate of 60 µmol H_2 h^{-1}(mg Chl)$^{-1}$ translates to 16.5 H_2 (PSI)$^{-1}$ s^{-1} or 33 electrons (PSI)$^{-1}$ s^{-1}. That is 10 times less than the rate obtained with the PSI-HydA2 chimera.[34] When no bicarbonate is added, maximal rates are higher for both ΨH2 and WT, indicating that competition for electrons between H_2 production and CO_2 fixation exists even at this early stage. Acetate has only a marginal effect on maximal H_2 production rates by ΨH2 under CO_2-limiting conditions on a short time scale. Net O_2 production rate in the early phase is less than what is expected from linear electron flow stoichiometry and is likely due to consumption of O_2 by respiratory processes. The observed CO_2 production in consistent with active respiration and lack of significant CO_2 fixation. The effect of DCMU shows that electrons from water oxidation are crucial for high rates of photobiological H_2 production in the ΨH2 mutant, in line with what was previously observed for WT algae [55].

The O_2 production observed in ΨH2 is significantly different from the ΨH1 strain, which only produced O_2 at very high light intensities, and this could be completely suppressed by the addition of acetate[34]. At the time we hypothesized that the low abundance of the PSI-HydA2 chimera resulted in a bottleneck in electron flow, which constrained upstream processes including water oxidation by PSII; we further postulated that the maximal O_2 production rate was sufficiently low that respiration could prevent O_2 from accumulating. The experiments with ΨH2 reported here have effectively tested this hypothesis. Despite the fact that the turnover rate of PSI-HydA1 is roughly half that of PSI-HydA2, its ~5-fold higher abundance results in much less of a constraint on PSII, such that the compensation point (where O_2 production exceeds uptake) is reached at much lower light intensities for ΨH2. This likely explains why O_2 never accumulated when the ΨH1 strain was grown with acetate in the light, and why H_2 production was sustained for days rather than hours.

The transitionary phase can be observed when no bicarbonate is added to the media and there is no significant inorganic carbon assimilation taking place. The duration of this phase seems to vary with the time it takes for cells to adapt to low CO_2 concentrations, which is likely a major source of variability between culture samples. Like the WT, the ΨH2 strain has a short transition when bicarbonate is added (e.g., compare panels B and C in **figure 3-16**). Addition of acetate to the media (without added bicarbonate) seemed to hinder CBB cycle activity despite higher dissolved CO_2 concentrations and could even postpone the transition for more than an hour in some instances (**figure 3-18 B, figure 3-19 B**).

In the negative stage of H_2 production, when the CBB cycle is active, we observed both H_2 uptake and CO_2 assimilation. The duration of H_2 uptake depends on the bicarbonate concentration (**figure 3-17 A and C**), unless H_2 itself is limiting. With acetate in the media, H_2 uptake continues until most of the H_2 is depleted (**figure 3-19**). The exemplary case of H_2 uptake was seen after addition of bicarbonate to anaerobic ΨH2 cells locked in a “steady state” (net H_2 production rate approaching zero) during illumination (**figure 3-18 B and C**). Unsurprisingly, there

is no significant O_2 rise until most of the H_2 is gone (**figure 3-17 A&C, figure 3-19**). The so-called oxyhydrogen reaction ($2H_2$ and O_2 assimilation), first reported by Gaffron [16], takes place at low (<1%) O_2 and is the most likely explanation for this phenomenon. That is especially true for ΨH2 cultures supplemented with acetate. H_2 uptake can also explain our long-term experiments with sealed cultures. With acetate in the media, cells consumed headspace H_2 to a greater extent before O_2 inactivated the PSI-HydA1 hydrogenase activity (**figure 3-10**). It is worth noting that H_2 partitions into the headspace and therefore the concentration of the dissolved H_2 is much lower.

We can explain the observed variability in the timing of the transition from the positive to the negative phase of H_2 production as variability in the timing of the onset of CO_2 fixation by the CBB cycle. Suboptimal rates of photosynthetic O_2 evolution and CO_2 assimilation, which we repeatedly saw in MIMS experiments without added bicarbonate, suggested that the CBB cycle activity was low in those instances. The fact that O_2 evolution and CO_2 uptake could be stimulated by addition of 2 mM bicarbonate at the beginning of the experiment point to substrate limitation as the origin of this effect. Green algae have a carbon-concentrating mechanism (CCM) that helps them cope with low CO_2 concentrations. The CCM is upregulated under low CO_2 conditions, but it requires high light under mixotrophic conditions to “sense” low CO_2[56]. This is likely due to uptake of acetate under high light conditions that preferentially enters the glyoxylate cycle, which was shown to be boosted by increased photorespiratory glycolate in *Chlorella sorokiniana*.[57] Increased demand for CO_2 may create a CO_2 shortage and subsequent CCM upregulation.[58] Under lower light, mixotrophy and aerobic conditions acting simultaneously, there is enough CO_2 made in the mitochondria from acetate oxidation to suppress the CCM[59]. Artificially imposed anoxia helps to maintain low-CO_2 conditions in cultures supplemented with acetate. We conclude that variability in the onset of CO_2 assimilation is a result of capturing cells at different stages of adaptation to low CO_2, which is extenuated by the inclusion of acetate.

Addition of glycolaldehyde inhibits the CBB cycle, and as a result ΨH2 continuously produces H_2 in the light for the time of the experiment (1 hour) (**figure 3-16 D and 3-17 D**),

consistent with our expectation that H_2 evolution competes with CO_2 assimilation activity.

Hydrogenase inactivation by O_2 quickly follows during the negative stage of H_2 production. The most O_2 was produced by ΨH2 cultures with added bicarbonate in the 30-min illumination experiment (**figure 3-16 C**). Since the algal hydrogenase are reversible [18], inactivation of the HydA active site can be detected by loss of H_2 uptake activity after the light is off. Our data shows that during the 30-min illuminations, some hydrogenase activity in the PSI-HydA1 chimera is preserved despite the O_2 increase (**figure 3-16 A** and **3-17 A**). It was previously reported that activity can be restored to algal hydrogenases after complete O_2 inactivation followed by anaerobic readaptation [60]. However, it was not clear whether the hydrogenase had to be re-expressed. As the hydrogenase domain of PSI-HydA1 is made by chloroplast ribosomes, rather than cytosolic ribosomes (which still make the maturases), we were able to separate expression of the hydrogenase catalytic domain from expression of the maturases. Using an inhibitor of chloroplastic translation, we showed that after complete inactivation by O_2, most (≥60%) of the hydrogenase activity of the PSI-HydA1 chimera can be restored in vivo after restoration of anoxia (**figure 3-9**). This is in line with previous findings that attack by O_2 dismantles the diiron site first and a new diiron site can be installed by the maturases in vitro [24].

A state-of-the-art technique involving continuous O_2 removal from the headspace (below <0.05%) with iron-based absorbent was tested with the ΨH2 strain to assess its potential for long-term photobiological H_2 production. The use of the absorbent resulted in increase in yields of H_2 produced of 50-200%. In the original method with WT algae, the level of preservation of hydrogenase activity after 96 h was ~2.5 times higher (as measured by RMVA) with O_2 absorber (~5% of the maximal) than without (~2% of the maximal) [30]. Since we showed that hydrogenase can be continuously reactivated *in vivo* without significant loss in activity, we speculate that with the help of O_2 absorber the equilibrium of inactivation/reactivation reactions is shifted towards reactivation. Higher yields of H_2 production in ΨH2 compared with D66 control are likely due to

higher and constitutive expression of PsaC-HydA1 as compared with endogenous hydrogenases of D66. Therefore, we conclude that PSI-HydA1 chimera is likely not significantly more O_2 resistant under the tested conditions than the algal endogenous hydrogenases and a search for O_2-resistant hydrogenase is needed.

Chlamydomonas PSI mutants that accumulate lower amounts of PSI have been known to exhibit inability to grow in the light and O_2, or what is also called light-sensitive phenotype[61]. We argue that light sensitivity can be traced back to the effect PSI-HydA1 bestows upon ΨH2 metabolism. Under aerobic, CO_2-replete conditions, we observed a significant decrease in the quantum yield of PSII in the ΨH2 strain compared to the parental strain only under high light conditions (>500 µmol m^{-2} s^{-1}) (**figure 3-15**). This indicates that linear electron flow under oxic conditions is barely hindered and the plastoquinol pool becomes reduced in the light by PSII when it encounters a bottleneck in the form of the PSI-HydA1 chimera (lacking H-cluster) only at very high light. This is consistent with our measurements of gross O_2 evolution rate, which was similar between ΨH2 and the parental strain under high light, aerobic and CO_2-replete conditions (**figure 3-14**), as well as MIMS data (**figure 3-16 C** and **3-17 C**). However, these experiments were done in relatively short time scales (2-30 min of illumination) and seemingly contradicted the long-term growth assay that shows no growth by ΨH2 on plates supplemented with bicarbonate in air (**figure 3-23**). The same cells could grow under microaerobic high-CO_2 conditions. Therefore, we conclude that there is a long-term detrimental effect of O_2 on ΨH2 cells. With acetate, ΨH2 growth lags parental strain on the 2nd day (**figure 3-23**) but only in air and the difference in growth is diminished when O_2 is diminished. We hypothesize that O_2 interacts with the acceptor side of the PSI-HydA1 chimera and destroys the H-cluster (including the [4Fe-4S] cluster) over time. Consequently, the light-sensitive PSI-less phenotype[61] emerges as electrons from PSI-HydA1 can no longer reach Fd, as it is the [4Fe-4S] cluster of the HydA1 domain that reduces ferredoxin (see below).

Strong evidence for Fd binding to the chimera in the ΨH2 strain suggested that, if our

PSI-HydA1 model (**figure 3-4**) is reliable, we should be able to demonstrate such an interaction with it as well. In WT PSI, Fd1 binds to the PsaC, PsaD, and PsaE subunits primarily via electrostatic interactions, resulting in the most energetically favorable model bringing the [2Fe-2S] cluster of Fd1 as close as 9.7 *Å* to F_B[62]. Using PsaC, PsaD and PsaE subunits of algal PSI (6JO5) and Fd1 (2N0S), we could dock Fd in a similar way using only a single distance restraint of 2-20 Å between Cys14 of PsaC and Cys42 of Fd. These residues correspond to the outermost cysteines coordinating iron-sulfur clusters (F_B and [2Fe-2S] of Fd) and are only ~5-7 *Å* apart from each other in the best model of [62]. When we used the same distant restraint for docking of Fd1 to the PsaC-HydA1/PsaD subunits of the PSI-HydA1 model, we were surprised to find Fd1 binding to the opposite side of the PsaD-PsaC ridge (**figure 3-24**) from what is seen with WT PSI. In the most favorable model of docked Fd1, its [2Fe-2S] cluster is actually closer to the [4Fe-4S] cluster of the HydA1 active site (13.0 Å) than to F_B (14.7 Å). Only 3 polar contacts of Fd1 with the PsaC-HydA1 polypeptide play a role in docking, while 10 are formed between Fd and PsaD (**table 3-5**). This suggests that PsaD binding to PSI-HydA1 complex is important for Fd binding and does not deviate significantly from that of WT PSI, which was assumed in our model. We did not consider using PsaE in the PSI-HydA1 model (or in docking) because its native site near PsaC is almost entirely occupied by the hydrogenase domain of the chimera and it is highly unlikely to bind in the same fashion as in WT PSI. Thus, as we concluded for PSI-HydA2 [34], it is most likely that electrons exit the PSI-HydA1 complex to Fd from the hydrogenase domain rather than from the PsaC domain.

The most favorable model of Fd1 binding to PsaC-HydA2/PsaD (using the same distance restraint) did not produce the same distances and overall predicted a binding site further from the electron transfer cofactors of PSI-HydA2. This difference is likely due to structural differences between the two chimeras, specifically in the opening between the PsaC and HydA domains. This is somewhat larger in the PSI-HydA1 model, mainly due to a larger angle between the HydA domain and the stromal surface of PSI. The size of the inter-domain space may depend on (1) the interaction of the HydA1 domain with PsaA and PsaF, (2) the size of the HydA1 domain (7

residues shorter than HydA2) and (3) the presence of alanine in the C-terminal linking region of HydA1 (as opposed to proline in HydA2). These results point to interesting structural differences between the PSI-HydA1 and PSI-HydA2 chimeric complexes, which were not initially expected. They also indicate that better structural predictions will be required in the future to make more rapid progress in chimeric protein design and testing.

To compare the PSI-HydA1 and PSI-HydA2 chimeras with wild type PSI in its ability to pass electrons to acceptors, we used an *in vitro* assay that relies on the ability of PSI to reduce flavodoxin to its semiquinone form, using flavodoxin reduction as a proxy for Fd reduction (**figure 3-21**). We found that electron flow towards flavodoxin is significantly hindered relative to WT PSI (~13% of the WT rate). In the same experiment, PSI-HydA2 showed an even lower ability to reduce flavodoxin (~11 % of WT) [34]. In a single flash experiment, we found that PSI-HydA1 is ~3 times better at giving electrons to flavodoxin than PSI-HydA2 (see **figure 3-22**). The discrepancy between the single flash and the multiple turnover experiments for PSI-HydA1 may reflect differences in dissociation of flavodoxin from the complex, which would play a role in the latter but not the former.

Our analysis of the flavodoxin reduction kinetic assay suggests that the PSI-HydA1 terminal iron sulfur clusters get inactivated by O_2 ~2 times slower than PSI-HydA2 (**table 3-4**). Together with the ~5-times higher accumulation of the PSI-HydA1 (as compared to PSI-HydA2) and better flavodoxin reduction (relative to PSI-HydA2), it can explain the higher quantum yields of PSII (**figure 3-15**), higher rates of CEF (**figure 3-20**) and O_2 evolution (**figure 3-16 C, 3-17 C**) observed in the short-term experiments than was observed previously with PSI-HydA2. We hypothesize that the eventual destruction of the terminal iron sulfur clusters leads to inability to grow phototrophically in the presence of O_2 (**figure 3-23**).

Conclusions

We have made a significant improvement in the stability and accumulation of the PSI-HydA1 chimera described here, which approaches wild-type PSI levels and 5 times more than our previously described PSI-HydA2 chimera. Its hydrogenase activity can be restored after complete inactivation by O_2, indicating that the active site can be reinserted into the same PsaC-HydA1 protein by the maturases and underscoring the advantage of performing H_2 production *in vivo*. The higher amount of PSI-HydA1 (and its higher propensity for Fd reduction) had the unfortunate consequence of allowing O_2 to accumulate, inhibiting long-term H_2 production, thus demonstrating that improvements to protein design do not always translate to improvements in the overall system. Finally, these results extend the universality of the *psaC*-internal fusion approach for insertion of redox enzymes into PSI and raise the possibility of using other hydrogenase enzymes with desirable properties (e.g., O_2-tolerance).

MAHIVKIYDTCIGCTQCVRACPLDVLEMVPWGGATATDAVPHVQQALAELAKPKDDPTRKHVCV
QVAPAVRVAIAETLGLAPGATTPKQLAEGLRRLGFDEVFDTLFGADLTIMEEGSELLHRLTEHLEA
HPHSDEPLPMFTSCCPGWIAMLEKSYPDLIPYVSSCKSPQMMLAAMVKSYLAEKKGIAPKDMVM
VSIMPCTRKQSEADRDWFCVDADPTLRQLDHVITTVELGNIFKERGINLAELPEGEWDNPMGVG
SGAGVLFGTTGGVMEAALRTAYELFTGTPLPRLSLSEVRGMDGIKETNITMVPAPGSKFEELLKH
RAAARAEAAAHGTPGPLAWDGGAGFTSEDGRGGITLRVAVANGLGNAKKLITKMQAGEAKYDF
VEIMACPAGCVGGGGQPRSTDKAITQKRQAALYNLDEKSTLRRSHENPSIRELYDTYLGEPLGH
KAHELLHTHYVAGGASQMASAPRTEDCVGCKRCETACPTDFLSVRVYLGSESTRSMGLSY

Figure 3-1. Coding sequence of the PsaC-HydA1 polypeptide. Highlighted residues indicate the PsaC fragments (green), N-terminal junction (cyan), linker sequence borrowed from PsaC-HydA2 chimera (magenta).

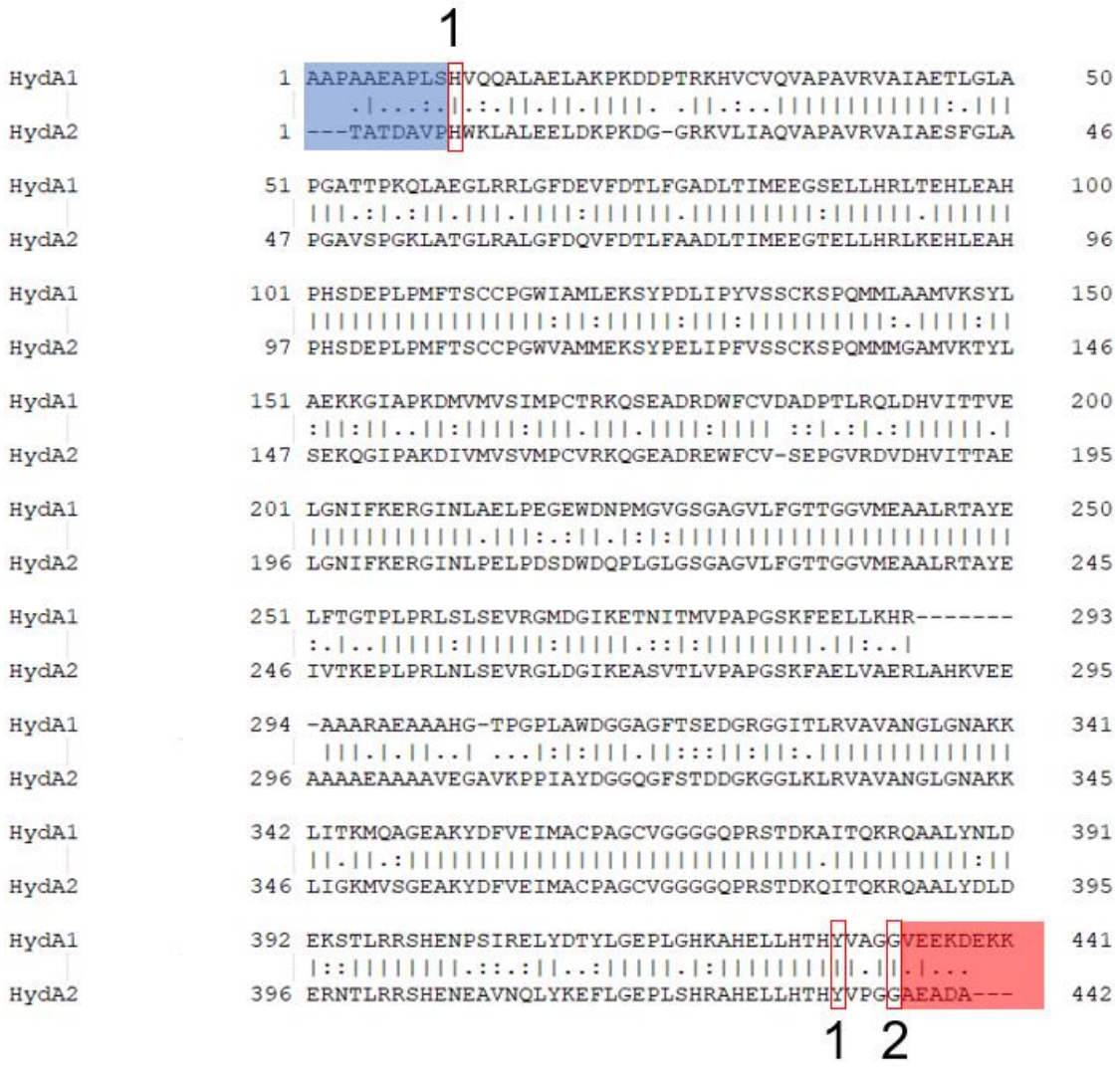

Figure 3-2. Pairwise sequence alignment (EMBOSS needle) of mature HydA1 and HydA2 polypeptides. Symbols between sequences indicates identical (I), similar (:), and dissimilar (.) residues; gaps (–) are indicated in sequence lines. Non-conserved N- (blue) and C- (red) terminal sequences are highlighted. Red frame with 1 on top indicates the first and the last conserved residue among hydrogenases from *Chlamydomonas reinhardtii* (HydA1, HydA2), *Scenedesmus obliquus* (HydA1, HydA2), as well as the bacterial *Clostridium pasteurianum* (*Cp*.H1), while 2 marks the last conserved residue among the algal hydrogenases, as shown by Forestier et al.[63]

Figure 3-3. Clustal alignment of PsaC-HydA2 chimera vs PsaC-HydA1. Symbols under alignment indicate identical (*), similar (.), and dissimilar ( ) residues; gaps (–) are indicated in sequence lines. Non-conserved N- (blue) and C- (red) terminal sequences are highlighted. Green highlights the original PsaC sequence. Blue and red boxes show N- and C- terminal linking sequences with respect to hydrogenase domain orientation.

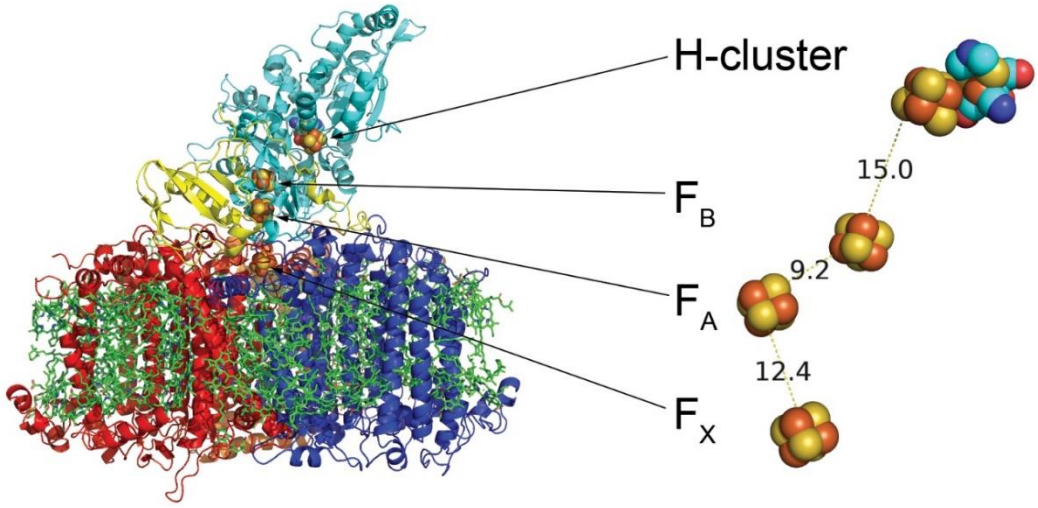

Figure 3-4. A model of PSI-HydA1. PsaA (red), PsaB(blue), PsaC-HydA1 (cyan), PsaD (yellow), PsaF (orange) are shown as cartoon representation, with pigments as green sticks and metallic clusters as space-filling models. On the right, the iron-sulfur clusters and H-cluster are magnified, with edge-to-edge distances indicated in Å.

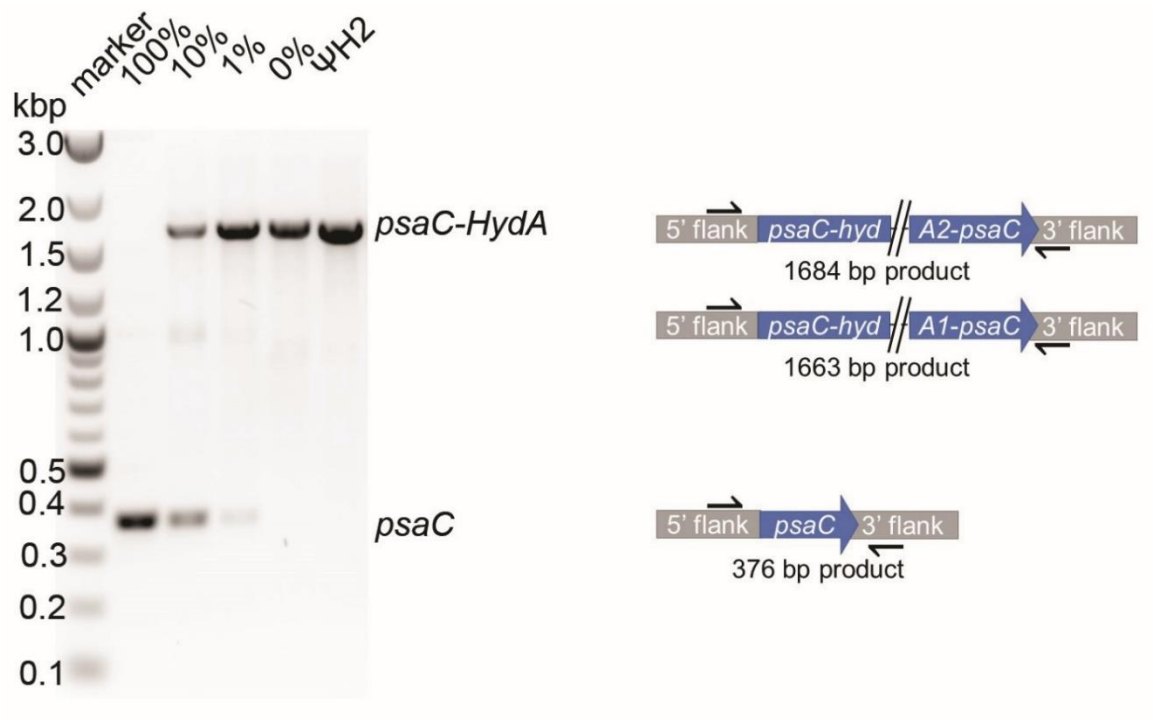

Figure 3-5. Agarose gel image of homoplasmicity detection PCR. Wild type genomic DNA (parental strain) indicated as a percentage of total DNA (diluted into ΨH1 genomic DNA containing *psaC-HydA2* in place of *psaC*). Total template DNA was 100 ng per reaction.

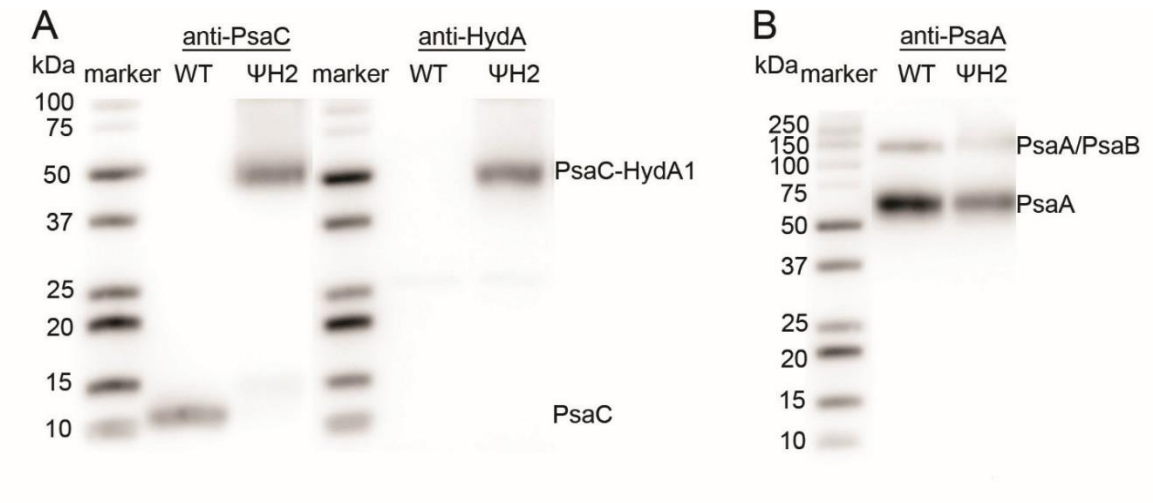

Figure 3-6. Immunoblots of solubilized thylakoid membranes, loaded based on equal amounts of photobleachable P_{700} (1.41 pmol) (**A**) or Chl (2 µg). (**B**). Blots were probed with antibodies against PsaC (**A**, left), HydA (**A**, right), or PsaA (**B**).

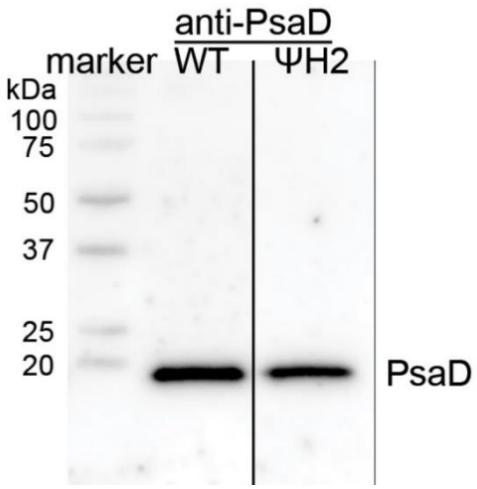

Figure 3-7. Immunoblots of solubilized thylakoids loaded on equal chlorophyll (2 µg). Integration of the anti-PsaD cross-reactive bands gave a ratio of 1:0.8 (PSI:PSI-HydA1).

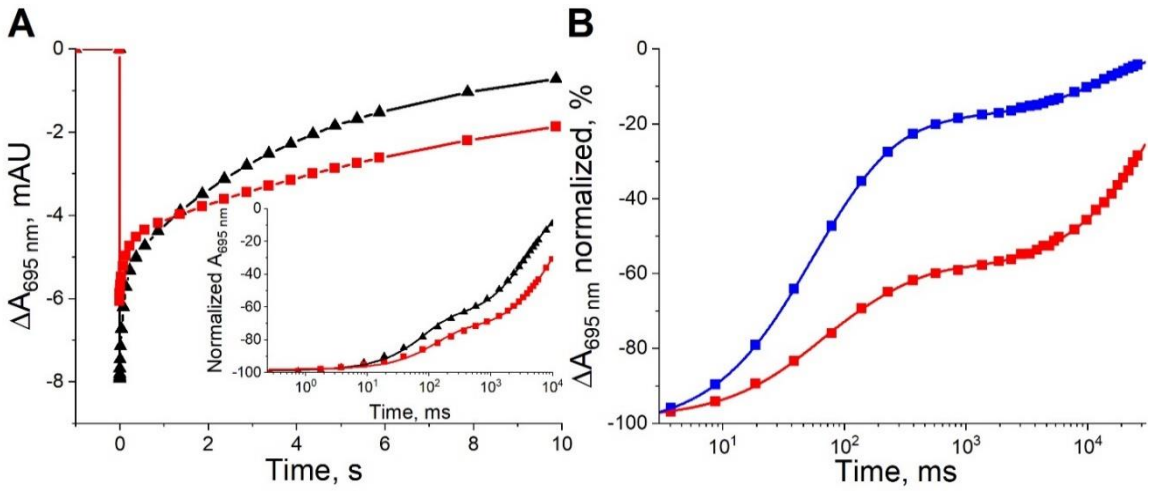

Figure 3-8. In vitro spectroscopic characterization of PSI-HydA1 chimera. (**A**) Transients of flash-induced P_{700} photobleaching and recovery in thylakoids (normalized to 60 µg/mL of total Chl) isolated from *hydA* (black triangles) and ΨH2 (red squares) cells grown aerobically. The inset shows the same transients normalized to the maximal bleaching on a log time scale. (**B**) Transients of P_{700} recovery after photooxidation in purified PSI-HydA1 particles prepared oxically (red squares) or anoxically (blue squares) from anaerobically adapted cells.

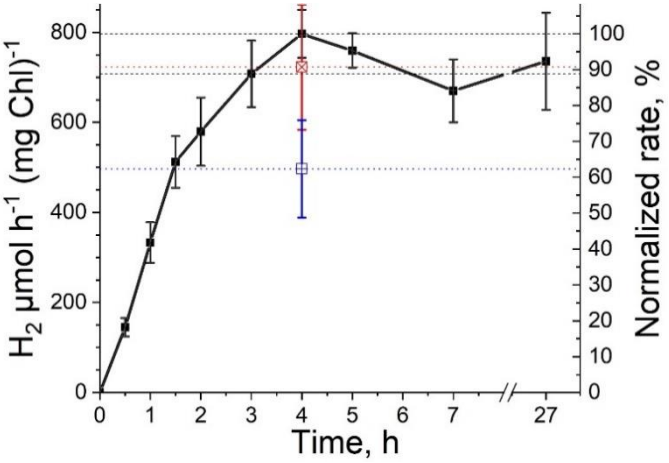

Figure 3-9. Absolute and normalized rates of H_2 production in the reduced methyl viologen assay (RMVA) on permeabilized cells (ΨH2 in TAP) as a function of anaerobic adaptation period. Black squares (solid) show permeabilized cells without CAM treatment, red square (x) – with 200 µg/mL CAM added at the onset of anaerobic induction (t = 0), blue square (+) represents a subset of untreated cells that went through 4 h of anaerobic adaptation followed by addition of 200 µg/mL CAM, 5 min of air treatment, and another 4 h of anaerobic adaptation. Horizontal dashed/dotted lines help visualize relevant rates on absolute and relative scales. Error bars represent standard error (n≥3).

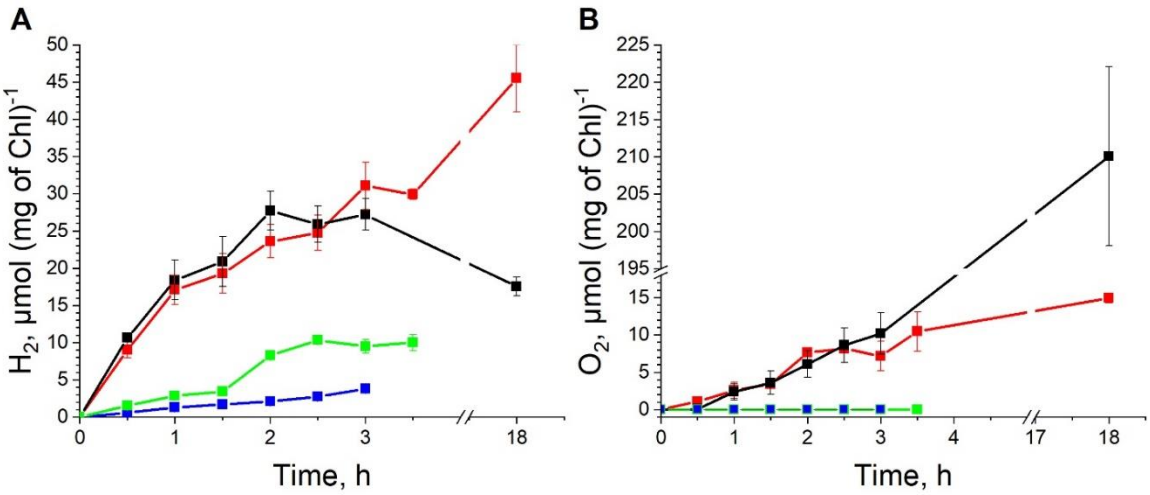

Figure 3-10. Net headspace H_2 (A) and O_2 (B) produced by ΨH2 in sealed bottles. The light and media conditions are indicated as follows: black (TAP + 200 µmol m^{-2} s^{-1}), blue (TAP + dark), red (TP + 200 µmol m^{-2} s^{-1}), green (TP+ 200 µmol m^{-2} s^{-1}+10 µM DCMU). All values are normalized to Chl. Error bars indicate standard error (n=3 for all except the dark sample for which n=6).

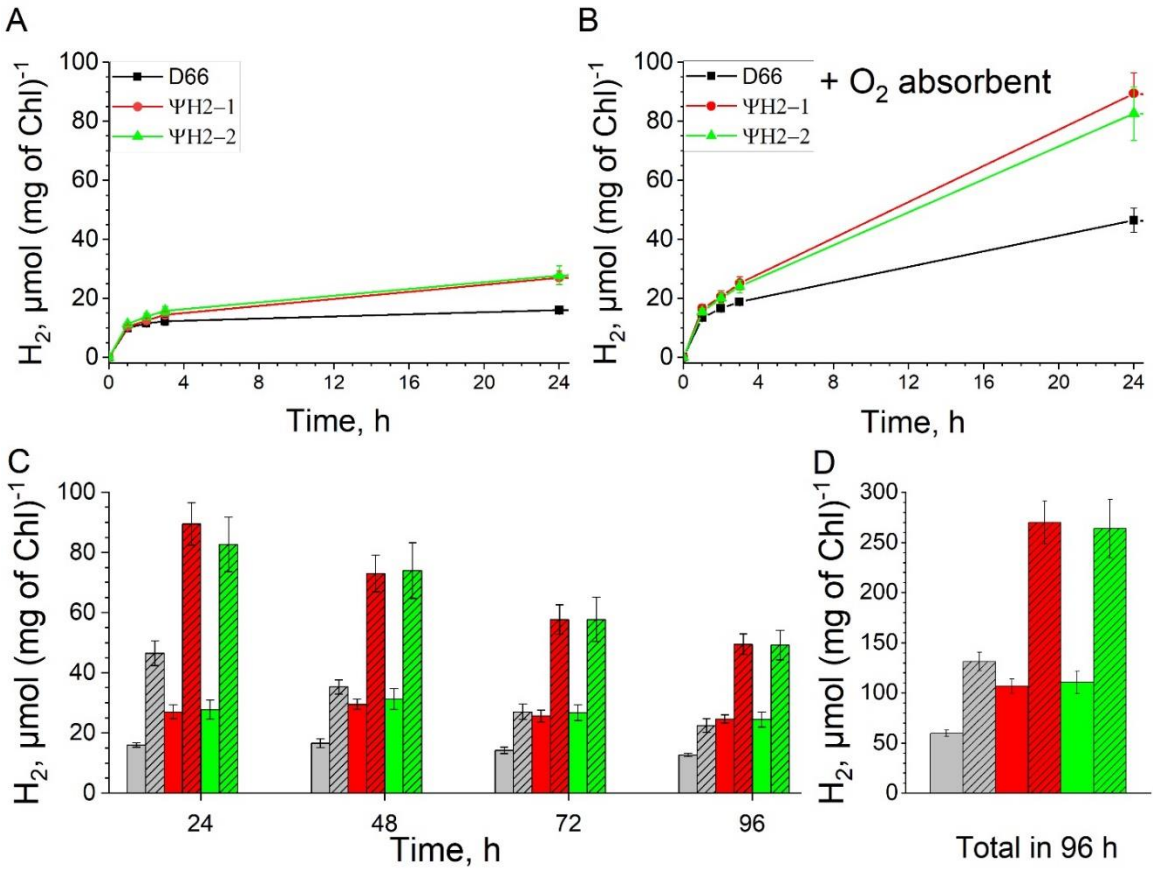

Figure 3-11. Effect of O_2 absorbent on anaerobiosis-induced photoautotrophic H_2 production in ΨH2 chimeras (red and green for 2 independent transformants) and D66 wild type strain (black/grey) in HS medium lacking acetate and bicarbonate under white light (200 µmol m^{-2} s^{-1} PAR). The first 24 h of H_2 production is shown in panels A and B. The headspace of the culture was flushed every 24 h with N_2 and the daily amount of H_2 produced is presented in panels C (hashed bars represent trials with O_2 absorbent). A sum of H_2 accumulation over 4 days is shown in panel D. The net amount of O_2 produced was below the detection limit of 0.05%. The Chl content was set to 4 - 5 µg Chl mL^{-1} at time 0. Error bars indicate standard error (n=5 for all samples).

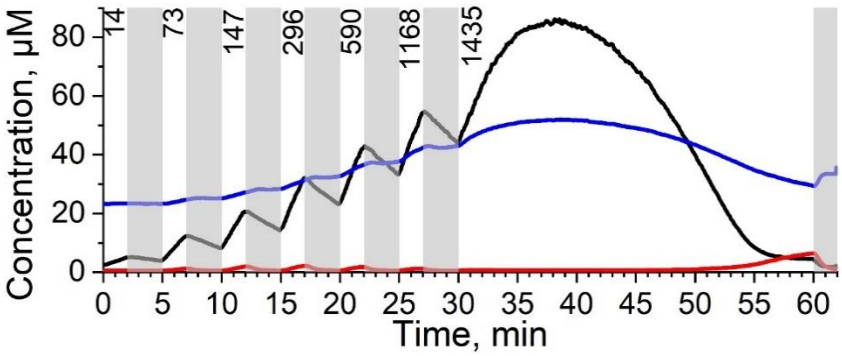

Figure 3-12. Concentration of dissolved gases: H_2 (black), O_2 (red), and CO_2 (blue) in a prototypical light sequence used for MIMS experiments on ΨH2 cells (suspended in TAP). A sample experiment is shown with greyed areas indicating periods of darkness and PAR (in µmol of photons m^{-2} s^{-1}) is indicated above the figure. For clarity, light saturation portion of the experiment (first 30 min) is presented separately (see figure 3-13) from the prolonged illumination (30-60 min) (see figures 3-16 through 3-19).

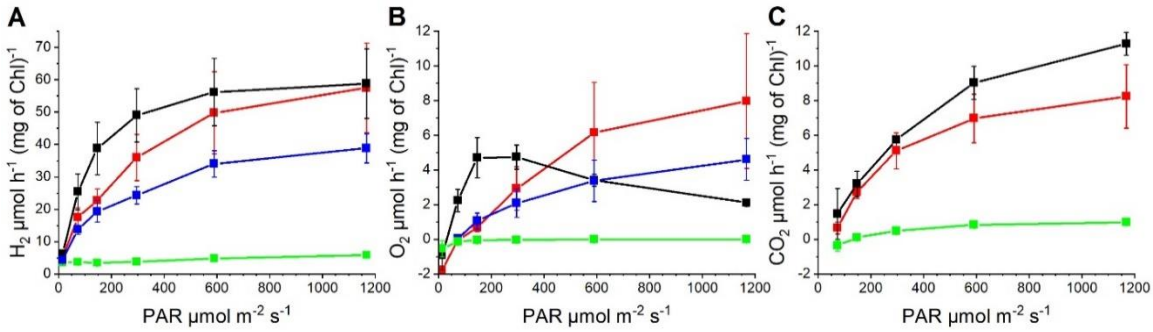

Figure 3-13. Light-induced maximal net production rates of H_2 (A), O_2 (B) and CO_2 (C) in ΨH2 cell culture, as measured by membrane inlet mass spectrometry (MIMS) during 2-min illumination periods at the indicated flux. The conditions are indicated as follows: black (TAP), red (TP), green (TP + 10 µM DCMU), blue (TP + 2mM bicarbonate). Error bars represent standard error (n=3), except for the TP sample (n=5). (The addition of 2 mM bicarbonate rendered the CO_2 traces very noisy, so they are not included in panel C.)

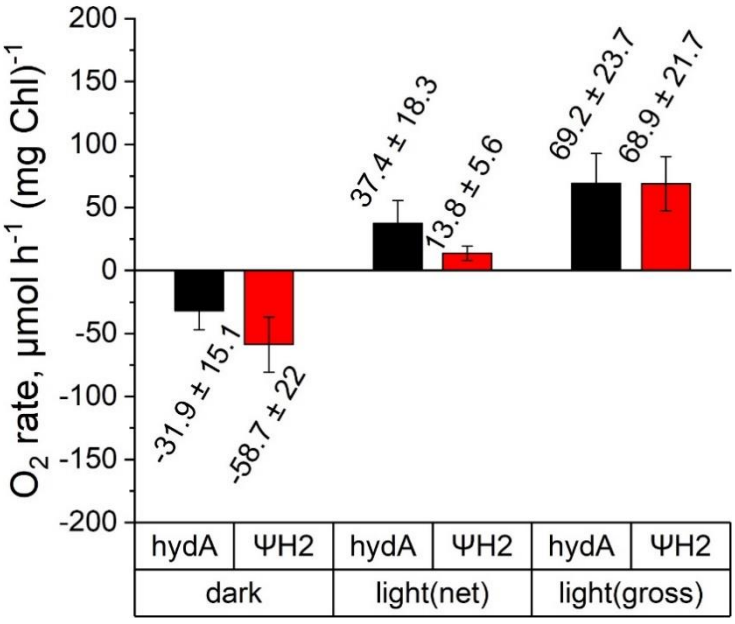

Figure 3-14. Oxygen uptake/production rates in algal cultures resuspended in TAP + 25 mM bicarbonate, as measured by FireSting-O_2 optical meter. Light condition corresponds to 1435 µmol m^{-2} s^{-1} PAR. Error bars represent standard error (n=3 for hydA and n=6 for ΨH2).

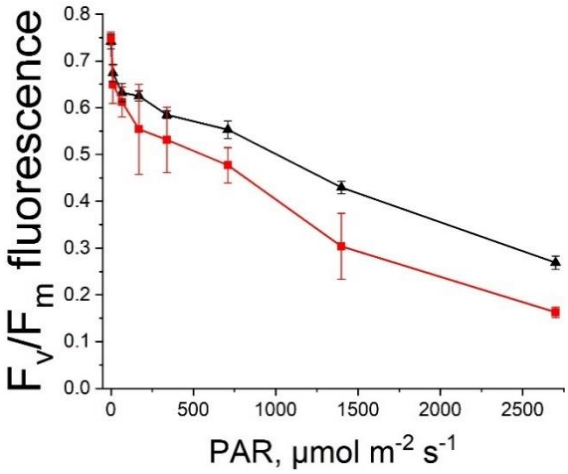

Figure 3-15. Fv/Fm fluorescence of PSII for hydA (black/triangle) and ΨH2 (red/square). Aerobically maintained cells were dark adapted for 5 min in sodium phosphate buffer (pH 7.0) containing 20% Ficoll and 2 mM sodium bicarbonate. Error bars represent standard error (n=3).

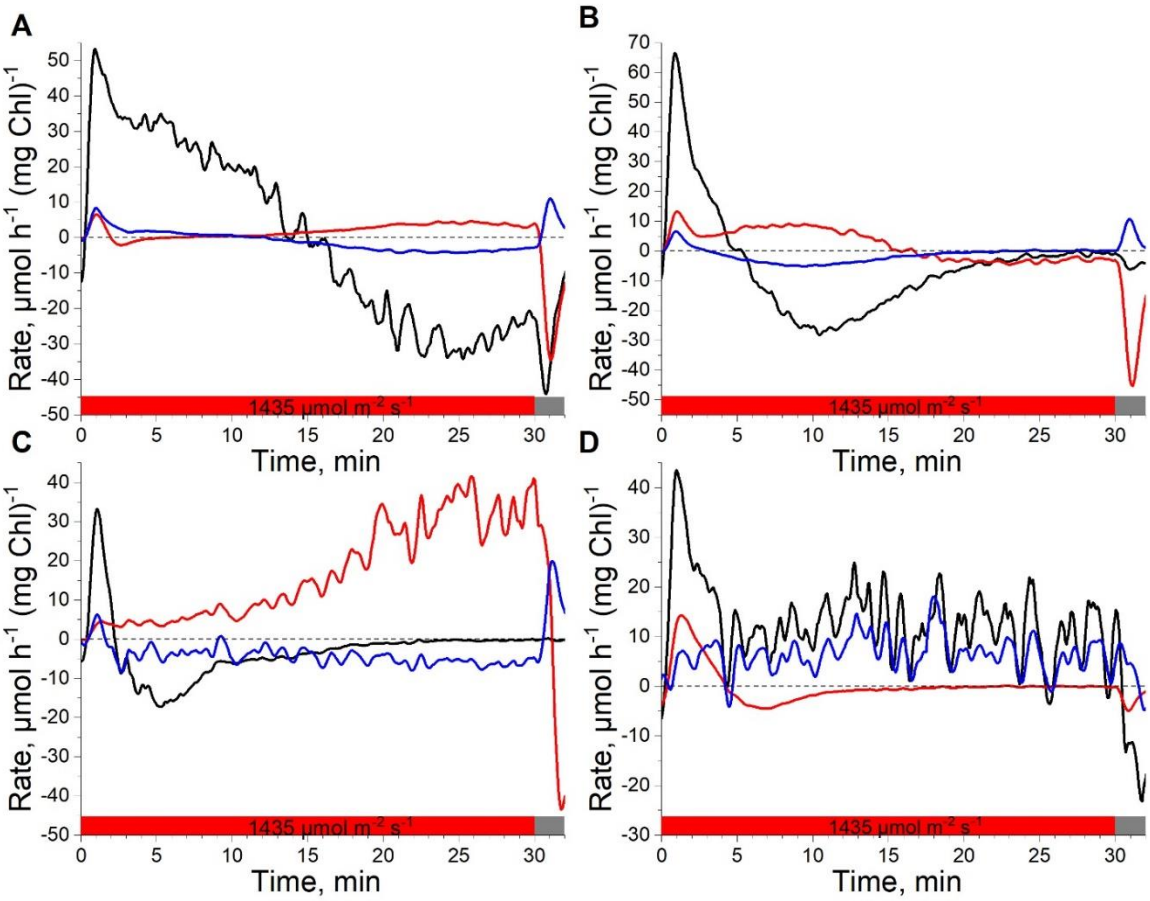

Figure 3-16. H_2 (black), O_2 (red), and CO_2 (blue) production rate averages (n=3) during prolonged illumination (30 min) followed by 2 minutes of darkness on ΨH2 cells resuspended in TP (A), D66 WT in TP (B), ΨH2 in TP+2 mM bicarbonate (C), ΨH2 in TP+2 mM bicarbonate+40 mM glycol aldehyde (GA). Error bars are not shown for clarity.

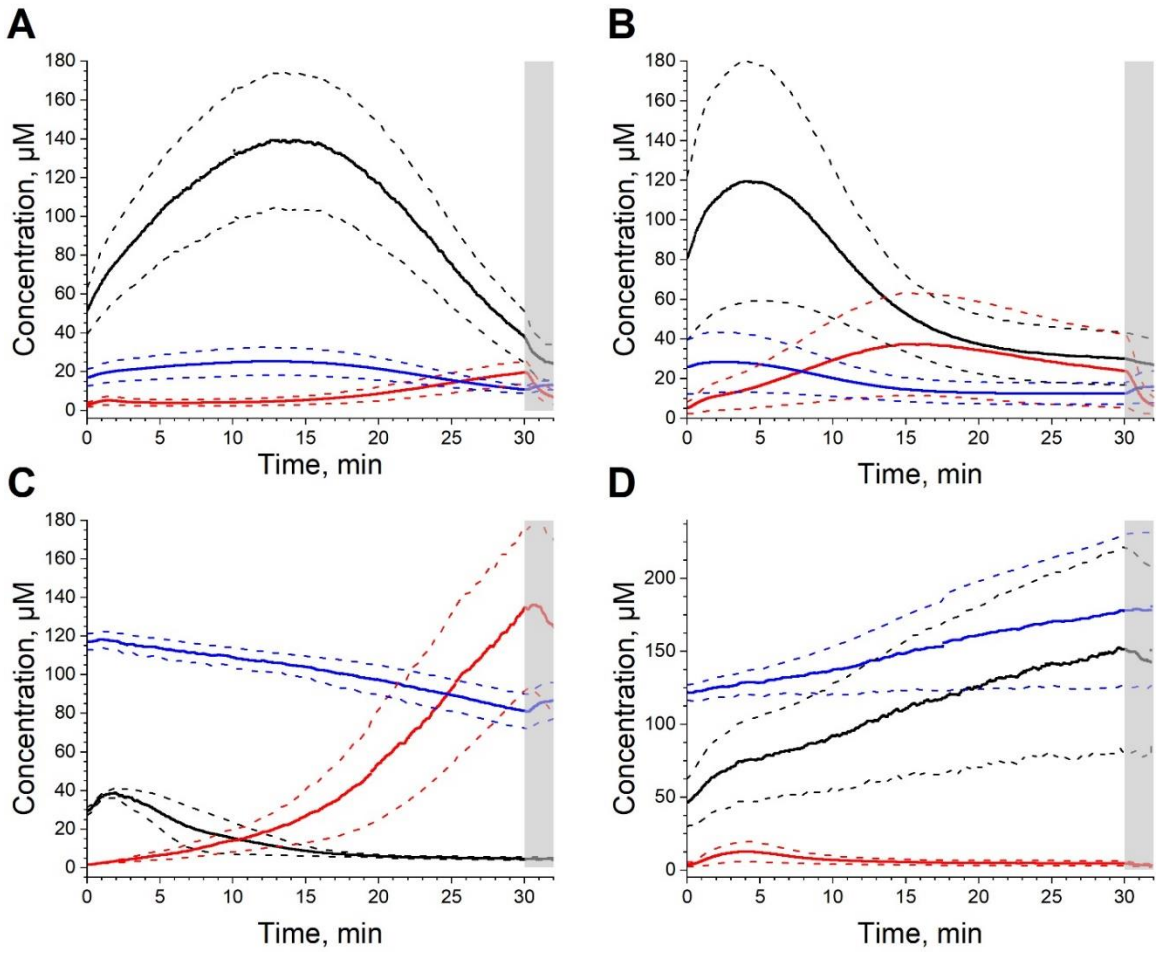

Figure 3-17. Concentration of dissolved gases: H_2 (black), O_2 (red), and CO_2 (blue), which were used to derive rates in **figure 3-16**. Cells of ΨH2 in TP (**A**), D66 in TP (**B**), ΨH2 in TP+ 2 mM bicarbonate(**C**) or ΨH2 in TP+2mM bicarbonate+ 40 mM GA (**D**) were exposed to continuous illumination of red light (1435 µmol m^{-2} s^{-1}) followed up by 2 min of darkness (shown as greyed rectangle). Dashed lines indicate the boundaries of standard error (n=3 for all, but panel A where n=5).

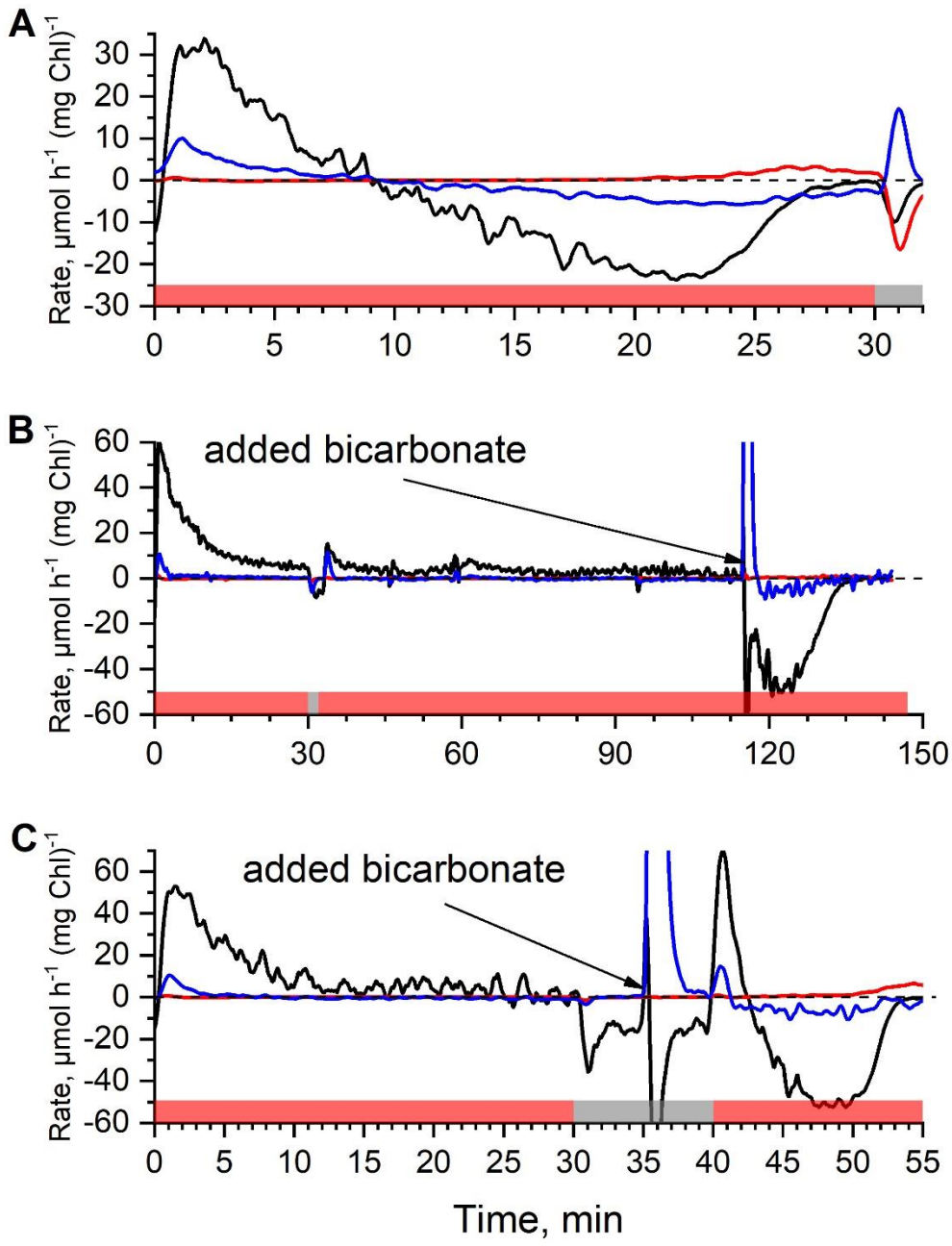

Figure 3-18. Variability in the metabolic switch onset for rates of H_2 (black), O_2 (red), and CO_2 (blue) generated by ΨH2 cells resuspended in TAP (acetate). Addition of bicarbonate solution to 2 mM (final) is indicated by arrows. In panel A, a typical light regimen resulted in H_2 uptake after 10 min, in panel (B) an extended illumination and addition of bicarbonate were required for onset of H_2 uptake, and in panel (C) bicarbonate was added after first 30 min of illumination following ~10 min of dark adaptation. Black dashed line shows zero rate. Rectangles above the abscissa indicate light conditions: red = 1435 µmol m^{-2} s^{-1} red LED; grey = dark.

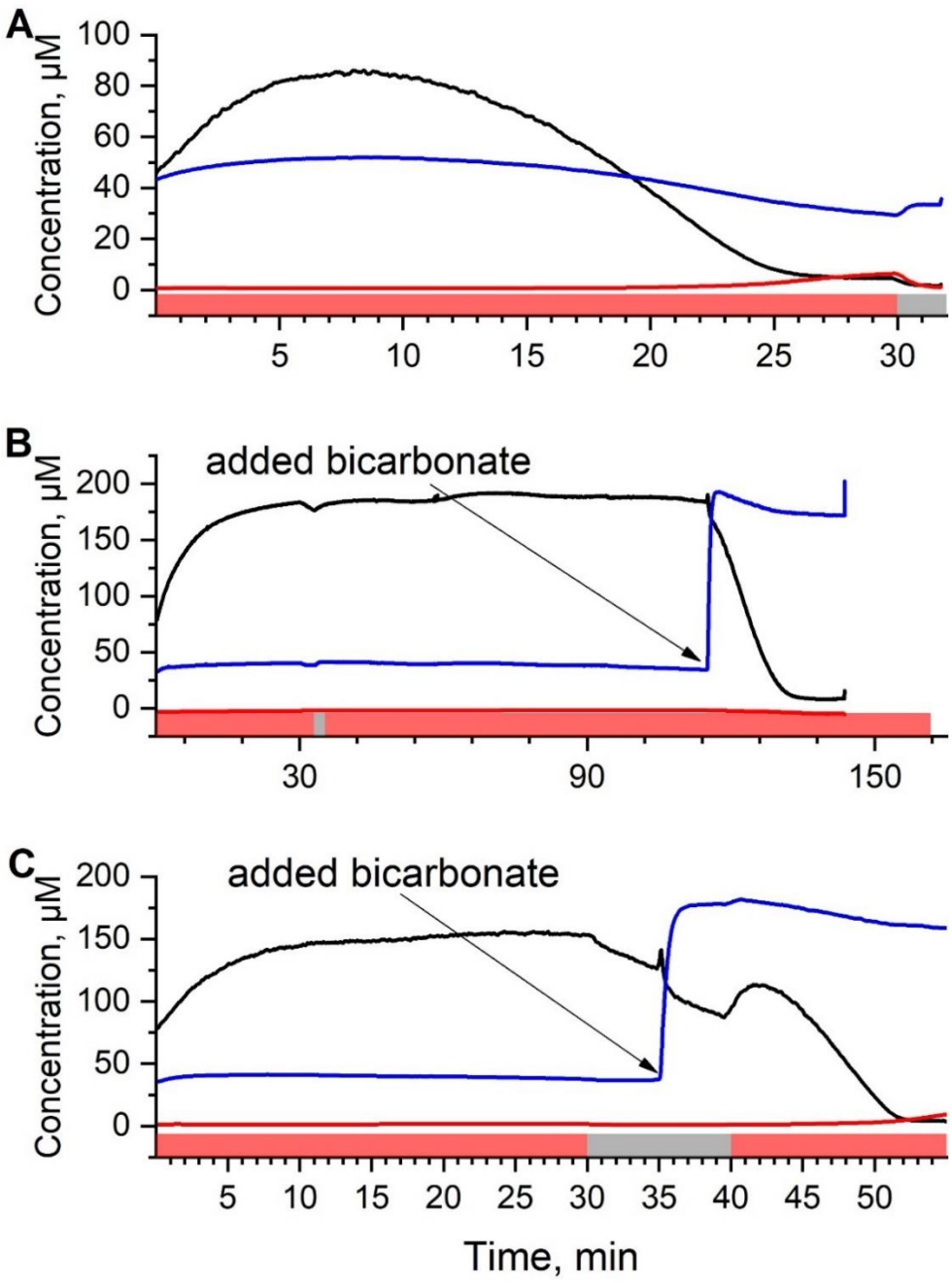

Figure 3-19. Concentration of dissolved gases that were used to derive rates in **figure 3-18**: H_2 (black), O_2 (red) and CO_2 (blue). Individual runs are shown. Addition of bicarbonate solution to 2 mM (final) is indicated by arrows. (A) regular regimen, (B) extended illumination with the spike of bicarbonate in the end, and (C) spiking bicarbonate in the dark after the regular regimen with more illumination

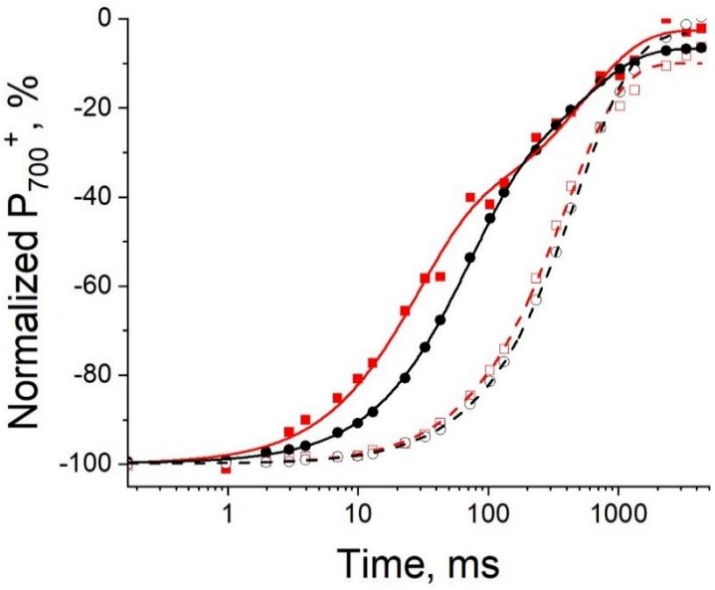

Figure 3-20. P_{700}^+ dark recovery kinetics in D66 (black) and ΨH2 (red) cells after 10 s of illumination with red light (630 nm) at a flux of ~500 photons PSI^{-1} s^{-1}. Cells had been grown in TAP under low light before being resuspended in phosphate/bicarbonate buffer, followed by addition of 10 µM DCMU (see Methods). Averages of P_{700}^+ reduction kinetics (n=5) in cells with DCMU (solid symbols) were fit to a biexponential decay (solid lines). Addition of 20 µM DBMIB to the same cells is indicated by hollow symbols; the transients were fit to a mono-exponential decay (dashed lines).

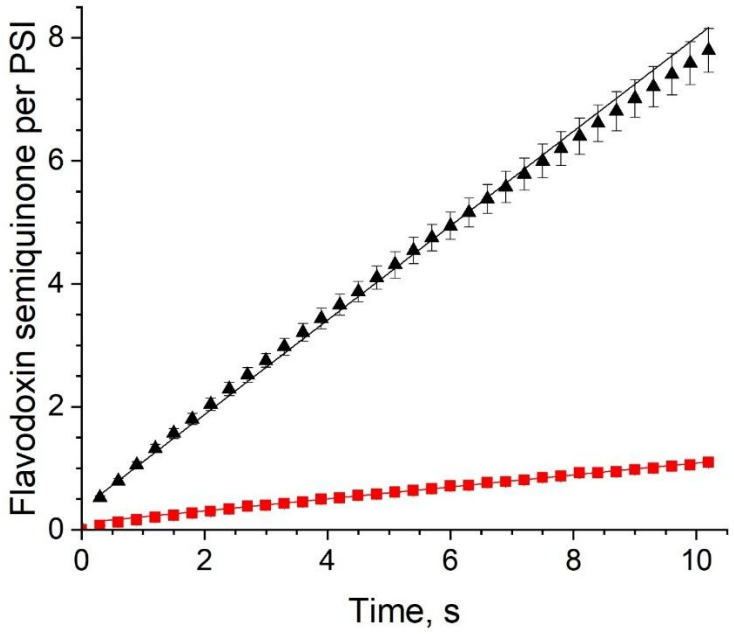

Figure 3-21. PSI activity towards flavodoxin photoreduction in vitro under saturating illumination. Flavodoxin is in 50-fold excess of PSI (black = hydA, red = ΨH2). Turnover rates are 0.8 s^{-1} (WT PSI) and 0.1 s^{-1} (PSI-HydA1).

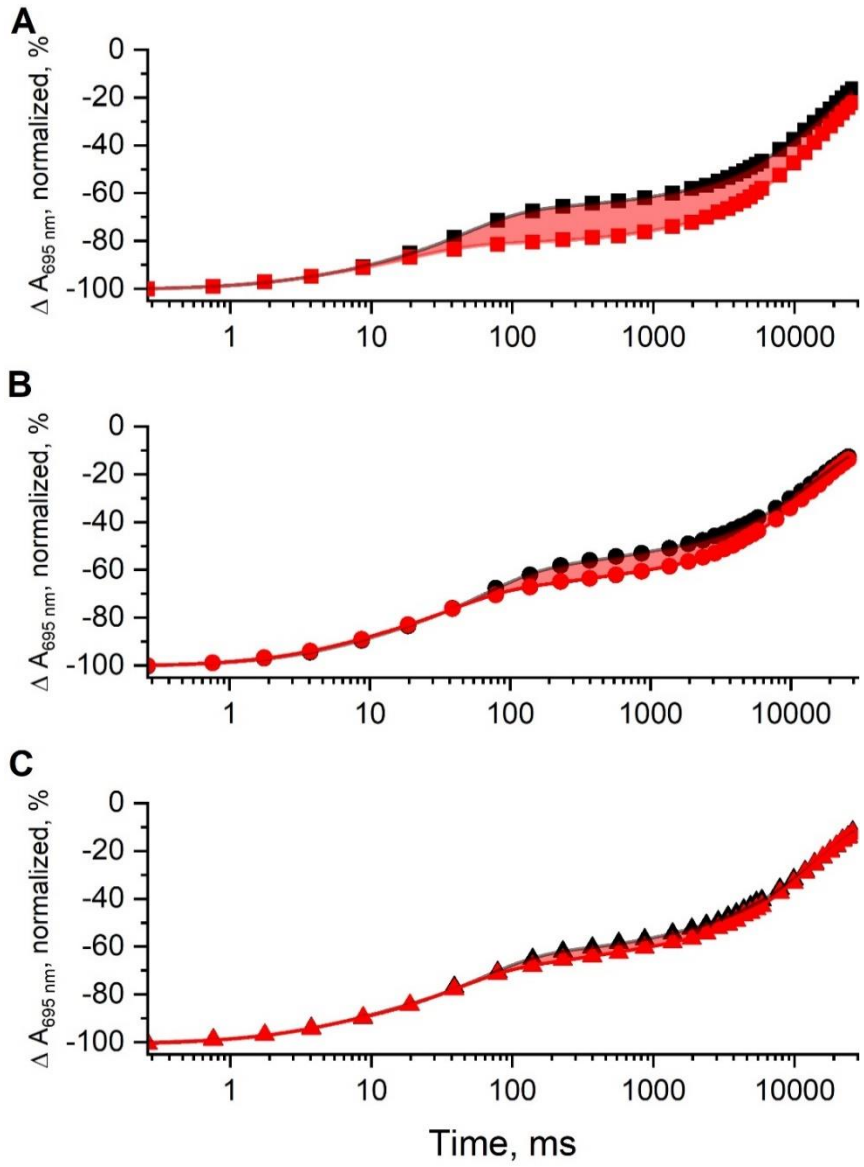

Figure 3-22. Effect of flavodoxin on charge recombination in vitro after a saturating laser flash in *hydA* (PSI) (A), ΨH2 (PSI-HydA1) (B) and ΨH1 (PSI-HydA2) (C). Each trace was fitted to a 4-component exponential decay function (shown as a line). Traces with flavodoxin are shown in red. Area between the fitted lines filled in red represent the fraction of electrons*ms that escaped to flavodoxin. Setup was the same as in the kinetic experiment, except that plastocyanin was not added.

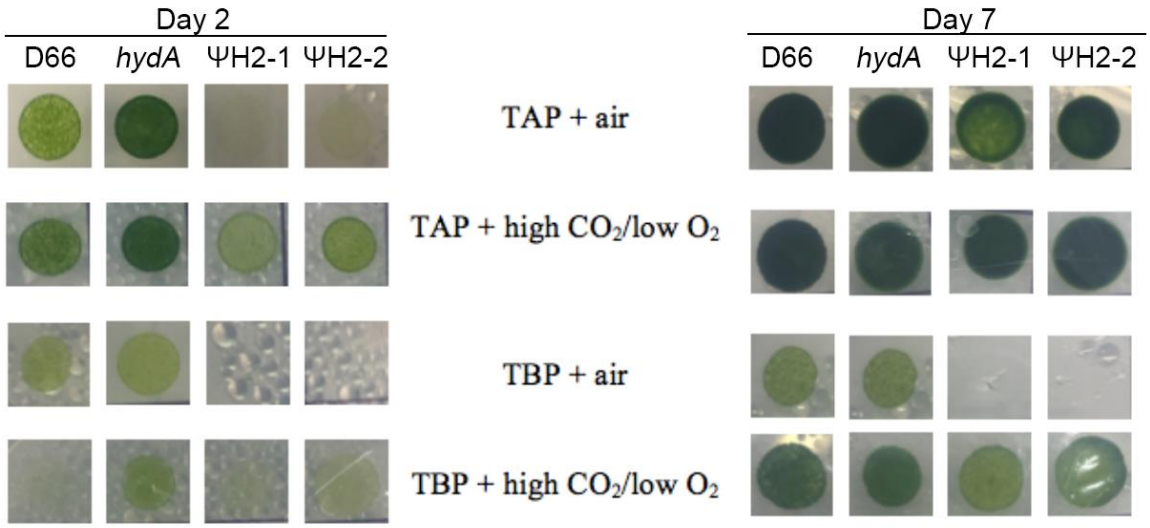

Figure 3-23. Growth assay on plates under 70 µmol m^{-2} s^{-1} of white fluorescent light. Columns are marked on top with the corresponding algal strain. Rows differentiate between different media conditions.

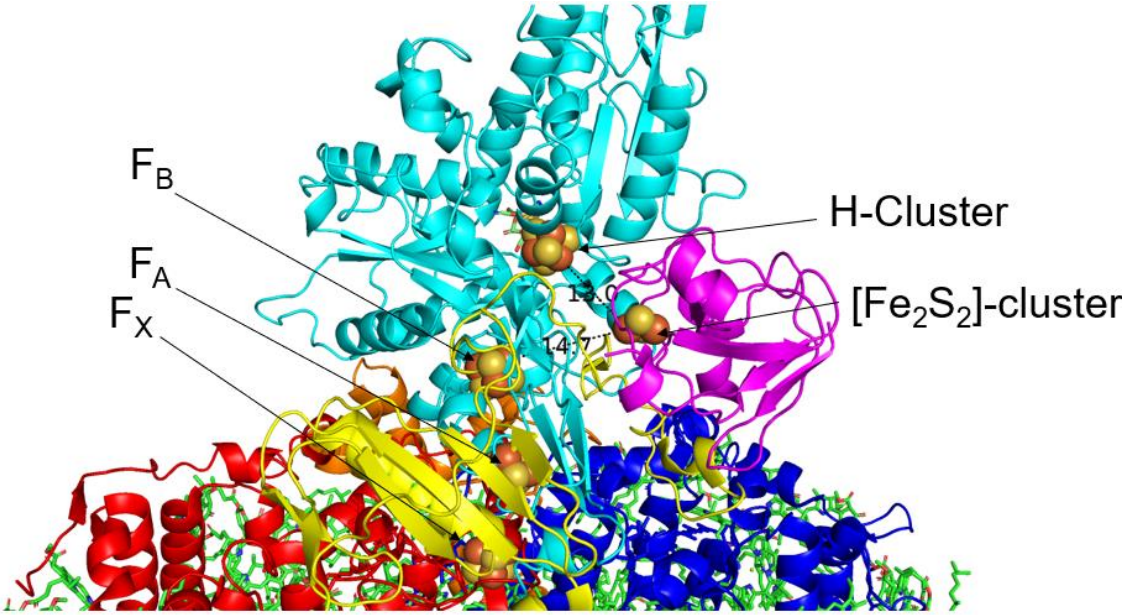

Figure 3-24. Fd1 (magenta) docking to the model of PsaC-HydA1 (cyan) and PsaD (yellow), using ClusPro2 [64]. For reference, PsaA (red), PsaB (blue), and PsaF (orange) polypeptides are shown as ribbons while Chl *a* are shown as stick figures (green). Black dashed lines indicate edge-to-edge distances (in Å) between the [2Fe-2S] cluster of Fd1 and either the H-cluster or F_B.

parameter	PSI	PSI-hydrogenase	Comments
τ_1	77 ± 4.5 ms	123 ± 9 ms	Decay constant of fast phase (ms)
A_1	31 ± 0.6 %	23.2 ± 0.6 %	Amplitude of fast phase (% of total)
τ_2	4.3 ± 0.1 s	10 ± 0.3 s	Decay constant of slow phase (s)
A_2	66 ± 0.5 %	71.1 ± 0.7 %	Amplitude of slow phase (% of total)
A_0	1.6 ± 0.3 %	3.7 ± 0.8 %	Non-decaying fraction (% of total)
R^2	0.99951	0.99931	Coefficient of determination

Table 3-1. Fitting coefficients of P_{700}^+ decay in thylakoids. Bi-exponential fitting coefficients of P_{700}^+ decay transients in vitro as shown in **figure 3-8A**. Function: $A(x) = A_0 + A_1 \exp(-x/t_1) + A_2 \exp(-x/t_2)$. Fast recovery phase parameters τ_1 and A_1 are likely due to charge recombination from $P_{700}^+(F_A/F_B)^-$ while τ_2 and A_2 result from a slow reduction of P_{700}^+ by ascorbate.

Phase assignment	Time constant ± SE, ms (relative amplitude, %)	
	PSI-HydA1 (oxic)	**PSI-HydA1 (anoxic)**
CR of $P_{700}^{+}(F_AF_B)^{-}$	42 ± 6 (19 ± 3) 183 ± 21 (20 ± 3)	29 ± 2 (28 ± 4) 86 ± 11 (40.5 ± 2.5)
CR of $P_{700}^{+}F_H^{-}$	N/A	269 ± 34 (13.5 ± 3.5)
ascorbate	40,000 ± 4100 (65 ± 5)	14500 ± 400 (17.8 ± 0.2)
Non-decaying	(5 ± 5)	– (1.3 ± 0.2)
R^2	0.99968	0.99999

Table 3-2. Fitting coefficients of P_{700}^{+} decay in isolated PSI-HydA1 particles. Fitting parameters for P_{700}^{+} recovery transients shown in **figure 3-8B**. Transients were fitted to a sum of exponentials $A(x) = A_0 + A_i \exp(-x/t_i)$, where *i* was 3 for oxic and 4 for anoxic.

Maximal rate μmol H_2 h^{-1} (mg Chl)$^{-1}$	**Conditions**
797 ± 53	RMVA in permeabilized cells after 4 h of anaerobic induction determined over 10-30 min interval (GC) (n=9)
723 ± 140	RMVA in permeabilized cells (GC) (n=3) with 200 μg/mL CAM added at the beginning of anaerobic adaptation (4 hours of anaerobic induction) determined over 10-30 min interval
18 ± 2	TP under ~200 μmol m^{-2} s^{-1} (white fluorescent) light (GC) (n=3) determined over 1-h interval
21 ± 1	TAP under ~200 μmol m^{-2} s^{-1} (white fluorescent) light (GC) determined over 1-h interval (n=3)
1.5 ± 0.3	TAP in the dark (GC) determined over 1 h interval (n=6)
3.1 ± 0.3	TP (+10 μM DCMU) under ~200 μmol m^{-2} s^{-1} (white fluorescent) light (GC) determined over 1-h interval (n=3)
58 ± 14	TP, under 1170 μmol m^{-2} s^{-1} (red LED) light (MIMS) determined over ~1-min interval (n=5)
59 ± 11	TAP, under 1170 μmol m^{-2} s^{-1} (red LED) light (MIMS) (n=3)
39 ± 5	TP (+2 mM bicarbonate), under 1170 μmol m^{-2} s^{-1} (red LED) light (MIMS) determined over ~1-min interval (n=3)
6 ± 1	TP (+10 μM DCMU) under 1170 μmol m^{-2} s^{-1} (red LED) light (MIMS) determined over ~1-min interval (n=3)
52 ± 18	TP (+2 mM bicarbonate + 40 mM GA), under 1170 μmol m^{-2} s^{-1} (red LED) light (MIMS) determined over ~1-min interval (n=3)

Table 3-3. Maximal H_2 production rates in ΨH2 under specified conditions with associated standard error.

	A	B	C
WT-PSI	-0.01	0.84 (100%)	0.3
PSI-HydA1	-0.0020	0.12 (14.3%)	0.05
PSI-HydA2	-0.0044	0.11 (13 %)	0.1
Interpretation	Once multiplied by 2, it indicates the decrease rate over time (absolute; taking first derivative of the quadratic function)	Indicates initial rate at time 0 (after taking first derivative of the quadratic function)	Amount of flavodoxin semiquinone per PSI at the beginning of the experiment. No meaning for the rate equation
	Normalized rate of decrease = 2A/B, expressed in s^{-1} or (%)		
WT-PSI	-0.025 (100%)		
PSI-HydA1	-0.030 (121%)		
PSI-HydA2	-0.082 (327%)		

Table 3-4. Coefficients for a quadratic fit of the flavodoxin reduction kinetic data shown in **figure 3-21:** $Y = At^2 + Bt + C$ and their meaning for kinetic analysis.

Ferredoxin 1 residue	PsaC-HydA1 residue	Distance (in Å)
E28	K407	2.6
Q59	K370	3.0
Y94	E26	1.9
	PsaD residue	
S9	G188	2.9
K12	S187	2.3
Y35	R173	3.2
Y35	Q177	1.9
Y35	V179	3.0
S43	G167	2.8
S44	N169	2.9 & 3.0
S44	Q170	3.2

Table 3-5. Polar contacts playing role in docking of Fd1 to (PsaC-HydA1+PsaD) for the model shown in **figure 3-24**.

References

[1] Blankenship RE, Tiede DM, Barber J, Brudvig GW, Fleming G, Ghirardi M, et al. Comparing Photosynthetic and Photovoltaic Efficiencies and Recognizing the Potential for Improvement. Science (80-) 2011;332:805–9. https://doi.org/10.1126/science.1200165.

[2] Eroglu E, Melis A. Microalgal hydrogen production research. Int J Hydrogen Energy 2016;41:12772–98. https://doi.org/https://doi.org/10.1016/j.ijhydene.2016.05.115.

[3] Bolatkhan K, Kossalbayev BD, Zayadan BK, Tomo T, Veziroglu TN, Allakhverdiev SI. Hydrogen production from phototrophic microorganisms: Reality and perspectives. Int J Hydrogen Energy 2019;44:5799–811. https://doi.org/10.1016/j.ijhydene.2019.01.092.

[4] Akhlaghi N, Najafpour-Darzi G. A comprehensive review on biological hydrogen production. Int J Hydrogen Energy 2020;45:22492–512. https://doi.org/10.1016/j.ijhydene.2020.06.182.

[5] Swartz J. Opportunities toward hydrogen production biotechnologies. Curr Opin Biotechnol 2020;62:248–55. https://doi.org/10.1016/j.copbio.2020.03.002.

[6] Stirbet A, Lazár D, Guo Y, Govindjee G. Photosynthesis: basics, history and modelling. Ann Bot 2020;126:511–37. https://doi.org/10.1093/aob/mcz171.

[7] Nawrocki WJ, Bailleul B, Picot D, Cardol P, Rappaport F, Wollman F-A, et al. The mechanism of cyclic electron flow. Biochim Biophys Acta - Bioenerg 2019;1860:433–8. https://doi.org/10.1016/j.bbabio.2018.12.005.

[8] Lubitz W, Ogata H, Rüdiger O, Reijerse E. Hydrogenases. Chem Rev 2014;114:4081–148. https://doi.org/10.1021/cr4005814.

[9] Winkler M, Kuhlgert S, Hippler M, Happe T. Characterization of the Key Step for Light-driven Hydrogen Evolution in Green Algae. J Biol Chem 2009;284:36620–7. https://doi.org/10.1074/jbc.M109.053496.

[10] Winkler M, Hemschemeier A, Jacobs J, Stripp S, Happe T. Multiple ferredoxin isoforms in *Chlamydomonas reinhardtii* – Their role under stress conditions and biotechnological implications. Eur J Cell Biol 2010;89:998–1004. https://doi.org/10.1016/J.EJCB.2010.06.018.

[11] Cournac L, Mus F, Bernard L, Guedeney G, Vignais PM, Peltier G. Limiting steps of hydrogen production in *Chlamydomonas reinhardtii* and *Synechocystis* PCC 6803 as analysed by light-induced gas exchange transients. Int J Hydrogen Energy 2002;27:1229–37. https://doi.org/10.1016/S0360-3199(02)00105-2.

[12] Clowez S, Godaux D, Cardol P, Wollman F-A, Rappaport F. The Involvement of Hydrogen-producing and ATP-dependent NADPH-consuming Pathways in Setting the Redox Poise in the Chloroplast of *Chlamydomonas reinhardtii* in Anoxia. J Biol Chem 2015;290:8666–76. https://doi.org/10.1074/jbc.M114.632588.

[13] Milrad Y, Schweitzer S, Feldman Y, Yacoby I. Green Algal Hydrogenase Activity Is Outcompeted by Carbon Fixation before Inactivation by Oxygen Takes Place. Plant Physiol 2018;177:918–26. https://doi.org/10.1104/pp.18.00229.

[14] Godaux D, Bailleul B, Berne N, Cardol P. Induction of Photosynthetic Carbon Fixation in Anoxia Relies on Hydrogenase Activity and Proton-Gradient Regulation-Like1-Mediated Cyclic Electron Flow in *Chlamydomonas reinhardtii*. Plant Physiol 2015;168:648–58. https://doi.org/10.1104/pp.15.00105.

[15] Burlacot A, Sawyer A, Cuiné S, Auroy-Tarrago P, Blangy S, Happe T, et al. Flavodiiron-Mediated O_2 Photoreduction Links H_2 Production with CO_2 Fixation during the Anaerobic Induction of Photosynthesis. Plant Physiol 2018;177:1639 LP – 1649. https://doi.org/10.1104/pp.18.00721.

[16] Gaffron H. Carbon Dioxide Reduction with Molecular Hydrogen in Green Algae. Am J Bot 1940;27:273. https://doi.org/10.2307/2436697.

[17] Stuart TS, Gaffron H. The Gas Exchange of Hydrogen-adapted Algae as Followed by Mass Spectrometry. Plant Physiol 1972;50:136–40. https://doi.org/10.1104/pp.50.1.136.

[18] Milrad Y, Schweitzer S, Feldman Y, Yacoby I. Bi-directional electron transfer between H_2 and NADPH mitigates light fluctuation responses in green algae. Plant Physiol 2021;186:168–79. https://doi.org/10.1093/plphys/kiab051.

[19] Posewitz MC, King PW, Smolinski SL, Zhang L, Seibert M, Ghirardi ML. Discovery of Two Novel Radical S -Adenosylmethionine Proteins Required for the Assembly of an Active [Fe] Hydrogenase. J Biol Chem 2004;279:25711–20. https://doi.org/10.1074/jbc.M403206200.

[20] Berggren G, Adamska A, Lambertz C, Simmons TR, Esselborn J, Atta M, et al. Biomimetic assembly and activation of [FeFe]-hydrogenases. Nature 2013;499:66–9. https://doi.org/10.1038/nature12239.

[21] Bai Y, Chen T, Happe T, Lu Y, Sawyer A. Iron–sulphur cluster biogenesis via the SUF pathway. Metallomics 2018;10:1038–52. https://doi.org/10.1039/C8MT00150B.

[22] Britt RD, Tao L, Rao G, Chen N, Wang L-P. Proposed Mechanism for the Biosynthesis of the [FeFe] Hydrogenase H-Cluster: Central Roles for the Radical SAM Enzymes HydG and HydE. ACS Bio Med Chem Au 2022;2:11–21. https://doi.org/10.1021/acsbiomedchemau.1c00035.

[23] Kubas A, Orain C, De Sancho D, Saujet L, Sensi M, Gauquelin C, et al. Mechanism of O_2 diffusion and reduction in FeFe hydrogenases. Nat Chem 2017;9:88–95. https://doi.org/10.1038/nchem.2592.

[24] Swanson KD, Ratzloff MW, Mulder DW, Artz JH, Ghose S, Hoffman A, et al. [FeFe]-Hydrogenase Oxygen Inactivation Is Initiated at the H Cluster 2Fe Subcluster. J Am Chem Soc 2015;137:1809–16. https://doi.org/10.1021/ja510169s.

[25] Stripp ST, Goldet G, Brandmayr C, Sanganas O, Vincent KA, Haumann M, et al. How oxygen attacks [FeFe] hydrogenases from photosynthetic organisms. Proc Natl Acad Sci 2009;106:17331–6. https://doi.org/10.1073/pnas.0905343106.

[26] Pinto TS, Malcata FX, Arrabaça JD, Silva JM, Spreitzer RJ, Esquível MG. Rubisco mutants of *Chlamydomonas reinhardtii* enhance photosynthetic hydrogen production. Appl Microbiol Biotechnol 2013;97:5635–43. https://doi.org/10.1007/s00253-013-4920-z.

[27] Melis A, Zhang L, Forestier M, Ghirardi ML, Seibert M. Sustained Photobiological Hydrogen Gas Production upon Reversible Inactivation of Oxygen Evolution in the Green Alga *Chlamydomonas reinhardtii*. Plant Physiol 2000;122:127–36. https://doi.org/10.1104/pp.122.1.127.

[28] Sun Y, Chen M, Yang H, Zhang J, Kuang T, Huang F. Enhanced H_2 photoproduction by down-regulation of ferredoxin-$NADP^+$ reductase (FNR) in the green alga *Chlamydomonas reinhardtii*. Int J Hydrogen Energy 2013;38:16029–37. https://doi.org/10.1016/J.IJHYDENE.2013.10.011.

[29] Kosourov S, Jokel M, Aro E-M, Allahverdiyeva Y. A new approach for sustained and efficient H_2 photoproduction by *Chlamydomonas reinhardtii*. Energy Environ Sci 2018;11:1431–6. https://doi.org/10.1039/C8EE00054A.

[30] Nagy V, Podmaniczki A, Vidal-Meireles A, Tengölics R, Kovács L, Rákhely G, et al. Water-splitting-based, sustainable and efficient H_2 production in green algae as achieved by substrate limitation of the Calvin–Benson–Bassham cycle. Biotechnol Biofuels 2018;11:69. https://doi.org/10.1186/s13068-018-1069-0.

[31] Ben-Zvi O, Dafni E, Feldman Y, Yacoby I. Re-routing photosynthetic energy for continuous hydrogen production in vivo. Biotechnol Biofuels 2019;12:266. https://doi.org/10.1186/s13068-019-1608-3.

[32] Eilenberg H, Weiner I, Ben-Zvi O, Pundak C, Marmari A, Liran O, et al. The dual effect of a ferredoxin-hydrogenase fusion protein in vivo: successful divergence of the photosynthetic electron flux towards hydrogen production and elevated oxygen tolerance. Biotechnol Biofuels 2016;9:182. https://doi.org/10.1186/s13068-016-0601-3.

[33] Yacoby I, Pochekailov S, Toporik H, Ghirardi ML, King PW, Zhang S. Photosynthetic electron partitioning between [FeFe]-hydrogenase and ferredoxin: $NADP^+$-oxidoreductase (FNR) enzymes in vitro. Proc Natl Acad Sci 2011;108:9396–401.

[34] Kanygin A, Milrad Y, Thummala C, Reifschneider K, Baker P, Marco P, et al. Rewiring photosynthesis: a photosystem I-hydrogenase chimera that makes H_2 *in vivo*. Energy Environ Sci 2020;13:2903–14. https://doi.org/10.1039/C9EE03859K.

[35] Happe T, Kaminski A. Differential regulation of the Fe-hydrogenase during anaerobic adaptation in the green alga *Chlamydomonas reinhardtii*. Eur J Biochem 2002;269:1022–32. https://doi.org/10.1046/j.0014-2956.2001.02743.x.

[36] Mulder DW, Boyd ES, Sarma R, Lange RK, Endrizzi JA, Broderick JB, et al. Stepwise [FeFe]-hydrogenase H-cluster assembly revealed in the structure of $HydA^{\Delta EFG}$. Nature 2010;465:248–51. https://doi.org/10.1038/nature08993.

[37] Su X, Ma J, Pan X, Zhao X, Chang W, Liu Z, et al. Antenna arrangement and energy transfer pathways of a green algal photosystem-I–LHCI supercomplex. Nat Plants 2019;5:273–81. https://doi.org/10.1038/s41477-019-0380-5.

[38] Song Y, DiMaio F, Wang RY-R, Kim D, Miles C, Brunette T, et al. High-Resolution Comparative Modeling with RosettaCM. Structure 2013;21:1735–42. https://doi.org/10.1016/j.str.2013.08.005.

[39] Schrödinger L. The {PyMOL} Molecular Graphics System, Version 2.4.0. 2015.

[40] Rumpel S, Siebel JF, Diallo M, Farès C, Reijerse EJ, Lubitz W. Structural Insight into the Complex of Ferredoxin and [FeFe] Hydrogenase from *Chlamydomonas reinhardtii*. ChemBioChem 2015;16:1663–9. https://doi.org/10.1002/cbic.201500130.

[41] Meuser JE, D'Adamo S, Jinkerson RE, Mus F, Yang W, Ghirardi ML, et al. Genetic disruption of both *Chlamydomonas reinhardtii* [FeFe]-hydrogenases: Insight into the role of HYDA2 in H_2 production. Biochem Biophys Res Commun 2012;417:704–9. https://doi.org/10.1016/j.bbrc.2011.12.002.

[42] Kropat J, Hong-Hermesdorf A, Casero D, Ent P, Castruita M, Pellegrini M, et al. A revised mineral nutrient supplement increases biomass and growth rate in *Chlamydomonas reinhardtii*. Plant J 2011;66:770–80. https://doi.org/10.1111/j.1365-313X.2011.04537.x.

[43] Porra RJ, Thompson WA, Kriedemann PE. Determination of accurate extinction coefficients and simultaneous equations for assaying chlorophylls a and b extracted with four different solvents: verification of the concentration of chlorophyll standards by atomic absorption spectroscopy. Biochim Biophys Acta - Bioenerg 1989;975:384–94. https://doi.org/10.1016/S0005-2728(89)80347-0.

[44] Fischer N, Sétif P, Rochaix JD. Targeted Mutations in the *psaC* Gene of *Chlamydomonas reinhardtii*: Preferential Reduction of F_B at Low Temperature Is Not Accompanied by Altered Electron Flow from Photosystem I to Ferredoxin. Biochemistry 1997;36:93–102. https://doi.org/10.1021/bi962244v.

[45] Gulis G, Narasimhulu K V, Fox LN, Redding KE. Purification of His_6-tagged Photosystem I from *Chlamydomonas reinhardtii*. Photosynth Res 2008;96:51–60. https://doi.org/10.1007/s11120-007-9283-9.

[46] Nagy V, Podmaniczki A, Vidal-Meireles A, Kuntam S, Herman É, Kovács L, et al. Thin cell layer cultures of *Chlamydomonas reinhardtii* L159I-N230Y, *pgrl1* and *pgr5* mutants perform enhanced hydrogen production at sunlight intensity. Bioresour Technol 2021;333:125217. https://doi.org/10.1016/j.biortech.2021.125217.

[47] Kosourov SN, Batyrova KA, Petushkova EP, Tsygankov AA, Ghirardi ML, Seibert M. Maximizing the hydrogen photoproduction yields in *Chlamydomonas reinhardtii* cultures: The effect of the H_2 partial pressure. Int J Hydrogen Energy 2012;37:8850–8. https://doi.org/10.1016/j.ijhydene.2012.01.082.

[48] Burlacot A, Burlacot F, Li-Beisson Y, Peltier G. Membrane Inlet Mass Spectrometry: A Powerful Tool for Algal Research. Front Plant Sci 2020;11. https://doi.org/10.3389/fpls.2020.01302.

[49] Genty B, Briantais J-M, Baker NR. The relationship between the quantum yield of photosynthetic electron transport and quenching of chlorophyll fluorescence. Biochim Biophys Acta - Gen Subj 1989;990:87–92. https://doi.org/10.1016/S0304-4165(89)80016-9.

[50] Zhao J, Li R, Bryant DA. Measurement of Photosystem I Activity with Photoreduction of Recombinant Flavodoxin. Anal Biochem 1998;264:263–70. https://doi.org/10.1006/abio.1998.2845.

[51] Kuhlgert S, Drepper F, Fufezan C, Sommer F, Hippler M. Residues PsaB Asp612 and PsaB Glu613 of Photosystem I Confer pH-Dependent Binding of Plastocyanin and Cytochrome c_6. Biochemistry 2012;51:7297–303. https://doi.org/10.1021/bi300898j.

[52] Meimberg K, Mühlenhoff U. Laser-flash absorption spectroscopy study of the competition between ferredoxin and flavodoxin photoreduction by Photosystem I in *Synechococcus* sp. PCC 7002: Evidence for a strong preference for ferredoxin. Photosynth Res 1999;61:253–67. https://doi.org/10.1023/A:1006308729990.

[53] Nikolova D, Heilmann C, Hawat S, Gäbelein P, Hippler M. Absolute quantification of selected photosynthetic electron transfer proteins in *Chlamydomonas reinhardtii* in the presence and absence of oxygen. Photosynth Res 2018;137:281–93. https://doi.org/10.1007/s11120-018-0502-3.

[54] Hoobert JK, Blobel G. Characterization of the chloroplastic and cytoplasmic ribosomes of *Chlamydomonas reinhardi*. J Mol Biol 1969;41:121–38. https://doi.org/10.1016/0022-2836(69)90130-2.

[55] Kosourov S, Nagy V, Shevela D, Jokel M, Messinger J, Allahverdiyeva Y. Water oxidation by photosystem II is the primary source of electrons for sustained H_2 photoproduction in nutrient-replete green algae. Proc Natl Acad Sci 2020;117:29629–36. https://doi.org/10.1073/pnas.2009210117.

[56] Tirumani S, Gothandam KM, J Rao B. Coordination between photorespiration and carbon concentrating mechanism in *Chlamydomonas reinhardtii*: transcript and protein changes during light-dark diurnal cycles and mixotrophy conditions. Protoplasma 2019;256:117–30. https://doi.org/10.1007/s00709-018-1283-4.

[57] Xie X, Huang A, Gu W, Zang Z, Pan G, Gao S, et al. Photorespiration participates in the assimilation of acetate in *Chlorella sorokiniana* under high light. New Phytol 2016;209:987–98. https://doi.org/10.1111/nph.13659.

[58] Polukhina I, Fristedt R, Dinc E, Cardol P, Croce R. Carbon Supply and Photoacclimation Cross Talk in the Green Alga *Chlamydomonas reinhardtii*. Plant Physiol 2016;172:1494–505. https://doi.org/10.1104/pp.16.01310.

[59] Johnson X, Alric J. Interaction between Starch Breakdown, Acetate Assimilation, and Photosynthetic Cyclic Electron Flow in *Chlamydomonas reinhardtii*. J Biol Chem 2012;287:26445–52. https://doi.org/10.1074/jbc.M112.370205.

[60] Urbig T, Schulz R, Senger H. Inactivation and Reactivation of the Hydrogenases of the Green Algae *Scenedesmus obliquus* and *Chlamydomonas reinhardtii*. Zeitschrift Für Naturforsch C 1993;48:41–5. https://doi.org/10.1515/znc-1993-1-208.

[61] Redding K, MacMillan F, Leibl W, Brettel K, Hanley J, Rutherford AW, et al. A systematic survey of conserved histidines in the core subunits of Photosystem I by site-directed mutagenesis reveals the likely axial ligands of P_{700}. EMBO J 1998;17:50–60. https://doi.org/10.1093/emboj/17.1.50.

[62] Cashman DJ, Zhu T, Simmerman RF, Scott C, Bruce BD, Baudry J. Molecular interactions between photosystem I and ferredoxin: an integrated energy frustration and experimental model. J Mol Recognit 2014;27:597–608. https://doi.org/10.1002/jmr.2384.

[63] Forestier M, King P, Zhang L, Posewitz M, Schwarzer S, Happe T, et al. Expression of two [Fe]-hydrogenases in *Chlamydomonas reinhardtii* under anaerobic conditions. Eur J Biochem 2003;270:2750–8. https://doi.org/10.1046/j.1432-1033.2003.03656.

[64] Xia B, Vajda S, Kozakov D. Accounting for pairwise distance restraints in FFT-based protein–protein docking. Bioinformatics 2016;32:3342–4. https://doi.org/10.1093/bioinformatics/btw306.

CHAPTER 4

EXPRESSING A HYDROGENASE FROM *MEGASPHAERA ELSDENII* AS A FUSION WITH PHOTOSYSTEM I IN THE GREEN ALGA *CHLAMYDOMONAS REINHARDTII*

Andrey Kanygin

School of Molecular Sciences, Center for Bioenergy & Photosynthesis, Box 871604 Arizona State University Tempe, Arizona 85287-1604

Abstract

Photosynthesis converts sunlight into other forms of energy storing surplus as a reduced carbon. Considering increasing global energy demand and carbon neutrality, we previously demonstrated a proof-of-principle fusion protein allowing for capturing photosynthetic electrons directly at Photosystem I (PSI) to drive hydrogen production in vivo thereby switching storage molecule. However, our efforts to reach high-efficiency energy conversion were stymied by the O_2 inactivation of the hydrogenase. Recently, the truncated [FeFe]-hydrogenase from *Megasphaera elsdenii* was shown to retain the native level of O_2 tolerance. Here a novel *psaC-MeHydA* chimera is presented in which N-terminal ferredoxin-like domain of the *Me*HydA is replaced with the PsaC domain of PSI. The resulting chimeric protein assembles on PSI, accumulates to ~25% wild-type PSI levels, and make H_2 in a light-dependent fashion. In addition, replacement of PSI with the PSI-*Me*HydA chimera results in impaired cyclic electron flow and a limitation in linear electron transport. It is proposed that this system harboring chimeric hydrogenase and endogenous hydrogenases with different oxygen resistances to be a good starting point for directed evolution experiments aimed for selecting oxygen tolerant hydrogenases.

Introduction

Photosynthesis has been driving biomass accumulation on Earth for over 3 billion years, using fleeting light energy conversion into stable chemical bonds by pigment-protein machinery [1]. As the oxygenic photosynthesis became dominant, the light could do the most work by splitting water into oxygen, protons, and reducing electrons. Low redox potential electrons traverse energetically downhill via photosynthetic electron transport chain using energy difference to generate proton gradient [2,3]. First, at acceptor side of Photosystem II the quinone is reduced to quinol taking two protons and two electrons from the stromal side and via the Q-cycle, involving cytochrome b_6f, releasing 4 protons (per 2 electrons transported) at the luminal side of the membrane. Then, these electrons are “reenergized” by Photosystem-I becoming highly reducing

(~-520-590 mV at PSI acceptor side cofactors) and readily go to ferredoxin (E_m^o=-430 mV). Ferredoxins are a logistical hub for electrons in the stroma; deliver based on the momentary needs of the cell. When electrons delivered to ferredoxin-NADP reductase (FNR) to make NADPH, it is called linear electron flow. When electrons are delivered back to the quinone pool (via cytochrome *b6f* or NAD(P)H:quinone oxidoreductase), it is called cyclic pathway [4]. The former is used for carbon fixation resulting in NADPH and ATP consumption, while the latter allows supplementary ATP synthesis via additional proton pumping.

Alternative pathways for reductant at ferredoxin level takes place when the linear pathway is stalling [5–7] or cyclic electron flow is impaired [8,9]. To prevent overreduction and damage to PSI, electrons can follow the path of O_2 reduction if O_2 is available: either directly via Mehler reaction [10] or flavodiiron proteins mediated pathway [11]. In the absence of oxygen, some microalga developed a mechanism that involves hydrogenases – metalloenzymes catalyzing reversible proton reduction [12–15], thusly, reductant changes phase from liquid to gaseous storing energy as molecular hydrogen that can be recaptured later and converted back to reduced ferredoxin [16].

There are wide variety of hydrogenases that are present in all 3 domains of life and estimated in more than one-third of all microorgansims [17]. [FeFe]-hydrogenases represent a class with the highest turnover rates for H_2 oxidation/H^+ reduction reaction; subdivided based on the presence of accessory domains [18]. The [FeFe]-hydrogenase from *Megasphaera elsdenii* (*Me*HydA) has been well characterized [19–21] and shown to have a catalytic bias towards hydrogen production [22]. Although oxygen sensitive, *Me*HydA exhibited 10 times slower inactivation rate by O_2 than *Chlamydomonas reinhardtii* HydA1 (*Cr*HydA1) and its oxygen tolerance was not attributed to the F-like domain of the first 80 residues coordinating 2 [Fe_4S_4] clusters [23].

Recently, we published a proof-of-principle work in which we show that we can capture some of the reducing power and redirect it from carbon fixation to proton reduction, hence,

changing the energy storage molecule from carbohydrate to molecular hydrogen [24,25]. In essence, we created a *psaC-hydA* gene and replaced the native *psaC* in the chloroplast, so that upon expression and assembly on PSI, the chimera would deliver PSI electrons to the active site of hydrogenase. In that work and our sequential work, endogenous hydrogenases of *Chlamydomonas reinhardtii* have been used, which are notoriously oxygen sensitive [26,27]. In both cases, we show hydrogenase function significantly suffers from oxygen inactivation as active oxygen removal methods [28] improve chimeric hydrogenase activity. Without a way to keep most of the chimeric protein active, photobiological hydrogen production cannot approach its theoretical maximum of solar-to-hydrogen conversion efficiency of ~13% [29,30] as electrons are diverted to alternative electron acceptors (O_2) and become feasible for industrial scale. A wild-type *Chlamydomonas* light-to-hydrogen energy conversion efficiency is typically an order of magnitude lower and is around 1.61% under conditions of mitigating O_2 by respiration [31]. To cope with negative effect of oxygen on hydrogenase activity, we explored the option of fusing a more oxygen tolerant hydrogenase from *Megasphaera elsdenii* with the PsaC subunit of PSI.

Materials and methods

Design of PsaC-MeHydA chimera and modeling

A protein sequence of PsaC-*Me*HydA is shown in **figure 4-1**. *Me*HydA sequence [32] (GenBank accession number AAF22114.1) was aligned with HydA1 GenBank accession number AAG00591.1) and HydA2 (GenBank accession number AAR04931.1) protein sequences (lacking transit peptide) (see **figure 4-2**) with the use of Clustal Omega tool [33] (https://www.ebi.ac.uk/Tools/msa/clustalo/). A model of the *Me*HydA was generated with Phyre2 server [34]. First 80 residues of *Me*HydA corresponding to ferredoxin domain and residues past the last conserved residue among all 3 hydrogenases (highlighted blue in **figure 4-2**) were removed in PyMOL [35]. In preparation for docking, PsaC residues D32-K35 of the *Chlamydomonas reinhardtii* PSI structure (PDB ID: 6JO5 [36]) were also removed in PyMOL. A rigid body docking of the truncated *Megasphaera elsdenii* hydrogenase domain (set as ligand) to

the PsaA, PsaB, PsaF and the modified PsaC subunits (set as receptor) was performed in ClusPro2 server [37] using a single distant restraint 1-25 Å between C14 of PsaC and C383 of *Me*HydA (original numbering). The most plausible docked model was used in design of the linking sequences. For N-terminus *Me*HydA junction with PsaC, a 10 amino acid residue (GGATATDAVP) linking sequence was used similarly to PsaC-HydA2 and PsaC-HydA1 constructs. For C-terminus junction of *Me*HydA, a 15 amino acid long sequence (HYSAGSGGGGSGAGG). A final model was built using Robetta's web server comparative modeling algorithm [38] providing the docked model coordinates as a template.

Generation of PSI-MeHydA algal mutants

The *psaC-MeHydA* fusion gene sequence was codon optimized for chloroplast expression and synthesized by Genscript (Piscataway, NJ USA). The gene construct was delivered on pBS-EP 5.8 vector [39], in which the fusion gene replaced the *psaC* gene. Transformations were carried out in the PBC4-2^{H6} strain lacking *psaC* and having hexahistidine tag on exon 1 of *psaA* [40] via biolistic transformation as previously described [24]. Positive transformants were selected on Tris-acetate-phosphate (TAP) plates with 100 mg L^{-1} spectinomycin in the dark. Positive transformants were confirmed by PCR with region specific

primers (PsaC5': TAATATGGAGATGACATATTTAG and PsaC3': GATCTCAC CAAGATACTCCC, also see **figure 4-3**).

Growth conditions

All strains were grown on TAP with revised mineral nutrients [41]. Mutants on plates were kept in the dark. Liquid cultures were grown under low room light (5-10 µmol m^{-2} s^{-1} PAR).

Chlorophyll (Chl) measurement

Chl *a+b* concentrations were determined in 80% acetone as described in [42].

Thylakoids and PSI preparation

Thylakoid membranes and PSI preparations were done as previously described [24] with minor modifications outlined below. In cell lysis step, ultrasonic cell disruption or French pressure cell was used.

For ultrasonic cell disruption, cell pellet (from 10 L mid-late log phase cultures, equivalent of 80-100 mg of Chl) was resuspended in breaking buffer (50 mM HEPES-KOH pH 7.5, 0.3 M sucrose, 10 mM EDTA-KOH, 1 mM phenylmethyl sulfonyl fluoride (PMSF)) to a final volume of 200 mL. Ultrasonic lysis was done in a thin-walled aluminum cup on ice with continuous stirring in the dark. Temperature was continuously monitored during sonication and was always at 4 ^{o}C. Branson sonifier S-450 was operated with ½" (12.7 mm) catenoidal horn at amplitude level 3 (10 % duty cycle) for 60 min. It approximately corresponded to 800 J per 10 mL of lysate as recommended for complete breakage of algal cells [43]. The lysate was spun down at 64000xg at 4 ^{o}C for 15 min, washed with H2 buffer (5 mM HEPES-KOH pH 7.5, 0.3 M sucrose, 10 mM

EDTA-KOH) and resuspended in buffer H3 (5 mM HEPES-KOH, 1.8 M sucrose, 10 mM EDTA-KOH). All the following steps of discontinuous sucrose gradient were as described in [24].

French press lysis protocol was followed exactly as previously described [24].

PSI isolation was done oxically using PROTEINDEX™ Ni-Penta™ agarose resin (Marvelgent Biosciences) as described in [40]. For oxygen removal, PSI elution samples were concentrated and exchanged buffer using Amicon™ stirred ultrafiltration cell (furnished with 100 kDa MWCO regenerated cellulose disc) inside the glovebox with a degassed solubilization buffer (25 mM HEPES-KOH, pH 7.5, 300 mM KCl, 5 mM $MgSO_4$, 10% glycerol, 0.03% n-dodecyl-β-D-maltoside (β-DDM)).

Laser-flash spectroscopy

Thylakoids were resuspended at ~60 µg *Chl* ml^{-1} in 25 mM HEPES-KOH (pH 7.5), 300 mM KCl, 10 % glycerol, 5 mM sodium ascorbate while PSI were resuspended at ~6 µg *Chl* ml^{-1} in with the same buffer with 0.03% β-DDM. Samples were kept on ice in the dark before measurements. Absorbance changes pumped by a saturating laser flash (532 nm, 6 ns, 20-25 mJ) were monitored at 696 nm with weak LED pulses (10 µs) using JTS-10 (Bio-Logic) kinetic

spectrophotometer. Background transients were collected by running the same sequence with laser shutter closed.

Gas chromatography

A model SRI 310 gas chromatograph with thermal conductivity detector and 5Å molecular sieve prepacked column (91.4 cm long) was used. Gas tight syringes (1700 series) with non-coring needles were used for probing headspace.

Immunoblotting

Western blots were carried out as described in [24]. Solubilized thylakoids were loaded on the same Chl (2 µg).

Membrane inlet mass spectrometry (MIMS)

MIMS measurements were carried out as described in [25].

In vivo P_{700} recovery measurements and Chl fluorescence measurements

Early log phase cells were washed and then resuspended in 10 mM sodium phosphate (pH 7.0), 2 mM sodium bicarbonate and 20% Ficoll™ PM400 (GE Healthcare) to ~30 µg/mL Chl (P_{700}) or ~9 µg Chl mL^{-1} (for Chl fluorescence measurements). Cells were dark adapted for 5 min. Aerobic conditions were ensured by occasional mixing and brief sparging with air (in between the measurements). P_{700}^{+} signal was measured at 696 nm as previously described [24]. Chlorophyll

steady state fluorescence was measured after 2 min of green LED (520 nm) of variable intensity as described in [25].

Flavodoxin photoreduction in vitro

The experiment was carried out as described in [25] with one major difference – no oxygen was expected as it was set up in the anaerobic chamber filled with 5% H_2/95% N_2 (Coy).

Results

Design and expression of PSI-MeHydA

To generate a reasonable model of PSI-*Me*HydA, we isolated the hydrogenase domain of our *Me*HydA homology model based on the work of Caserta et al [23] and a multiple sequence alignment with *Cr*HydAs (see **figure 4-2**). The first 80 residues corresponding to a ferredoxin-like domain were removed, as well as all residues past the last consensus residue (T452, See **figure 4-2**). The model of the truncated *Me*HydA hydrogenase domain was docked to PsaC, PsaA, PsaB and PsaF subunits of PSI (PDB ID:6JO5, [36]) with a single distant restraint (1-25 Å) between adjacent to surface cysteines of F_b (Cys14) and H-cluster (Cys383). Four residues (Asp32-Lys35) of the PsaC outer loop (point of the fusion) were removed in PyMOL prior to docking. The most plausible model placed N-terminal junction residues ~12 Å apart from each other, while the C-terminal junction gap was ~22 Å. To connect N-terminal junction, we tried the native N-terminus sequence to bridge hydrogenase and F-domains with added G (GGAIVE), while a YFSDKSGG sequence (native C-terminal sequence of *Me*HydA) was used for the C-terminal junction. When introduced into *Chlamydomonas reinhardtii,* no stable chimeric PSI-*Me*HydA complex was detected (see **figure 4-4**, for multiple sequence alignment of various PsaC-HydA). For the second attempt, we made the N-terminal junction slightly longer (GGATATDAVP) and the same as in previously made PsaCHydA1 and PsaCHydA2 chimeras. We made the C-terminal junction like HydA1/HydA2 by replacing YF with HY and extending the

length (and flexibility) by 7 residues (HYSAGSGGGGSGAGG). A model of this version of PSI-*Me*HydA is shown on **figure 4-5.**

The designed *psaC-hydA* gene was delivered to the chloroplast of the PBC4-2 strain, which lacks the *psaC* gene and harbors a His_6-tagged version of *psaA* [40], by particle bombardment. Transformants were selected for spectinomycin/streptomycin resistance. Homologous recombination with the chloroplast chromosome should result in replacement of *psaC* with the *psaC-hydA* gene. Positive transformants were confirmed by PCR with region-specific primers (**figure 4-3**) and Sanger sequencing of the amplicons. For brevity, PBC4-2[PsaC-*Me*HydA] will be referred as $\Psi H3^{H6}$, and PBC4-2[pBSEP5.8] expressing wild type *psaC* as WT^{H6}. Expression of PsaC-*Me*HydA was confirmed by Western blot using solubilized thylakoids prepared from aerobically grown cells (**figure 4-6**). Samples were loaded on equal Chl amounts (2 µg per lane). When the blot was probed with anti-PsaC antibodies (**figure 4-6 A**), the WT^{H6} lane showed a single 10 kDa band corresponding to the PsaC subunit. A single ~50 kDa band appeared in the $\Psi H3^{H6}$, which is most likely the band corresponding to PsaC-*Me*HydA (predicted MW = 51.2 kDa). We also confirmed that the PsaD subunit is present in thylakoids of $\Psi H3^{H6}$ (**figure 4-6 B**). Given that PsaD is an extrinsic subunit of PSI, this indicates that PsaD is assembled onto the PSI-*Me*HydA complex, as seen before for PSI-HydA1 and PSI-HydA2 [24,25].

Spectroscopic characterization of the PSI-MeHydA

A primary function of reaction centers – conversion of absorbed light energy into a stable charge separation – requires all cofactors of the electron transfer chain to be assembled. The PsaC domain of PsaC-MeHydA carries two terminal $[Fe_4S_4]$ clusters: F_A and F_B. They can only be inserted upon proper folding of the PsaC domain from the first 30 and last 46 residues of the chimeric polypeptide. To test assembly and accumulation of PSI-*Me*HydA, we prepared thylakoids oxically via 2 methods: ultrasonic cell disruption and French Press. The former has

advantage of potentially being used under complete anoxia (inside the glovebox), while the latter is a standard thylakoid preparation.

First, we look at the amplitude of P_{700}^+ formation in thylakoids prepared via sonication. After a saturating laser flash in the presence of ascorbate (to ensure P_{700} is reduced before the flash), we observed 67% accumulation of PSI-*Me*HydA relative to the WT^{H6} signal (**figure 4-7 A**). Since WT^{H6} mutant was made of the photosynthetically inactive PBC4-2 strain lacking *psaC*, which was maintained heterotrophically for some time, we tested another WT control – JVD-$1B^{H6}$. When amplitudes of P_{700}^+ in thylakoids are compared between $\Psi H3^{H6}$ and JVD-$1B^{H6}$, we find ~38% relative photoaccumulation of the chimera. The Chl/P_{700}^+ ratio for $\Psi H3^{H6}$, WT^{H6} and JVD-$1B^{H6}$ were 6540, 4390 and 2480, respectively. In thylakoids prepared by French press (**figure 4-7 B**), we find a ~2 times larger amplitude of P_{700}^+ and a lower Chl/P_{700} ratio (3410 and 3520) for two independent transformants of $\Psi H3^{H6}$.

Second, we examine recovery of P_{700} signal in the dark. Upon charge separation in the absence of available electron acceptors, the reduced iron sulfur clusters of PSI harbored by PsaC will eventually backreact with P_{700}^+. Charge recombination of the $P_{700}^+(F_A/F_B)^-$ state typically happens with a time constant(s) of 40-200 ms and if F_AF_B are not available (e.g., PsaC is absent or F_A/F_B is reduced), charge recombination from F_X^- would happen with a time constant of ≤1 ms [44]. We fitted the P_{700}^+ transients (see **figure 4-7 A and B insets**) to a triexponential decay function (See **table 4-1** for parameters). All preparations exhibited a component corresponding to charge recombination of $P_{700}^+(F_A/F_B)^-$, confirming that the PsaC domain had folded correctly. It is worth pointing out that all thylakoids prepared via sonication show signs of shorter decay time constants than expected from a typical P_{700}^+-$(F_A/F_B)^-$ and likely result from some fraction of reaction centers having lost PsaC-MeHydA. The slowest decay component (on the order of seconds) is due to P_{700}^+ being reduced by ascorbate, because electrons had escaped from the iron sulfur clusters to exogenous acceptors (such as O_2). This phase was especially prevalent in

the French press preparations (60-70% amplitude) while also present in the ultrasonically disrupted cells (10-15% amplitude).

To get rid of dissolved oxygen, we concentrated PSI prepared from sonicated thylakoids under anoxia. In P_{700} bleaching and recovery kinetic experiment (**figure 4-7 C**), we observed a diminished slow phase (3-10% amplitude, see **table 4-2**). WT^{H6} PSI showed a typical biphasic kinetic (24 ± 1.4 ms and 98 ± 5.7 ms) for charge recombination P_{700}^{+}-$(F_A/F_B)^{-}$. PSI-*Me*HydA sample on the other hand showed biphasic kinetics that are significantly slower than WT PSI (51 ± 2.5 ms and 211 ± 16 ms).

In vitro activity toward flavodoxin photoreduction

An ideal PSI-HydA chimera would direct all electrons to the hydrogenase domain. In such a situation, the rate of reduction of its normal electron acceptor would approach zero. To test the ability of PSI-*Me*HydA to reduce cyanobacterial flavodoxin, we used purified PSI or PSI-*Me*HydA complexes under anoxia with a ~50-fold excess of flavodoxin exposed to brief illuminations of saturating actinic light. We found that the linear rate determined over a ~1 s interval (as shown in **figure 4-8**) is ~15.9 ± 2.4 % that of to WT^{H6} and 12.3 ± 2.4 % relative to JVD-$1B^{H6}$ PSI. Thus, the addition of the MeHydA domain to PsaC lowers Flvd reduction by a factor of 6-8. Please note that the interval between the actinic light was switched ON and the following detection point was excluded from linear analysis.

Another way to look at electron escape from terminal iron-sulfur clusters of PSI to exogenous acceptors (flavodoxin) is to measure a charge recombination kinetics after a single turnover laser flash without and with flavodoxin added. Under anoxic conditions, the substitution of a fast charge recombination P_{700}^{+}-$(F_A/F_B)^{-}$ with a very slow phase of reduction by ascorbate is expected solely due to electrons leaving for flavodoxin. To account for different time constants in slow phase of reduction kinetics, we integrated areas under the decay curves and subtracted the area without flavodoxin from the area with flavodoxin (see **figure 4-9**). The resulting areas represent a fraction of slow reductant in units of (electrons*ms) that was needed due to

replenishing electrons gone to flavodoxin. Finally, multiplying area difference by the decay rate constants (1/ms) corresponding to the slowest phase of decay (with flavodoxin added, see **table 4-3**), we find that fraction of electrons went to flavodoxin are 45%, 39% and 32% for JVD-1b^{H6}, WT^{H6} and ΨH3^{H6} respectively.

In vivo photosynthetic activity of ΨH3^{H6} strain

When analyzing hydrogen production/oxidation activity of the ΨH3^{H6} strain, it is important to keep in mind that it has 3 hydrogenases enzymes: two endogenous enzymes (HydA1 and HydA2) and the chimeric PSI-*Me*HydA. We first examine this mutant's ability to produce H_2 without added bicarbonate or acetate on a relatively short time scale using MIMS (**figure 4-10 panels A, B**). The experiment consisted of 2 parts: a light-saturation portion (2 min light ON followed by 3 min OFF) and continuous maximal light portion. During the light-saturation portion, the H_2 evolution rate plateaued at ~1170 µmol m^{-2} s^{-1} PAR with ~37 µmol H_2 h^{-1} (mg Chl)$^{-1}$. On continuous light, the H_2 rate gradually dropped down to ~5 µmol H_2 h^{-1} (mg Chl)$^{-1}$ as the dissolved H_2 concentration approached 120 µM. Just after the light was switched off, a maximal H_2 uptake rate of ~-17 µmol H_2 h^{-1} (mg Chl)$^{-1}$ was observed. The O_2 concentration remained low throughout the experiment with small spikes appearing during dark-to-light transitions. The net O_2 production rate saturated with light, reaching its maximal value of ~2 µmol O_2 h^{-1} (mg Chl)$^{-1}$ at 100% light intensity. The CO_2 concentration started at ~9 µM at the beginning of the experiment and more than doubled at the end of the continuous illumination portion. The CO_2 production rate coincided with O_2 spikes and saturated at maximal light intensity with the value of 6.3 µmol CO_2 h^{-1} (mg Chl)$^{-1}$. No net CO_2 uptake was detected during illumination of cells.

When bicarbonate was added to the cells at the beginning of the experiment (**figure 4-10 C and D**), there was about 2 times less H_2 produced in the light saturation portion and the maximal H_2 concentration was ~ 3 times less overall in comparison to the trial in which no bicarbonate was added. The H_2 production rate saturated with light at the highest intensity tested (1.4 mmol photons m^2 s^{-1}), reaching 27 µmol H_2 h^{-1} (mg Chl)$^{-1}$. In the continuous-illumination portion, the H_2

evolution rate dropped and became negative within 5 minutes of the onset. Towards the end of the illumination phase, the H_2 uptake rate suddenly accelerated, reaching ~15 µmol H_2 h^{-1} (mg Chl)$^{-1}$, resulting in complete consumption of H_2. The O_2 concentration stayed low and only started significantly increasing once all H_2 was consumed. Spikes of transient O_2 production were observed at each dark-light transition, but they were low (~1 µmol O_2 h^{-1} (mg Chl)$^{-1}$ at the highest light intensity). When H_2 was exhausted towards the end of the illumination, the O_2 production rate rose to 6 µmol O_2 h^{-1} (mg Chl)$^{-1}$ before the lights were turned off. Spikes of CO_2 production were also observed after each light-dark transition, saturating at 8 µmol CO_2 h^{-1} (mg Chl)$^{-1}$ under maximal illumination. During continuous illumination, the CO_2 production rate followed the H_2 evolution rate, transitioning to CO_2 uptake 2 min after maximal illumination commenced.

Next, we wanted to assess H_2 production on a longer scale, so we set up a sealed bottle experiment with anaerobically adapted cultures and periodically probed the headspace using GC (**figure 4-11**). Cells were resuspended with acetate-containing media to increase respiration and thereby protect hydrogenase from rapid inactivation. We found a significant difference in H_2 production by the ΨH3^{H6} strain in comparison to the WT^{H6} control. The initial H_2 production rate for ΨH3^{H6} was 19.5 ± 0.6 µmol H_2 h^{-1} (mg Chl)$^{-1}$ and remained quasi-linear for 3 hours at ~16 µmol H_2 h^{-1} (mg Chl)$^{-1}$. After overnight illumination, headspace H_2 had decreased, presumably due to uptake. The initial H_2 production rate of the WT^{H6} control was ~2-fold lower (11 ± 0.1 µmol H_2 h^{-1} (mg Chl)$^{-1}$) and rapidly declined, with headspace H_2 plateauing for the next 3 hours. Thus, the ΨH3^{H6} culture produced roughly 4 times more H_2 than the WT^{H6} control culture during a 4-h illumination period under these conditions.

Net O_2 was initially evolved at 9.5 ± 1.5 µmol O_2 h^{-1} (mg Chl)$^{-1}$ by ΨH3^{H6} for the first hour and then remained fairly stable at about 0.05% for the next 3 h. The amount of O_2 doubled overnight. In contrast, WT^{H6} exhibited a linear rate of O_2 evolution in the first 4 hours at an average rate of 10.7 µmol O_2 h^{-1} (mg Chl)$^{-1}$; O_2 reached 0.2% in the headspace and did not significantly change overnight.

It was also of interest to know how the ΨH3^{H6} strain would perform under fully aerobic conditions, as it must initially be grown this way. We used Chl fluorescence of Photosystem II to characterize its photosynthetic capacity for linear electron flow. ΨH3^{H6} strain saturates with relatively low light: at 67 µmol m^{-2} s^{-1} PAR (green LED at 520 nm) the quantum yield of PSII drops below 0.2. It takes almost 1500 µmol m^{-2} s^{-1} PAR for the WT^{H6} control for a comparable decrease in quantum yield (See **figure 4-9**).

We blocked PSII activity with 3-(3,4-dichlorophenyl)-1,1-dimethylurea (DCMU) and measured the rate of P_{700}^{+} decay to estimate cyclic electron flow (CEF) around PSI (**figure 4-13**). We found ~2.2 times lower CEF in ΨH3^{H6} chimeric strain (~3 e^{-} PSI^{-1} s^{-1}) compared to WT^{H6}. Addition of the cytochrome *b_6f* inhibitor 2,5-dibromo-6-isopropyl-3-methyl-1,4-benzoquinone (DBMIB) resulted in the rate of P_{700}^{+} re-reduction dropping >6-fold for the WT^{H6} strain and 2-fold for ΨH3^{H6}, approaching 1 e^{-} PSI^{-1} s^{-1} for both.

Discussion

Design considerations

In this work, we created a new PSI chimera in *C. reinhardtii* chloroplast with a heterologous hydrogenase domain of *Megasphaera elsdenii* [FeFe]-hydrogenase that can make photosynthetic H_2 *in vivo*. Our previous work on PSI-hydrogenase chimeras clearly demonstrated the need for a more O_2-resistant candidate for carrying out proton reduction in the context of oxygenic photosynthesis. The hydrogenase of *M. elsdenii* was particularly interesting, for it was shown to be relatively O_2 tolerance, exhibiting a ~10-fold lower O_2 inactivation rate compared to algal hydrogenases. Furthermore, this property was retained after removal of the F-domain, an N-terminal extension that is similar to a dicluster ferredoxin [23]. This domain is typically found in bacterial hydrogenases, but not in the algal enzymes, and it had been thought that it contributed to the O_2 tolerance. Another compelling reason for making a chimera with heterologous hydrogenase was the observed electron escape to ferredoxin/flavodoxin from our constructs with algal hydrogenases, which seemed to be from the hydrogenase domain. Given that the algal

hydrogenases must be able to bind and oxidize/reduce the algal ferredoxin, it was reasonable to think that replacement with a bacterial hydrogenase that has not evolved to interact with chloroplast ferredoxin might result in less electron escape. The *Me*HydA domain is indeed very different from algal hydrogenases: 30.7 % identity (43.1 % similarity) against HydA1 and 31.5 % identity (43.0 % similarity) against HydA2 (see **figure 4-2**). It had been shown that *Cpl* HydA from *Clostridium pasteurianum* could be expressed and activated in the algal chloroplast *in vivo* [45], so it was not unrealistic to expect that another bacterial HydA domain could also be activated by the algal HydEF/HydG maturases. However, since *Me*HydA shares only 31.3% sequence identity (41.4 % similarity) with *Cpl*HydA, it was not guaranteed that the algal maturation machinery could insert the H-cluster into this foreign hydrogenase. Our work has thus expanded the concept that the maturases are capable of working with a wider variety of HydA domains than once thought.

The other risk of incorporating *Me*HydA into the PSI-HydA chimera was that we had to use a truncated version of the bacterial hydrogenase lacking the F-domain to generate the same type of chimera as was previously made with algal HydA1 and HydA2. A hard docking model of truncated *Me*HydA bound to PsaC (along with PsaA, PsaB and PsaF) showed that the terminal iron sulfur cluster of PSI (F_B) could be as close as 12.3 Å (edge-to-edge) to the iron-sulfur cubane of the H-cluster (**figure 4-5**). This is closer than in our published models for PSI-HydA2 (14.8 Å) [24] or PSI-HydA1(15 Å) [25]. This difference could be due to the smaller *Me*HydA domain: the truncated polypeptide is 41 residues shorter than algal HydA1 trimmed of N- and C-terminal nonconserved residues. The structural similarity of PsaC to the F-domain of *Me*HydA might play a role in such a close docking, in that one ferredoxin-like domain is being replaced with another, albeit with a different connectivity. Based on Marcus electron transfer theory, the forward electron transfer rate in the PSI-*Me*HydA chimera might be faster than in the previously designed chimeras, assuming that the reorganization energy and driving force of the reaction are not significantly different.

The first attempt at generating a PSI-*Me*HydA chimera failed, due to insufficient length of the N-(GGAIVE) and C-terminal (YFSDKSGG) linkers. The mutant was unable to accumulate any PSI-HydA chimera: there was no PSI, no hydrogenase activity, and no photobiological hydrogen production (data not shown). Our initial assumption was that an average distance of 3.7 A between α-carbons of consecutive residues in the linker would satisfy distances obtained with the docking model, but this did not account for the extra length needed for folding the PsaC domain, and perhaps for obtaining a more relaxed conformation of the polypeptide backbone. A proven N-terminal linker sequence (used in the PsaC-HydA2 and PsaC-HydA1 chimeras) and increasing the C-terminal linker length and flexibility resulted in a stably assembled PSI-*Me*HydA, present at 25% - 67 % the WT PSI level.

Structure and operation of the PSI-MeHydA chimeric protein

A chloroplast vector carrying the second version of *psaC-MeHydA* was introduced into the PBC4-2 strain lacking *psaC* and having hexahistidine-tagged *psaA* exon 1. There were no mutations to the endogenous hydrogenases that would impair H_2 production in that strain, as evidenced by hydrogenase activity of the WT^{H6} strain (**figure 4-10)**. Therefore, we expected a contribution of endogenous hydrogenases to H_2 evolution and uptake in $\Psi H3^{H6}$. Expression and stable assembly of PSI-*Me*HydA was verified by immunoblots of purified thylakoids (**figure 4-6**). PsaD is present in PSI-*Me*HydA (as seen before in previous chimeras) and likely interacts with the N-terminal junction of the chimera (**figure 4-5**).

PSI-*Me*HydA chimera accumulation, as measured by the amplitude of P_{700}^+ signal under saturating laser flash, varies with the method of thylakoid preparation. Under a gentle protocol requiring French press for cell breakage, we observed 3410-3520 Chl/P_{700}^+ ratio (averages from independent transformants, See **figure 4-7 B**). These numbers, when compared with previously made chimeras (prepared with French press protocol): 5650 for PSI-HydA2 (~15%), 1100 for PSI-HydA1, place PSI-*Me*HydA accumulation at 24-25 % of typical WT level. With ultrasonic cell disruption protocol providing 800 J/10 mL of lysate [43], despite precautions aimed at reducing

global temperature rise of the solution (and no such rise was detected in 200 mL of lysate solution at any point during cell lysis), we observed a much higher Chl/P_{700}^{+} ratio: 6540, 4390 and 2480 for ΨH3^{H6}, WT^{H6} and JVD-1B^{H6}, respectively. This is likely due to local hot spots formed upon resonant bubble implosions, following sonolysis of water [46] (formation of OH· and H· radicals – strong oxidant and reductant) resulting in partial protein damage and faster charge recombination reactions in the affected reaction centers (if electron transfer chain is cut short). It might be possible that faster charge recombination reactions were partially due to a strong reductant generated in the process of sonolysis of water since we do not observe very fast phase of charge recombination in the purified PSI (see **figure 4-7 C, table 4-2**). The ratio of Chl/P_{700}^{+} of ~430 (PSI^{H6}) and ~690 (PSI^{H6}-*Me*HydA) suggests that purified PSI from sonicated cells have some inactive reaction centers as a mere contribution from PSI-LHCI (219 Chl/P_{700}^{+}, PDB ID: 6JO5) or even PSI-LHCI-LHCII (332 Chl/P_{700}^{+}, PDB ID: 7D0J) cannot explain such a high ratio. A typical PSI IMAC purification from French Pressed algal cells doesn't exceed 220 Chl/P_{700}^{+} and usually less.

Kinetics of P_{700}^{+} reduction after a saturating laser flash and in the absence of exogenous electron acceptors (e.g., ferredoxins or O_2) usually suggest stable charge-separated states formed during excitation. In purified PSI^{H6}, under anoxic conditions there is a typical biphasic decay of P_{700}^{+} due to $P_{700}^{+}(F_AF_B)^{-}$ charge recombination, accounting for most (95%) of the total signal (see **figure 4-7 C, table 4-2**). In PSI-*Me*HydA the time constants of the decay are significantly longer than in the WT with the longest (211 ± 16 ms, 32 ± 3 % amplitude of total decay vs 98 ± 6 ms, 46 ± 3 % amplitude in chimeric PSI and WT^{H6}, respectively) suggesting stable charge separation P_{700}^{+}-$(F_H)^{-}$ may be formed. This is in line with our previous examination of PSI-HydA1 and PSI-HydA2 P_{700}^{+} decay kinetics. A shorter time constant may also confirm F_H cluster of PSI-*Me*HydA being closer to P_{700} than in PSI-HydA2 or PSI-HydA1.

Direct reduction of flavodoxin (or ferredoxin) by PSI-*Me*HydA *in vitro* could be viewed as a reciprocal function of proton reduction activity by the chimeric complex since the 2 processes

are in competition when the hydrogenase active site is functional. Flavodoxin and ferredoxin share the binding interface on PSI, which requires the collaboration of PsaC, PsaD and PsaE forming a stromal ridge [47]. Moreover, PSI lacking the F_B cluster show no flavodoxin reduction from the remaining F_A cluster of PsaC [48]. We only used the initial 4 points to determine steady-state rate of flavodoxin reduction. Thusly, 6-8 times drop in flavodoxin steady-state photoreduction rate (per PSI complex) by PSI-*Me*HydA is comparable to previously made constructs. This suggests that flavodoxin "binding" might not involve interaction with hydrogenase domain of the chimeric complex and perhaps is limited to PsaC domain and linking regions. It is important to remember that this *in vitro* experiment is not representative of what is occurring in vivo, as the hydrogenase active site is damaged during purification of the PSI-HydA chimera – thus, there is no competition with proton reduction.

To find a probable site for Fd binding on PSI-*Me*HydA, we used the generated PsaC-*Me*HydA with PsaA, PsaB, PsaD, and PsaF subunits as a receptor for Fd hard docking as previously described [25]. With a single distant restraint between C14 (F_B) and outermost C42 of Fd (limited to 20 Å), the most likely docking model places Fd in a different position than typical WT ferredoxin site (**figure 4-14**). The distance between ferredoxin [2Fe-2S] cluster and F_B is ~15.2 Å and is larger than the docked model of Fd with PSI-HydA1. Polar interactions with *Me*HydA domain play a significant role in the proposed model (see **table 4-4**) but overall has less significant pairs than PSI-HydA1-Fd model.

Physiology of the ΨH3^{H6} mutant

Photobiological H_2 production of the ΨH3^{H6} strain on a short time scale had a maximal rate of 37 µmol h^{-1} (mg Chl)$^{-1}$, as measured by MIMS. Using the ratio of 3420 Chl per P_{700} determined for strain ΨH3^{H6}-1, this would correspond to a turnover rate of ~31 H_2 s^{-1}, assuming that each PSI-*Me*HydA complex is active. This number is comparable to the rate obtained for PSI-HydA2 in the ΨH1 strain – ~52 H_2 s^{-1}. The PSI-*Me*HydA turnover rate is about twice as high as PSI-HydA1 (16 H_2 s^{-1}). A reciprocal relation of turnover number vs accumulation level of the

PSI-HydA chimera may indicate that inactivation of the hydrogenase domain occurs faster and to a greater degree in a higher accumulating chimera.

The reduction in net H_2 production rate upon bicarbonate addition indicates the likely involvement of endogenous hydrogenases in concomitant H_2/CO_2 uptake processes competing with H_2 evolution processes by PSI-*Me*HydA. The H_2/CO_2 uptake eventually wins over as the CBB cycle activates, creating a large electron since, until H_2 is completely consumed and O_2 starts to build up (**figure 4-10 C**). This creates an electron transport chain: PSI-*Me*HydA $\rightarrow$ H_2 $\rightarrow$ HydA1/2 $\rightarrow$ ferredoxin $\rightarrow$ NADPH $\rightarrow$ carbon fixation. We note that this system has potential for directed evolution system of a more O_2 resistant hydrogenase *in vivo*. Assuming that O_2 inactivation of chimeric PSI-*Me*HydA is 10 times slower than algal endogenous hydrogenases, there should be available electrons from photosynthesis to drive H_2/CO_2 uptake by endogenous hydrogenases. Thus, by slowly allowing steady-state O_2 levels to rise in a photobioreactor setting, it may be possible to select mutants with more O_2-tolerant hydrogenases over many generations.

Longer term H_2 production in the $\Psi H3^{H6}$ strain was measured in a sealed-bottle experiment after 3 hours of dark anaerobic adaptation in media containing acetate to mitigate anticipated photosynthetic O_2 by mitochondrial respiration (**figure 4-11 A**). A quasi-linear rate of H_2 production by $\Psi H3^{H6}$ strain over a 3-hour period is very different from the isogenic control strain (WT^{H6}), which ceased most hydrogenase activity within 1 hour of illumination. The CBB cycle of WT activates after ~1 min of irradiation [5] and electrons are directed to CO_2 fixation as evidenced by a linear O_2 evolution rate (**figure 4-11 B**). $\Psi H3^{H6}$ doesn't show the same linearity to O_2 production and that could be due to increased mitochondrial respiration needed to compensate for the significantly reduced CEF in $\Psi H3^{H6}$ (**figure 4-13**). This is in line with previous findings on the *pgr5* mutant lacking CEF [9]. Another likely case for decreased O_2 evolution by $\Psi H3^{H6}$ is inactivation of PSI-*Me*HydA by O_2. That would turn the chimeric protein into a bottleneck for electron transport chain as evidenced by PSII Chl fluorescence even at low light intensities (**figure 4-12**).

Conclusions

We have created a chimeric PSI fused to a very different (and more oxygen tolerant than algal counterpart) hydrogenase from *Megasphaera elsdenii*. The algal maturation system is capable of inserting the H-cluster into PSI-*Me*HydA. Accumulation and stability of chimeric PSI-*Me*HydA is superior to PSI-HydA2 but not as high as PSI-HydA1. However, this lower accumulation level may be optimal for long term hydrogen production as the “bottleneck” in electron transport chain may restrain PSII oxygen evolution activity, provided no endogenous hydrogenases can fuel carbon fixation via H_2 uptake. Moreover, ΨH3 strain may serve as a starting point for directed evolution experiments in search for higher oxygen resistant hydrogenase.

MAHIVKIYDTCIGCTQCVRACPLDVLEMVPWGGATATDAVPNDVDKVKAALKDPEKIVIFQTAPA
VRVGLGEAFGMDPGTFVEGKMVAALRTLGADYVFDTDFGADLTIMEEATELLHRLQSEEIPIPQF
TSCCPAWVEFAETFYPDLLQHLSSTKSPISILSPVIKTYFAQQKNIDPKKIVNVCVTPCTAKKAEIR
RPELSASGLFWDEPEIRDTDICITTRELAQWIQDENIDFASLEDSKFDKAFGEASGGGRIFGNSG
GVMEAAIRTAYHMFTGRPAPKDFIPFEPVRGLQGVKKATVIFGHFVLHVAAISGLGNARAFIDDLI
KNDAFEDYSFIEVMACPGGCIGGGGQPKVKLPQVKKVQEARTASIYKSDEETDIKASWQNPEIET
LYEAFLDEPLSEMAEFTLHTHYSAGSGGGGSGAGGASQMASAPRTEDCVGCKRCETACPTDFL
SVRVYLGSESTRSMGLSY

Figure 4-1. Coding sequence of the PsaC-*Me*HydA polypeptide (474 residues). Highlighted residues indicate the PsaC fragment (green), N-terminus junction (cyan), HydA2 N-terminus linker sequence (magenta), and C-terminus linker (red).

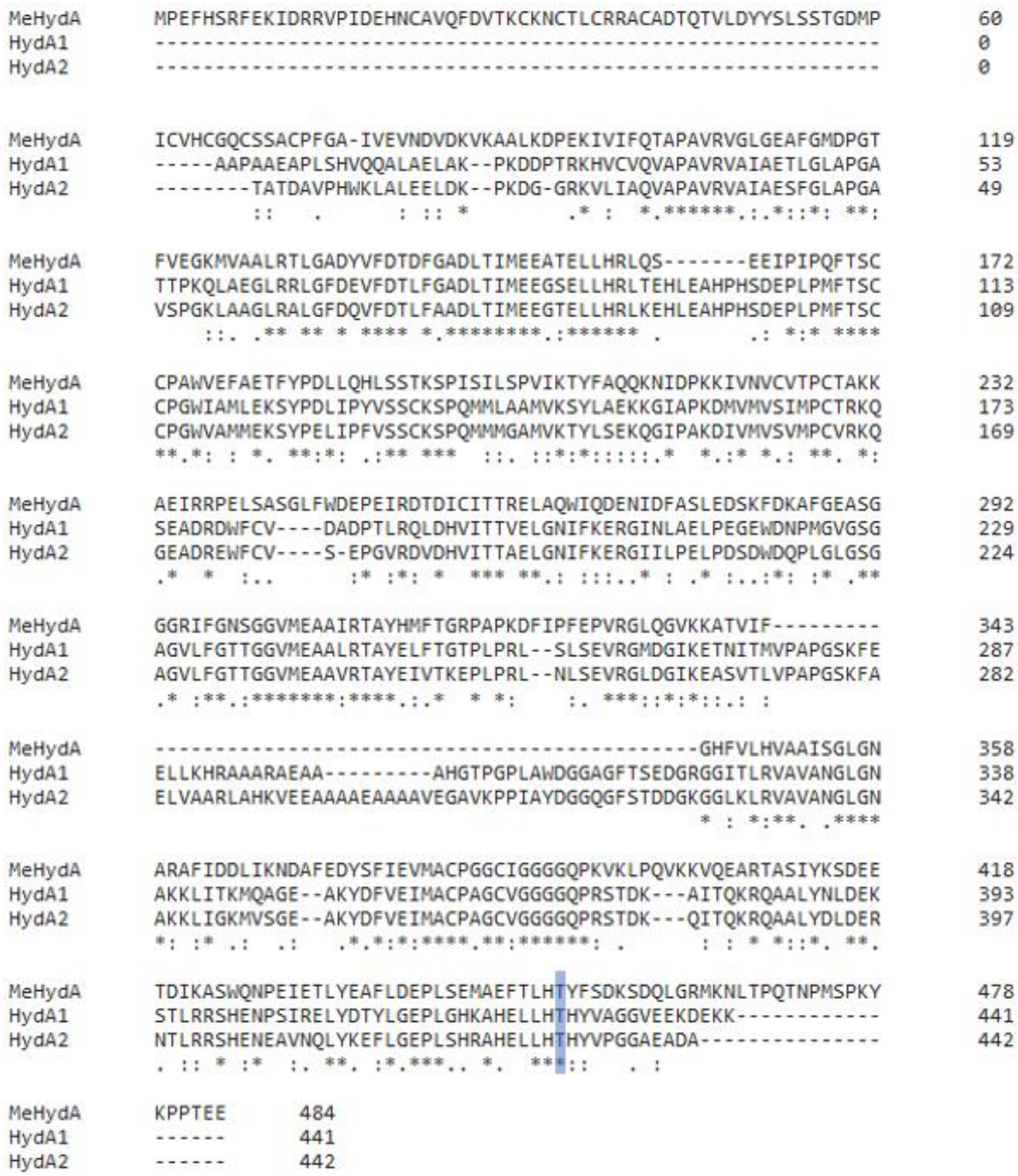

Figure 4-2. Clustal Omega (1.2.4) multiple sequence alignment of *Me*HydA to the mature (transit peptide removed) HydA1 and HydA2 hydrogenase sequences. (*) indicates fully conserved residues, (:) indicates residues with strongly similar properties, (.) indicates residues with weakly similar properties. Blue highlight shows the last conserved residue among all 3 sequences.

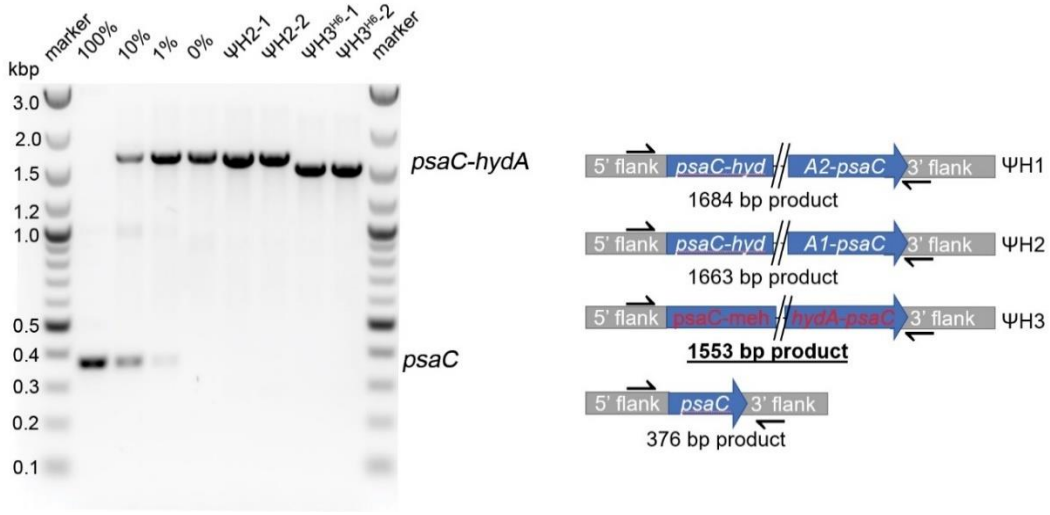

Figure 4-3. Homoplasmicity detection PCR. Wild type genomic DNA (WT^{H6}) indicated as a percentage of total DNA (diluted into ΨH1 genomic DNA containing psaC-HydA2 in place of psaC). ΨH2 genomic DNA is shown for comparison. Total DNA per reaction was 100 ng.

Figure 4-4. Clustal omega (1.2.4) multiple sequence alignment of PsaC-MeHydA with previously constructed chimeras. N-terminal junction is highlighted in blue, C-terminal junction is highlighted in red.

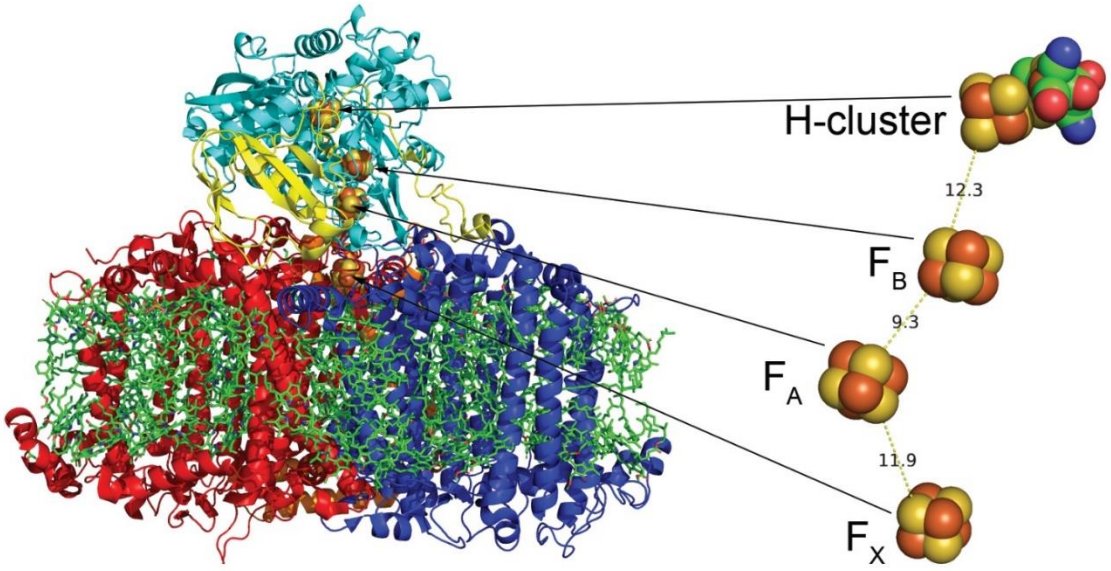

Figure 4-5. A model of PSI-*Me*HydA. PsaA (red), PsaB(blue), PsaC-*Me*HydA (cyan), PsaD (yellow), PsaF (orange) are shown as cartoon representation, with pigments as green sticks and metallic clusters as space-filling models. On the right, an exploded view of the acceptor side cofactors (with edge-to-edge distances in Å) is shown.

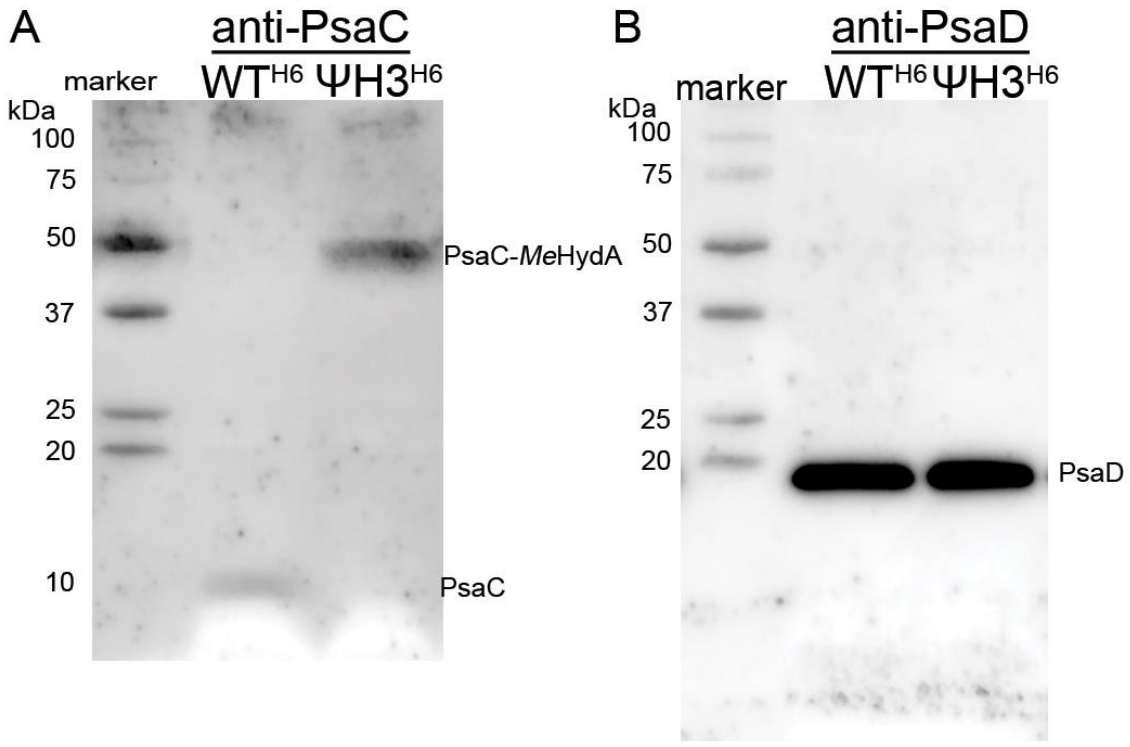

Figure 4-6. Immunoblots of solubilized thylakoids, loaded on equal amount of Chl (2 µg) and probed with antibodies against PsaC (A) or PsaD (B).

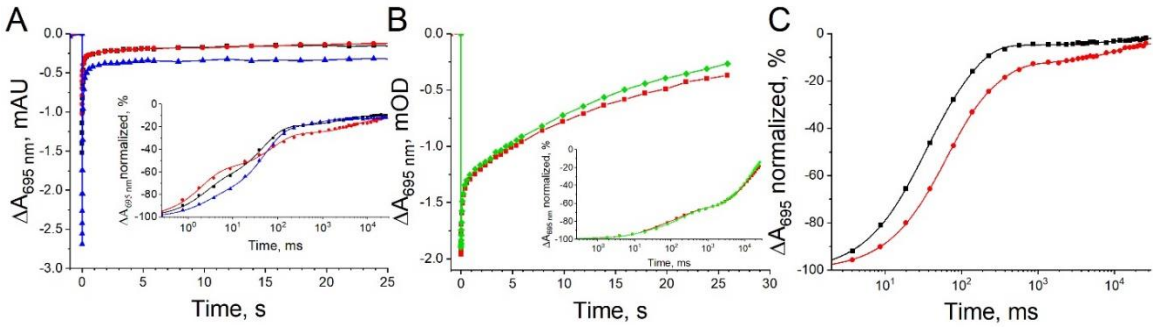

Figure 4-7. P_{700} photooxidation and recovery in thylakoids (A, B) or purified PSI (C). (A) Thylakoids (WT^{H6} – black squares, JVD-$1B^{H6}$ – blue triangles, Ψ$H3^{H6}$-1 -red circles, were prepared via sonication protocol in air or (B) Thylakoids (Ψ$H3^{H6}$-1 -red circles, Ψ$H3^{H6}$-2 – green diamonds) prepared via French press protocol in air. Transients normalized to 60 µg/ml of Chl. Insets show dark reduction of P_{700}^{+} with time shown on a log-scale. Average of 3 technical replicates. (C) Recovery kinetics of P_{700} in purified WT^{H6}-PSI (black squares) or Ψ$H3^{H6}$-1 (red circles) under anoxia from thylakoids in (A), Transients represent average of 3 technical replicates.

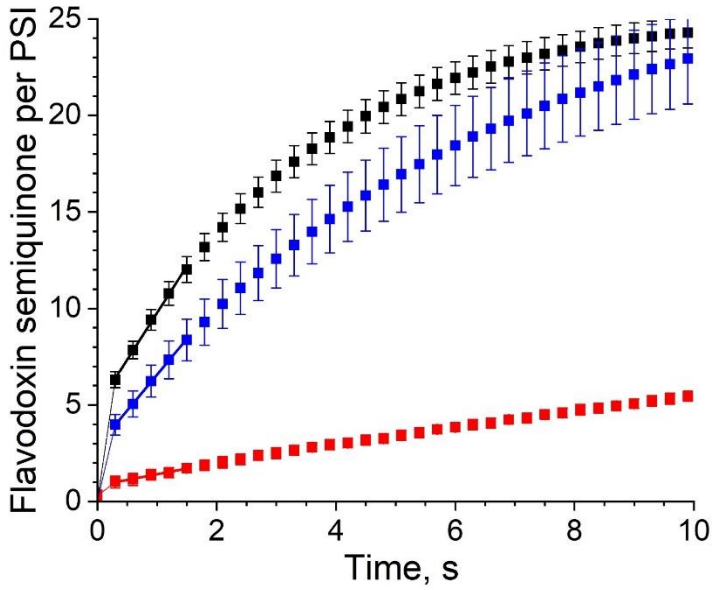

Figure 4-8. Flavodoxin photoreduction by PSI (0.1 µM) *in vitro* under saturating (3000 µmol m^{-2} s^{-1} PAR red light) illumination. Flavodoxin is ~50 fold excess of PSI (black=JVD-1B^{-H6}, blue=WT^{H6} and red= ΨH3^{H6}). Ascorbate (5 mM) and plastocyanin (5 µM) were used as electron donors to P_{700}^{+}. Turnover rates (derived from a linear fit as shown in bold line) are 5.7 ± 0.3 Flvd s^{-1} $(PSI)^{-1}$, 4.4 ± 0.6 Flvd s^{-1} $(PSI)^{-1}$ and 0.7 ± 0.1 Flvd s^{-1} $(PSI)^{-1}$ for WT-PSI: JVD-1B^{-H6}, WT^{H6}, and PSI-*Me*HydA respectively. Error bars represent standard error (n=3).

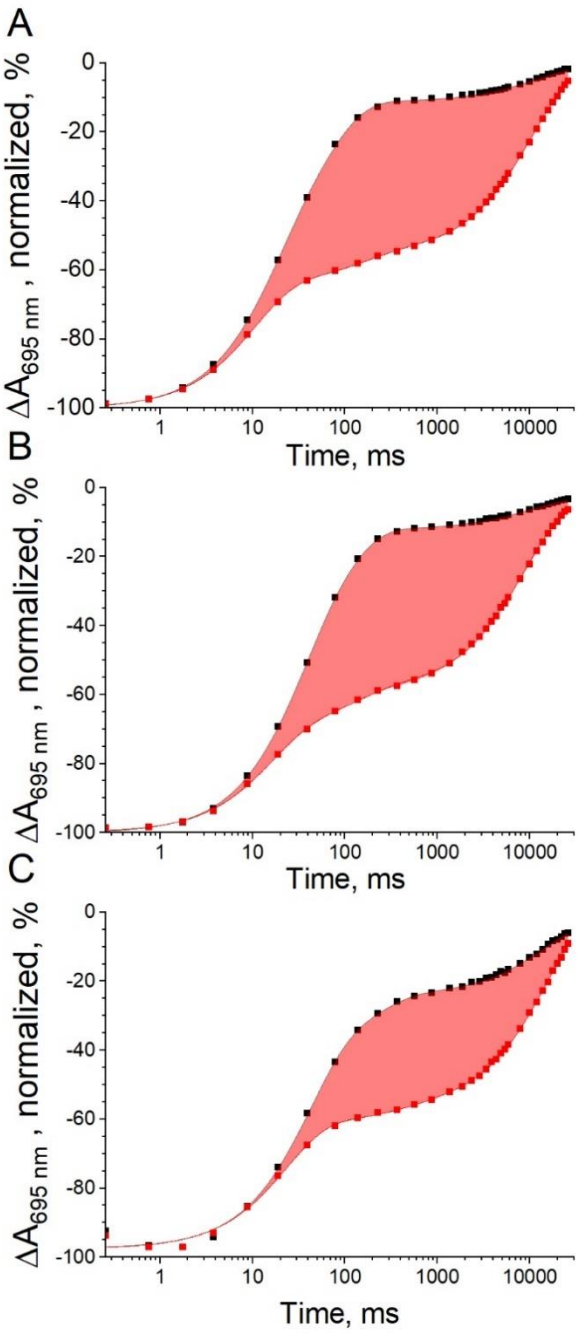

Figure 4-9. Effect of flavodoxin on charge recombination in vitro after a saturating laser flash in JVD-1B$^{-\ H6}$ (PSI) (panel A), WT^{H6} (panel B) and ΨH3^{H6} (panel C). Each trace was fitted to a 3-component exponential decay function (shown as a line). Traces with flavodoxin are shown in red, without flavodoxin - black. Area between the fitted lines filled in red represent a quantity of (electrons*ms) that escaped to flavodoxin. Setup was the same as in the kinetic experiment, except that plastocyanin was not added.

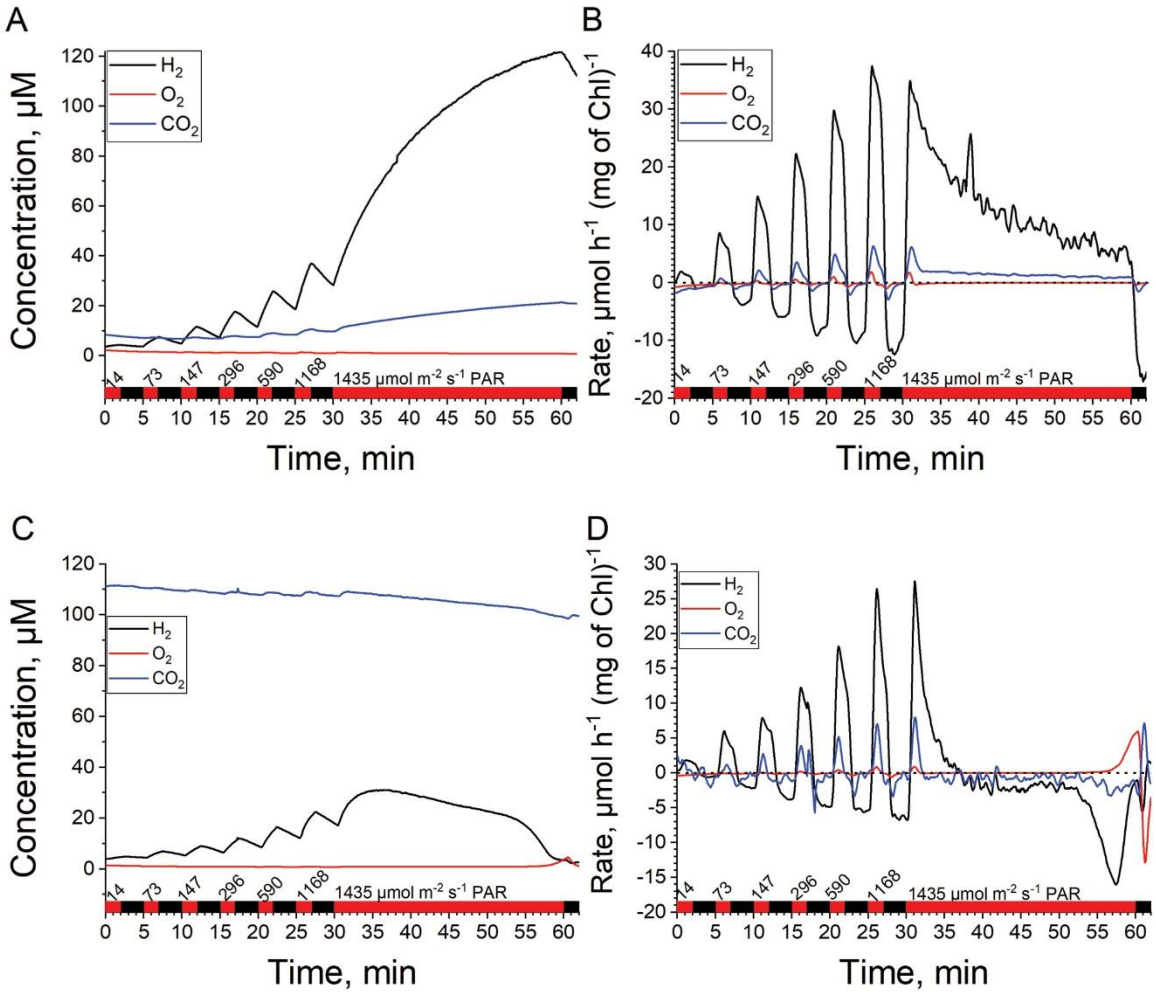

Figure 4-10. H_2 (black), O_2 (red) and CO_2 (blue) concentrations (A, C) and the derivatives of their concentrations (B, D) in cultures of $\Psi H3^{H6}$ cells resuspended in TP without added carbon source (A, B) or with 2 mM bicarbonate (C, D). Dotted line in B and D indicates zero rate. A bar above abscissa indicates intervals of specified light intensity or darkness. A single trial is reported.

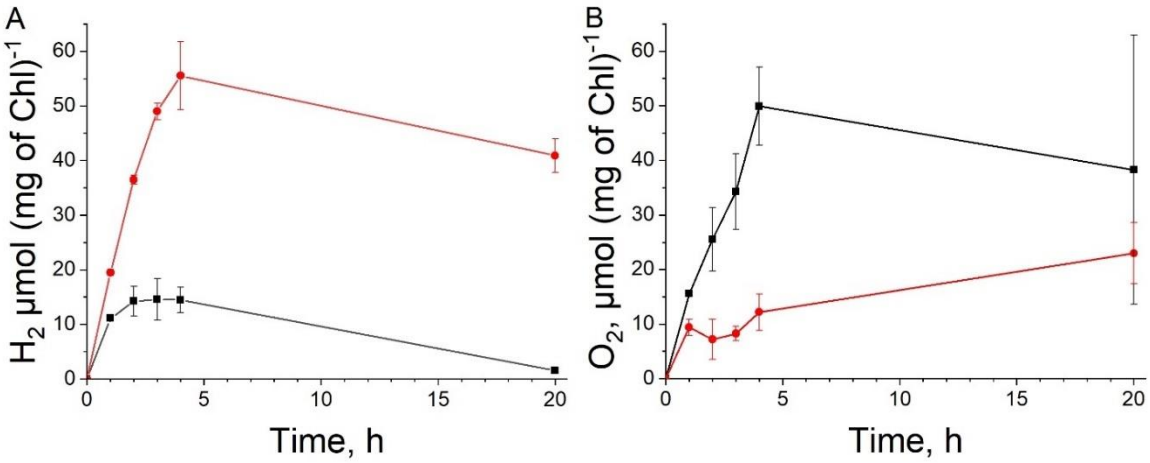

Figure 4-11. Net headspace H_2 (A) and O_2 (B) produced by ΨH3^{H6} (red) or WT^{H6} (black) resuspended in TAP after 2 h anaerobic adaptation in the dark followed up by ~200 µmol m^{-2} s^{-1} PAR emitted by white LEDs. The net amount of H_2 or O_2 was normalized to the initial Chl values. The sealed bottles were constantly agitated (except for headspace withdrawal). Error bars represent standard error (n=3).

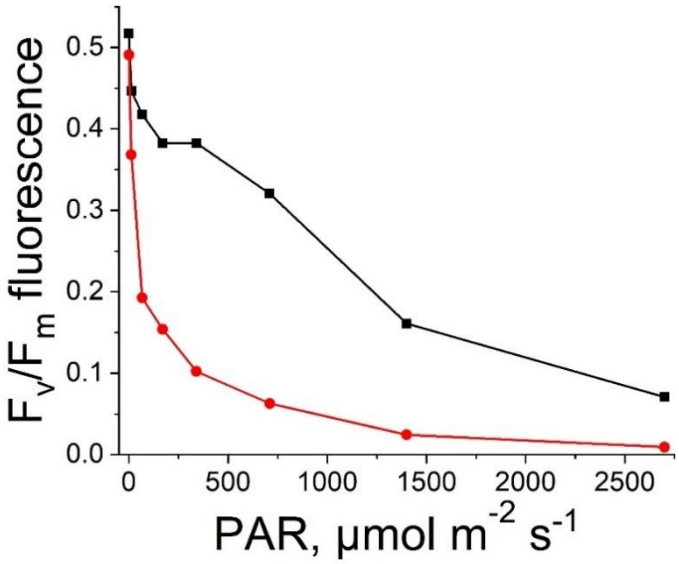

Figure 4-12. F_v/F_m of PSII for WT^{H6} (black/square) and $\Psi H3^{H6}$ (red/circle). Cells were resuspended in sodium phosphate buffer (pH 7.0) containing 20% Ficoll and 2 mM sodium bicarbonate, and dark adapted for 5 min prior to measurements. Aerobic conditions were maintained by brief sparging with air.

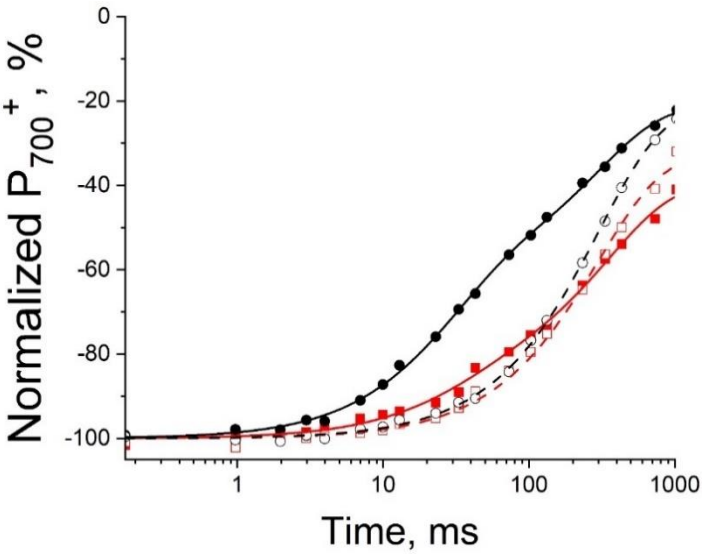

Figure 4-13. P_{700} dark recovery kinetics in WT^{H6} (black) and $\Psi H3^{H6}$ (red) cells after 10 s of illumination with red light (~630 nm) at a flux of ~500 photons $PSI^{-1}\,s^{-1}$. Cells were grown in TAP under low light before being resuspended in phosphate bicarbonate buffer, followed by addition of 10 µM DCMU (see Methods). Averages of P_{700}^+ reduction kinetics (n=5) in cells with DCMU (solid symbols) were fit to a biexponential decay (solid lines). Addition of 20 µM DBMIB to the same cells is indicated by hollow symbols; these transients were fit to a mono-exponential decay (dashed lines).

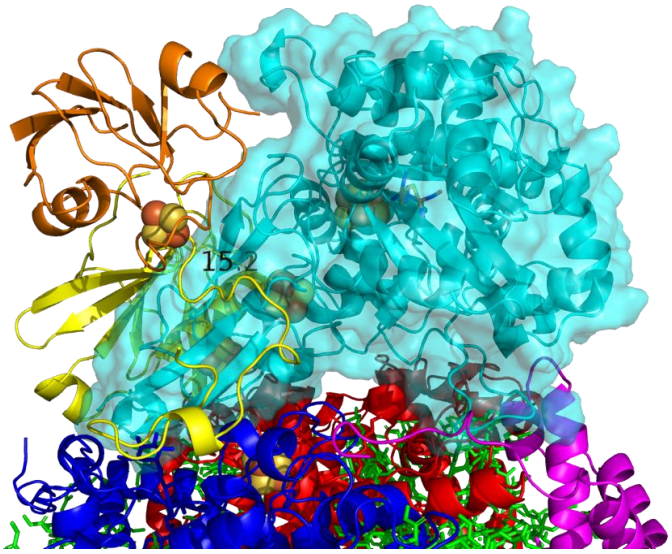

Figure 4-14. Fd1 docking to PSI-*Me*HydA model. Subunits of the chimeric PSI are PsaC-*Me*HydA (cyan), PsaA (red), PsaB (blue), PsaD (yellow) and PsaF (magenta) with Chl shown as green sticks. Fd shown as orange cartoon. Edge-to-edge distance between [2Fe-2S] cluster of Fd and F_B is 15.2 Å.

Parameter	Sonication protocol			French press protocol	
	WT^{H6}	JVD-$1b^{H6}$	$\Psi H3^{H6}$-1	$\Psi H3^{H6}$-1	$\Psi H3^{H6}$-2
τ_1 (ms)	2.3 ± 0.3	2.3 ± 0.4	2.0 ± 0.3	23.4 ± 4.5	13.9 ± 3.1
A_1 (%)	30 ± 1.4	16.5 ± 1.2	41 ± 1.8	11.4 ± 1.5	8.0 ± 0.9
τ_2 (ms)	47 ± 3	52 ± 2.5	76 ± 9	192 ± 21	184 ± 13
A_2 (%)	50 ± 1.3	61.5 ± 1.2	32 ± 1.4	19 ± 1.4	22.4 ± 1
τ_3 (s)	2.9 ± 0.4	0.85 ± 0.2	5.5 ± 0.9	15.2 ± 0.6	16.4 ± 0.6
A_3 (%)	9.9 ± 0.6	9.6 ± 1	14 ± 0.8	60 ± 1	69 ± 1
A_0 (%)	10.1 ± 0.3	12.6 ± 0.2	12.8 ± 0.6	8.1 ± 1.1	0.3 ± 1.2
R^2	0.99895	0.99941	0.9968	0.99964	0.9997

Table 4-1. Fitting coefficients of P_{700}^+ decay in thylakoids as shown in **figure 4-7 A and B.**

Parameter	Sonication protocol	
	WT^{H6}	$\Psi H3^{H6}$-1
τ_1 (ms)	24.3 ± 1.4	51.4 ± 2.5
A_1 (%)	48.9 ± 3.4	54.9 ± 2.9
τ_2 (ms)	98.1 ± 5.7	210.7 ± 16.3
A_2 (%)	46.4 ± 3.4	31.8 ± 2.9
τ_3 (s)	13.4 ± 5.5	11.0 ± 1.3
A_3 (%)	3.3 ± 0.5	9.7 ± 0.3
A_0 (%)	1.6 ± 0.6	3.6 ± 0.4
R^2	0.99989	0.99986

Table 4-2. Fitting coefficients of P_{700}^+ decay in purified PSI under anoxia as shown in **figure 4-7C**

Parameter	JVD-1b^{H6}		WT^{H6}		ΨH3^{H6}-1	
	- Fld	+ Fld	- Fld	+ Fld	- Fld	+ Fld
τ_1 (ms)	28 ± 2	15 ± 1	14 ± 1	10.3 ± 0.3	39 ± 5	23 ± 2
A_1 (%)	44 ± 5	28 ± 2	41 ± 2	35.5 ± 0.6	56 ± 7	36 ± 1.4
τ_2 (ms)	85 ± 6	122 ± 19	60 ± 2	148 ± 17	198 ± 80	391 ± 240
A_2 (%)	44 ± 5	12 ± 1	48 ± 2	9.2 ± 0.6	17 ± 7	5 ± 1
τ_3 (s)	10 ± 1	8.8 ± 0.2	11.7 ± 0.9	10.8 ± 0.2	14.4 ± 3.6	15.7 ± 1.4
A_3 (%)	9 ± 0.3	55 ± 0.3	10.5 ± 0.3	54.6 ± 0.3	21.7 ± 2	58.6 ± 2
A_0 (%)	2.7 ± 0.3	3.9 ± 0.4	0.7 ± 0.3	0.7 ± 0.4	2.3 ± 2.5	1.7 ± 2.4
R^2	0.99992	0.99979	0.99994	0.99987	0.99849	0.99881

Table 4-3. Fitting coefficients of P_{700}^+ decay in flavodoxin experiment as shown in **figure 4-9.**

Ferredoxin 1 residue	**PsaC-MeHydA residue**	**Distance (in Å)**
S43	G32	2.6
Y94	G33	2.5
Y94	L359	2.4
	PsaD residue	
H88	A163	3.2

Table 4-4. Important pairs of residues involved in Fd1 docking to PSI-*Me*HydA (**figure 4-14**).

References

[1] Hohmann-Marriott MF, Blankenship RE. Evolution of Photosynthesis. Annu Rev Plant Biol 2011;62:515–48. https://doi.org/10.1146/annurev-arplant-042110-103811.

[2] Nelson N, Ben-Shem A. The complex architecture of oxygenic photosynthesis. Nat Rev Mol Cell Biol 2004;5:971.

[3] Nelson N, Junge W. Structure and Energy Transfer in Photosystems of Oxygenic Photosynthesis. Annu Rev Biochem 2015;84:659–83. https://doi.org/10.1146/annurev-biochem-092914-041942.

[4] Nawrocki WJ, Bailleul B, Picot D, Cardol P, Rappaport F, Wollman F-A, et al. The mechanism of cyclic electron flow. Biochim Biophys Acta - Bioenerg 2019;1860:433–8. https://doi.org/10.1016/j.bbabio.2018.12.005.

[5] Milrad Y, Schweitzer S, Feldman Y, Yacoby I. Green Algal Hydrogenase Activity Is Outcompeted by Carbon Fixation before Inactivation by Oxygen Takes Place. Plant Physiol 2018;177:918–26. https://doi.org/10.1104/pp.18.00229.

[6] Pinto TS, Malcata FX, Arrabaça JD, Silva JM, Spreitzer RJ, Esquível MG. Rubisco mutants of *Chlamydomonas reinhardtii* enhance photosynthetic hydrogen production. Appl Microbiol Biotechnol 2013;97:5635–43. https://doi.org/10.1007/s00253-013-4920-z.

[7] Sun Y, Chen M, Yang H, Zhang J, Kuang T, Huang F. Enhanced H_2 photoproduction by down-regulation of ferredoxin-$NADP^+$ reductase (FNR) in the green alga *Chlamydomonas reinhardtii*. Int J Hydrogen Energy 2013;38:16029–37. https://doi.org/10.1016/J.IJHYDENE.2013.10.011.

[8] Dang K-V, Plet J, Tolleter D, Jokel M, Cuiné S, Carrier P, et al. Combined Increases in Mitochondrial Cooperation and Oxygen Photoreduction Compensate for Deficiency in Cyclic Electron Flow in *Chlamydomonas reinhardtii*. Plant Cell 2014;26:3036–50. https://doi.org/10.1105/tpc.114.126375.

[9] Elman T, Hoai Ho TT, Milrad Y, Hippler M, Yacoby I. Enhanced chloroplast-mitochondria crosstalk promotes ambient algal-H_2 production. Cell Reports Phys Sci 2022;3:100828. https://doi.org/10.1016/j.xcrp.2022.100828.

[10] Kozuleva M, Petrova A, Milrad Y, Semenov A, Ivanov B, Redding KE, et al. Phylloquinone is the principal Mehler reaction site within photosystem I in high light. Plant Physiol 2021;186:1848–58. https://doi.org/10.1093/plphys/kiab221.

[11] Chaux F, Burlacot A, Mekhalfi M, Auroy P, Blangy S, Richaud P, et al. Flavodiiron Proteins Promote Fast and Transient O_2 Photoreduction in *Chlamydomonas*. Plant Physiol 2017;174:1825 LP – 1836. https://doi.org/10.1104/pp.17.00421.

[12] Lubitz W, Ogata H, Rüdiger O, Reijerse E. Hydrogenases. Chem Rev 2014;114:4081–148. https://doi.org/10.1021/cr4005814.

[13] Engelbrecht V, Liedtke K, Rutz A, Yadav S, Günzel A, Happe T. One isoform for one task? The second hydrogenase of *Chlamydomonas reinhardtii* prefers hydrogen uptake. Int J Hydrogen Energy 2021;46:7165–75. https://doi.org/10.1016/j.ijhydene.2020.11.231.

[14] Eroglu E, Melis A. Microalgal hydrogen production research. Int J Hydrogen Energy 2016;41:12772–98. https://doi.org/https://doi.org/10.1016/j.ijhydene.2016.05.115.

[15] Cournac L, Mus F, Bernard L, Guedeney G, Vignais PM, Peltier G. Limiting steps of hydrogen production in *Chlamydomonas reinhardtii* and *Synechocystis* PCC 6803 as analysed by light-induced gas exchange transients. Int J Hydrogen Energy 2002;27:1229–37. https://doi.org/10.1016/S0360-3199(02)00105-2.

[16] Milrad Y, Schweitzer S, Feldman Y, Yacoby I. Bi-directional electron transfer between H_2 and NADPH mitigates light fluctuation responses in green algae. Plant Physiol 2021;186:168–79. https://doi.org/10.1093/plphys/kiab051.

[17] Søndergaard D, Pedersen CNS, Greening C. HydDB: A web tool for hydrogenase classification and analysis. Sci Rep 2016;6:34212. https://doi.org/10.1038/srep34212.

[18] Land H, Senger M, Berggren G, Stripp ST. Current State of [FeFe]-Hydrogenase Research: Biodiversity and Spectroscopic Investigations. ACS Catal 2020;10:7069–86. https://doi.org/10.1021/acscatal.0c01614.

[19] DIJK C, MAYHEW SG, GRANDE HJ, VEEGER C. Purification and Properties of Hydrogenase from *Megasphaera elsdenii*. Eur J Biochem 1979;102:317–30. https://doi.org/10.1111/j.1432-1033.1979.tb04246.x.

[20] DIJK C, GRANDE HJ, MAYHEW SG, VEEGER C. Properties of the Hydrogenase of *Megasphaera elsdenii*. Eur J Biochem 1980;107:251–61. https://doi.org/10.1111/j.1432-1033.1980.tb04645.x.

[21] FILIPIAK M, HAGEN WR, VEEGER C. Hydrodynamic, structural and magnetic properties of *Megasphaera elsdenii* Fe hydrogenase reinvestigated. Eur J Biochem 1989;185:547–53. https://doi.org/10.1111/j.1432-1033.1989.tb15148.x.

[22] Butt JN, Filipiak M, Hagen WR. Direct Electrochemistry of *Megasphaera Elsdenii* Iron Hydrogenase. Definition of the Enzyme's Catalytic Operating Potential and Quantitation of the Catalytic Behaviour over a Continuous Potential Range. Eur J Biochem 1997;245:116–22. https://doi.org/10.1111/j.1432-1033.1997.00116.x.

[23] Caserta G, Papini C, Adamska-Venkatesh A, Pecqueur L, Sommer C, Reijerse E, et al. Engineering an [FeFe]-Hydrogenase: Do Accessory Clusters Influence O_2 Resistance and Catalytic Bias? J Am Chem Soc 2018;140:5516–26. https://doi.org/10.1021/jacs.8b01689.

[24] Kanygin A, Milrad Y, Thummala C, Reifschneider K, Baker P, Marco P, et al. Rewiring photosynthesis: a photosystem I-hydrogenase chimera that makes H_2 *in vivo*. Energy Environ Sci 2020;13:2903–14. https://doi.org/10.1039/C9EE03859K.

[25] Kanygin A, Smith A, Nagy V, Tóth SZ, Redding KE. Interplay between hydrogen production and photosynthesis in a green alga expressing an active photosystem I-hydrogenase chimera. Int J Hydrogen Energy 2022;47:21969–83. https://doi.org/10.1016/j.ijhydene.2022.03.096.

[26] Swanson KD, Ratzloff MW, Mulder DW, Artz JH, Ghose S, Hoffman A, et al. [FeFe]-Hydrogenase Oxygen Inactivation Is Initiated at the H Cluster 2Fe Subcluster. J Am Chem Soc 2015;137:1809–16. https://doi.org/10.1021/ja510169s.

[27] Ghirardi ML, Togasaki RK, Seibert M. Oxygen sensitivity of algal H_2-production. Appl Biochem Biotechnol 1997;67:182. https://doi.org/10.1007/BF02787851.

[28] Nagy V, Podmaniczki A, Vidal-Meireles A, Tengölics R, Kovács L, Rákhely G, et al. Water-splitting-based, sustainable and efficient H_2 production in green algae as achieved by substrate limitation of the Calvin–Benson–Bassham cycle. Biotechnol Biofuels 2018;11:69. https://doi.org/10.1186/s13068-018-1069-0.

[29] Torzillo G, Scoma A, Faraloni C, Giannelli L. Advances in the biotechnology of hydrogen production with the microalga *Chlamydomonas reinhardtii*. Crit Rev Biotechnol 2015;35:485–96. https://doi.org/10.3109/07388551.2014.900734.

[30] Redding KE, Appel J, Boehm M, Schuhmann W, Nowaczyk MM, Yacoby I, et al. Advances and challenges in photosynthetic hydrogen production. Trends Biotechnol 2022. https://doi.org/10.1016/j.tibtech.2022.04.007.

[31] Hwang J-H, Lee WH. Continuous photosynthetic biohydrogen production from acetate-rich wastewater: Influence of light intensity. Int J Hydrogen Energy 2021;46:21812–21. https://doi.org/10.1016/j.ijhydene.2021.04.052.

[32] Atta M, Meyer J. Characterization of the gene encoding the [Fe]-hydrogenase from *Megasphaera elsdenii*. Biochim Biophys Acta - Protein Struct Mol Enzymol 2000;1476:368–71. https://doi.org/10.1016/S0167-4838(99)00245-9.

[33] Sievers F, Wilm A, Dineen D, Gibson TJ, Karplus K, Li W, et al. Fast, scalable generation of high-quality protein multiple sequence alignments using Clustal Omega. Mol Syst Biol 2011;7:539. https://doi.org/10.1038/msb.2011.75.

[34] Kelley LA, Mezulis S, Yates CM, Wass MN, Sternberg MJE. The Phyre2 web portal for protein modeling, prediction and analysis. Nat Protoc 2015;10:845–58. https://doi.org/10.1038/nprot.2015.053.

[35] Schrödinger L. The {PyMOL} Molecular Graphics System, Version 2.4.0. 2015.

[36] Suga M, Ozawa S-I, Yoshida-Motomura K, Akita F, Miyazaki N, Takahashi Y. Structure of the green algal photosystem I supercomplex with a decameric light-harvesting complex I. Nat Plants 2019;5:626–36. https://doi.org/10.1038/s41477-019-0438-4.

[37] Kozakov D, Hall DR, Xia B, Porter KA, Padhorny D, Yueh C, et al. The ClusPro web server for protein–protein docking. Nat Protoc 2017;12:255. https://doi.org/10.1038/nprot.2016.169.

[38] Song Y, DiMaio F, Wang RY-R, Kim D, Miles C, Brunette T, et al. High-Resolution Comparative Modeling with RosettaCM. Structure 2013;21:1735–42. https://doi.org/10.1016/j.str.2013.08.005.

[39] Fischer N, Sétif P, Rochaix JD. Targeted Mutations in the *psaC* Gene of *Chlamydomonas reinhardtii*: Preferential Reduction of F_B at Low Temperature Is Not Accompanied by Altered Electron Flow from Photosystem I to Ferredoxin. Biochemistry 1997;36:93–102. https://doi.org/10.1021/bi962244v.

[40] Gulis G, Narasimhulu K V, Fox LN, Redding KE. Purification of His_6-tagged Photosystem I from *Chlamydomonas reinhardtii*. Photosynth Res 2008;96:51–60. https://doi.org/10.1007/s11120-007-9283-9.

[41] Kropat J, Hong-Hermesdorf A, Casero D, Ent P, Castruita M, Pellegrini M, et al. A revised mineral nutrient supplement increases biomass and growth rate in *Chlamydomonas reinhardtii*. Plant J 2011;66:770–80. https://doi.org/10.1111/j.1365-313X.2011.04537.x.

[42] Porra RJ, Thompson WA, Kriedemann PE. Determination of accurate extinction coefficients and simultaneous equations for assaying chlorophylls a and b extracted with four different solvents: verification of the concentration of chlorophyll standards by atomic absorption spectroscopy. Biochim Biophys Acta - Bioenerg 1989;975:384–94. https://doi.org/10.1016/S0005-2728(89)80347-0.

[43] Gerde JA, Montalbo-Lomboy M, Yao L, Grewell D, Wang T. Evaluation of microalgae cell disruption by ultrasonic treatment. Bioresour Technol 2012;125:175–81. https://doi.org/10.1016/j.biortech.2012.08.110.

[44] Brettel K. Electron transfer and arrangement of the redox cofactors in photosystem I. Biochim Biophys Acta - Bioenerg 1997;1318:322–73. https://doi.org/10.1016/S0005-2728(96)00112-0.

[45] Sawyer A, Bai Y, Lu Y, Hemschemeier A, Happe T. Compartmentalisation of [FeFe]-hydrogenase maturation in *Chlamydomonas reinhardtii*. Plant J 2017;90:1134–43. https://doi.org/10.1111/tpj.13535.

[46] Suslick KS. Sonochemistry. Science (80-) 1990;247:1439–45. https://doi.org/10.1126/science.247.4949.1439.

[47] Sétif P. Ferredoxin and flavodoxin reduction by photosystem I. Biochim Biophys Acta - Bioenerg 2001;1507:161–79. https://doi.org/https://doi.org/10.1016/S0005-2728(01)00205-5.

[48] Vassiliev IR, Jung Y-S, Yang F, Golbeck JH. PsaC Subunit of Photosystem I Is Oriented with Iron-Sulfur Cluster F_B as the Immediate Electron Donor to Ferredoxin and Flavodoxin. Biophys J 1998;74:2029–35. https://doi.org/10.1016/S0006-3495(98)77909-3.

CHAPTER 5

PHOTOSYSTEM-I-HYDROGENASE CHIMERA MODELLING: THE ALPHAFOLD2 PERSPECTIVE

Andrey Kanygin

School of Molecular Sciences, Center for Bioenergy & Photosynthesis, Box 871604 Arizona State University Tempe, Arizona 85287-1604

Abstract

In silico simulations can be of great help in protein design, however, until recent breakthrough in protein folding, some challenging sequences could not be fold accurately. In this chapter, Alphafold2 was used to generate models of previously made chimeras. Comparisons with hard-docking models were made with alphafold2 models having much less internal clashes. However, the relatively low pLDDT score for PsaC domain that was also supported by PsaC domain alignment analysis suggest the need for further molecular dynamics simulations.

Introduction

Recent advances in machine learning at Google ushered an era of high resolution protein structure prediction from a protein sequence alone [1]. Alphafold2 uses a combination of evolutionary (similarities between sequences), physical, and geometric constraints to train neural engine for high accuracy models. In CASP14, the Alphafold2 was declared a winner with average RMSD (C_α at 95% confidence) slightly below 1 Å resolution. Such high accuracy enabled correct orientation of coordinating residues (e.g., side chains of Cys or His) in a protein tertiary structure without explicitly inserting heteroatoms of the ligand molecule. Essentially, they took homology modeling to an entirely new level.

Assessing quality of computed model can be accomplished by comparison with the experimentally determined structures and in the early days of Critical assessment of techniques for protein structure prediction (CASP), they used scoring system based on the global superposition (or alignment) of the two models and root-mean-square deviation (RMSD) calculations [2]. RMSD is calculated by superimposing two models and finding the root-mean-square distances between aligned atoms in the model or only polypeptide backbone atoms such as alpha-carbons. There are several disadvantages with the RMSD scoring: it is insensitive to the missing parts in the experimental model; it is heavily biased by outliers; it is dependent on the quality of superposition (algorithm), and for two or more domains even slight deviations in relative positions could skew the results in global alignment. Although, variations of the superposition-based scores have been developed such as global distance test (GDT) [3] to diminish the weight

of the outliers by setting a cutoff distance, such methods usually cannot adequately score quality of multi-domain models. One alternative to superposition-based methods is local distance difference test (lDDT), which compares how well atomic interactions in the reference protein compares with the generated model [4]. lDDT calculates as an average of fractions of preserved distances (within the thresholds of 0.5, 1, 2, and 4 Å) that could be found within a predefined inclusion radius. Alphafold2 uses internal accuracy system based on the predicted local distance difference test (plDDT) [1] on alpha-carbons in the model. The model is divided into 50 bins and scoring algorithms are used against high quality ground truth structures (up to 3.0 A resultion from PDB database). On the alphafold web-site (https://alphafold.ebi.ac.uk/faq) the pLDDT scores are sorted on high-accuracy (>90), well-modeled regions (70-90), low confidence (50-70), disordered regions (<50) that may be structured but only as a part of the complex.

Stability of Photosystem I (PSI) assembly is depended upon PsaC binding to PsaA/PsaB heterodimer and in the absence of PsaC, PsaA and PsaB are quickly recycled *in vivo* [5]. Crystal structure of cyanobacterial PSI (PDB ID: 1JB0 [6] suggested what residues make up the interface between PsaC and PsaA/PsaB subunits. Mutagenesis and reconstitution experiments on PsaC subunit of PSI showed importance of ionic interactions in creating a tight binding between PsaC and heterodimer, while in the absence of such, charge recombination kinetics [P_{700}^{+} -F_A/F_B^{-}] was significantly slower [7]. In this work, we use Alphafold2 models to address important questions with regard to stability of chimeric PSI and limitations to electron transfer in the engineered reaction centers.

Methods

Alphafold2 modeling

The Alphafold version 2.1.2 was run on Agave high performance computing cluster at Arizona State University using singularity container-built image from the docker repository of University of Virginia research computing (https://github.com/uvarc/rivanna-docker/tree/master/alphafold/2.1.2). The most up-to-date databases were downloaded from

Google's DeepMind repository: https://github.com/deepmind/alphafold. Genetic search was preset with full BFD database. Alphafold2 was run with the monomer flag.

Visualization and model analysis

Model coordinates (as pdb files) were visualized and analyzed with PyMOL[8]. Domain alignment was performed with the PyMOL command *align* with selection of the 2-31 and 36-70 residues of PsaC subunit (PDB ID=6JO5 [9]) against corresponding residues of the chimeric PsaC domain. For determination of the selected atoms RMSD, the number of outlier rejections was set to zero (cycles=0). For all other alignments, a default outlier rejection cutoff (2 Å) was used with 20 cycles of refinement.

Analysis of steric clashes with MolProbity.

Webserver (http://molprobity.biochem.duke.edu/) was used to analyze pairwise clashes [10,11] between the PsaC-HydA chimeras (excluding the C-terminus residues: SESTRSMGLSY; heteroatoms of cofactors) and PSI subunits: PsaA, PsaB, PsaD and PsaE. For PsaA and PsaB only polypeptide chains were used (heteroatoms removed). PsaC domain of the chimera was aligned with the PsaC subunit of PSI as described above. Uploaded coordinates were first stripped off hydrogen atoms, then all hydrogen atoms were remodeled with electron-cloud x-H bond lengths and Van der Waals (vdW) radii.

Maximal photobleaching in purified thylakoids

Thylakoids purification and P_{700}^{+} single flash photobleaching experiments were performed as described in [12].

Unpublished PsaC-hydrogenase chimera variations

PsaC-HydA2 group (**Table 5-1**) has 4 mutants varying in the length of the glycine residues linking C-terminus (truncated) of HydA2 to the PsaC residue A36. 0G sequence is the reference sequence published in [12], and has no extra glycines, hence, zero G. 2G, 3G, and 4G have the respective amount of extra glycines in the abovementioned junction. These mutants were made in *fud7* strain and photoaccumulation was compared to the parental control.

PsaC-HydA1 group (**Table 5-1**) has reference sequence published in [13]. Variant "2Q" has two

point mutations relative to the reference sequence: K370Q and K371Q.

Variant “4Q” has four point mutations relative reference sequence: R202Q, K371Q, K372Q, and K408Q.

Variant “4Q_short linker” has deletion of TATDAVP linking residues (located near W30 of PsaC and N-terminus of HydA1 sequence) and 4Q point mutations relative reference sequence.

PsaC-*Me*HydA group (**Table 5-1**) has reference sequence and “null” variant published in previous chapter.

PsaC-CpI: for sequence and annotation see **figure 5-1**.

Results and discussion

Quality of PsaC domain folding in Alphafold2 models

Before development of Alphafold2, no freely available homology or *ab initio* modeling tools could predict the folding of the PsaC domain of the existing PsaC-HydA chimeras, although most of them were able to produce plausible models of the hydrogenase domain. A stable assembly of PsaC-HydA chimeras on the PsaA/PsaB heterodimer are predicated on proper folding of the PsaC domain, which is split between the 30 N-terminal and 44 C-terminal residues flanking the hydrogenase domain on either side (**figure 5-2**). Moreover, both iron-sulfur clusters of PsaC use 3 Cys from one fragment and 1 Cys from the other. To assess the similarity of the chimeric PsaC domain (in general) to the PsaC subunit of PSI (6JO5), we calculated RMSD (root-mean-square deviation) between the aligned and superimposed atomic coordinates of 490 atoms comprising the core PsaC subunit. We also calculated RMSDs for PsaC residues making strong ionic interactions with PsaA/PsaB (K52, R53 and R66 or KRR for short), and the cysteine residues ligating the F_A and F_B clusters (see **table 5-1**).

After reviewing 11 various PsaC-hydrogenase fusions for which P_{700} photobleaching data was available, we found a very weak correlation ($R^2 \approx 0.15$) between the level of photoaccumulation (relative to the wild-type control) and RMSD_490 value (see **figure 5-3**). This is in line with the DeepMind team explicitly stating that Alphafold2 cannot be used to determine stability of proteins, nor could the model distributions (**table 5-1**) be used for such an endeavor

[1]. Additional scores such as RMSD_KRR, RMSD_F_A, and RMSD_F_B may be useful in instances where RMSD_490 was close to 4 Å for the best model (see **table 5-1**, PsaC-HydA1_4Q dataset), but RMSD_KRR is rather large, due to misplacement of the Arg66 analog in the chimera.
The statistics for the most plausible model of 5 for each variant (highlighted in bold in **Table 5-1**) was further analyzed with respect to inter-cofactor distances (**figure 5-4**). To our surprise, the PsaC-HydA chimeras exhibit much shorter distances between the terminal cofactor of PSI (F_B) and the iron sulfur cluster of hydrogenase (F_H) than previously modeled with hard docking (see **fugure 5-5**) [12,13]. Distances between F_A and F_B of the chimeric PsaC domain are mostly the same as in the PsaC subunit of PSI (9.3 Å), with a minor exception (PsaC-HydA1) that had it at 8.5 Å, which is likely due to the error of Alphafold2 prediction for coordinating cysteines of the model (see **table 5-2** for full list of inter-cofactor distances).

The selected models that we determined as the most plausible by PsaC domain alignment (in bold, **table 5-1**) were further analyzed with Alphafold2 internal scoring system (see **table 5-3**). For the published PsaC-HydA2 and PsaC-HydA1 chimeras the PsaC domain pLDDT score was 60 and 58, respectively. Variations for other models were not consistent with the level of accumulation. So, a further modeling and optimization is needed with conjunction to PsaA/PsaB heterodimer as well as PsaD.

Interaction of chimeric models with the core PsaA and PsaB subunits.

The RMSD data from PsaC domain alignments indicated deviations in the atom positions (on average from 2 to 4 Å) for the PsaC domain of accumulating mutants. This deviation is much smaller (1-2 Å) for 3 important residues forming ionic bonds with PsaA and PsaB subunits (K52/R53/R66) and anchoring PsaC domain in place for stably assembled chimeras. Moreover, simple rotamer adjustments could optimize RMSDs for the 3 residues (only R66-equivalent is typically misplaced in the chimera and skews RMSD for the average). This prompted us to ask how many steric clashes there are between the PsaC domain of the chimera and the PsaA/PsaB interface without any adjustments (i.e., based on the superposition of the PsaC domains alone). We estimated the steric clashes between the chimeras and PsaA/PsaB with MolProbity [10] and

found that there are quite a few – about 80 serious steric clashes (≥ 0.4 Å of vdW radii) on average between 4 models, and no correlation with the amount of accumulation (see t**able 5-4**). When wild type PsaC (PDB ID: 6JO5) was used in the same analysis, only 1 steric clash was found.

Interaction of chimeric models with PsaD and PsaE

Alignment of the chimeric PsaC domain between models and PsaC subunit of PSI (in **figure 5-4)** allows us to compare the relative position of the hydrogenase domain in space. At a glance, the PsaE subunit would have serious steric clashes with the hydrogenase domain (in all observed chimeras) if it attempted to occupy its native binding site. Using MolProbity we found that 25-45% of all PsaE atoms would sterically clash with chimera hydrogenase domain (see **table 5-5**). PsaD, on the other hand, has fewer clashes (17-23 % of total PsaD atoms), with the majority of them happening in the flexible coil that goes around of PsaC domain. Since PsaD was detected in PSI-HydA2, PSI-HydA1, and PSI-*Me*HydA, it is safe to assume that it underwent conformational changes for binding to the chimeric PsaC domain.

Comparison of Alphafold2 and hard docking models (HDMs)

Inter-cofactor distances set limitations on the intraprotein electron transfer rates, which can be estimated using the Moser-Dutton approximation [14]. Therefore, it is important to know how close the two cofactors supported by protein scaffold can be in the design of the chimera. Previously published HDMs of PSI-HydA2 [12], PSI-HydA1 [13], and PSI-*Me*HydA served primarily for that purpose. In **figure 5-5**, it is shown a side-by-side comparison between HDMs (left) vs Alphafold2 models (right) for the three chimeras. The most exciting finding was the greatly reduced distance between terminal iron sulfur cluster of PSI (F_B) and H-cluster of hydrogenase domain (F_H). Under assumption of average protein packing (density) between cofactors and Gibbs free energy matching reorganization energy, we find that electron transfer rates to H-cluster would not be limited by distance from F_B to F_H as preceding cofactor distance (F_X-F_A) is almost 12 Å). We expect the rate of electron transfer between F_B and F_H to be on the order of 10^9-10^{10} e^- s^{-1}. This may have a profound implication on our previous results regarding

charge recombination kinetics in PSI-hydrogenase chimeras. We previously hypothesized that the long distance between F_H and F_B was the likely reason for additional component of P_{700} recovery kinetic with longer decay time (and relatively small amplitude). Recent modeling data suggest that the longer time components could be due to other factors such as altered midpoint potential of one of the iron-sulfur clusters.

When we compare the overall quality of models in **figure 5-5**, Alphafold2 models lead with relatively low clash scores on the order of of 1-2 clashes per 1000 atoms in the model (similar to X-ray crystallography or cryoEM models). This is not surprising as Alphafold2 models are relaxed with AMBER molecular dynamics simulations [15] and therefore, any wrinkles posed by the folding algorithm are ironed out. Ideally, we should subject the HDMs to AMBER simulations for a fair comparison.

There were attempts to generate multimeric models with Alphafold2 of the chimeric protein with other PSI subunits (PsaA, PsaB, PsaD and PsaE). After various combinations were attempted and failed (mostly due to severe steric clashes between subunits) it is concluded that Alphafold2 (2.1.2 version) cannot handle such a complex protein as Photosystem I.

To make Alphafold2 models more useful in predicting stability and assembly on PSI, I suggest using molecular dynamics simulations on the aligned (PsaC-domain) chimera and PSI (substituting PsaC). We expect that steric clashes between chimeric PsaC domain and nearby subunits may be reduced to a such degree that would be reflective of the stability of the complex *in vivo*.

Conclusions

Alphafold2 proclaimed accuracy continues to impress with such a challenging fusion protein as PsaC-hydrogenase. Highly accurate prediction of coordinating cysteines allowed us to estimate inter-cofactor distance in the chimera and confirm that proximity of F_B to F_H should not be a limiting factor in electron transfer. To that effect, a longer charge recombination component seen in the P_{700} recovery experiments in chimeric PSI could be a result of imperfect binding of PsaC domain. As multimeric setting fell short of producing sterically sound models of chimeric PSI at

this point and pLDDT socres of PsaC domain are relatively low indicating the need to have other subunits for proper (stable) assembly, we suggest that structure alignments and molecular dynamics simulations may prove useful for generating more realistic models i.e., predicting stability of PSI-hydrogenase chimeras in silico.

MAHIVKIYDTCIGCTQCVRACPLDVLEMVPWGGATATDAVPSHMDRVKNALNAPEKHVIVAMAP
SVRASIGELFNMGFGVDVTGKIYTALRQLGFDKIFDINFGADMTIMEEATELVQRIENNGPFPMFT
SCCPGWVRQAENYYPELLNNLSSAKSPQQIFGTASKTYYPSISGLDPKNVFTVTVMPCTSKKFE
ADRPQMEKDGLRDIDAVITTRELAKMIKDAKIPFAKLEDSEADPAMGEYSGAGAIFGATGGVMEA
ALRSAKDFAENAELEDIEYKQVRGLNGIKEAEVEINNNKYNVAVINGASNLFKFMKSGMINEKQY
HFIEVMACHGGCVNGGGQPHVNPKDLEKVDIKKVRASVLYNQDEHLSKRKSHENTALVKMYQN
YFGKPGEGRAHEILHFKYKKSAWSHPQFEKAGGASQMASAPRTEDCVGCKRCETACPTDFLSV
RVYLGSESTRSMGLSY

Figure 5-1. Coding sequence for PsaC-*Cp*IHydA. PsaC (green), N-terminus linking sequence (magenta), Strep-II tag (cyan), C-terminus linking sequences (red), CpI hydrogenase domain (no color).

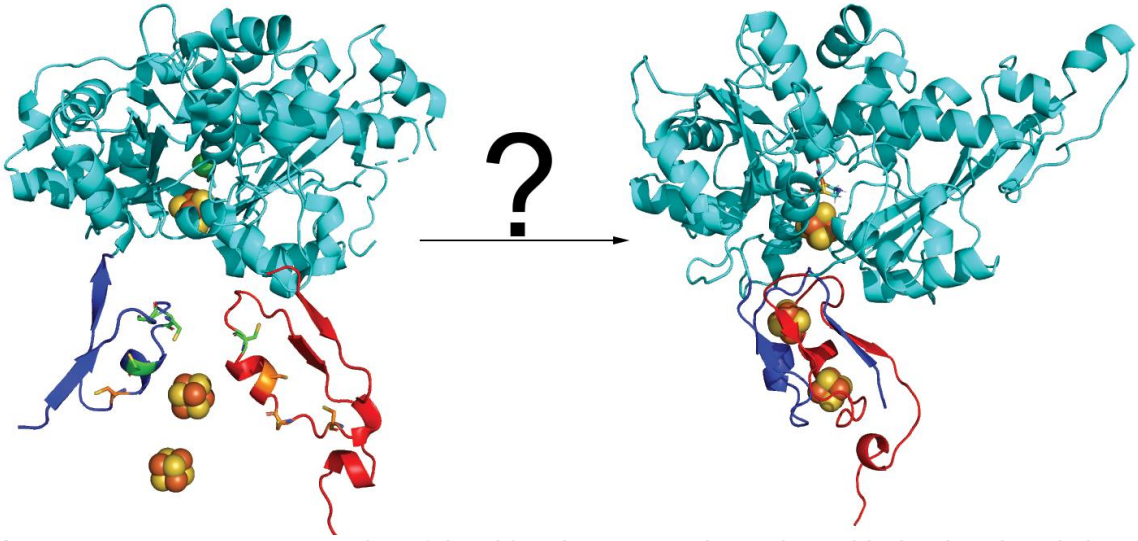

Figure 5-2. Cartoon representation of the chimeric PsaC-HydA1 polypeptide (HydA1 domain in cyan, N-terminus PsaC – blue, C-terminus PsaC – red) showing unfolded PsaC domain on the left and folded PsaC domain on the right (as in [13]). Green sticks show cysteines that make up F_B while orange sticks – F_A.

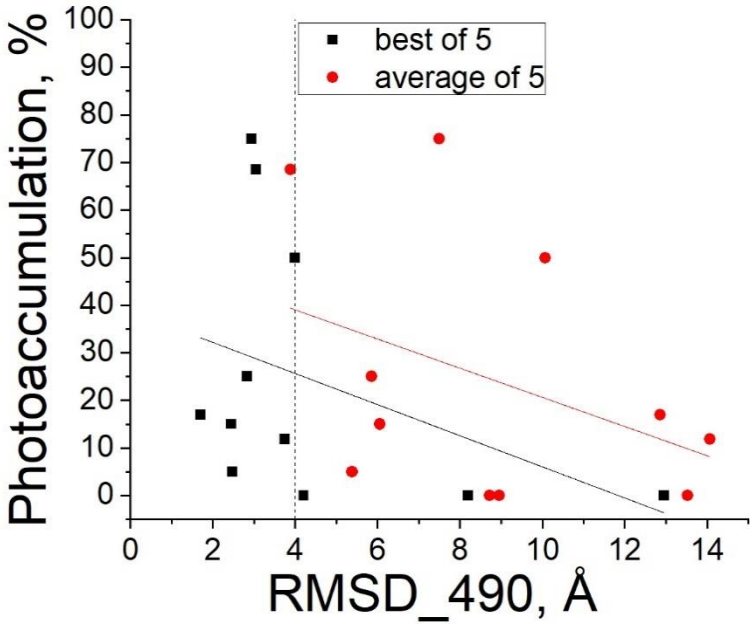

Figure 5-3. Photoaccumulation of functional PSI-hydrogenase chimeras in purified thylakoids as a function of the PsaC domain similarity score (RMSD_490). The black squares show the best of 5 models RSMD_490 score, while the red circles show the average of 5 models score. Coefficient of determination (R^2) is very low (~0.15) for both datasets. Vertical dashed line indicates empirical cutoff RMSD_490 value (4 Å) for best of 5 dataset, above which no stable assembly was observed.

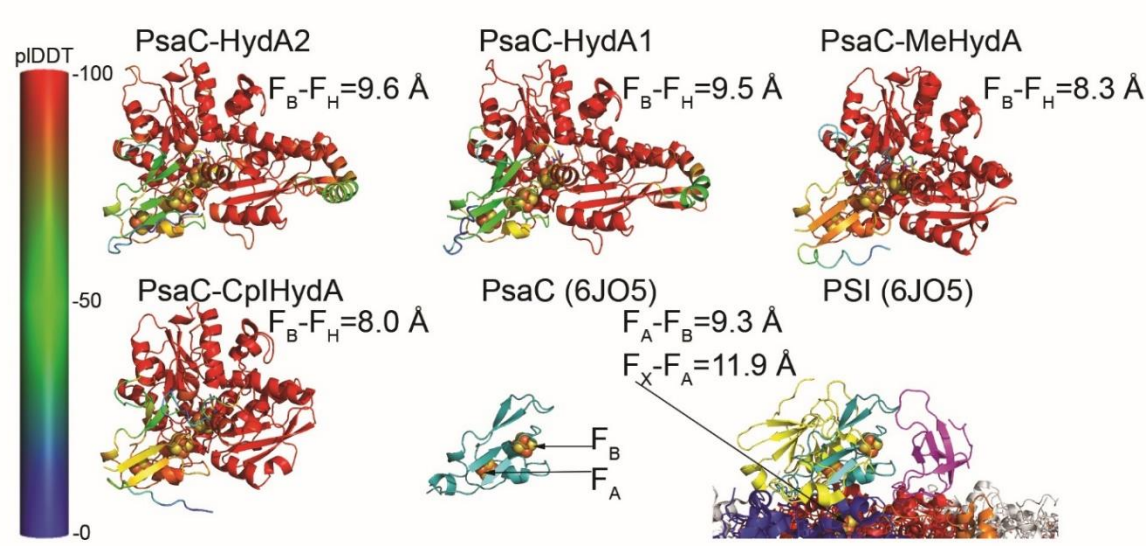

Figure 5-4. Alignment of PsaC domain in the selected chimeras and PSI (PsaA – red, PsaB – blue, PsaC – teal, PsaD – yellow, PsaE – magenta, PsaF – orange). Cartoon color in chimeras corresponds to the plDDT score, which can be approximated with the spectrum bar on the left side of the figure. Edge-to-edge distances between cofactors is indicated for each chimera and the PSI complex.

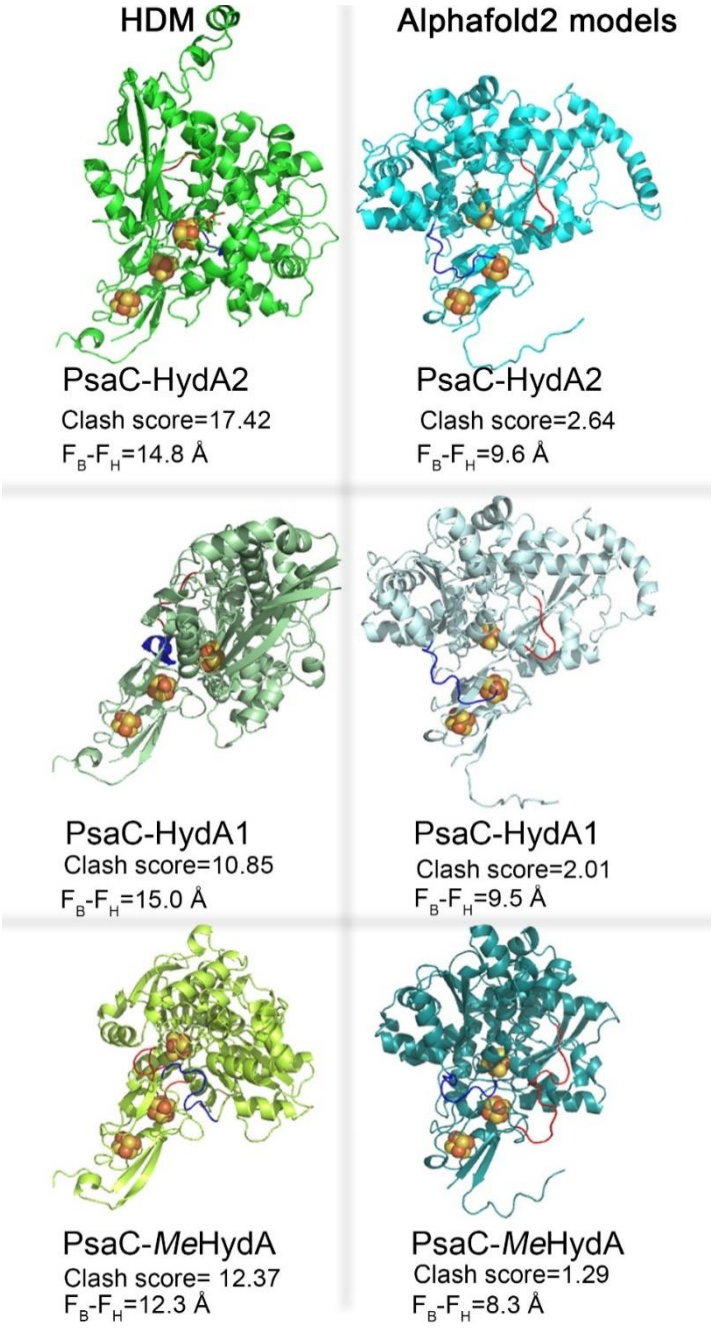

Figure 5-5. PsaC domain alignments of the HDMs (left column) in comparison to Alphafold2 models (right column). N-terminus junction is shown in blue, C-terminus junction is shown in red.

Group	Model name (subgroup)	plDDT score	RMSD_490	RMSD_KRR	RMSD_F_A	RMSD F_B	P_{700}, %
PsaC-HydA2	0G (ref)	83.7	5.0	1.2	0.39	0.34	15%
		83.3	**2.4**	**1.2**	**0.31**	**0.36**	
		82.4	5.0	2.6	0.37	0.37	
		80.5	4.1	2.0	0.57	0.43	
		80.0	13.8	11.8	12.16	7.87	
	2G	**82.2**	**3.7**	**2.5**	**0.37**	**0.35**	11.8
		81.1	18.0	11.7	15.87	8.27	
		80.4	19.3	15.3	16.41	7.63	
		80.1	8.3	5.6	1.50	0.52	
		77.9	20.9	16.1	17.87	9.53	
	3G	**83.0**	**3.4**	**2.1**	**0.35**	**0.45**	68.5
		82.6	3.0	2.4	0.26	0.43	
		82.4	6.2	3.7	0.59	0.47	
		82.4	3.6	2.1	0.36	0.41	
		81.9	3.1	2.2	0.32	0.37	
	4G	**85.4**	**1.7**	**1.0**	**0.35**	**0.37**	**17**
		81.9	20.0	8.3	18.93	13.86	
		80.9	10.0	7.0	2.84	0.75	
		80.4	24.0	9.1	17.91	16.84	
		80.2	8.5	6.2	1.33	0.85	
PsaC-HydA1	(ref)	**86.31**	**2.9**	**1.1**	**0.41**	**0.42**	75
		84.00	12.7	8.0	10.89	8.41	
		83.14	5.5	2.1	0.40	0.40	
		80.28	4.6	4.8	0.31	0.61	
		78.52	11.7	10.6	7.65	3.12	
	2Q	84.27	12.7	5.9	8.14	10.90	50
		83.75	11.4	7.0	6.43	10.44	
		81.70	**4.0**	**2.0**	**0.41**	**0.41**	
		80.89	10.3	7.7	3.84	1.30	
		79.14	12.0	9.0	7.00	6.35	
	4Q_short linker	85.15	13.3	5.4	9.91	8.47	0
		84.86	13.6	6.0	10.45	8.52	
		81.98	13.0	5.4	9.87	8.12	
		80.78	14.2	7.7	10.29	7.56	
		79.28	13.6	6.6	9.37	6.96	
	4Q	84.61	8.6	6.5	2.49	0.79	0

		84.36	13.4	9.4	12.22	8.45	
		82.93	4.6	4.0	0.43	0.38	
		80.41	4.2	3.3	0.48	0.51	
		77.68	12.9	10.6	10.82	7.93	
PsaC-*Me*HydA	(ref)	**88.64**	**3.0**	**1.0**	**0.40**	**0.36**	**25**
		86.96	2.8	1.4	0.30	0.38	
		86.24	3.2	1.5	0.22	0.40	
		85.10	8.3	2.7	0.40	0.46	
		84.51	12.0	5.0	3.53	1.15	
	null	88.41	8.2	2.2	2.07	0.39	0
		87.62	8.2	2.3	2.26	0.35	
		87.59	11.2	2.9	2.95	0.32	
		87.40	8.2	2.3	2.31	0.52	
		86.55	9.0	2.4	1.90	0.32	
PsaC-*Cpl* HydA		89.83	3.9	1.1	0.34	0.36	5
		88.74	3.2	1.1	0.24	0.36	
		88.68	**2.5**	**1.2**	**0.23**	**0.35**	
		88.19	2.8	1.1	0.30	0.35	
		85.67	14.6	8.5	5.08	10.71	

Table 5-1. Alphafold2 model comparison with the focus on PsaC domain alignments. The selected best fit representative of the group of 5 is indicated in bold.

Model name	Distance (edge-to-edge) in Å	
	Fa-Fb	Fb-Fh
PsaC-HydA2		
reference (0G)	9.1	9.6
2G	9.3	9.3
3G	9.2	8.5
4G	9.1	9.1
PsaC-HydA1		
reference	8.5	9.5
2Q	9	8.8
PsaC-*Me*HydA	9.3	8.3
PsaC-*CpI* HydA	9.3	8
PsaC (6JO5)	9.3	n/a

Table 5-2. Intercofactor distances in the most plausible models of Alphafold2. Iron sulfur clusters were inserted by alignment in PyMOL.

Model	490 atoms	“K52”	“R53”	“R65”	F_A	F_B
PsaC-HydA2	59.9	75.5	75.3	48.8	73.7	70.1
PsaC-HydA1	57.8	72.5	71.9	45	69.4	68.4
PsaC-MeHydA	74.1	83.9	83.4	77.9	82.8	82.7
PsaC-CpIHydA	72.9	84.8	84.2	72.3	82.6	85.4
PsaC-HydA2-2G	53.7	67.4	67.6	35.6	66.4	67.4
PsaC-HydA2-3G	64.6	80	79.4	50.9	78.3	77.3
PsaC-HydA2-4G	78.8	87.5	86.2	84.0	87.2	82.2
PsaC-HydA1_2Q	56.3	70	67.8	38.7	68	72.3

Table 5-3. Internal Alphafold2 score (pLDDT) for the selected models. Representative models from **table 5-1** are shown here.

PsaC-chimera or PsaC (atoms in a model)	total atoms in a model	Clash score (serious steric overlaps per 1000 atoms)	Number of interface clashes	% interface clashes (realtive to atoms in the chimera)
PsaC-HydA2 (7574)	30415	5.26	82	1.08
PsaC-HydA1 (7471)	30315	5.67	99	1.33
PsaC-*Me*HydA (6960)	29804	4.5	67	0.96
PsaC-*CpI* HydA (6949)	29793	4.83	72	1.04
PsaC (1028)	23874	2.6	1	0.10

Table 5-4. Steric clashes between chimeras and PsaA+PsaB subunits of PSI.

PsaC-chimera or PsaC (atoms in a model)	total atoms in a model	Clash score (serious steric overlaps per 1000 atoms)	Number of interface clashes	interface clashes % (realtive to atoms in the PsaE)
PsaC-HydA2 (7569)	8502	29.76	232	24.9
PsaC-HydA1 (7456)	8388	41.85	335	35.9
PsaC-*Me*HydA (6943)	7878	55.47	427	45.7
PsaC-*Cpl* HydA(6936)	7876	49.64	376	40.0
PsaC (1028)	1984	2.52	2	0.2

Table 5-5. Steric clashes between chimeras and PsaE subunit.

PsaC-chimera or PsaC (atoms in a model)	total atoms in a model	Clash score (serious steric overlaps per 1000 atoms)	Number of interface clashes	interface clashes % (realtive to atoms in the PsaD)
PsaC-HydA2 (7565)	9832	54.41	509	22.5
PsaC-HydA1 (7461)	9724	37.74	346	15.3
PsaC-*Me*HydA (6945)	9219	32.87	288	12.7
PsaC-*Cpl* HydA(6936)	9194	43.29	378	16.7
PsaC (1028)	3310	3.63	3	0.1

Table 5-6. Steric clashes between chimeras and PsaD subunit.

References

[1] Jumper J, Evans R, Pritzel A, Green T, Figurnov M, Ronneberger O, et al. Highly accurate protein structure prediction with AlphaFold. Nature 2021;596:583–9. https://doi.org/10.1038/s41586-021-03819-2.

[2] Hubbard TJP. RMS/Coverage graphs: A qualitative method for comparing three-dimensional protein structure predictions. Proteins Struct Funct Bioinforma 1999;37:15–21. https://doi.org/https://doi.org/10.1002/(SICI)1097-0134(1999)37:3+<15::AID-PROT4>3.0.CO;2-Z.

[3] Zemla A. LGA: a method for finding 3D similarities in protein structures. Nucleic Acids Res 2003;31:3370–4. https://doi.org/10.1093/nar/gkg571.

[4] Mariani V, Biasini M, Barbato A, Schwede T. lDDT: a local superposition-free score for comparing protein structures and models using distance difference tests. Bioinformatics 2013;29:2722–8. https://doi.org/10.1093/bioinformatics/btt473.

[5] Takahashi Y, Goldschmidt-Clermont M, Soen SY, Franzén LG, Rochaix JD, Franzen LG, et al. Directed chloroplast transformation in *Chlamydomonas reinhardtii*: insertional inactivation of the *psaC* gene encoding the iron sulfur protein destabilizes photosystem I. EMBO J 1991;10:2033.

[6] Jordan P, Fromme P, Witt HT, Klukas O, others. Three-dimensional structure of cyanobacterial photosystem I at 2.5 angstrom resolution. Nature 2001;411:909.

[7] Jagannathan B, Golbeck JH. Understanding of the Binding Interface between PsaC and the PsaA/PsaB Heterodimer in Photosystem I. Biochemistry 2009;48:5405–16. https://doi.org/10.1021/bi900243f.

[8] Schrödinger L. The {PyMOL} Molecular Graphics System, Version 2.4.0. 2015.

[9] Suga M, Ozawa S-I, Yoshida-Motomura K, Akita F, Miyazaki N, Takahashi Y. Structure of the green algal photosystem I supercomplex with a decameric light-harvesting complex I. Nat Plants 2019;5:626–36. https://doi.org/10.1038/s41477-019-0438-4.

[10] Chen VB, Arendall WB, Headd JJ, Keedy DA, Immormino RM, Kapral GJ, et al. MolProbity : all-atom structure validation for macromolecular crystallography. Acta Crystallogr Sect D Biol Crystallogr 2010;66:12–21. https://doi.org/10.1107/S0907444909042073.

[11] Williams CJ, Headd JJ, Moriarty NW, Prisant MG, Videau LL, Deis LN, et al. MolProbity: More and better reference data for improved all-atom structure validation. Protein Sci 2018;27:293–315. https://doi.org/10.1002/pro.3330.

[12] Kanygin A, Milrad Y, Thummala C, Reifschneider K, Baker P, Marco P, et al. Rewiring photosynthesis: a photosystem I-hydrogenase chimera that makes H_2 *in vivo*. Energy Environ Sci 2020;13:2903–14. https://doi.org/10.1039/C9EE03859K.

[13] Kanygin A, Smith A, Nagy V, Tóth SZ, Redding KE. Interplay between hydrogen production and photosynthesis in a green alga expressing an active photosystem I-hydrogenase chimera. Int J Hydrogen Energy 2022;47:21969–83. https://doi.org/10.1016/j.ijhydene.2022.03.096.

[14] Moser CC, Keske JM, Warncke K, Farid RS, Dutton PL. Nature of biological electron transfer. Nature 1992;355:796–802. https://doi.org/10.1038/355796a0.

[15] Salomon-Ferrer R, Case DA, Walker RC. An overview of the Amber biomolecular simulation package. Wiley Interdiscip Rev Comput Mol Sci 2013;3:198–210. https://doi.org/10.1002/wcms.1121.

CHAPTER 6

CONCLUSION

Andrey Kanygin

School of Molecular Sciences

Arizona State University, Tempe, AZ 85287

In this work, 3 different PSI-hydrogenase chimeras (PSI-HydA2, PSI-HydA1 and PSI-*Me*HydA) were analyzed in detail with respect to their activity in vivo and in vitro, as well as their impact on the PETC and metabolism in the green microalgae *Chlamydomonas reinhardtii*. The PsaC subunit of PSI resembles bacterial ferredoxins, and it is suggested that “acquisition” of such a protein by the ancestral heterodimeric type I RC was an evolutionary adaptation to oxygenation of the Earth’s atmosphere provided several distinct advantages: (1) additional iron-sulfur clusters allowed for stable charge separation with longer lifetimes (~100 ms) and lower energy of charge separated state, thusly greatly reducing the risk of back reactions leading to triplet chlorophyll formation that would in turn generate very reactive singlet oxygen; (2) two additional electrons could be temporarily stored in the terminal cofactors when PSI electron acceptors are lacking; (3) a stromal bump formed by PsaC and adjacent PsaD and PsaE could adapt to better ferredoxin binding with the potential for supercomplex formations, such as ferredoxin-FNR. Here it was shown that by re-engineering PsaC as a fusion to the redox enzyme (hydrogenase), a further specialization of heterodimeric type I reaction center can be achieved, diminishing its native affinity for ferredoxin and generating a specialized reaction center with designed properties to drive selected redox chemistries.

In all PsaC-hydrogenase internal fusions, it is assumed that hydrogenase domain (larger) folds first and the PsaC domain (smaller) follows, after which the N- and C- terminal fragments of the fusion protein can come together to form PsaC. The three chimeras were able to fold the PsaC domain, although the in vivo accumulation of PSI-hydrogenase varied from about 15% (relative to WT level) to 75%. One plausible explanation would be differences in the binding interface between the PsaC domain and the PsaA/PsaB heterodimer, which is facilitated by PsaD “clamping down” PsaC domain from the other side and complicated by the bulky hydrogenase domain. Alphafold2 models of PsaC-hydrogenase chimeras display near native conformations for the K52R53 residues (PsaC numbering) with high internal confidence scores (plDDT more than 75%), while R65 is significantly misplaced with low plDDT confidence scores (~50%). All 3 residues form ionic bonds with the PsaA/B heterodimer that are important for stable assembly of

PSI. The stand-alone PsaC-hydrogenase alphafold2 models cannot explain subtle variations in accumulation levels. Therefore, it is suggested that in the future one should perform soft docking of the PsaC domain with the core heterodimers (and PsaD) for optimization of R65 conformation/position and other residues (e.g., forming stabilizing hydrogen bonds). The anticipated energy minimizations may provide better models for comparison between various PSI-hydrogenase chimeras and may help with the design of more stable fusion proteins with desired characteristics. Alphafold2 must be used with caution as the low coverage regions (e.g., longer unnatural linkers) tend to be difficult to model with high confidence by the current version of the algorithm.

The examined PSI-hydrogenases exhibit successful charge separation all the way to the terminal iron sulfur clusters located in the chimeric subunit, as judged by charge recombination kinetics in the absence of external electron acceptors. A novel longer time constant in the analysis of CR kinetics suggests that it may be due to an additional iron-sulfur cluster from the hydrogenase H-cluster. The alphafold2 PsaC-hydrogenase models place the H-cluster much closer to F_B than in the hard-docking models, so that the inter-cofactor F_A-F_B and F_B-F_H distances are about the same (~ 9.5 Å), and F_X-F_A (~ 12 Å) is the longest. This may suggest that other possibilities (aside from F_B-F_H distance), such as altered midpoint potential of one of the 3 clusters, could contribute to the longer component of CR kinetics. As mentioned earlier, a better soft-docking model may alter the relative position of the hydrogenase domain to PsaC, perhaps slightly increasing the distance between F_H and F_B. A structural model (e.g., via cryo-EM) could potentially give us an insight about the relative orientations of the two domains. However, such efforts have been thwarted by the tendency of the chimeric PSI to precipitate at higher concentrations.

All three chimeras show reduced capability for flavodoxin photoreduction in vitro (as well as ferredoxin for PSI-HydA2). Decreased rates of flavodoxin photoreduction (by ~ 8 times) relative to wild-type control suggest that the hydrogenase domain effectively blocks the native Fd binding site (in agreement with our modeling efforts). Alternative modes of ferredoxin binding may

involve the hydrogenase domain or PsaC domain, but we have no direct evidence for either one. Indirect evidence of Fd binding to the chimeric PS-HydA complex comes from H_2 evolution experiments in vivo in the dark, where reduced Fd was the sole electron donor. However, the results are hard to interpret quantitatively across different chimeras due to varied amounts of accumulation between them in the respective mutant strains. In vivo CEF measurements suggest that Fd can bind well to PSI-HydA1, while PSI-HydA2 and PSI-*Me*HydA show almost no CEF. The difference in accumulation levels as well as a potential supercomplex formation might also contribute to the observed differences in CEF. We cannot exclude the adaptation of one of the ferredoxins to bind PSI-HydA1, as selective pressure would favor such mutations over time; however, it is considered unlikely. Ultimately, Fd binding to chimeric PSI determines if mutant strains can actively fix inorganic carbon via the CBB cycle. Our results indicate that under anoxia, both PSI-HydA1 and PSI-HydA2 (reduced in comparison to WT) can do that; the PSI-*Me*HydA situation is less obvious due to the presence of active endogenous hydrogenases in the parental strain.

The PSI-hydrogenase chimeras studied here can make hydrogen in vivo in a light-dependent fashion, deriving electrons mostly from water oxidation by PSII, as originally intended. The relatively high light (around 1000 µmol m^{-2} s^{-1} PAR) needed to achieve saturation of in vivo H_2 production rate is likely due to a requirement for 2 electrons residing on terminal cofactors of the PSI-HydA complex to make one hydrogen molecule and outcompete the potential theft of an electron by Fd. The maximal turnover numbers for in vivo hydrogen production correlate negatively with the relative photoaccumulation of chimeric PSI. PSI-HydA2 (accumulating to 15%) exhibits the highest turnover rate 170 H_2 s^{-1} (equivalent of 340 electrons s^{-1}) under enforced anoxia conditions. This correlation implies that the higher accumulating chimeras may have lower apparent turnover numbers due to significant inactivation of hydrogenase by oxygen evolved at PSII. This conclusion is supported by improved H_2 production results under enforced anoxia conditions, which strongly suggests the need for more oxygen tolerant hydrogenase to make photobiological hydrogen production feasible in the future.

REFERENCES

Akhlaghi, N., & Najafpour-Darzi, G. (2020). A comprehensive review on biological hydrogen production. *International Journal of Hydrogen Energy*, *45*(43), 22492–22512. https://doi.org/10.1016/j.ijhydene.2020.06.182

Allen, J. P., & Williams, J. C. (1998). Photosynthetic reaction centers. *FEBS Letters*, *438*(1–2), 5–9. https://doi.org/10.1016/S0014-5793(98)01245-9

Alric, J. (2010). Cyclic electron flow around photosystem I in unicellular green algae. *Photosynthesis Research*, *106*(1), 47–56. https://doi.org/10.1007/s11120-010-9566-4

Alric, J., & Johnson, X. (2017). Alternative electron transport pathways in photosynthesis: a confluence of regulation. *Current Opinion in Plant Biology*, *37*, 78–86. https://doi.org/10.1016/j.pbi.2017.03.014

Alric, J., Lavergne, J., & Rappaport, F. (2010). Redox and ATP control of photosynthetic cyclic electron flow in *Chlamydomonas reinhardtii* (I) aerobic conditions. *Biochimica et Biophysica Acta (BBA) - Bioenergetics*, *1797*(1), 44–51. https://doi.org/10.1016/j.bbabio.2009.07.009

Asada, K. (2000). The water–water cycle as alternative photon and electron sinks. *Philosophical Transactions of the Royal Society of London. Series B: Biological Sciences*, *355*(1402), 1419–1431. https://doi.org/10.1098/rstb.2000.0703

Atta, M., & Meyer, J. (2000). Characterization of the gene encoding the [Fe]-hydrogenase from *Megasphaera elsdenii*. *Biochimica et Biophysica Acta (BBA) - Protein Structure and Molecular Enzymology*, *1476*(2), 368–371. https://doi.org/10.1016/S0167-4838(99)00245-9

Bai, Y., Chen, T., Happe, T., Lu, Y., & Sawyer, A. (2018). Iron–sulphur cluster biogenesis via the SUF pathway. *Metallomics*, *10*(8), 1038–1052. https://doi.org/10.1039/C8MT00150B

Barber, J. (2009). Photosynthetic energy conversion: natural and artificial. *Chem. Soc. Rev.*, *38*(1), 185–196. https://doi.org/10.1039/B802262N

Ben-Zvi, O., Dafni, E., Feldman, Y., & Yacoby, I. (2019). Re-routing photosynthetic energy for continuous hydrogen production in vivo. *Biotechnology for Biofuels*, *12*(1), 266. https://doi.org/10.1186/s13068-019-1608-3

Berggren, G., Adamska, A., Lambertz, C., Simmons, T. R., Esselborn, J., Atta, M., Gambarelli, S., Mouesca, J.-M., Reijerse, E., Lubitz, W., Happe, T., Artero, V., & Fontecave, M. (2013). Biomimetic assembly and activation of [FeFe]-hydrogenases. *Nature*, *499*(7456), 66–69. https://doi.org/10.1038/nature12239

Blankenship, R. E., & Prince, R. C. (1985). Excited-state redox potentials and the Z scheme of photosynthesis. *Trends in Biochemical Sciences*, *10*(10), 382–383. https://doi.org/10.1016/0968-0004(85)90059-3

Blankenship, R. E., Tiede, D. M., Barber, J., Brudvig, G. W., Fleming, G., Ghirardi, M., Gunner, M. R., Junge, W., Kramer, D. M., Melis, A., Moore, T. A., Moser, C. C., Nocera, D. G., Nozik, A. J., Ort, D. R., Parson, W. W., Prince, R. C., & Sayre, R. T. (2011). Comparing Photosynthetic and Photovoltaic Efficiencies and Recognizing the Potential for Improvement. *Science*, *332*(6031), 805–809. https://doi.org/10.1126/science.1200165

BOHME, H. (1978). Quantitative Determination of Ferredoxin, Ferredoxin-$NADP^+$ Reductase and Plastocyanin in Spinach Chloroplasts. *European Journal of Biochemistry*, *83*(1), 137–141. https://doi.org/10.1111/j.1432-1033.1978.tb12077.x

Bolatkhan, K., Kossalbayev, B. D., Zayadan, B. K., Tomo, T., Veziroglu, T. N., & Allakhverdiev, S. I. (2019). Hydrogen production from phototrophic microorganisms: Reality and perspectives. *International Journal of Hydrogen Energy*, *44*(12), 5799–5811. https://doi.org/10.1016/j.ijhydene.2019.01.092

Brettel, K. (1997). Electron transfer and arrangement of the redox cofactors in photosystem I. *Biochimica et Biophysica Acta (BBA) - Bioenergetics*, *1318*(3), 322–373. https://doi.org/10.1016/S0005-2728(96)00112-0

Britt, R. D., Tao, L., Rao, G., Chen, N., & Wang, L.-P. (2022). Proposed Mechanism for the Biosynthesis of the [FeFe] Hydrogenase H-Cluster: Central Roles for the Radical SAM Enzymes HydG and HydE. *ACS Bio & Med Chem Au*, *2*(1), 11–21. https://doi.org/10.1021/acsbiomedchemau.1c00035

Buchert, F., Scholz, M., & Hippler, M. (2022). Electron transfer via cytochrome b_6f complex displays sensitivity to antimycin A upon STT7 kinase activation. *Biochemical Journal*, *479*(1), 111–127. https://doi.org/10.1042/BCJ20210802

Burlacot, A., Burlacot, F., Li-Beisson, Y., & Peltier, G. (2020). Membrane Inlet Mass Spectrometry: A Powerful Tool for Algal Research. *Frontiers in Plant Science*, *11*. https://doi.org/10.3389/fpls.2020.01302

Burlacot, A., Sawyer, A., Cuiné, S., Auroy-Tarrago, P., Blangy, S., Happe, T., & Peltier, G. (2018). Flavodiiron-Mediated O_2 Photoreduction Links H_2 Production with CO_2 Fixation during the Anaerobic Induction of Photosynthesis. *Plant Physiology*, *177*(4), 1639 LP – 1649. https://doi.org/10.1104/pp.18.00721

Burlacot, Peltier, & Li-Beisson. (2019). Subcellular Energetics and Carbon Storage in *Chlamydomonas*. *Cells*, *8*(10), 1154. https://doi.org/10.3390/cells8101154

Butt, J. N., Filipiak, M., & Hagen, W. R. (1997). Direct Electrochemistry of *Megasphaera Elsdenii* Iron Hydrogenase. Definition of the Enzyme's Catalytic Operating Potential and Quantitation of the Catalytic Behaviour over a Continuous Potential Range. *European Journal of Biochemistry*, *245*(1), 116–122. https://doi.org/10.1111/j.1432-1033.1997.00116.x

Byrdin, M., Santabarbara, S., Gu, F., Fairclough, W. V, Heathcote, P., Redding, K., & Rappaport, F. (2006). Assignment of a kinetic component to electron transfer between iron–sulfur clusters F_X and $F_{A/B}$ of Photosystem I. *Biochimica et Biophysica Acta (BBA) - Bioenergetics*, *1757*(11), 1529–1538. https://doi.org/10.1016/j.bbabio.2006.06.016

Caserta, G., Papini, C., Adamska-Venkatesh, A., Pecqueur, L., Sommer, C., Reijerse, E., Lubitz, W., Gauquelin, C., Meynial-Salles, I., Pramanik, D., Artero, V., Atta, M., del Barrio, M., Faivre, B., Fourmond, V., Léger, C., & Fontecave, M. (2018). Engineering an [FeFe]-Hydrogenase: Do Accessory Clusters Influence O_2 Resistance and Catalytic Bias? *Journal of the American Chemical Society*, *140*(16), 5516–5526. https://doi.org/10.1021/jacs.8b01689

Cashman, D. J., Zhu, T., Simmerman, R. F., Scott, C., Bruce, B. D., & Baudry, J. (2014). Molecular interactions between photosystem I and ferredoxin: an integrated energy frustration and experimental model. *Journal of Molecular Recognition*, *27*(10), 597–608. https://doi.org/10.1002/jmr.2384

Chang, C. H., King, P. W., Ghirardi, M. L., & Kim, K. (2007). Atomic Resolution Modeling of the Ferredoxin:[FeFe] Hydrogenase Complex from *Chlamydomonas reinhardtii*. *Biophysical Journal*, *93*(9), 3034–3045. https://doi.org/10.1529/biophysj.107.108589

Chapman, S. P., Paget, C. M., Johnson, G. N., & Schwartz, J.-M. (2015). Flux balance analysis reveals acetate metabolism modulates cyclic electron flow and alternative glycolytic pathways in *Chlamydomonas reinhardtii*. *Frontiers in Plant Science*, *6*, 474. https://doi.org/10.3389/fpls.2015.00474

Chaux, F., Burlacot, A., Mekhalfi, M., Auroy, P., Blangy, S., Richaud, P., & Peltier, G. (2017). Flavodiiron Proteins Promote Fast and Transient O_2 Photoreduction in *Chlamydomonas*. *Plant Physiology*, *174*(3), 1825 LP – 1836. https://doi.org/10.1104/pp.17.00421

Chen, V. B., Arendall, W. B., Headd, J. J., Keedy, D. A., Immormino, R. M., Kapral, G. J., Murray, L. W., Richardson, J. S., & Richardson, D. C. (2010). MolProbity : all-atom structure validation for macromolecular crystallography. *Acta Crystallographica Section D Biological Crystallography*, *66*(1), 12–21. https://doi.org/10.1107/S0907444909042073

Clowez, S., Godaux, D., Cardol, P., Wollman, F.-A., & Rappaport, F. (2015). The Involvement of Hydrogen-producing and ATP-dependent NADPH-consuming Pathways in Setting the Redox Poise in the Chloroplast of *Chlamydomonas reinhardtii* in Anoxia. *Journal of Biological Chemistry*, *290*(13), 8666–8676. https://doi.org/10.1074/jbc.M114.632588

Cournac, L., Mus, F., Bernard, L., Guedeney, G., Vignais, P. M., & Peltier, G. (2002). Limiting steps of hydrogen production in *Chlamydomonas reinhardtii* and *Synechocystis* PCC 6803 as analysed by light-induced gas exchange transients. *International Journal of Hydrogen Energy*, *27*(11–12), 1229–1237. https://doi.org/10.1016/S0360-3199(02)00105-2

Dang, K.-V., Plet, J., Tolleter, D., Jokel, M., Cuiné, S., Carrier, P., Auroy, P., Richaud, P., Johnson, X., Alric, J., Allahverdiyeva, Y., & Peltier, G. (2014). Combined Increases in Mitochondrial Cooperation and Oxygen Photoreduction Compensate for Deficiency in Cyclic Electron Flow in *Chlamydomonas reinhardtii*. *The Plant Cell*, *26*(7), 3036–3050. https://doi.org/10.1105/tpc.114.126375

Decottignies, P., Flesch, V., Gérard-Hirne, C., & Le Maréchal, P. (2003). Role of positively charged residues in *Chlamydomonas reinhardtii* ferredoxin-$NADP^+$-reductase. *Plant Physiology and Biochemistry*, *41*(6–7), 637–642. https://doi.org/10.1016/S0981-9428(03)00061-5

Decottignies, P., Lemarechal, P., Jacquot, J. P., Schmitter, J. M., & Gadal, P. (1995). Primary Structure and Post-translational Modification of Ferredoxin-NADP Reductase from *Chlamydomonas reinhardtii*. *Archives of Biochemistry and Biophysics*, *316*(1), 249–259. https://doi.org/https://doi.org/10.1006/abbi.1995.1035

Desplats, C., Mus, F., Cuiné, S., Billon, E., Cournac, L., & Peltier, G. (2009). Characterization of Nda2, a Plastoquinone-reducing Type II NAD(P)H Dehydrogenase in *Chlamydomonas* Chloroplasts. *Journal of Biological Chemistry*, *284*(7), 4148–4157. https://doi.org/10.1074/jbc.M804546200

DIJK, C., GRANDE, H. J., MAYHEW, S. G., & VEEGER, C. (1980). Properties of the Hydrogenase of *Megasphaera elsdenii*. *European Journal of Biochemistry*, *107*(1), 251–261. https://doi.org/10.1111/j.1432-1033.1980.tb04645.x

DIJK, C., MAYHEW, S. G., GRANDE, H. J., & VEEGER, C. (1979). Purification and Properties of Hydrogenase from *Megasphaera elsdenii*. *European Journal of Biochemistry*, *102*(2), 317–330. https://doi.org/10.1111/j.1432-1033.1979.tb04246.x

Eilenberg, H., Weiner, I., Ben-Zvi, O., Pundak, C., Marmari, A., Liran, O., Wecker, M. S., Milrad, Y., & Yacoby, I. (2016). The dual effect of a ferredoxin-hydrogenase fusion protein in vivo: successful divergence of the photosynthetic electron flux towards hydrogen production and elevated oxygen tolerance. *Biotechnology for Biofuels*, *9*(1), 182. https://doi.org/10.1186/s13068-016-0601-3

Elman, T., Hoai Ho, T. T., Milrad, Y., Hippler, M., & Yacoby, I. (2022). Enhanced chloroplast-mitochondria crosstalk promotes ambient algal-H_2 production. *Cell Reports Physical Science*, *3*(4), 100828. https://doi.org/10.1016/j.xcrp.2022.100828

Energy Technology Perspectives 2020. (2020). In *Energy Technology Perspectives 2020*. OECD. https://doi.org/10.1787/ab43a9a5-en

Engelbrecht, V., Liedtke, K., Rutz, A., Yadav, S., Günzel, A., & Happe, T. (2021). One isoform for one task? The second hydrogenase of *Chlamydomonas reinhardtii* prefers hydrogen uptake. *International Journal of Hydrogen Energy*, *46*(10), 7165–7175. https://doi.org/10.1016/j.ijhydene.2020.11.231

Erbes, D. L., King, D., & Gibbs, M. (1979). Inactivation of Hydrogenase in Cell-free Extracts and Whole Cells of *Chlamydomonas reinhardi* by Oxygen. *Plant Physiology*, *63*(6), 1138 LP – 1142. https://doi.org/10.1104/pp.63.6.1138

Eroglu, E., & Melis, A. (2016). Microalgal hydrogen production research. *International Journal of Hydrogen Energy*, *41*(30), 12772–12798. https://doi.org/https://doi.org/10.1016/j.ijhydene.2016.05.115

FILIPIAK, M., HAGEN, W. R., & VEEGER, C. (1989). Hydrodynamic, structural and magnetic properties of *Megasphaera elsdenii* Fe hydrogenase reinvestigated. *European Journal of Biochemistry*, *185*(3), 547–553. https://doi.org/10.1111/j.1432-1033.1989.tb15148.x

Fischer, N. (1998). The PsaC subunit of photosystem I provides an essential lysine residue for fast electron transfer to ferredoxin. *The EMBO Journal*, *17*(4), 849–858. https://doi.org/10.1093/emboj/17.4.849

Fischer, N., Sétif, P., & Rochaix, J. D. (1997). Targeted Mutations in the *psaC* Gene of *Chlamydomonas reinhardtii*: Preferential Reduction of F_B at Low Temperature Is Not Accompanied by Altered Electron Flow from Photosystem I to Ferredoxin. *Biochemistry*, *36*(1), 93–102. https://doi.org/10.1021/bi962244v

Fischer, N., Stampacchia, O., Redding, K., & Rochaix, J.-D. (1996). Selectable marker recycling in the chloroplast. *Molecular and General Genetics MGG*, *251*(3), 373–380. http://files/570/Fischer et al. - 1996 - Selectable marker recycling in the chloroplast.pdf

Fiser, A., Do, R. K. G., & Šali, A. (2000). Modeling of loops in protein structures. *Protein Science*, *9*(9), 1753–1773. https://doi.org/10.1110/ps.9.9.1753

Forestier, M., King, P., Zhang, L., Posewitz, M., Schwarzer, S., Happe, T., Ghirardi, M. L., & Seibert, M. (2003). Expression of two [Fe]-hydrogenases in *Chlamydomonas reinhardtii* under anaerobic conditions. *European Journal of Biochemistry*, *270*(13), 2750–2758. https://doi.org/10.1046/j.1432-1033.2003.03656

Gaffron, H. (1940). Carbon Dioxide Reduction with Molecular Hydrogen in Green Algae. *American Journal of Botany*, *27*(5), 273. https://doi.org/10.2307/2436697

Genty, B., Briantais, J.-M., & Baker, N. R. (1989). The relationship between the quantum yield of photosynthetic electron transport and quenching of chlorophyll fluorescence. *Biochimica et Biophysica Acta (BBA) - General Subjects*, *990*(1), 87–92. https://doi.org/10.1016/S0304-4165(89)80016-9

Gerde, J. A., Montalbo-Lomboy, M., Yao, L., Grewell, D., & Wang, T. (2012). Evaluation of microalgae cell disruption by ultrasonic treatment. *Bioresource Technology*, *125*, 175–181. https://doi.org/10.1016/j.biortech.2012.08.110

Gfeller, R. P., & Gibbs, M. (1984). Fermentative Metabolism of *Chlamydomonas reinhardtii*. *Plant Physiology*, *75*(1), 212–218. https://doi.org/10.1104/pp.75.1.212

Gfeller, R. P., & Gibbs, M. (1985). Fermentative Metabolism of *Chlamydomonas reinhardtii*. *Plant Physiology*, *77*(2), 509–511. https://doi.org/10.1104/pp.77.2.509

Ghirardi, M. L., Togasaki, R. K., & Seibert, M. (1997). Oxygen sensitivity of algal H_2-production. *Applied Biochemistry and Biotechnology*, *67*(1–2), 182. https://doi.org/10.1007/BF02787851

Ghysels, B., Godaux, D., Matagne, R. F., Cardol, P., & Franck, F. (2013). Function of the Chloroplast Hydrogenase in the Microalga *Chlamydomonas*: The Role of Hydrogenase and State Transitions during Photosynthetic Activation in Anaerobiosis. *PLoS ONE*, *8*(5), e64161. https://doi.org/10.1371/journal.pone.0064161

Gibbs, M., Gfeller, R. P., & Chen, C. (1986). Fermentative Metabolism of *Chlamydomonas reinhardii*. *Plant Physiology*, *82*(1), 160–166. https://doi.org/10.1104/pp.82.1.160

Girolomoni, L., Cazzaniga, S., Pinnola, A., Perozeni, F., Ballottari, M., & Bassi, R. (2019). LHCSR3 is a nonphotochemical quencher of both photosystems in *Chlamydomonas reinhardtii*. *Proceedings of the National Academy of Sciences*, *116*(10), 4212–4217. https://doi.org/10.1073/pnas.1809812116

Godaux, D., Bailleul, B., Berne, N., & Cardol, P. (2015). Induction of Photosynthetic Carbon Fixation in Anoxia Relies on Hydrogenase Activity and Proton-Gradient Regulation-Like1-Mediated Cyclic Electron Flow in *Chlamydomonas reinhardtii*. *Plant Physiology*, *168*(2), 648–658. https://doi.org/10.1104/pp.15.00105

Godman, J. E., Molnár, A., Baulcombe, D. C., & Balk, J. (2010). RNA silencing of hydrogenase(-like) genes and investigation of their physiological roles in the green alga *Chlamydomonas reinhardtii*. *Biochemical Journal*, *431*(3), 345–352. https://doi.org/10.1042/BJ20100932

Gulis, G., Narasimhulu, K. V, Fox, L. N., & Redding, K. E. (2008). Purification of His_6-tagged Photosystem I from *Chlamydomonas reinhardtii*. *Photosynthesis Research*, *96*(1), 51–60. https://doi.org/10.1007/s11120-007-9283-9

Gurrieri, L., Fermani, S., Zaffagnini, M., Sparla, F., & Trost, P. (2021). Calvin–Benson cycle regulation is getting complex. *Trends in Plant Science*, *26*(9), 898–912. https://doi.org/10.1016/j.tplants.2021.03.008

Happe, T., & Kaminski, A. (2002). Differential regulation of the Fe-hydrogenase during anaerobic adaptation in the green alga *Chlamydomonas reinhardtii*. *European Journal of Biochemistry*, *269*(3), 1022–1032. https://doi.org/10.1046/j.0014-2956.2001.02743.x

Happe, T., & Naber, J. D. (1993). Isolation, characterization and N-terminal amino acid sequence of hydrogenase from the green alga *Chlamydomonas reinhardtii*. *European Journal of Biochemistry*, *214*(2), 475–481. https://doi.org/10.1111/j.1432-1033.1993.tb17944.x

Harris, E. H. (2001). *Chlamydomonas* as a Model Organism. *Annual Review of Plant Physiology and Plant Molecular Biology*, *52*(1), 363–406. https://doi.org/10.1146/annurev.arplant.52.1.363

Hemschemeier, A., Fouchard, S., Cournac, L., Peltier, G., & Happe, T. (2008). Hydrogen production by *Chlamydomonas reinhardtii*: an elaborate interplay of electron sources and sinks. *Planta*, *227*(2), 397–407. https://doi.org/10.1007/s00425-007-0626-8

Hohmann-Marriott, M. F., & Blankenship, R. E. (2011). Evolution of Photosynthesis. *Annual Review of Plant Biology*, *62*(1), 515–548. https://doi.org/10.1146/annurev-arplant-042110-103811

Hoobert, J. K., & Blobel, G. (1969). Characterization of the chloroplastic and cytoplasmic ribosomes of *Chlamydomonas reinhardi*. *Journal of Molecular Biology*, *41*(1), 121–138. https://doi.org/10.1016/0022-2836(69)90130-2

Houille-Vernes, L., Rappaport, F., Wollman, F.-A., Alric, J., & Johnson, X. (2011). Plastid terminal oxidase 2 (PTOX2) is the major oxidase involved in chlororespiration in *Chlamydomonas*. *Proceedings of the National Academy of Sciences*, *108*(51), 20820–20825. https://doi.org/10.1073/pnas.1110518109

Hubbard, T. J. P. (1999). RMS/Coverage graphs: A qualitative method for comparing three-dimensional protein structure predictions. *Proteins: Structure, Function, and Bioinformatics*, *37*(S3), 15–21. https://doi.org/https://doi.org/10.1002/(SICI)1097-0134(1999)37:3+<15::AID-PROT4>3.0.CO;2-Z

Hwang, J.-H., & Lee, W. H. (2021). Continuous photosynthetic biohydrogen production from acetate-rich wastewater: Influence of light intensity. *International Journal of Hydrogen Energy*, *46*(42), 21812–21821. https://doi.org/10.1016/j.ijhydene.2021.04.052

Jagannathan, B., & Golbeck, J. H. (2009). Understanding of the Binding Interface between PsaC and the PsaA/PsaB Heterodimer in Photosystem I. *Biochemistry*, *48*(23), 5405–5416. https://doi.org/10.1021/bi900243f

Johnson, X., & Alric, J. (2012). Interaction between Starch Breakdown, Acetate Assimilation, and Photosynthetic Cyclic Electron Flow in *Chlamydomonas reinhardtii*. *Journal of Biological Chemistry*, *287*(31), 26445–26452. https://doi.org/10.1074/jbc.M112.370205

Johnson, X., & Alric, J. (2013). Central Carbon Metabolism and Electron Transport in *Chlamydomonas reinhardtii*: Metabolic Constraints for Carbon Partitioning between Oil and Starch. *Eukaryotic Cell*, *12*(6), 776–793. https://doi.org/10.1128/EC.00318-12

Jordan, P., Fromme, P., Witt, H. T., Klukas, O., & others. (2001). Three-dimensional structure of cyanobacterial photosystem I at 2.5 angstrom resolution. *Nature*, *411*(6840), 909. http://search.proquest.com/openview/d2e4a1fb74ddc35524db2fe4428d5072/1?pq-origsite=gscholar&cbl=40569

Jumper, J., Evans, R., Pritzel, A., Green, T., Figurnov, M., Ronneberger, O., Tunyasuvunakool, K., Bates, R., Žídek, A., Potapenko, A., Bridgland, A., Meyer, C., Kohl, S. A. A., Ballard, A. J., Cowie, A., Romera-Paredes, B., Nikolov, S., Jain, R., Adler, J., … Hassabis, D. (2021). Highly accurate protein structure prediction with AlphaFold. *Nature*, *596*(7873), 583–589. https://doi.org/10.1038/s41586-021-03819-2

Kanygin, A., Milrad, Y., Thummala, C., Reifschneider, K., Baker, P., Marco, P., Yacoby, I., & Redding, K. E. (2020). Rewiring photosynthesis: a photosystem I-hydrogenase chimera that makes H_2 *in vivo*. *Energy & Environmental Science*, *13*(9), 2903–2914. https://doi.org/10.1039/C9EE03859K

Kanygin, A., Smith, A., Nagy, V., Tóth, S. Z., & Redding, K. E. (2022). Interplay between hydrogen production and photosynthesis in a green alga expressing an active photosystem I-hydrogenase chimera. *International Journal of Hydrogen Energy*, *47*(52), 21969–21983. https://doi.org/10.1016/j.ijhydene.2022.03.096

Kelley, L. A., Mezulis, S., Yates, C. M., Wass, M. N., & Sternberg, M. J. E. (2015). The Phyre2 web portal for protein modeling, prediction and analysis. *Nature Protocols*, *10*(6), 845–858. https://doi.org/10.1038/nprot.2015.053

Kosourov, S., Jokel, M., Aro, E.-M., & Allahverdiyeva, Y. (2018). A new approach for sustained and efficient H_2 photoproduction by *Chlamydomonas reinhardtii*. *Energy & Environmental Science*, *11*(6), 1431–1436. https://doi.org/10.1039/C8EE00054A

Kosourov, S. N., Batyrova, K. A., Petushkova, E. P., Tsygankov, A. A., Ghirardi, M. L., & Seibert, M. (2012). Maximizing the hydrogen photoproduction yields in *Chlamydomonas reinhardtii* cultures: The effect of the H_2 partial pressure. *International Journal of Hydrogen Energy*, *37*(10), 8850–8858. https://doi.org/10.1016/j.ijhydene.2012.01.082

Kosourov, S., Nagy, V., Shevela, D., Jokel, M., Messinger, J., & Allahverdiyeva, Y. (2020). Water oxidation by photosystem II is the primary source of electrons for sustained H_2 photoproduction in nutrient-replete green algae. *Proceedings of the National Academy of Sciences*, *117*(47), 29629–29636. https://doi.org/10.1073/pnas.2009210117

Kozakov, D., Hall, D. R., Xia, B., Porter, K. A., Padhorny, D., Yueh, C., Beglov, D., & Vajda, S. (2017). The ClusPro web server for protein–protein docking. *Nature Protocols*, *12*(2), 255. https://doi.org/10.1038/nprot.2016.169

Kozuleva, M., Petrova, A., Milrad, Y., Semenov, A., Ivanov, B., Redding, K. E., & Yacoby, I. (2021). Phylloquinone is the principal Mehler reaction site within photosystem I in high light. *Plant Physiology*, *186*(4), 1848–1858. https://doi.org/10.1093/plphys/kiab221

Kropat, J., Hong-Hermesdorf, A., Casero, D., Ent, P., Castruita, M., Pellegrini, M., Merchant, S. S., & Malasarn, D. (2011). A revised mineral nutrient supplement increases biomass and growth rate in *Chlamydomonas reinhardtii*. *The Plant Journal*, *66*(5), 770–780. https://doi.org/10.1111/j.1365-313X.2011.04537.x

Kubas, A., Orain, C., De Sancho, D., Saujet, L., Sensi, M., Gauquelin, C., Meynial-Salles, I., Soucaille, P., Bottin, H., Baffert, C., Fourmond, V., Best, R. B., Blumberger, J., & Léger, C. (2017). Mechanism of O_2 diffusion and reduction in FeFe hydrogenases. *Nature Chemistry*, *9*(1), 88–95. https://doi.org/10.1038/nchem.2592

Kuhlgert, S., Drepper, F., Fufezan, C., Sommer, F., & Hippler, M. (2012). Residues PsaB Asp612 and PsaB Glu613 of Photosystem I Confer pH-Dependent Binding of Plastocyanin and Cytochrome c_6. *Biochemistry*, *51*(37), 7297–7303. https://doi.org/10.1021/bi300898j

Land, H., Senger, M., Berggren, G., & Stripp, S. T. (2020). Current State of [FeFe]-Hydrogenase Research: Biodiversity and Spectroscopic Investigations. *ACS Catalysis*, *10*(13), 7069–7086. https://doi.org/10.1021/acscatal.0c01614

Li, Y., Lucas, M.-G., Konovalova, T., Abbott, B., MacMillan, F., Petrenko, A., Sivakumar, V., Wang, R., Hastings, G., Gu, F., van Tol, J., Brunel, L.-C., Timkovich, R., Rappaport, F., & Redding, K. (2004). Mutation of the Putative Hydrogen-Bond Donor to P_{700} of Photosystem I. *Biochemistry*, *43*(39), 12634–12647. https://doi.org/10.1021/bi036329p

Liran, O., Semyatich, R., Milrad, Y., Eilenberg, H., Weiner, I., & Yacoby, I. (2016). Microoxic Niches within the Thylakoid Stroma of Air-Grown *Chlamydomonas reinhardtii* Protect [FeFe]-Hydrogenase and Support Hydrogen Production under Fully Aerobic Environment. *Plant Physiology*, *172*(1), 264 LP – 271. https://doi.org/10.1104/pp.16.01063

Lubitz, W., Ogata, H., Rüdiger, O., & Reijerse, E. (2014). Hydrogenases. *Chemical Reviews*, *114*(8), 4081–4148. https://doi.org/10.1021/cr4005814

Lubner, C. E., Applegate, a. M., Knorzer, P., Ganago, a., Bryant, D. a., Happe, T., & Golbeck, J. H. (2011). Solar hydrogen-producing bionanodevice outperforms natural photosynthesis. *Proceedings of the National Academy of Sciences*, *108*(52), 20988–20991. https://doi.org/10.1073/pnas.1114660108

Malone, L. A., Proctor, M. S., Hitchcock, A., Hunter, C. N., & Johnson, M. P. (2021). Cytochrome *b6f* – Orchestrator of photosynthetic electron transfer. *Biochimica et Biophysica Acta (BBA) - Bioenergetics*, *1862*(5), 148380. https://doi.org/10.1016/j.bbabio.2021.148380

Marco, P., Kozuleva, M., Eilenberg, H., Mazor, Y., Gimeson, P., Kanygin, A., Redding, K., Weiner, I., & Yacoby, I. (2018). Binding of ferredoxin to algal photosystem I involves a single binding site and is composed of two thermodynamically distinct events. *Biochimica et Biophysica Acta (BBA) - Bioenergetics*, *1859*(4), 234–243. https://doi.org/10.1016/j.bbabio.2018.01.001

Mariani, V., Biasini, M., Barbato, A., & Schwede, T. (2013). lDDT: a local superposition-free score for comparing protein structures and models using distance difference tests. *Bioinformatics*, *29*(21), 2722–2728. https://doi.org/10.1093/bioinformatics/btt473

Meimberg, K., Fischer, N., Rochaix, J.-D., & Mühlenhoff, U. (1999). Lys35 of PsaC is required for the efficient photoreduction of flavodoxin by photosystem I from *Chlamydomonas reinhardtii*. *European Journal of Biochemistry*, *263*(1), 137–144. https://doi.org/10.1046/j.1432-1327.1999.00474.x

Meimberg, K., & Mühlenhoff, U. (1999). Laser-flash absorption spectroscopy study of the competition between ferredoxin and flavodoxin photoreduction by Photosystem I in *Synechococcus* sp. PCC 7002: Evidence for a strong preference for ferredoxin. *Photosynthesis Research*, *61*(3), 253–267. https://doi.org/10.1023/A:1006308729990

Melis, A., Zhang, L., Forestier, M., Ghirardi, M. L., & Seibert, M. (2000). Sustained Photobiological Hydrogen Gas Production upon Reversible Inactivation of Oxygen Evolution in the Green Alga *Chlamydomonas reinhardtii*. *Plant Physiology*, *122*(1), 127–136. https://doi.org/10.1104/pp.122.1.127

Meuser, J. E., D'Adamo, S., Jinkerson, R. E., Mus, F., Yang, W., Ghirardi, M. L., Seibert, M., Grossman, A. R., & Posewitz, M. C. (2012). Genetic disruption of both *Chlamydomonas reinhardtii* [FeFe]-hydrogenases: Insight into the role of HYDA2 in H_2 production. *Biochemical and Biophysical Research Communications*, *417*(2), 704–709. https://doi.org/10.1016/j.bbrc.2011.12.002

Meyer zu Tittingdorf, J. M. W., Rexroth, S., Schäfer, E., Schlichting, R., Giersch, C., Dencher, N. A., & Seelert, H. (2004). The stoichiometry of the chloroplast ATP synthase oligomer III in *Chlamydomonas reinhardtii* is not affected by the metabolic state. *Biochimica et Biophysica Acta (BBA) - Bioenergetics*, *1659*(1), 92–99. https://doi.org/10.1016/j.bbabio.2004.08.008

Milrad, Y., Schweitzer, S., Feldman, Y., & Yacoby, I. (2018). Green Algal Hydrogenase Activity Is Outcompeted by Carbon Fixation before Inactivation by Oxygen Takes Place. *Plant Physiology*, *177*(3), 918–926. https://doi.org/10.1104/pp.18.00229

Milrad, Y., Schweitzer, S., Feldman, Y., & Yacoby, I. (2021). Bi-directional electron transfer between H_2 and NADPH mitigates light fluctuation responses in green algae. *Plant Physiology*, *186*(1), 168–179. https://doi.org/10.1093/plphys/kiab051

Moser, C. C., Keske, J. M., Warncke, K., Farid, R. S., & Dutton, P. L. (1992). Nature of biological electron transfer. *Nature*, *355*(6363), 796–802. https://doi.org/10.1038/355796a0

Mulder, D. W., Boyd, E. S., Sarma, R., Lange, R. K., Endrizzi, J. A., Broderick, J. B., & Peters, J. W. (2010). Stepwise [FeFe]-hydrogenase H-cluster assembly revealed in the structure of $HydA^{\Delta EFG}$. *Nature*, *465*(7295), 248–251. https://doi.org/10.1038/nature08993

Nagy, V., Podmaniczki, A., Vidal-Meireles, A., Kuntam, S., Herman, É., Kovács, L., Tóth, D., Scoma, A., & Tóth, S. Z. (2021). Thin cell layer cultures of *Chlamydomonas reinhardtii* L159I-N230Y, *pgrl1* and *pgr5* mutants perform enhanced hydrogen production at sunlight intensity. *Bioresource Technology*, *333*, 125217. https://doi.org/10.1016/j.biortech.2021.125217

Nagy, V., Podmaniczki, A., Vidal-Meireles, A., Tengölics, R., Kovács, L., Rákhely, G., Scoma, A., & Tóth, S. Z. (2018). Water-splitting-based, sustainable and efficient H_2 production in green algae as achieved by substrate limitation of the Calvin–Benson–Bassham cycle. *Biotechnology for Biofuels*, *11*, 69. https://doi.org/10.1186/s13068-018-1069-0

Nawrocki, W. J., Bailleul, B., Picot, D., Cardol, P., Rappaport, F., Wollman, F.-A., & Joliot, P. (2019). The mechanism of cyclic electron flow. *Biochimica et Biophysica Acta (BBA) - Bioenergetics*, *1860*(5), 433–438. https://doi.org/10.1016/j.bbabio.2018.12.005

Nelson, N., & Ben-Shem, A. (2004). The complex architecture of oxygenic photosynthesis. *Nature Reviews Molecular Cell Biology*, *5*, 971. https://doi.org/10.1038/nrm1525

Nelson, N., & Junge, W. (2015). Structure and Energy Transfer in Photosystems of Oxygenic Photosynthesis. *Annual Review of Biochemistry*, *84*(1), 659–683. https://doi.org/10.1146/annurev-biochem-092914-041942

Nikkanen, L., Solymosi, D., Jokel, M., & Allahverdiyeva, Y. (2021). Regulatory electron transport pathways of photosynthesis in cyanobacteria and microalgae: Recent advances and biotechnological prospects. *Physiologia Plantarum*, *173*(2), 514–525. https://doi.org/10.1111/ppl.13404

Nikolova, D., Heilmann, C., Hawat, S., Gäbelein, P., & Hippler, M. (2018). Absolute quantification of selected photosynthetic electron transfer proteins in *Chlamydomonas reinhardtii* in the presence and absence of oxygen. *Photosynthesis Research*, *137*(2), 281–293. https://doi.org/10.1007/s11120-018-0502-3

Noth, J., Krawietz, D., Hemschemeier, A., & Happe, T. (2013). Pyruvate:Ferredoxin Oxidoreductase Is Coupled to Light-independent Hydrogen Production in *Chlamydomonas reinhardtii*. *Journal of Biological Chemistry*, *288*(6), 4368–4377. https://doi.org/10.1074/jbc.M112.429985

Ostersetzer, O., & Adam, Z. (1997). Light-stimulated degradation of an unassembled Rieske FeS protein by a thylakoid-bound protease: the possible role of the FtsH protease. *The Plant Cell*, *9*(6), 957–965. http://www.plantcell.org/content/9/6/957.short

Peltier, G., Aro, E.-M., & Shikanai, T. (2016). NDH-1 and NDH-2 Plastoquinone Reductases in Oxygenic Photosynthesis. *Annual Review of Plant Biology*, *67*(1), 55–80. https://doi.org/10.1146/annurev-arplant-043014-114752

Pinto, T. S., Malcata, F. X., Arrabaça, J. D., Silva, J. M., Spreitzer, R. J., & Esquível, M. G. (2013). Rubisco mutants of *Chlamydomonas reinhardtii* enhance photosynthetic hydrogen production. *Applied Microbiology and Biotechnology*, *97*(12), 5635–5643. https://doi.org/10.1007/s00253-013-4920-z

Polle, J. E. W., Benemann, J. R., Tanaka, A., & Melis, A. (2000). Photosynthetic apparatus organization and function in the wild type and a chlorophyll *b* -less mutant of *Chlamydomonas reinhardtii* . Dependence on carbon source. *Planta*, *211*(3), 335–344. https://doi.org/10.1007/s004250000279

Polukhina, I., Fristedt, R., Dinc, E., Cardol, P., & Croce, R. (2016). Carbon Supply and Photoacclimation Cross Talk in the Green Alga *Chlamydomonas reinhardtii*. *Plant Physiology*, *172*(3), 1494–1505. https://doi.org/10.1104/pp.16.01310

Porra, R. J., Thompson, W. A., & Kriedemann, P. E. (1989). Determination of accurate extinction coefficients and simultaneous equations for assaying chlorophylls a and b extracted with four different solvents: verification of the concentration of chlorophyll standards by atomic absorption spectroscopy. *Biochimica et Biophysica Acta (BBA) - Bioenergetics*, *975*(3), 384–394. https://doi.org/10.1016/S0005-2728(89)80347-0

Posewitz, M. C., King, P. W., Smolinski, S. L., Zhang, L., Seibert, M., & Ghirardi, M. L. (2004). Discovery of Two Novel Radical S -Adenosylmethionine Proteins Required for the Assembly of an Active [Fe] Hydrogenase. *Journal of Biological Chemistry*, *279*(24), 25711–25720. https://doi.org/10.1074/jbc.M403206200

Redding, K., Cournac, L., Vassiliev, I. R., Golbeck, J. H., Peltier, G., & Rochaix, J.-D. (1999). Photosystem I Is Indispensable for Photoautotrophic Growth, CO_2 Fixation, and H_2 Photoproduction in *Chlamydomonas reinhardtii*. *Journal of Biological Chemistry*, *274*(15), 10466–10473. https://doi.org/10.1074/jbc.274.15.10466

Redding, K. E., Appel, J., Boehm, M., Schuhmann, W., Nowaczyk, M. M., Yacoby, I., & Gutekunst, K. (2022). Advances and challenges in photosynthetic hydrogen production. *Trends in Biotechnology*. https://doi.org/10.1016/j.tibtech.2022.04.007

Redding, K., MacMillan, F., Leibl, W., Brettel, K., Hanley, J., Rutherford, A. W., Breton, J., & Rochaix, J.-D. (1998). A systematic survey of conserved histidines in the core subunits of Photosystem I by site-directed mutagenesis reveals the likely axial ligands of P_{700}. *The EMBO Journal*, *17*(1), 50–60. https://doi.org/10.1093/emboj/17.1.50

Reifschneider-Wegner, K., Kanygin, A., & Redding, K. E. (2014). Expression of the [FeFe] hydrogenase in the chloroplast of *Chlamydomonas reinhardtii*. *International Journal of Hydrogen Energy*, *39*(8), 3657–3665. https://doi.org/10.1016/j.ijhydene.2013.12.157

Rumpel, S., Siebel, J. F., Diallo, M., Farès, C., Reijerse, E. J., & Lubitz, W. (2015). Structural Insight into the Complex of Ferredoxin and [FeFe] Hydrogenase from *Chlamydomonas reinhardtii*. *ChemBioChem*, *16*(11), 1663–1669. https://doi.org/10.1002/cbic.201500130

Salomon-Ferrer, R., Case, D. A., & Walker, R. C. (2013). An overview of the Amber biomolecular simulation package. *Wiley Interdisciplinary Reviews: Computational Molecular Science*, *3*(2), 198–210. https://doi.org/10.1002/wcms.1121

Santabarbara, S., Redding, K. E., & Rappaport, F. (2009). Temperature Dependence of the Reduction of P_{700}^{+} by Tightly Bound Plastocyanin in Vivo. *Biochemistry*, *48*(43), 10457–10466. https://doi.org/10.1021/bi901052c

Saroussi, S. I., Wittkopp, T. M., & Grossman, A. R. (2016). The Type II NADPH Dehydrogenase Facilitates Cyclic Electron Flow, Energy-Dependent Quenching, and Chlororespiratory Metabolism during Acclimation of *Chlamydomonas reinhardtii* to Nitrogen Deprivation. *Plant Physiology*, *170*(4), 1975–1988. https://doi.org/10.1104/pp.15.02014

Saroussi, S., Karns, D. A. J., Thomas, D. C., Bloszies, C., Fiehn, O., Posewitz, M. C., & Grossman, A. R. (2019). Alternative outlets for sustaining photosynthetic electron transport during dark-to-light transitions. *Proceedings of the National Academy of Sciences*, *116*(23), 11518–11527. https://doi.org/10.1073/pnas.1903185116

Sawyer, A., Bai, Y., Lu, Y., Hemschemeier, A., & Happe, T. (2017). Compartmentalisation of [FeFe]-hydrogenase maturation in *Chlamydomonas reinhardtii*. *The Plant Journal*, *90*(6), 1134–1143. https://doi.org/10.1111/tpj.13535

Schrödinger, L. (2015). *The {PyMOL} Molecular Graphics System, Version 2.4.0*.

Sétif, P. (2001). Ferredoxin and flavodoxin reduction by photosystem I. *Biochimica et Biophysica Acta (BBA) - Bioenergetics*, *1507*(1), 161–179. https://doi.org/https://doi.org/10.1016/S0005-2728(01)00205-5

Sétif, P., Fischer, N., Lagoutte, B., Bottin, H., & Rochaix, J. D. (2002). The ferredoxin docking site of photosystem I. *Biochimica et Biophysica Acta - Bioenergetics*, *1555*(1–3), 204–209. https://doi.org/10.1016/S0005-2728(02)00279-7

Sharkey, T. D. (2019). Discovery of the canonical Calvin–Benson cycle. *Photosynthesis Research*, *140*(2), 235–252. https://doi.org/10.1007/s11120-018-0600-2

Shepard, E. M., Mus, F., Betz, J. N., Byer, A. S., Duffus, B. R., Peters, J. W., & Broderick, J. B. (2014). [FeFe]-Hydrogenase Maturation. *Biochemistry*, *53*(25), 4090–4104. https://doi.org/10.1021/bi500210x

Sicher, R. C. (1984). Glycolaldehyde Inhibition of Photosynthetic Carbon Assimilation by Isolated Chloroplasts and Protoplasts. In C. Sybesma (Ed.), *Advances in Photosynthesis Research: Proceedings of the VIth International Congress on Photosynthesis, Brussels, Belgium, August 1--6, 1983* (pp. 413–416). Springer Netherlands. https://doi.org/10.1007/978-94-017-4973-2_94

Sievers, F., Wilm, A., Dineen, D., Gibson, T. J., Karplus, K., Li, W., Lopez, R., McWilliam, H., Remmert, M., Söding, J., Thompson, J. D., & Higgins, D. G. (2011). Fast, scalable generation of high-quality protein multiple sequence alignments using Clustal Omega. *Molecular Systems Biology*, *7*(1), 539. https://doi.org/10.1038/msb.2011.75

Søndergaard, D., Pedersen, C. N. S., & Greening, C. (2016). HydDB: A web tool for hydrogenase classification and analysis. *Scientific Reports*, *6*(1), 34212. https://doi.org/10.1038/srep34212

Song, Y., DiMaio, F., Wang, R. Y.-R., Kim, D., Miles, C., Brunette, T., Thompson, J., & Baker, D. (2013). High-Resolution Comparative Modeling with RosettaCM. *Structure*, *21*(10), 1735–1742. https://doi.org/10.1016/j.str.2013.08.005

Stirbet, A., Lazár, D., Guo, Y., & Govindjee, G. (2020). Photosynthesis: basics, history and modelling. *Annals of Botany*, *126*(4), 511–537. https://doi.org/10.1093/aob/mcz171

Stripp, S. T., Goldet, G., Brandmayr, C., Sanganas, O., Vincent, K. A., Haumann, M., Armstrong, F. A., & Happe, T. (2009). How oxygen attacks [FeFe] hydrogenases from photosynthetic organisms. *Proceedings of the National Academy of Sciences*, *106*(41), 17331–17336. https://doi.org/10.1073/pnas.0905343106

Stroebel, D., Choquet, Y., Popot, J.-L., & Picot, D. (2003). An atypical haem in the cytochrome *b6f* complex. *Nature*, *426*(6965), 413–418. https://doi.org/10.1038/nature02155

Stuart, T. S., & Gaffron, H. (1972). The Gas Exchange of Hydrogen-adapted Algae as Followed by Mass Spectrometry. *Plant Physiology*, *50*(1), 136–140. https://doi.org/10.1104/pp.50.1.136

Su, X., Ma, J., Pan, X., Zhao, X., Chang, W., Liu, Z., Zhang, X., & Li, M. (2019). Antenna arrangement and energy transfer pathways of a green algal photosystem-I–LHCI supercomplex. *Nature Plants*, *5*(3), 273–281. https://doi.org/10.1038/s41477-019-0380-5

Suga, M., Ozawa, S.-I., Yoshida-Motomura, K., Akita, F., Miyazaki, N., & Takahashi, Y. (2019). Structure of the green algal photosystem I supercomplex with a decameric light-harvesting complex I. *Nature Plants*, *5*(6), 626–636. https://doi.org/10.1038/s41477-019-0438-4

Sun, Y., Chen, M., Yang, H., Zhang, J., Kuang, T., & Huang, F. (2013). Enhanced H_2 photoproduction by down-regulation of ferredoxin-$NADP^+$ reductase (FNR) in the green alga *Chlamydomonas reinhardtii*. *International Journal of Hydrogen Energy*, *38*(36), 16029–16037. https://doi.org/10.1016/J.IJHYDENE.2013.10.011

Suslick, K. S. (1990). Sonochemistry. *Science*, *247*(4949), 1439–1445. https://doi.org/10.1126/science.247.4949.1439

Swanson, K. D., Ratzloff, M. W., Mulder, D. W., Artz, J. H., Ghose, S., Hoffman, A., White, S., Zadvornyy, O. A., Broderick, J. B., Bothner, B., King, P. W., & Peters, J. W. (2015). [FeFe]-Hydrogenase Oxygen Inactivation Is Initiated at the H Cluster 2Fe Subcluster. *Journal of the American Chemical Society*, *137*(5), 1809–1816. https://doi.org/10.1021/ja510169s

Swartz, J. (2020). Opportunities toward hydrogen production biotechnologies. *Current Opinion in Biotechnology*, *62*, 248–255. https://doi.org/10.1016/j.copbio.2020.03.002

Takahashi, H., Clowez, S., Wollman, F.-A., Vallon, O., & Rappaport, F. (2013). Cyclic electron flow is redox-controlled but independent of state transition. *Nature Communications*, *4*, 1954. https://doi.org/10.1038/ncomms2954

Takahashi, Y., Goldschmidt-Clermont, M., Soen, S. Y., Franzén, L. G., Rochaix, J. D., Franzen, L. G., & Rochaix, J. D. (1991). Directed chloroplast transformation in *Chlamydomonas reinhardtii*: insertional inactivation of the *psaC* gene encoding the iron sulfur protein destabilizes photosystem I. *The EMBO Journal*, *10*(8), 2033. https://www.ncbi.nlm.nih.gov/pmc/articles/PMC452884/

Tirumani, S., Gothandam, K. M., & J Rao, B. (2019). Coordination between photorespiration and carbon concentrating mechanism in *Chlamydomonas reinhardtii*: transcript and protein changes during light-dark diurnal cycles and mixotrophy conditions. *Protoplasma*, *256*(1), 117–130. https://doi.org/10.1007/s00709-018-1283-4

Torzillo, G., Scoma, A., Faraloni, C., & Giannelli, L. (2015). Advances in the biotechnology of hydrogen production with the microalga *Chlamydomonas reinhardtii*. *Critical Reviews in Biotechnology*, *35*(4), 485–496. https://doi.org/10.3109/07388551.2014.900734

Tóth, S. Z., & Yacoby, I. (2019). Paradigm Shift in Algal H_2 Production: Bypassing Competitive Processes. *Trends in Biotechnology*, *37*(11), 1159–1163. https://doi.org/10.1016/j.tibtech.2019.05.001

Urbig, T., Schulz, R., & Senger, H. (1993). Inactivation and Reactivation of the Hydrogenases of the Green Algae *Scenedesmus obliquus* and *Chlamydomonas reinhardtii*. *Zeitschrift Für Naturforschung C*, *48*(1–2), 41–45. https://doi.org/10.1515/znc-1993-1-208

Vassiliev, I. R., Jung, Y.-S., Yang, F., & Golbeck, J. H. (1998). PsaC Subunit of Photosystem I Is Oriented with Iron-Sulfur Cluster F_B as the Immediate Electron Donor to Ferredoxin and Flavodoxin. *Biophysical Journal*, *74*(4), 2029–2035. https://doi.org/10.1016/S0006-3495(98)77909-3

Veeravalli, S. S., Shanmugam, S. R., Ray, S., Lalman, J. A., & Biswas, N. (2019). Biohydrogen Production From Renewable Resources. In M. Hosseini (Ed.), *Advanced Bioprocessing for Alternative Fuels, Biobased Chemicals, and Bioproducts* (pp. 289–312). Woodhead Publishing. https://doi.org/10.1016/B978-0-12-817941-3.00015-2

von Abendroth, G., Stripp, S., Silakov, A., Croux, C., Soucaille, P., Girbal, L., & Happe, T. (2008). Optimized over-expression of [FeFe] hydrogenases with high specific activity in *Clostridium acetobutylicum*. *International Journal of Hydrogen Energy*, *33*(21), 6076–6081. https://doi.org/10.1016/j.ijhydene.2008.07.122

Wang, L., Gong, W., Lin, A., & Hu, B. (2014). Analysis of photosynthetically active radiation under various sky conditions in Wuhan, Central China. *International Journal of Biometeorology*, *58*(8), 1711–1720. https://doi.org/10.1007/s00484-013-0775-3

Weiß, D., Schneider, G., Niemann, B., Guttmann, P., Rudolph, D., & Schmahl, G. (2000). Computed tomography of cryogenic biological specimens based on X-ray microscopic images. *Ultramicroscopy*, *84*(3–4), 185–197. https://doi.org/10.1016/S0304-3991(00)00034-6

Williams, C. J., Headd, J. J., Moriarty, N. W., Prisant, M. G., Videau, L. L., Deis, L. N., Verma, V., Keedy, D. A., Hintze, B. J., Chen, V. B., Jain, S., Lewis, S. M., Arendall, W. B., Snoeyink, J., Adams, P. D., Lovell, S. C., Richardson, J. S., & Richardson, D. C. (2018). MolProbity: More and better reference data for improved all-atom structure validation. *Protein Science*, *27*(1), 293–315. https://doi.org/10.1002/pro.3330

Winkler, M., Hemschemeier, A., Jacobs, J., Stripp, S., & Happe, T. (2010). Multiple ferredoxin isoforms in *Chlamydomonas reinhardtii* – Their role under stress conditions and biotechnological implications. *European Journal of Cell Biology*, *89*(12), 998–1004. https://doi.org/10.1016/J.EJCB.2010.06.018

Winkler, M., Kuhlgert, S., Hippler, M., & Happe, T. (2009). Characterization of the Key Step for Light-driven Hydrogen Evolution in Green Algae. *Journal of Biological Chemistry*, *284*(52), 36620–36627. https://doi.org/10.1074/jbc.M109.053496

Witt, H., Bordignon, E., Carbonera, D., Dekker, J. P., Karapetyan, N., Teutloff, C., Webber, A., Lubitz, W., & Schlodder, E. (2003). Species-specific differences of the spectroscopic properties of P700: analysis of the influence of non-conserved amino acid residues by site-directed mutagenesis of photosystem I from *Chlamydomonas reinhardtii*. *The Journal of Biological Chemistry*, *278*(47), 46760–46771. https://doi.org/10.1074/jbc.M304776200

World Energy Council. (2013). Energy Resources: Solar. *World Energy Council 2013 World Energy Resources: Solar*, 1–28. http://www.worldenergy.org/wp-content/uploads/2013/10/WER_2013_8_Solar_revised.pdf

Xia, B., Vajda, S., & Kozakov, D. (2016). Accounting for pairwise distance restraints in FFT-based protein–protein docking. *Bioinformatics*, *32*(21), 3342–3344. https://doi.org/10.1093/bioinformatics/btw306

Xie, X., Huang, A., Gu, W., Zang, Z., Pan, G., Gao, S., He, L., Zhang, B., Niu, J., Lin, A., & Wang, G. (2016). Photorespiration participates in the assimilation of acetate in *Chlorella sorokiniana* under high light. *New Phytologist*, *209*(3), 987–998. https://doi.org/10.1111/nph.13659

Yacoby, I., Pochekailov, S., Toporik, H., Ghirardi, M. L., King, P. W., & Zhang, S. (2011). Photosynthetic electron partitioning between [FeFe]-hydrogenase and ferredoxin: $NADP^+$-oxidoreductase (FNR) enzymes in vitro. *Proceedings of the National Academy of Sciences*, *108*(23), 9396–9401. http://www.pnas.org/content/108/23/9396.short

Zemla, A. (2003). LGA: a method for finding 3D similarities in protein structures. *Nucleic Acids Research*, *31*(13), 3370–3374. https://doi.org/10.1093/nar/gkg571

Zhao, J., Li, R., & Bryant, D. A. (1998). Measurement of Photosystem I Activity with Photoreduction of Recombinant Flavodoxin. *Analytical Biochemistry*, *264*(2), 263–270. https://doi.org/10.1006/abio.1998.2845

APPENDIX A

PERMISSION TO REPRODUCE CHAPTERS 2 AND 3 FROM THE ENERGY & ENVIRONMENTAL SCIENCE JOURNAL AND INTERNATIONAL JOURNAL OF HYDROGEN ENERGY, RESPECTIVELY

Sales Operations
Thomas Graham House
Science Park, Milton Road
Cambridge CB4 0WF, UK

Tel +44 (0) 1223 420066

Email contracts-copyright@rsc.org

www.rsc.org

Permission Request Form for RSC Material

To request permission to use material from material published by The Royal Society of Chemistry (RSC), please complete and return this form.

From: Name: Andrey Kanygin E-mail: akanygin@asu.edu
Address: 502 E Mitchell dr
Phoenix, AZ, 85012, USA

I am preparing the following work for publication:

Article/Chapter Title	Rewiring photosynthesis: a photosystem I-hydrogenase chimera that makes H2 in vivo
Journal/Book Title	Engineering the next-generation type I reaction centers specializing in H2 production in vivo.
Editor/Author(s)	Andrey Kanygin
Publisher	ProQuest

I would very much appreciate your permission to use the following material:

Journal/Book Title	Energy & Environmental Science
Article/Chapter Title	Rewiring photosynthesis: a photosystem I-hydrogenase chimera that makes H2 in vivo
Editor/Author(s)	Andrey Kanygin
DOI	10.1039/C9EE03859K
Year of Publication	2020
Description of Material	Journal Article
Page(s)	2903-2914

I will acknowledge the original source as specified at the https://rsc.li/permissions.

Signed: Date: 05/30/2022

The Royal Society of Chemistry hereby grants permission for the use of the material specified above in the work described and in all subsequent editions of the work for distribution throughout the world, in all media including electronic and microfilm. You may use the material in conjunction with computer-based electronic and information retrieval systems, grant permissions for photocopying, reproductions and reprints, translate the material and to publish the translation, and authorise document delivery and abstracting and indexing services. Please note that if the material specified above or any part of it appears with credit or acknowledgement to a third party then you must also secure permission from that third party before reproducing that material. The Royal Society of Chemistry is a signatory to the STM Guidelines on Permissions (available on request).

Signed: DocuSigned by: Gill Cockhead 4C6AE64E6C064B5... Date: 30/5/2022 | 10:40 AM BST

VAT registration number GB 342 1784 71 Registered charity number 207890

Andrey Kanygin <akanygin@asu.edu>

Re: Permission to use my article in the dissertation [220629-004216]

Permissions Helpdesk <permissionshelpdesk@elsevier.com> Wed, Jun 29, 2022 at 6:54 AM
Reply-To: Permissions Helpdesk <permissionshelpdesk@elsevier.com>
To: akanygin@asu.edu

Dear Andrey Kanygin,

We hereby grant you permission to reprint the material below at no charge in your thesis subject to the following conditions:

RE: Interplay between hydrogen production and photosynthesis in a green alga expressing an active photosystem I-hydrogenase chimera, International Journal of Hydrogen Energy, Volume 47, Issue 52, 2022, Pages 21969-21983, Kanygin et al

1. If any part of the material to be used (for example, figures) has appeared in our publication with credit or acknowledgement to another source, permission must also be sought from that source. If such permission is not obtained then that material may not be included in your publication/copies.

2. Suitable acknowledgment to the source must be made, either as a footnote or in a reference list at the end of your publication, as follows:

"This article was published in Publication title, Vol number, Author(s), Title of article, Page Nos, Copyright Elsevier (or appropriate Society name) (Year)."

3. Your thesis may be submitted to your institution in either print or electronic form.

4. Reproduction of this material is confined to the purpose for which permission is hereby given.

5. This permission is granted for non-exclusive world English rights only. For other languages please reapply separately for each one required. Permission excludes use in an electronic form other than submission. Should you have a specific electronic project in mind please reapply for permission.

6. As long as the article is embedded in your thesis, you can post/share your thesis in the University repository.

7. Should your thesis be published commercially, please reapply for permission.

8. Posting of the full article/ chapter online is not permitted. You may post an abstract with a link to the Elsevier website www.elsevier.com, or to the article on ScienceDirect if it is available on that platform.

Kind regards,

Roopa Lingayath
Senior Copyrights Coordinator
ELSEVIER | HCM - Health Content Management

Visit Elsevier Permissions

APPENDIX B

COAUTHOR APPROVALS AND CONTRIBUTIONS

COAUTHOR APPROVALS

All coauthors have granted permission for use of previously published material presented in chapters 2 and 3 for the purpose of this dissertation.

AUTHOR CONTRIBUTIONS

Chapter 2

Andrey Kanygin. Designed research. Performed research. Analyzed data. Wrote the paper.

Yuval Milrad. Designed research. Performed research. Analyzed data.

Chandrasekhar Thummala. Performed research.

Kiera Reifschneider. Designed research.

Patricia Baker. Performed research.

Pini Marco. Performed research.

Iftach Yacoby. Designed research.

Kevin E. Redding. Designed research. Wrote the paper.

Chapter 3

Andrey Kanygin. Designed research. Performed research. Analyzed data. Wrote the paper.

Alec Smith. Performed research. Analyzed data.

Valéria Nagy. Performed research. Analyzed data.

Szilvia Z. Tóth. Designed research.

Kevin E. Redding. Designed research. Wrote the paper.